NNT : 2024AIXM0280

THÈSE DE DOCTORAT

Soutenue à Aix-Marseille Université
le 02 Octobre 2024 par

Despoina PERVIZOU

Caractérisation des cellules immunitaires au sein de la prostate murine saine et cancéreuse

Discipline
Biologie santé

Spécialité
Immunologie

École doctorale
ED62- Sciences de la Vie et de la Sante

Laboratoire
Centre d'Immunologie de Marseille Luminy (CIML)

Composition du jury

Julie HELFT — **Rapportrice**
Directrice de Recherche, Institut Cochin, Paris

Benoît MARTEYN — **Rapporteur**
Directeur de Recherche, IBMC, Strasbourg

Nathalie BENDRISS-VERMARE — **Examinatrice**
Chargée de Recherche, CRCL, Lyon

Bernard MALISSEN — **Examinateur**
Directeur de Recherche, CIML, Marseille

Sandrine HENRI — **Directrice de thèse**
Directrice de Recherche, CIML, Marseille

Romain RONCAGALLI — **Président du jury**
Directeur de Recherche, CIML, Marseille

Affidavit

I, undersigned, **Despoina PERVIZOU**, hereby declare that the work presented in this manuscript is my own work, carried out under the scientific supervision of Sandrine HENRI, in accordance with the principles of honesty, integrity and responsibility inherent to the research mission. The research work and the writing of this manuscript have been carried out in compliance with both the French national charter for Research Integrity and the Aix-Marseille University charter on the fight against plagiarism.

This work has not been submitted previously either in this country or in another country in the same or in a similar version to any other examination body.

Place : Marseille, Date : 8 juillet 2024

Cette œuvre est mise à disposition selon les termes de la Licence Creative Commons Attribution - Pas d'Utilisation Commerciale - Pas de Modification 4.0 International.

List of publications

Submitted Research Article (Complete article in Appendix)

"p53-loss induced prostatic epithelial cell plasticity and invasion is driven by a crosstalk with the tumor microenvironment"
Darya Yanushko, Beatriz German Falcon, Rana El Bizri, **Despoina Pervizou**, Céline Keime, Tao Ye, Christelle Thibault-Carpentier, Sandrine Henri, Gilles Laverny and Daniel Metzger.
Submitted in *Cell Death and Disease*, 17th June 2024.

Abstract

Prostate cancer is a heterogeneous disease with a slow progression and a highly variable clinical outcome. The tumor suppressor genes *PTEN* and *TP53* are frequently mutated in prostate cancer and predictive of an early metastatic dissemination and unfavorable patient outcome. The progression of solid tumors to metastasis is often associated with increased cell plasticity, but the complex events underlying *TP53*-loss induced disease aggressiveness remain incompletely understood. Using genetically engineered mice, we show that *Trp53* deficiency in *Pten*-null prostatic epithelial cells (PECs) does not impact the early cell proliferation and neoplasia formation, nor growth arrest and senescence entry at later time. However, *Trp53*-deficiency enhances invasive adenocarcinoma development and promotes metastatic cell dissemination. Importantly, our single-cell transcriptomic and chromatin accessibility analyses combined with histological examinations uncovered an epithelial cell population characterized by an induction of Jak/Stat3 signaling and displaying mesenchymal features. Moreover, our *in vivo* and organoid-based co-culture experiments provide evidence that PEC plasticity occurs through a bi-directional communication with cancer-associated fibroblasts (CAFs). Thus, our study demonstrates that p53 loss induces a protumorigenic crosstalk between PECs and CAFs and identifies new vulnerabilities that might be targeted to limit cancer progression.

Awards & Fellowships

Laureate of Best oral communication
Annual seminar Canceropole PACA 2023; Saint Raphael; France 05/07/2023

Laureate of Fellowship for 4th year of PhD studies
Fondation de Recherche Médicale (FRM) 09/05/2023

Laureate of Best poster communication
ARTP symposium, Paris, France 16/11/2022

Laureate of 2nd Best oral communication
16th PhD workshop in CIML, Marseille, France 25/11/2021

Laureate of Fellowship for 3-years PhD studies
ED62-Aix-Marseille Université, Marseille, France 01/10/2020-2023

Laureat of Travel Grant
European Network of Immunology Institutes for Summer School – 1 week in Sardinia

Laureat of Travel Grant
Europe's Civic University Alliance for Summer School – 1 week in Tubingen

Summer School attendance

12-19/05/23 **16th ENII EFIS EJI Summer School - Advanced Immunology**, Sardinia, Italy
Poster communication

24/06/2022 **CIVIS Summer School- Basics & translational approaches in cancer immunotherapy**, Tübingen University, Germany
Poster communication

06/07/2021 **1st ICI-CIVIS Summer School - Single Cell Approaches in Tumor and Immune Cell Heterogeneity**, Aix Marseille University, France
Poster communication

Conference participation & Awards

06-10/05/24 **Keystone -Myeloid Targeting Strategies for Cancer Treatment**, Killarney, Ireland
Poster Communication

22/11/2023 **32nd Prostate cancer Symposium ARTP**, Paris, France
Oral communication

05/07/2023 **Annual seminar Canceropole PACA 2023**, Saint Raphael, France
Oral communication - *Best oral communication award*

30/05/2023 **30th Doctoral School 62 Symposium**, Marseille, France
Poster communication

16/11/2022 **31nd Prostate cancer Symposium ARTP**, Paris, France
Poster communication -*Best poster communication award*

28/10/2022 **IGBMC, Invited by Dr. Daniel Metzger,** Strasbourg, France
Oral communication

26/09/2022 **CIML, Internal Seminar**, Marseille, France
Oral communication

05/07/2022 **Annual seminar Canceropole PACA**, Saint Raphael, France
Poster communication

31/03/2022 **3rd Annual Conference ICI**, Marseille, France
Poster communication

25/11/2021 **16th PhD workshop in CIML**, Marseille, France
Oral Communication - *2nd Best oral communication award*

Trainings

07-08/11/23	**Spectral Cytometry training - Cytek Aurora/Northern Lights Training** (Introduction to Full Spectrum Profiling)
31-23/06/21	**Imaging Training by Centuri** (Optics & Imaging techniques - Image analysis & programming)
18/01/2021	**Expérimentation Animale - Niveau Concepteur**
16/11/2020	**Research Integrity in scientific professions** (MOOC - AMU)
01/11/2020	**Research Ethics** (MOOC - AMU)

Membership

2022-2024	**Member of the Association pour la Recherche sur les Tumeurs de la Prostate (ARTP)**
2022	**Member of the organization & evaluation committee of "17th PhD workshop in CIML"**

Résumé

Le cancer de la prostate (PCa) est le cancer le plus fréquemment diagnostiqué et la deuxième cause de décès par cancer chez les hommes des sociétés occidentales. Le PCa évolue lentement, commençant par une néoplasie intraépithéliale prostatique (PIN), progressant jusqu'au stade de l'adénocarcinome et aboutissant enfin à des niches métastatiques. Récemment, le domaine de l'immunologie du cancer a été révolutionné par les inhibiteurs du point de contrôle immunitaire (ICI). Cependant, la plupart des essais d'immunothérapie ont échoué pour le cancer de la prostate et l'implication des cellules immunitaires dans le développement des tumeurs de la prostate n'a été abordée que récemment.

La nouveauté de notre étude réside dans la caractérisation détaillée des cellules immunitaires résidant dans la prostate murine saine et recrutées au cours de la progression du cancer de la prostate chez les souris PTEN$^{(i)pe-/-}$. Dans ce modèle de souris, le gène PTEN est délété sélectivement dans les cellules épithéliales luminales prostatiques à l'âge adulte (PSA-Cre^{ERT2}), reproduisant l'occurrence et les caractéristiques du PCa humain. La progression de la tumeur est lente, atteignant le stade PIN seulement 3 mois après l'invalidation du gène, et le stade adénocarcinome après 9 mois. Ainsi, le contrôle temporel strict de la déplétion de la PTEN, la progression lente de la tumeur et son analogie avec la pathologie humaine font du modèle de souris PTEN$^{(i)pe-/-}$ un outil puissant pour caractériser l'infiltration immunitaire tout au long de la progression de la tumeur et pour tester des stratégies thérapeutiques.

En utilisant des techniques avancées, dont le séquençage de l'ARN sur cellule unique, des modèles de souris rapportrices, la cytométrie de flux multiparamétrique et la microscopie confocale, j'ai effectué une analyse longitudinale approfondie des infiltrats myéloïdes et lymphoïdes dans la prostate murine saine et cancéreuse. Grâce à ces méthodes, j'ai établi un atlas immunitaire de haute résolution de la prostate et observé la dynamique de recrutement des certaines cellules immunes au cours du développement du PCa murin, de la néoplasie à l'adénocarcinome. Parallèlement, j'ai effectué une caractérisation avancée des différentes populations de macrophages résidant dans la prostate saine de souris, et déterminé leur localisation, leur taux de renouvellement, leur tropisme au Csf-1, ce qui représente la première exploration détaillée de cet organe.

Nos résultats révèlent de profonds changements dans le compartiment immunitaire à dominante myéloïde tout au long de la progression du PCa, caractérisé par une signature immunosuppressive dominante. Les neutrophiles apparaissent comme la population dominante et sont très hétérogènes, répartis en huit états distincts. Notamment, les états ISG- et dcTRAIL-R1 prédominent aux stades PIN et adénocarcinome, respectivement, indiquant un processus de reprogrammation et de diversification fonctionnelle des neutrophiles au fur et à mesure de l'évolution de la tumeur. Le stade PIN est en outre marqué par la présence de lymphocytes T CD8 épuisés (PD1^{+}Tim3^{+}) et de macrophages Trem2^{+}, ces derniers portant une forte signature métabolique et immunosuppressive.

Dans l'ensemble, l'étude présentée dans cette thèse élucide la diversité et la plasticité des cellules immunitaires lors du développement du PCa, des stades précoces aux stades avancés, indiquant que les tumeurs PTEN$^{(i)pe-/-}$ sont à dominante myéloïde et ouvrant la voie à de nouvelles stratégies immunothérapeutiques qui bénéficieront au domaine de l'immunologie des tumeurs.

Mots clés : cancer de la prostate, cellules immunitaires, immunothérapie, Neutrophiles associés à la tumeur (TAN), Macrophages associés à la tumeur (TAM), scRNAseq, modèle murin PSA-PTEN

Abstract

Prostate cancer (PCa) is the most commonly diagnosed cancer and the second leading cause of cancer related death among men of western societies. PCa progresses slowly, starting with Prostatic Intraepithelial Neoplasia (PIN), progressing to adenocarcinoma stage, and eventually leading to metastatic niches. Recently, the field of cancer immunology has been revolutionized by Immune Checkpoint Inhibitors (ICI). However, most immunotherapy trials for PCa have been unsuccessful and the involvement of immune cells in prostate tumor development has been only recently explored.

The novelty of my PhD study lies on the comprehensive characterization of immune cells residing in healthy murine prostate and those recruited during PCa progression in PTEN$^{(i)pe-/-}$ mice. In this mouse model, the *PTEN* gene is selectively ablated in prostatic luminal epithelial cells at adulthood (PSA-Cre^{ERT2}), reproducing the occurrence and features of human PCa. Importantly, tumor progression is slow, reaching the PIN stage 3 months after the gene invalidation, and the adenocarcinoma stage after 9 months. Thus, the strict temporal control of *PTEN* depletion together with the slow tumor progression and similarity to human PCa, renders the PTEN$^{(i)pe-/-}$ mouse model a powerful tool for characterizing the immune infiltration throughout tumor progression and for testing therapeutic strategies.

Using advanced techniques including single-cell RNA sequencing, reporter mouse models, multiparametric flow cytometry, and confocal microscopy, I conducted a comprehensive longitudinal analysis of the myeloid and lymphoid infiltrates in both healthy and cancerous murine prostate. This analysis allowed me to establish a high-resolution immune atlas of murine prostate and to observe the dynamics of immune cell recruitment during murine PCa development, from neoplasia to adenocarcinoma. Additionally, I conducted a comprehensive characterization of the different macrophage populations residing in the healthy mouse prostate, determining their localization, renewal rates, and tropism to Csf-1, representing the first detailed exploration of this organ.

Our findings reveal profound changes in the myeloid-dominant immune compartment throughout PCa progression, characterized by a dominant immunosuppressive signature. Neutrophils emerge as the dominant immune cell population and exhibit high heterogeneity, resolved into eight distinct states. Notably, the ISG- and dcTRAIL-R1-states predominate at the PIN and adenocarcinoma stages, respectively, indicating a process of neutrophil reprogramming and functional diversification as the tumor evolves. The PIN stage is further marked by the presence of exhausted PD1^{+}Tim3^{+}CD8^{+} T cells and Trem2^{+} tumor-associated macrophages, the latter bearing a strong metabolic and immunosuppressive signature.

Altogether, the study presented in this thesis elucidates to the diversity and plasticity of immune cell upon PCa development from early to late stages, indicating that PTEN$^{(i)pe-/-}$ tumors are myeloid dominant and paving the way for new immunotherapeutic strategies that will benefit the tumor immunology field.

Keywords: prostate cancer, immune cells, immunotherapy, Tumor-associated neutrophils (TAN), Tumor-associated macrophages (TAM), scRNAseq, mouse model PSA-PTEN

Acknowledgements

The present PhD study was carried out from 2020 to 2024 at the Centre d'Immunologie Marseille Luminy (CIML) in the team of Dr. Bernard Malissen under the supervision of Dr. Sandrine Henri.

First of all, I would like to express my appreciation to each jury member for accepting to be part of my PhD defense and evaluate my research. I am grateful to Dr. Julie Helft and Dr. Benoît Marteyn for accepting to review this manuscript, as well as to Dr. Nathalie Bendriss-Vermare and Dr. Bernard Malissen for accepting to be the examiners. I am also thankful to Dr. Romain Roncagalli for accepting to be the president of the jury. Dr. Romain Roncagalli was also the president of the jury when I was awarded the PhD fellowship from Aix-Marseille University at the concours de l'Ecole Doctoral in June of 2020, to start my PhD. Thus, a beautiful journey that started with him as president now comes full circle.

I would like to express my sincere gratitude to Dr. Bernard & Marie Malissen for welcoming me to their team initially for my Erasmus internship and subsequently for my PhD studies. I am deeply grateful Bernard for your strong support and trust throughout these years. I'd like to kindly thank you for the scientific opportunities you offered to me and the great inspiration for science that you have transmitted to me during this journey. It is an honor to have learned from you all these years and now have you as part of my PhD jury.

An immense thank you from heart to my thesis director, Dr. Sandrine Henri, for warmly welcoming me into the DC/Myeloid enthusiasts subgroup of the team when I arrived as an Erasmus intern and ever since, during the four years of PhD that followed. Sandrine, I would like to deeply thank you for the trust and strong support you have shown me since day one. You have been a great example of proper scientific practice, transmitting me your knowledge and passion for myeloid cells and flow cytometry expertise. Thank you for all the opportunities you offered me to participate in many summer schools and conferences all over Europe, that allowed me to travel, exchange with peers and brink back to the lab new knowledge and even prices of best oral communications! Indeed, all your advice and suggestions as I was preparing for scientific communications came handy. Thank you for your support on applying for a 4th year grand in order to stay for an extra year in the lab to continue our beautiful study on the prostate project. I deeply appreciate your hard work and dedication from the beginning of the project and especially the last months on preparing together our scientific article while having to balance also your well-deserved role as a Group leader in Tours. Thank you also for all the comments and corrections on my thesis manuscript. You have been an inspiration as a hard-working woman in science, and I have learned so much working by your side, gaining aptitudes that will accompany me for the rest of my career. I have grown both scientifically and personally over the past five years, learning to give always my best self.

I would like also to sincerely thank my thesis godfather, Dr. Pierre Golstein, for his valuable mentorship throughout my PhD studies. Our frequent discussions on the project were always enriching, providing an external perspective that significantly contributed to its advancement. Additionally, I extend my gratitude to Dr. Nathalie Bendriss-Vermare, my external supervisor, for monitoring my annual progress. Thank you for your valuable

suggestions on the project, and your support for applying for a fourth-year fellowship of PhD. It will be an honor to have you as examiner of my thesis.

An immense thank you to Joanna De Chiara, for being the greatest colleague/super engineer I could have asked for working side by side during my PhD journey. Joanna, thank you for all the hard work and the passion you brought into this project. Thank you for the long experiments we have been doing together, started very early and finishing past midnight. We have shared a lot of drama but also a of fun together. Thank you for taking care of our mice and making sure that everything is running smoothly at the bench, but also thank you for initiating and taking in charge the confocal microscopy aspect of the project that enabled us to visualize the immune cells on our beautiful butterfly-shaped prostate tissue. I deeply appreciate your being always there for me, on the great joys but also on the difficult moments of the PhD. You gave a unique energy to our lab life all those years (by singing/dancing and hard-working at the same time). I could not imagine this PhD without you, as it wouldn't have been the same both in terms of data amount as well as in personal level. We made an awesome binôme and you know that you have a special place in my heart. Un grand merci pour tout, ma JoJo, et merci for the beautiful soul and amazing friend that you are!

A big thanks to Dr. Lionel Spinelli, from the Bioinformatics platform of CIML (CB2M), for his immense work on performing the thorough bioinformatic analysis of our scRNAseq dataset. Thank you, Lionel, for all the hard work, dedication and scientific advice on how to interpret and proceed with the generated information at each point. We could not have reached this level of resolution without your expertise. A great thanks also to Lionel Chasson from the Histology platform of CIML, for performing tissue sections and paraffin samples always with a smile. Thanks, Lionel, for always being so welcoming, for the chats on the corridor and the beers over Happy Hours! Special thanks also to Sylvain Bigot and Marc Barad from the cytometry platform for their expert guidance and input on FACS cell sorting. I would also like to express my gratitude to Dr. Pierre Milpied, for the scientific discussions and advice on the scRNA sequencing procedure, as well as Dr. Hugues Lelouard and Dr. Marc Bajénoff for sharing their knowledge in fluorescent microcopy and providing reporter mouse models. At last, I would like to thank collectively all the platforms of CIML (Cytometry, Genomics, Microscopy, Bioinformatics, Histology, Animal Facility) and the individuals within them for their support and experimental assistance and for their contribution to the project.

At this point I would also like to thank our collaborators from IGBMC in Strasbourg, Dr. Daniel Metzger and Dr. Gilles Laverny for sharing the innovative inducible prostate cancer mouse models PTEN$^{(i)pe-/-}$ & PTEN/p53$^{(i)pe-/-}$, as well as for their suggestions and advice over our project. I appreciated the warm welcome in their lab in Strasbourg and the opportunity to present my PhD work at IGBMC. Special thanks also to Dr. Kateryna Len, who recently defended her PhD, and to the soon-to-be Dr. Darya Yanoushko, for their efforts in organizing and preparing the prostate samples for scRNA sequencing at IGBMC, as well as the discussions around the project data.

A deeply thank you to Dr. Julliane Souza-Lanza and Dr. Fanghui Zhang, my two favorite post-docs, whom I cherish for having met them and learned from them. My dear friends, you are an inspiration for young women in science, each in your own special way! Thank you for all the scientific advice and personal support during those years. I am grateful that our paths

crossed and for all the wonderful memories that we created together in the lab, on our beautiful trips and night-outs. Our shared passion for immunology brought us together in CIML, and we built a strong friendship that will undoubtedly reunite us in the future, whether in China, France, Greece, or Brazil. Cheers to that!

Gracias to mi amigo Javier, post doc and next-desk neighbor on the office, for his support and nice discussions all over those years. I'd also like to thank Guillaume and Romain for discussions over coffee and scientific advice. I am thankful for having met each and every one of the past and present members of the Bernard and Marie Malissen group: Lea, Anais, Lena, Valentin M., Emilie, Killian, Jeanne, Sophie, Philippe, Alice, George, Carine, Yunhao, Daiki and Le for all the good times we spent together. Special thanks to Valentin Le Guen, past post-doc member of our lab for sharing his passions on flow cytometry and nature. I'd like also to thank Maya Nestor Martin, that performed her M2 internship in our team on this project and initiated, along with Joanna and Sandrine, the confocal microscopy analysis. Special thanks to all my friends from CIML that bonded over drinks and night outs. Cecilia, Fanny, Eve, Sergio, Joachim, Apurwa, Julie, Gaby, Toufik you made the life in Marseille a unique experience.

A PhD journey abroad was an incredibly enriching and life-changing opportunity. I will be forever grateful for the people who supported me both professionally and personally. However, embarking on a life abroad means leaving a part of yourself behind in your home country. I would like to dedicate the following section to emphasize the immense importance of the support I received from my family and friends during my PhD studies. A deep thank you from the bottom of my heart to my parents for always encouraging and believing in me and for strongly supporting me during the four years of my thesis. They are everything to me and this dissertation is dedicated to them. Μαμά, μπαμπά σας ευχαριστώ για την αμέτρητη αγάπη και τη στήριξή σας σε αυτήν την πορεία που λέγεται διδακτορικό στο εξωτερικό. Παρότι είμαστε μακριά και μου λείπετε, θέλω να ξέρετε ότι σας νιώθω πάντα δίπλα μου. Είμαι απεριόριστα ευγνώμων που έχω την τύχη να είστε γονείς μου. Αυτή η διατριβή είναι αφιερωμένη σε εσάς με πολλή αγάπη.

My dear friends, Νικολέτα, Δανάη, Αλεξάνδρα, Κατερίνα, Πέτρο, Γιώργο I am deeply grateful for your unwavering support that comes straight from the heart throughout all these years. I thank you a million for always being there for me, listening to me, (even through group videocalls and chats) de-stressing me and for always believing in me. We might be scattered all over Europe, but we are always there for each other no matter what.

At last, my love, Αποστόλη, words are not enough to express my gratitude for your presence in my life. I met you at the beginning of this journey and we have been moving forward together ever since. Thank you for always listening to me and being there in joyful moments and difficult times that came along with the PhD. Thank you for reminding me that there is a whole beautiful forest ahead when I was lost seeing only the trees. You brink the best out of me, and these years wouldn't have been as wonderful and adventurous as they were without you. Cheers to the many more to come! Finally, I cannot overlook the greatest companion, my little cat, Mozzarella, who was sitting by my side (literally), or sometimes on the laptop, when I was writing my dissertation. The best dissertation-pall I could ever have.

Thank you very much, merci beaucoup, ευχαριστώ πολύ, to all the people that made the PhD journey a life-changing experience that I will cherish for life.

Table of Contents

Affidavit ***1***
List of publications ***2***
Résumé ***5***
Abstract ***7***
Acknowledgements ***8***
Table of Contents ***11***
Abbreviations ***13***
Introduction ***20***
Chapter 1: An overview of prostate & prostate cancer ***23***

1.1 Anatomy & physiological function of physiological prostate in human and mouse 23

1.1.1 Human prostate 23
1.1.2 Mouse prostate 25
1.1.3 Homology of human and mouse prostate 25
1.1.4 Cellular composition of human and mouse prostate 26

1.2 Prostate cancer (PCa) 27

1.2.1 Epidemiology 27
1.2.2 Etiology 28
1.2.2.1 Age 28
1.2.2.2 Geographical factor and ethnicity 28
1.2.2.3 Exogenous factors 28
1.2.2.4 Genetic factors 28
1.2.3 Development and staging 32
1.2.3.1 Benign Prostatic Hyperplasia (BPH) 33
1.2.3.2 Prostatic Intraepithelial Neoplasia (PIN) 33
1.2.3.3 Prostatic Carcinoma 34
1.2.3.4 Castrating resistant prostate cancer (CRPC) & Metastasis 34
1.2.4 Diagnosis & Grading of PCa 34

Chapter 2: Mouse models in Prostate Cancer research ***39***

2.1 Principle PCa mouse models 40

2.1.1 Gain-of-function 40
2.1.2 Whole-body knockout 41
2.1.3 Conditional knockout with spatial specificity 42
2.1.4 Conditional knockout with spatial & temporal specificity 43
2.1.4.1 Mouse model PSA-CreER^{T2}/PTEN$^{L2/L2}$ 44
2.1.4.2 Mouse model PSA-CreER^{T2}/PTEN$^{L2/L2}$/P53$^{L2/L2}$ 46

Chapter 3: Immunity in healthy prostate and prostate cancer ***49***

3.1 Interplay of innate and adaptive immunity 49
3.2 Role of immunity in cancer pathogenesis 52
3.3 A focus on Neutrophils in health & cancer 53
3.3.1 Properties & functions 54
3.3.2 Implication in cancer 55
3.3.3 Attraction to the tumor site 56
3.3.4 Heterogeneity and plasticity in cancer 57
3.3.5 Clinical aspect of neutrophils in cancer 58
3.3.6 Resolving the Myeloid Derived Suppressor Cells (MDSCs) nomenclature 58
3.4 A focus on Macrophages in health & cancer 60
3.4.1 Understanding their origins 60
3.4.2 Impact of the environmental niche 64
3.4.3 Macrophages in cancer 65
3.4.3.1 Macrophage polarization: the M1/M2 paradigm 65
3.4.3.2 Macrophage heterogeneity in the single cell era 68
3.4.3.3 Commonly used markers to identify macrophages in mouse tissue 71
3.5 Lymphoid cells in cancer 74
3.6 Elements of an immunosuppressive tumor microenvironment 77
3.6.1 Association of PTEN deficiency with an immunosuppressive TME 77
3.7 Treatment landscape of PCa 79
3.7.1 A focus on immunotherapy 81
3.7.2 Vaccine-based immunotherapy 81
3.7.3 Immune Checkpoint Inhibitors (ICI) as monotherapy 83
3.7.3.1 CTLA-4 83
3.7.3.2 PD-1 / PD-L1 84
3.7.3.3 ICI in combination with other treatments 85
3.7.4 Myeloid targeting treatments 86
3.7.5 Adoptive Cellular Therapy 87
Thesis Objectives 89
Results: Scientific Article 91
Discussion & Perspectives 163
General Conclusions 180
Appendix: Contributing author in submitted article 183
Literature 216

Abbreviations

A

ACT	Adoptive Cellular Therapy
ADCC	Antibody-Dependent Cytotoxicity
ADT	Androgen Deprivation Therapy
AGI	After Gene Invalidation
AGM	Aorta-Gonad Mesonephros
AP	Anterior Prostate
APCs	Antigen Presenting Cells
AR	Androgen Receptor
AREs	Androgen Response Elements
ARG1	Arginase 1
ARG2	Arginase 2
ARPC	Androgen Receptor Pathway-Positive Prostate Cancer
ATP	Adenosine Triphosphate
AZ	Anterior Zone

B

BCL-2	B-Cell Leukemia/lymphoma 2 Protein
BCR	B Cell Receptor
BiTE	Bispecific T cell Engager
BM	Bone Marrow
BP	Biological Process
BPH	Benign Prostatic Hyperplasia
BTLA	Band T Lymphocyte Attenuator

C

C5AR1	Complement component 5a Receptor 1
CAF	Cancer Associated Fibroblasts
CAR-T	Chimeric Antigen Receptor T cells
CBP	CREB-Binding Protein
CCR2	C-C chemokine receptor type 2
CD	Cluster of Differentiation
cDC1	Conventional Dendritic Cells Type I
cDC2	Conventional Dendritic Cells Type II
CGD	Chronic Granulomatous Disease
CK	Cytokeratins
CLP	Common Lymphoid Progenitor
CMP	Common Myeloid Progenitor
COPD	Chronic Obstructive Pulmonary Disease
COX2	Cyclooxygenase-2
CRE	Cyclization Recombinase
CREB	Camp-Response Element-Binding Protein
CRPC	Castrating Resistant Prostate Cancer
CSF-1	Colony Stimulating Factor 1

CTLA-4	Cytotoxic T Lymphocyte Antigen-4
CTLs	Cytolytic T Lymphocytes
CX3CR1	CX3C motif chemokine receptor 1
CXCL	C-X-C motif chemokine Ligand
CXCR	C-X-C motif chemokine Receptor
CZ	Central Zone

D

DAMPs	Damage Associated Molecular Patterns
DC	Dendritic Cells
DC-SIGN	Dendritic Cell-Specific Intercellular Adhesion Molecule 3 (ICAM-3)-Grabbing Nonintegrin
DEG	Differential Gene Expression
DHT	Dihydrotestosterone
DL	Dorsolateral
DLPs	Dorso-Lateral Prostates
dMMR	Mismatch Repair-Deficient
DN DCs	Double Negative Dendritic Cells
DNA	Deoxyribonucleic Acid
Doce	Docetaxel
DP	Dorsal Prostate
DRE	Digital Rectal Examination
DT	Diphtheria Toxin
DTH	Dihydrotestosterone
DTR	Diphtheria Toxin Receptor

E

E	Embryonic day
ECM	Extracellular Matrix
EDTA	Ethylenediaminetetraacetic Acid
EGF	Epidermal Growth Factor
EMT	Epithelial to Mesenchymal Transition
EMTc	Epithelial-to-Mesenchymal Transition Cells
EOMES	Eomesodermin
ER	Estrogen Receptor
ERG	ETS-Related Gene
ETS	E26 Transformation-Specific

F

FACS	Fluorescence-Activated Cell Sorting
FAS	Fatty Acid Synthesis
FCS	Fetal Calf Serum
FDA	Food And Drug Administration
FIRE	Fms-Intronic Regulatory Element
FMO	Fluorescent Minus One
FOLR2	Folate Receptor Beta

G

G/PMN-MDSCs	Granulocytic or Polymorphonuclear Myeloid-Derived Suppressor Cells

G-CSF	Granulocyte-Colony Stimulating Factor
GEMMs	Genetically Engineered Mouse Models
GM-CSF	Granulocyte-Macrophage Colony-Stimulating Factor
GnRH	Gonadotropin-Releasing Hormone
GO	Gene Ontology
GPCR	G-protein Coupled Receptor
GR	Glucocorticoid Receptor
GzmB	Granzyme B

H

H/E	Hematoxylin/Eosin
H2O2	Hydrogen Peroxide
HCC	Hepatocellular Carcinoma
HGPIN	High-Grade PIN
Hif-1	Hypoxia Inducible Factor-1
HSCs	Hematopoietic Stem Cells
HSPs	Heat-Shock Proteins

I-J

i.p.	Intraperitoneal
i.v.	Intravenous
iCAFs	Inflammatory Cancer Associated Fibroblasts
ICAM1	Intercellular Adhesion Molecule 1
ICB	Immune Checkpoint Blockade
ICI	Immune Checkpoint Inhibitors
IDO	Indoleamine 2,3-Dioxygenase
IFNγ	Interferon-γ
Ig	Immunoglobulin
IL	Interleukin
IL-1RA	Interleukin-1 Receptor Antagonist
ILCs	Innate Lymphoid Cells
iNOS	Inducible Nitric Oxide Synthase
IN-seq	Intracellular protein immunodetection by scRNA-seq
IRES	Internal Ribosome Entry Sites
IRF3	Interferon Regulatory Factor 3
ISG	Interferon-Stimulated Gene
ISG	Interferon-Stimulated Gene

K

KCs	Kupffer cells
KEGG	Kyoto Encyclopedia of Genes and Genomes

L

LAG-3	Lymphocyte Activation Gene 3 protein
LCMV	Lymphocytic Choriomeningitis Virus Infection
LCs	Langerhans Cells
LGPIN	Low-Grade Prostatic Intraepithelial Neoplasia
LH	Leuteinizing Hormone
LNCaP	Lymph Node Carcinoma of the Prostate

LoxP	Locus of X-over of P1
LP	Lateral Prostate
LPB	Large Probasin Promoter
LumC	Luminal-C
LYVE-1	Lymphatic Vessel Endothelial Hyaluronan Receptor 1

M

M1	Macrophage 1
M2	Macrophage 2
MBC	Metastatic Breast Cancer
mCRPC	Metastatic Castrating Resistant Prostate Cancer
MDA-PCa	MD Anderson Prostate Cancer
MDSCs	Myeloid-Derived Suppressor Cells
MEKi	Inhibitors Of the Mitogen-Activated Protein Kinase
Mf or Mac	Macrophages
MHC	Major Histocompatibility Complex
MIF	Macrophage Migration Inhibitory Factor
M-MDSCs	Monocytic Myeloid-Derived Suppressor Cells
MMP-9	Matrix Metalloproteinase 9
MNP	Mononuclear Phagocyte
mo-DC	Monocyte-derived Dendritic Cells
mo-macs	Monocyte-derived Macrophages
MPS	Mononuclear Phagocyte System
Mreg	Monocytic regulatory cells
mRNA	Messenger RNA
MSI-H	Microsatellite Instability-High
MSPC	Mesenchymal and Stem-like Prostate Cancer
myCAFs	Myofibroblastic Cancer Associated Fibroblasts

N

N1	Neutrophil 1
N2	Neutrophil 2
NADPH	Nicotinamide-Adenine Dinucleotide Phosphate
NCCN	National Comprehensive Cancer Network
NE	Neuroendocrine
NE	Neutrophil Elastase
NEPC	Neuroendocrine Prostate Cancer
NETs	Neutrophil Extracellular Traps
NK	Natural Killer cells
NKT	Natural Killer T cells
NLR	Neutrophil-to-Lymphocyte Ratio
NLRs	NOD-like receptors
NSCLC	Non-Small Cell Lung Cancer

O

OIS	Oncogene-Induced Senescence

P

PAD4	Protein-Arginine Deaminase Type 4

PAMPs	Pathogen Associated Molecular Patterns
PAP	Prostatic Acid Phosphatase
PB	Probasin Promoter
PBS	Phosphate-Buffered Saline
PC-3	Prostate Cancer cells-3
PCa	Prostate Cancer
PD-1	Programmed Death-1
PDAC	Pancreatic Ductal Adenocarcinoma
PD-L1	Programmed Death-Ligand 1
PECs	Prostatic Epithelial Cells
PI3K	Phosphoinositide 3-Kinase
PIN	Prostatic Intraepithelial Neoplasia
PPP	Pentose Phosphate Pathway
PRRs	Pattern Recognition Receptors
PSA	Prostatic Specific Antigen
PSC	Prostatic Stem Cells
PSMA	Prostate-Specific Membrane Antigen
PtdIns(3,4,5)P3	Phosphatidylinositol 3,4,5-Trisphosphate
PTEN	Phosphatase and TENsin homolog
PVMs	Perivascular Macrophages
PZ	Peripheral Zone

Q

QC	Quality Control

R

RB	Retinoblastoma Protein
RNA	Ribonucleic Acid
RNS	Reactive Nitrogen Species
ROS	Reactive Oxygen Species
RTMs	Resident-Tissue Macrophages

S

SASP	Senescence-Associated Secretory Phenotype
SBRT	Stereotactic Body Radiotherapy
scFv	single-chain variable Fragment
sc-RNA seq	Single cell-RNA sequencing
SHBG	Sex Hormone-Binding Globulin
SIRPα	Signal regulatory protein α
snATACseq	single-nuclei Assay for Transposase Accessible Chromatin sequencing
SPF	Specific Pathogen Free mice
SV40 Tag	Sivian Virus 40 large T and small t antigens

T

TAA	Tumor-Associated Antigens
Tam	Tamoxifen
TAMs	Tumor-Associated Macrophages
TANs	Tumor Associated Neutrophils
TBP	TATA-Box-Binding Protein

TCA	Tricarboxylic Acid
TCGA	The Cancer Genome Atlas
TCR	T Cell Receptor
TGF-β	Transforming growth factor beta
Th	T-Helper Cells
THPO	Thrombopoietin
TIGIT	Tyrosine-Based Inhibitory Motif Domain
TILs	Tumor Infiltrating Lymphocytes
TIM-3	T-cell Immunoglobulin domain and mucin Domain protein 3
TIM-4	T-cell Immunoglobulin and Mucin domain 4
TLRs	Toll-like receptors
TME	Tumor Microenvironment
TMPRSS2	Transmembrane Protease Serine 2
TNF-α	Tumor Necrosis Factor-a
TNM	Tumor, Nodes, Metastasis
TP53 or P53	Tumor Protein 53
TRAMP	Transgenic Adenocarcinoma of the Mouse Prostate
Treg	Regulatory T Cells
TREM2	Triggering Receptor Expressed on Myeloid Cells 2
TRUS	Trans-Rectal Ultrasound
TZ	Transitional Zone

U

UGS	Urogenital Sinus
UMAP	Uniform Manifold Approximation and Projection
UMIs	Unique Molecular Identifiers

V-Z

VCap	Vertebral-Cancer of the Prostate
VEGF	Vascular Endothelial Growth Factor
VP	Ventral Prostate
WT	Wild Type

« À mes parents »

Introduction

~CHAPTER 1~

An overview of prostate & prostate cancer

Chapter 1: An overview of prostate & prostate cancer

1.1 Anatomy & physiological function of physiological prostate in human and mouse

1.1.1 Human prostate

The prostate is an exocrine gland and a component of the male reproductive system. It has the size of a walnut in humans and, anatomically, it is located below the bladder, surrounding the proximal portion of urethra *(**Figure 1**)*.

The word prostate comes from the Ancient Greek "*προστάτης*", prostátēs, meaning "one who stands before", "protector", "guardian". As indicated by its name, the main function of prostate gland is to "protect" the sperm, by producing 30% of the seminal fluids, providing ions, nutrients, and enzymes necessary for the survival of the spermatozoids during their journey to the female reproductive track. The sperm, after being produced in the testicles, moves into a coiled mass, known as the epididymis for maturation. It then goes into two muscular tubes known as the vas deferens, which coil around the bladder and seminal vesicles. The seminal vesicle can store sperm for several days until ejaculation. The prostate contributes to sperm delivery via its smooth muscle fiber contraction, controlled by the autonomic nervous system, propelling sperm into the prostatic urethra and towards the tip of the penis. Although the prostate gland is involved in fertility, it is not essential for reproduction.

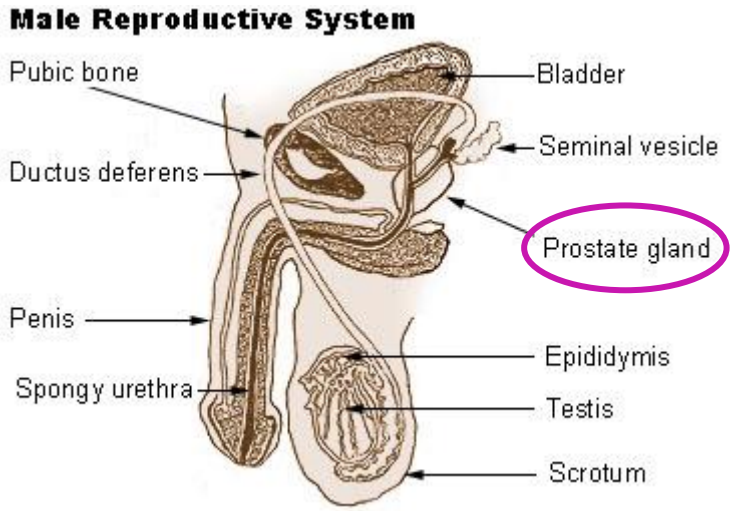

***Figure 1. Schematic representation of the human male reproductive system**. The arrows indicate the various organs, with the organ of prostate being highlighted. (Source: Official website of National Cancer Institute, visited on 23/01/2024 https://training.seer.cancer.gov/anatomy/reproductive/male/)*

The average weight of a healthy adult prostate is approximately 20 grams. It is encapsulated by a layer of fibroelastic tissue, leading to septa extending inwards and dividing the prostate into different lobes. The lobes contain around 50 irregularly branched saccular glands, excretory ducts, stroma (connective tissue cells), muscle cells, blood vessels and

nerves. This transitional epithelium or urothelium has the ability to contract and expand according to fluid volume (Berry et al., 1984).

The prostate gland is of significant importance in men's health, being susceptible to clinical pathologies such as prostatitis, prostate hyperplasia and prostate cancer. Understanding the prostate anatomy is crucial for specialized disease treatment. The structural anatomy of human prostate has been delineated by McNeal into 4 distinct zones: peripheral zone (PZ), central zone (CZ), transitional zone (TZ) and anterior zone (AZ) (McNeal, 1981) (***Figure 2A***).

The peripheral zone, located postero-laterally, is the largest area of the gland and, is the site where most carcinomas develop (75%). The central zone, which constitutes 25% of the prostate, is positioned anterior to the peripheral zone, with fewer than 5% of prostate cancers arising in this region (Toivanen and Shen, 2017). The transitional zone encircles the urethra, comprises only 10% of the prostate volume and is the primary site for benign prostatic hyperplasia (BPH), a non-malignant enlargement of tissue. Lastly, the anterior fibro-muscular zone, which lacks glandular components, forms the anterior surface of the prostate (Chughtai et al., 2016).

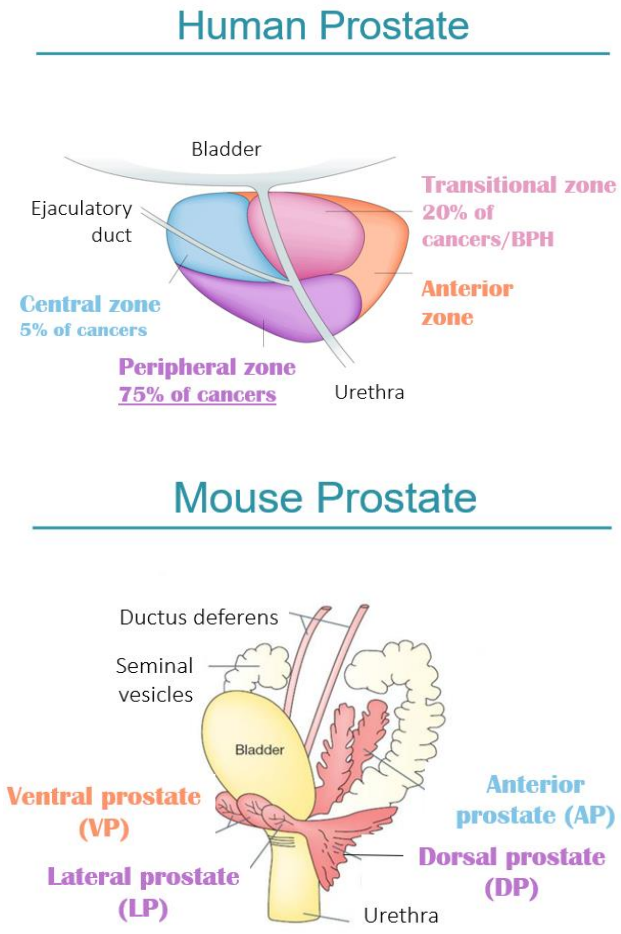

Figure 2. Schematic illustration of human (A) and mouse (B) prostate and adjacent structures. *(A) Human prostate showing the location of the zones of the prostate and their likelihood of developing cancerous lesions. (B) Mouse urogenital system in which the organ of prostate is depicted in red. The various lobes of the prostate are highlighted. The color code of the human prostate zones is indicating the equivalent lobes on the murine prostate. Figures adapted from Sathianathen et al., 2018 (A) and Toivanen et al., 2017 (B).*

1.1.2 Mouse prostate

While studies of human tissue samples have provided descriptive understandings of prostate development and function in health and pathology, the use of genetically engineered mouse models allows to decipher further pathological mechanisms. It is thus, of great importance to consider interspecies similarities and differences in order to develop and use the most accurate model for our studies. It is thus, important to highlight that prostate exhibits unique anatomical morphology across species. Although both human and mouse prostate originate from the urogenital sinus, they display significant anatomical and morphological differences.

While the human prostate is a uni-lobular organ, the murine prostate consists of four separate pair of lobes named after their spatial orientation (Timms, 2008). The anterior prostate (AP), dorsal prostate (DP), lateral prostate (LP) and ventral prostate (VP) lobe. Specifically, the AP lobes are adjacent to the seminal vesicles, while the DP lobes are located at the base of seminal vesicles and found on the dorsolateral side of the bladder. The VP lobes surround the urethra ventrally ending to the LP lobes which lay on both sides of the urethra (***Figure 2B***). DP and LP are often referred together as the dorsolateral prostate (DLP) despite some histological differences. These lobes display patterns characteristic of ductal branching and secretory protein production similar to those in humans (Cunha et al., 1987; Hayashi et al., 1991; Sugimura et al., 1986).

1.1.3 Homology of human and mouse prostate

Anatomical interspecies analysis regarding the homology of the murine prostate lobes to the human prostate zones, revealed that the mRNA expression signature of the murine DLP lobes corresponds to the human PZ, where 75-85% of the human adenocarcinomas occur. Similarly, the AP lobes are homologous to the human CZ. However, there is no mouse homologue for the human TZ zone, where most benign hyperplasia lesions occur. Despite anatomical differences, the prostate epithelium between human and mouse is histologically similar, being glandular, bi-stratified and composed of basal and luminal cells (Oliveira et al., 2016).

An additional interspecies difference of the prostate gland is the occurrence of various pathologies. Notably, while prostate cancer is the most common diagnosed cancer of male humans, and appears frequently in dogs too, mice and rats rarely develop spontaneous prostate cancer (Mitsumori and Elwell, 1988; Valkenburg and Williams, 2011). This can be partially explained due to the fact that the advanced age is one of the main risk factors of prostate cancer, with 60% of diagnoses occurring in men 65 years of age or older, while mice have a much shorter life span (~3 years) and subsequently less time for genetic alterations to accumulate. Additionally, while human prostate cancer harbors between 10 and 100 nonsynonymous mutations and multiple chromosomal rearrangements and somatic copy number aberrations (Taylor et al., 2010), most mouse prostate tumors rarely show karyotypic abnormalities and present very few somatic copy number alterations (Hubbard et al., 2016). On the top of that, telomeres in mice are five to 10 times longer than in humans, making them less prone to telomere-induced aging and subsequent genetic alterations.

The fact that mice do not spontaneously develop prostate cancer (PCa), is a limitation of their use as a spontaneous PCa model. Nevertheless, tumors can be induced through genetic or environmental manipulation. Therefore, Genetically Engineered Mouse Models (GEMMs) are now the model of choice for studying prostate cancer *in vivo*, allowing to disentangle the molecular and cellular mechanisms underlying prostate tumor initiation and progression, and to evaluate new therapies.

1.1.4 Cellular composition of human and mouse prostate

Within the prostatic epithelium, there are at least three distinct cell types, distinguished by their morphological characteristics, functional significance, and relevance for carcinogenesis. Notably, the prostate glandular epithelium is composed of an inner monolayer of secretory luminal epithelial cells and an outer monolayer of basal epithelial cells surrounding the luminal cells and being in contact with the basement membrane, which serves as a barrier between the epithelial and stromal compartments (***Figure 3***).

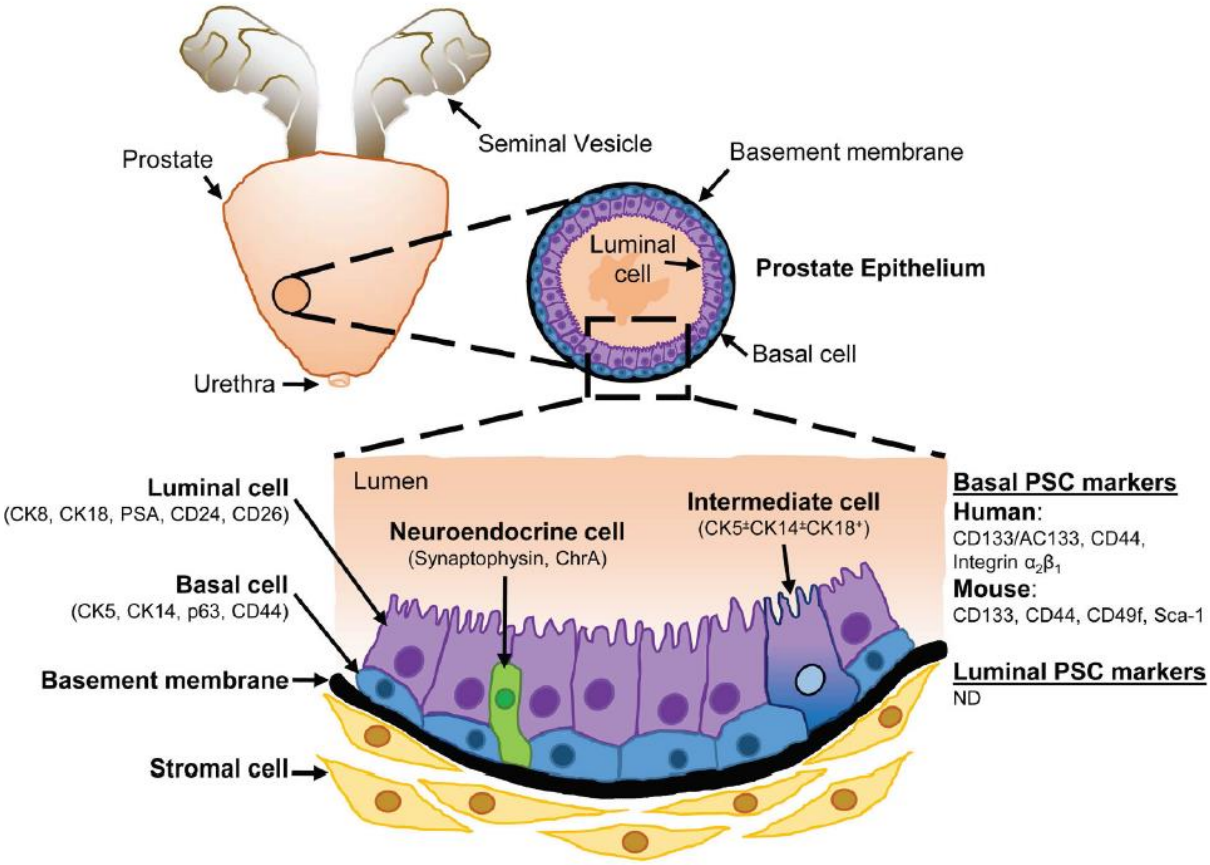

Figure 3. Schematic representation of differentiated cell types in the adult prostate. *The epithelial compartment is composed of basal cells that line the basement membrane, secretory luminal cells, and rare intermediate and neuroendocrine cell populations. These epithelial ducts are adjacent to a stromal compartment that includes smooth muscle cells, fibroblasts, and vascular and neural components. Source figure adapted from (Rybak et al., 2015).*

The luminal cells are a differentiated androgen-dependent cell type, characterized by the expression of androgen receptor (AR). These tall columnar epithelial cells secrete prostatic

acid phosphatase (PAP), prostatic specific antigen (PSA) and human kallikrein-2 into the lumen of the gland along the seminal fluid. They are distinguished by the surface protein expression of the cytokeratines (CK) 8 and 18, CD24, CD26. In contrast, the basal cells are located below the luminal layer and are non-secretory cells. These cuboidal cells are characterized by the expression of CD44, Trp63, CK14, CK5, display a low AR protein level and lack of PSA production both in humans and mice. Within the basal layer appears often an intermediate cell type, displaying both luminal and basal markers, not yet determined whether they represent a distinct cell type.

Moreover, the prostate epithelium contains a scattered long-term surviving population of prostate stem cells (PSC) exhibiting either a basal or luminal self-renewing phenotype. Additionally, there is another rare population, called neuroendocrine cells, expressing secreted neuropeptides and other hormones. Prostate mesenchyma is also rich in distinct differentiated cell types. It includes a layer of smooth muscle cells, encircling the epithelium and exhibiting contractile activity, and a substantial population of mature fibroblasts that secrete extracellular matrix. There are also other components of stroma including blood vessels, lymphatics, nerves and immune cells, that are involved in homeostatic maintenance as well as in tumorigenesis within the prostate (Rybak et al., 2015; Toivanen and Shen, 2017). A detailed description (*Chapter 3*) is dedicated to the prostatic immune cell characteristics and function in health and cancer.

1.2 Prostate cancer (PCa)

1.2.1 Epidemiology

The prostate is highly susceptible to oncogenic transformation with a frequency significantly greater than other male secondary sexual tissues. Prostate cancer (PCa) is the most frequent malignancy and the second leading cause of cancer-related deaths after lung cancer (***Figure 4***) (Siegel et al., 2024). 90% of men are being diagnosed with PCa between 55 and 64 years of age, with a 5-year relative survival rate in Europe at 83% (Marhold et al., 2022).

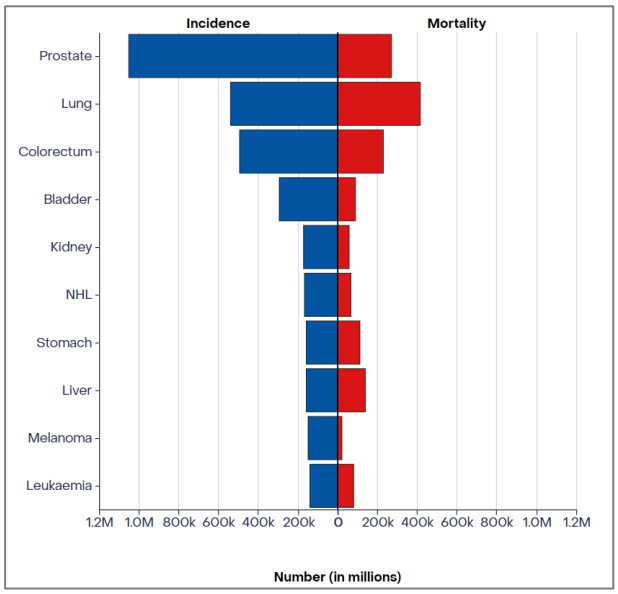

Figure 4. Incidence and mortality numbers of the top 10 cancer types in males in 2022. *The continents included in the study are Europe, Africa, Northern America, Latin America, and the Caribbean. (Source: Official website of World Health Organization - International agency for Cancer Research- Cancer Today, visited on 06/07/2024 https://gco.iarc.fr/today/en/).*

1.2.2 Etiology

The PCa incidence show great variability globally due to a wide range of etiology. Well-established risk factors for prostate cancer are increasing age, african ancestry, family history of the disease, and certain inherited genetic conditions (e.g., Lynch syndrome and BRCA1 and BRCA2 mutations) (Rawla, 2019).

1.2.2.1 Age

As prostate cancer is a cancer of elder people, over the age of 65, the age is considered as a primary risk factor. Notably, in view of the ageing population, this major risk factor may partly explain the increasing numbers of prostate cancers incidences each year.

1.2.2.2 Geographical factor and ethnicity

Prostate cancer is more prevalent in North America, North-West Europe, Australia, and the Caribbean islands, as opposed to Asia, Africa, Central America and South Africa. This disparity may be partly due to better screening and treatment access in developed countries, along with geographical factors such as diets sun exposure. Ethnicity is also associated to prostate cancer. African American men in the USA and the Caribbean have the highest documented prostate cancer incidence and mortality rates in the world. Nevertheless, the reasons for these ethnic differences remain unclear (Pernar et al., 2018).

1.2.2.3 Exogenous factors

Several exogenous factors, such as dietary habits, can influence the development of prostate (Gathirua-Mwangi and Zhang, 2014). High consumption of red meat, saturated fat, and calcium coupled with low fruit and vegetable intake, has been associated to an increased risk for advanced prostate cancer. Additional studies have suggested that men who consume calcium, either through diet or supplementation, have a higher risk of developing prostate cancer (Ahn et al., 2007). Other exogenous factors can increase the risk of developing prostate cancer, such as obesity, smoking, exposure to chemical agents, sexually transmitted infections, inflammation of the prostate and vasectomy (Gann, 2002). The factors that may increase the risk of aggressive and/or fatal disease are smoking and excess body weight.

1.2.2.4 Genetic factors

As with other cancers (e.g. breast cancer, colorectal cancer), a family history is a risk factor in the development of prostate cancer. Having a first-degree relative with prostate cancer increases the risk by two to three times due to the genetic susceptibility. Besides the hereditary mutations, additional genetic alterations play crucial roles in prostate carcinogenesis.

1.2.2.4.1 Androgens & Androgen receptor

The androgens are steroid hormones that play a crucial role in the expression of the male phenotypical and behavioral characteristic. The prostate is a gland whose physiological growth and function is dependent on androgens. Androgens, like testosterone, are primarily synthesized by the Leydig cells located in the testes, under the control of luteinizing hormone (LH) secreted by the anterior pituitary gland. The secretion of LH is regulated by gonadotropin-releasing hormone (GnRH) by the hypothalamus in the brain (***Figure 5A***). Once synthesized, testosterone largely circulates bound to serum sex hormone-binding globulin (SHBG) and albumin. The unbound or free form of testosterone can enter prostate cells by binding to the androgen receptor expressed by the prostatic epithelial and stromal cells (Heinlein and Chang, 2004). The androgen receptor (AR) belongs to the Type I class of nuclear hormone transcription factors along with the estrogen receptor (ER), progesterone receptor (PR), and glucocorticoid receptor (GR). In the absence of ligand, the AR is located on the cell cytoplasm. After ligand binding, AR is translocated into the nucleus stimulating downstream expression of androgen-dependent genes.

When testosterone enters prostate cells, 90% is converted to dihydrotestosterone (DHT) by the enzyme 5α-reductase. DHT is a more potent androgen that has a five-fold higher affinity for AR compared to testosterone. Within the nucleus, the AR dimers bind to androgen response elements (AREs) located in the promoter regions of target genes, such as prostate-specific antigen (PSA) and transmembrane protease serine 2 (TMPRSS2). This binding event facilitates the recruitment of various coregulatory proteins, aiding in transcription and ultimately resulting in responses such as growth and survival (Tan et al., 2015) (***Figure 5B***). The PI3K/AKT pathway, which is strongly implicated in cancer, is also a downstream target of AR signaling (Sarker et al., 2009).

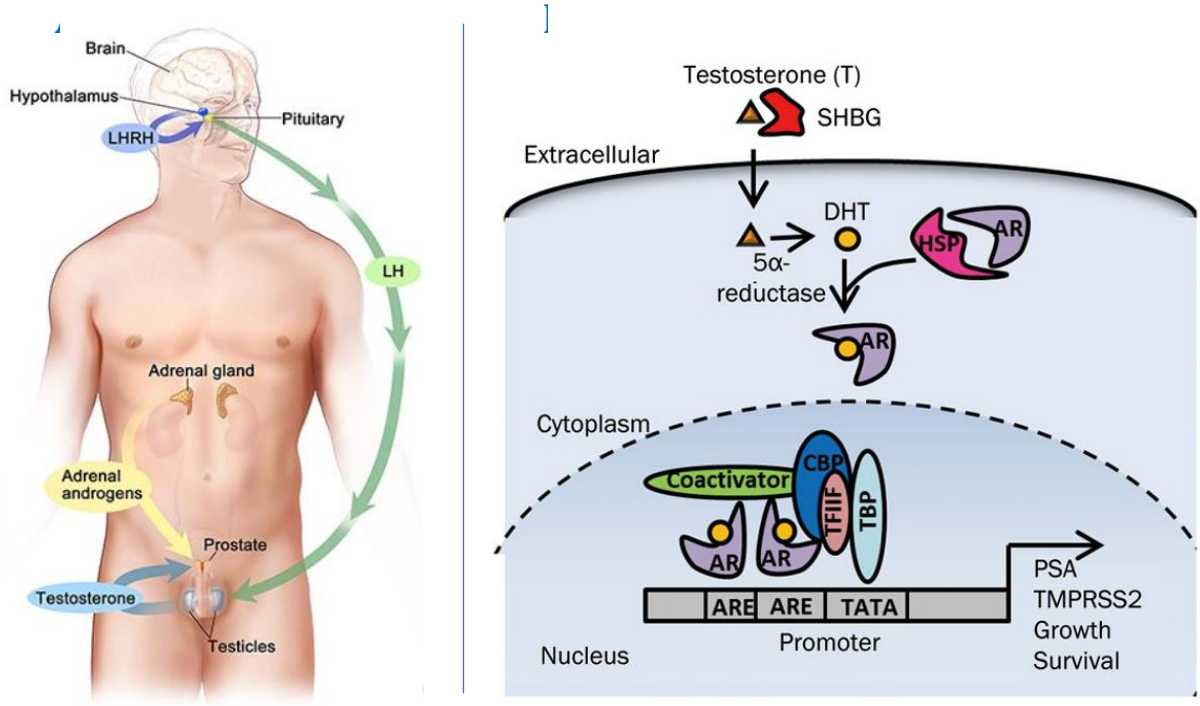

Figure 5. Androgen and AR signaling in prostate. A) Testosterone production. *The hypothalamus releases LHRH (luteinizing hormone-releasing hormone), which stimulates the*

release of LH from the pituitary gland. LH acts on specific cells in the testes to produce the majority of testosterone in the body. Most of the remaining androgens are produced by the adrenal glands. Androgens are taken up by prostate cells. Figure source from https://www.cancer.gov/ accessed on 09/03/2024 "National Hormone Therapy for Prostate Cancer" was originally published by the National Cancer Institute. ***B) AR signaling in prostate cells.*** *Following synthesis in the testes, testosterone is transported to target tissues like the prostate, where it undergoes conversion to dihydrotestosterone (DHT) by the enzyme 5-α-reductase. DHT binds to the ligand-binding pocket of the androgen receptor (AR), promoting the dissociation of heat-shock proteins (HSPs) from the AR. Subsequently, the AR translocates into the nucleus, where it dimerizes and binds to the androgen response element (ARE) located in the promoter region of target genes such as prostate-specific antigen (PSA) and TMPRSS2. At the promoter site, the AR is capable of recruiting members of the basal transcription machinery, including TATA-box-binding protein (TBP) and transcription factor IIF (TFIIF), along with other coregulators like members of the p160 family of coactivators and cAMP-response element-binding protein (CREB)-binding protein (CBP). Additionally, testosterone largely circulates bound to serum sex hormone-binding globulin (SHBG). Figure source adapted from (Tan et al., 2015).*

One of the first observations related to prostate cancer progression was the increase of AR molecules on the cell surface of tumor cells (Abeshouse et al., 2015; Abida et al., 2019). Current clinical and experimental data suggest that prostate cancer progression is largely due to the alteration of the normal androgenic axis via deregulation of AR activity by signal transduction cascades, altered expression of AR co-regulators and mutations that enable AR to be transcriptionally active in response to ligands in addition to DHT. Due to its many downstream effects, antiandrogen therapies have long been of therapeutic interest, with AR antagonists often in combination with conventional chemotherapy or radiation therapy (Heinlein and Chang, 2004). AR has been also shown to contribute to the formation of metastases. *In vitro*, increased AR expression in prostate tumors also led to the formation of metastatic niches and induction of the epithelial to mesenchymal transition (EMT). Through this process, cells lose their polarity, gain the ability to migrate and become invasive (Lin et al., 2018).

1.2.2.4.2 PTEN

The Phosphatase and TENsin homolog deleted on chromosome 10 (*PTEN*) gene is widely identified as a tumor suppressor gene, frequently mutated in a large number of cancers. In fact, the pan-cancer analysis, reveals that PTEN is the second most commonly inactivated gene across cancer types and is most frequently altered in uterine, glioblastoma, prostate, lung and melanoma cancer (Luongo et al., 2019).

The major biological function of PTEN protein is to regulate one of the most significant cell growth and pro-survival signaling pathways, the PI3K/AKT/mTOR. PTEN protein acts by dephosphorylating the phosphatidylinositol 3,4,5-trisphosphate (PtdIns(3,4,5)P3) to PtdIns(4,5)P2 and therefore inhibiting the PI3K/AKT/mTOR signaling pathway to regulate cell proliferation, metabolism, survival, polarity, migration and angiogenesis (***Figure 6***). Loss of

PTEN leads to over-activation of Akt which, in turn, promotes cell survival, uncontrolled cell proliferation, angiogenesis and migration.

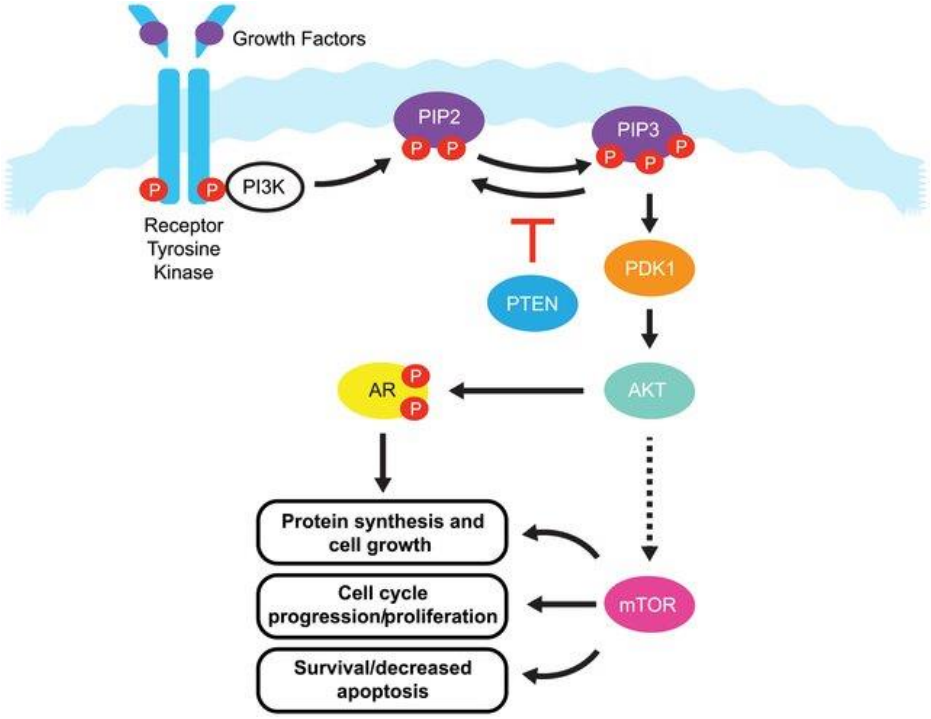

Figure 6. The PI3K-PTEN-Akt pathway. *The main function of PTEN consists in the regulation of the PI3K/Akt/mTOR. In response to extracellular stimuli (e.g., presence of insulin, growth factors, chemokines), PI3K is activated by tyrosine kinase receptors or G-protein-coupled receptors, and it phosphorylates PIP2 to generate PIP3 which in turn phosphorylates and activates Akt. PTEN is a lipid phosphatase that antagonizes the action of PI3K by dephosphorylating PIP3 to generate PIP2 and thus, blocking the PI3K signaling cascade. Source figure from (Phin et al., 2013).*

PTEN loss in PCa is associated with 20% primary and 40.7% metastatic PCa leading to lethal progression (Abeshouse et al., 2015; Robinson et al., 2015). Multiple functional studies using cell lines, xenografts, and mouse models underscore the role of PTEN as a critical tumor suppressor in prostate cancer. Moreover, high AR expression with low PTEN expression in prostate cancer patients, has been established as a predictive biomarker for poor clinical outcomes and progression to metastatic castrating resistant prostate cancer (Sircar et al., 2009).

1.2.2.4.3 P53

The Tumor protein 53, also known as Tp53 or p53, encoded by the *TP53* tumor suppressor gene in humans, has been extensively studied since its discovery in 1979 and is recognized as a multifaceted protein. Initially known as a stress-sensing protein crucial for maintaining genome integrity by regulating genes involved in cell cycle arrest, apoptosis, and DNA repair, the understanding of the role of p53 has expanded to encompass a broader array of biological processes, facilitating cell adaptation to their environment. Notably, its involvement in cancer-related pathways is well-documented, as p53 mutations are found in nearly half of human cancers (Marcel et al., 2018). While p53 is not indispensable for normal

cell growth and development, it plays a crucial role in orchestrating cellular responses to DNA damage and diverse stressors. Upon stress signals, p53 accumulates and stabilizes through post-translational modifications like phosphorylation, methylation, and acetylation, subsequently inhibiting or reducing proliferation via cell cycle arrest or apoptosis, often in collaboration with other cellular components (Brooks and Gu, 2006).

The *TP53* gene is commonly mutated in local and metastatic prostate adenocarcinoma. Approximately 25-30% of clinically localized cancers contain mutations in TP53, indicating that these alterations are not exclusively late events in the genomic history of the disease (Barbieri et al., 2013). Additionally, p53 mutations exhibit a strong correlation with PTEN loss, and this association extends to prostate cancer aggressiveness, resistance to anti-androgen therapy, as well as relapse and metastasis, indicating that p53 mutation represents a positively selected event in aggressive tumor cells (Eastham et al., 1995; Hatano and Nonomura, 2022).

1.2.2.4.4 Others

Other molecular players have been implicated in prostate carcinogenesis, spanning from the initiation to metastatic stages. The most prevalent alterations in prostate cancer genomes involve fusions of androgen-regulated promoters with the E26 transformation-specific (ETS) family of transcription factors and especially with the ERG (ETS-related gene). Specifically, the TMPRSS2-ERG fusion represents the most common molecular alteration in prostate cancer, occurring in approximately 40% to 50% of prostate tumor foci (Abeshouse et al., 2015). Also, the Nkx3.1, an androgen regulated tumor suppressor transcription factor, is critical in the normal differentiation of prostatic epithelium, and its loss is an initiating event in prostate carcinogenesis (Abate-Shen et al., 2008; Bhatia-Gaur et al., 1999). It is lost in 78% of metastatic prostate cancers. Additionally, the loss of RB (Retinoblastoma protein) is frequently observed in prostatic neoplasia. RB1 alterations have been recently associated with poor survival and serves as a strong predictive marker for poor clinical outcome (Abida et al., 2019). The genes *BRCA1*, *BRCA2* and *ATM* have also been implicated in PCa development and progression (Hatano and Nonomura, 2022).

1.2.3 Development and staging

Prostate cancer development is characterized by the abnormal division of prostate gland cells resulting in abnormal prostate gland growth. As mentioned before, most cancer lesions occur in the peripheral zone of the gland, fewer in the transition zone and almost none in the central zone. Benign prostatic hyperplasia (BPH) characterized by an increased proliferation of normal cells is not considered a precursor lesion to PCa, since BPH patients have not been correlated with increased incidence of PCa. However, the eminent proliferation of atypical epithelial cells contained within the glands leads to pre-neoplastic lesions, known as prostatic intraepithelial neoplasia (PIN). PIN progress to malignant adenocarcinoma, and eventually form metastatic niches (Grabowska et al., 2014). The progression of human prostate tumorigenesis has been defined in specific stages (***Figure 7***).

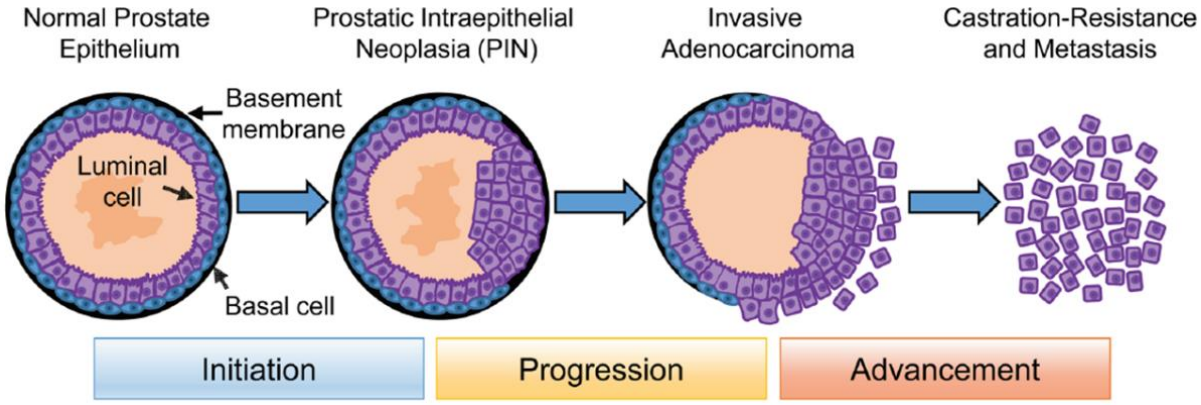

Figure 7. Prostate cancer progression (Rybak et al., 2015).

1.2.3.1 Benign Prostatic Hyperplasia (BPH)

The organ of prostate undergoes maturation during puberty and is completely mature on adulthood. Impressively, it is one of the few mature organs that continue to grow by ageing throughout adulthood. Thus, BPH is a very common disease in older men and can involve both stromal and epithelial growth. BPH is considered a normal event of the ageing process. It is estimated that 20% of men in their 40s will have BPH, rising to 80-90% of men in their 70s and 80s (Roehrborn, 2008). Due to prostate's anatomical location, increased prostatic volume leads to urinary disorders. Although the mechanisms of BPH are not fully elucidated to date, it is known to result from an imbalance between cell growth and apoptosis in the transitional zone of prostate (Chughtai et al., 2016). However, there is no association between BPH and the later development or increased risk of prostate cancer (Schenk et al., 2011).

1.2.3.2 Prostatic Intraepithelial Neoplasia (PIN)

The prostatic intraepithelial neoplasia (PIN) is characterized by luminal epithelial hyperplasia, enlarged nuclei and nucleoli and a reduction in basal cells while maintaining an intact basement membrane, and is considered as a pre-neoplastic lesion in humans (McNeal and Bostwick, 1986). PIN is classified into two types: Low-Grade PIN (LGPIN), where the epithelium has thickened as a result of cell proliferation of luminal cells, but still the lumen remains predominant and High-Grade PIN (HGPIN), where the epithelium is very thick, completely disorganized, and the epithelial nuclei are larger and richer in nucleoli, with little or no apparent lumen. In HGPIN there is complete or partial preservation of the basal cell layer but no invasion into the surrounding stroma. HGPIN is asymptomatic and unlike BPH, it is highly correlated with increased risk and progression to malignant adenocarcinoma (Merrimen et al., 2009).

1.2.3.3 Prostatic Carcinoma

PIN lesions can remain latent for several years, before progressing to carcinoma, which is characterized by stromal invasion of atypical epithelial cells and loss of basal cells and basement membrane. The process begins with biological changes within the cancer cells, which enhance their motility, leading to local invasion, intravasation into blood and lymphatic vessels, transit through the invaded circulatory system, and extravasation from the vessel into the parenchyma of distinct tissue. When HGPIN lesions progress to carcinoma, the majority (99%) of cases are adenocarcinoma, while the remaining 1% includes sarcomatoid tumors or neuroendocrine (NE) carcinoma, which, as the name suggests, is the result of a carcinogenic process in the rare prostatic neuroendocrine cells. Prostate carcinoma is classified as microinvasive or invasive carcinoma, based on the extend of infiltration and destructive growth. Invasive carcinoma involves neoplastic proliferation beyond the ducts and invasion of contiguous local structures within and beyond the prostate. Then, the formation of small nodules of cancer cells (micro-metastases) will grow into large macro-metastatic lesions, at secondary sites (Hanahan and Weinberg, 2011).

1.2.3.4 Castrating resistant prostate cancer (CRPC) & Metastasis

Prostate cancer is highly driven by androgen receptor signal. Notably, the androgens fuel the cancerous luminal cells, making androgen deprivation a common treatment (Sehgal et al., 2019). Nevertheless, after a remission phase of 18 to 36 months, most patients who are hormone-sensitive, will eventually relapse to a hormone-resistant form, which is more aggressive and is called Castrating Resistant Prostate Cancer (CRPC) progressing to metastatic stage (mCRPC) (Wadosky and Koochekpour, 2016). Most common metastatic niches are the bones and the lymph nodes. Localized prostate cancer, although painful (dysuria, hematuria) is not lethal. Mortality from prostate cancer mainly occurs due to metastasis, with about 15% of patients presenting with metastatic disease, and 90% of them involve prostatic skeletal metastasis which are largely osteoblastic. Prostate cancer cells can also spread to pelvic and retroperitoneal lymph nodes, spinal cord, bladder, rectum, bone and brain (Morrissey and Vessella, 2007).

1.2.4 Diagnosis & Grading of PCa

At the early stages prostate cancer is asymptomatic making it difficult to be diagnosed. The symptoms start with the prostate enlargement which presses the urethra and causes difficulties and pain in urination. The most reported symptoms include dysuria, pollakiuria (frequent urination), and nocturia (urination during night), which also occur in patients with prostatic hypertrophy. At an advanced stage, urinary retention is common, as well as back pain, since the axis skeleton is the most usual site of metastasis (Rawla, 2019). The common diagnostic approaches are the digital rectal examination (DRE), the trans-rectal ultrasound (TRUS), the blood test PSA (Prostate Specific Antigen), and the prostate biopsy to assess histological characteristics. Each test can identify only a proportion of cancers, with higher

rates of detection when used combined. The results can also indicate tumor stage and curability (Grozescu and Popa, 2017).

Prostate Specific Antigen (PSA) blood test is the most common and less invasive PCa diagnostic tool. PSA is a serine protease normally expressed by the luminal epithelial prostatic cells and prevents semen coagulation during ejaculation. PSA is mainly secreted into the semen with small quantities found in the urine and blood. PSA blood levels are currently used for risk stratification for men with localized prostate cancer and has also been used in assessing response to treatment and disease progression. However, it is important to highlight, that PSA testing can result in a lot of false positive diagnosis, thus a tissue biopsy is usually performed for confirmation (Schatten, 2018; Welch and Black, 2010).

Once a patient has been diagnosed with a prostate tumor, the latter must be staged to determine if it has spread beyond the prostate. Staging also provides a better insight into the risk of the disease spreading further and guides the treatment options. The Gleason grading system of prostate cancer, developed by Donald Gleason, remains the strongest prognostic tool for prostate cancer (Gleason, 1966). It is based on the histological appearance of prostate cancer cells on a scale of 1 to 5, based on the extent of glandular differentiation and the pattern of growth in the stroma. Grade 1 is almost identical to a normal prostate gland, grade 3 indicates the appearance of small, almost continuous glands, while grade 5 shows the complete destruction of the glands, with only tumor cell clusters present (***Figure 8A***). Since 2014, a simplified grading nomenclature based on Gleason Score has been agreed by the International Society of Urological Pathology (ISUP), defining 5 prognostic groups (***Figure 8B***) (Epstein et al., 2016).

The clinical classification “TNM” developed by D’Amico complements the Gleason grading system (D’Amico et al., 1998). The letter T stands for tumor size; the letter N indicates whether or not lymph nodes have been invaded; the letter M indicates the presence or absence of metastases. The TNM consensus is used to assess the risk of recurrence and thus adjust the treatment. It is based on the PSA level at diagnosis, the size and extent of local tumor invasion, and the Gleason score.

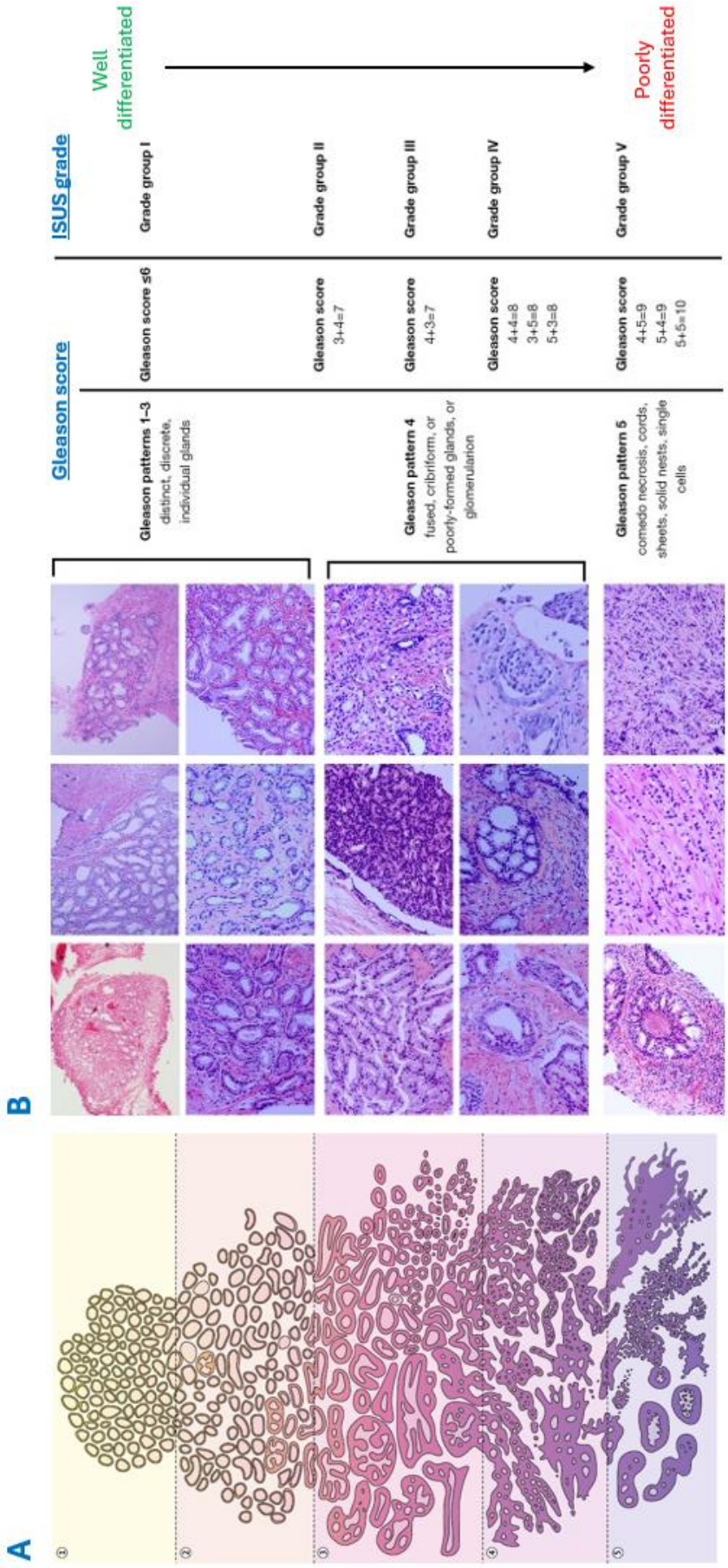

Figure 8. Gleason score and the ISUS Grade system.

A) *Schematical illustration of Gleason patterns. Figure source adapted from (Humphrey, 2004).*

B) *Typical Gleason patterns of the modern Gleason grading system & the corresponding new ISUS Grade Group system (H&E: 100×–200×). Figure source adapted from (Chen and Zhou, 2016).*

~Chapter 2~

Mouse models in prostate cancer research

Chapter 2: Mouse models in Prostate Cancer research

Understanding how certain factors promote or reduce the incidence or aggressiveness of cancer is challenging, due to limitations in using normal human fetal tissue for scientific research. To overcome these limitations, numerous studies have been carried out using immortalized prostate cancer cell lines, such as LNCaP, VCap, PC-3, DU-145 or MDA-PCa (Van Bokhoven et al., 2003). The *in vitro* preclinical studies using primary cell cultures have provided valuable insights for designing novel approaches for chemotherapy and radiotherapy. However, these cell lines derive from advanced and/or metastatic tumors, preventing us to recapitulate the different stages of human disease, and they have been obtained from patients 20-30 years ago, with their original features likely being altered through time and usage. Moreover, *in vitro* studies do not reflect their interaction with the various cellular compartments of the prostate tumor microenvironment, such as basal and neuroendocrine epithelial cells, stromal or metastatic cells, vascular and immune cells (Peehl, 2005).

In addition to *in vitro* experiments with PCa cell lines, and due to their lack of histopathologic features, human xenograft models began to serve as valuable tools to evaluate the efficacy of new therapeutics in prostate cancer. However, although they allow a rapid screening of the efficacy of new drugs, subcutaneous injection of tumor cell lines, does not reproduce an appropriate tumor microenvironment or vascularization, nor the heterogeneity of human tumors. Moreover, these models rely on immunodeficient host animals, that lack crucial modulators of tumorigenesis, thus rendering them even farer from a real-life PCa patient (Grabowska et al., 2014; Van Weerden et al., 2009).

Alternatively, the induced tumors in GEMMs stand as a powerful tool that can provide valuable resources for precision cancer prevention. One of their major advantages, is that they allow both longitudinal and molecular analyses of precancerous and cancerous lesions in defined genetic contexts and under environmentally controlled conditions, which would be exceedingly difficult to accomplish solely by studying human cancer. This has led to the continuing need for appropriate animal models, with the principle that there are satisfactory homologies to extrapolate the findings to humans. In terms of anatomy, there have been many parallel animal studies (Le Magnen et al., 2016).

Various mammalian models are currently used for prostate cancer studies, helping to significantly advance the knowledge on the prostate tumor biology. At present, mouse models, rat models and dog models are used for the preclinical prostate cancer research. The dog is most similar to humans in terms of PCa characteristics and natural PCa occurrence which is also age-related (LeRoy and Northrup, 2009). Nevertheless, the high costs, the long gestation period, and the difficulty of genetic manipulation make the dog an unrealistic experimental model. On the other hand, mice rarely develop prostate cancer spontaneously, but they can easily be manipulated to develop lesions induced by genetic engineering. Therefore, the use of GEMMs is strongly favored by the scientific community for preclinical research on prostate cancer as they offer many practical advantages over the other animal models. These include easier genetic manipulation at relatively low cost, compared to larger organisms, and a relatively short lifespan with fast breeding and time course of tumor progression.

2.1 Principle PCa mouse models

There are several molecular events involved in tumor progression that have been used to develop transgenic models for prostate cancer. The GEMMs can be divided in 3 categories based on their genetic manipulation for the PCa occurrence: gain-of-function, whole-body knockouts, conditional knockouts.

2.1.1 Gain-of-function

30 years ago, there were no GEMMs for prostate cancer. Today, a PubMed search for "prostate cancer mouse model" yields 9,854 publications and this list continues to grow. The history of the first transgenic mouse models for prostate cancer starts in 1995 with the TRAMP (Transgenic Adenocarcinoma of the Mouse Prostate) model which is the most widely used mouse model for PCa (Greenberg et al., 1995). In this model, the rat minimal probasin promoter (PB) is used to induce prostate-specific expression of the large T and small t antigens of Sivian Virus 40 (SV40 Tag). Probasin was defined as an androgen-dependent secretory product restricted to the rat dorsolateral prostate. Transcription of the probasin gene is regulated by 2 androgen response elements in the proximal promoter gene. Thus, the PB promoter was initially used to drive a tissue specific expression of various genes for the study of prostate cancer. The SV40 Tag on the other hand, is a viral oncogene encoded by the SV40 early sequence, known to inactivate important tumor suppressor proteins (e.g. p53 and Rb). TRAMP mice exhibit low-grade prostatic intraepithelial neoplasia (LGPIN) as early as 4–6 weeks of age, advancing to high-grade PIN (HGPIN) between 6 and 10 weeks, and eventually developing well-differentiated neuroendocrine carcinoma between 10 and 16 weeks in the dorsolateral prostate. However, this progression is not observed in the ventral or anterior prostate lobes. The tumor eventually metastasizes to distal sites (peri-aortic lymph nodes, lungs, and occasionally to the kidney) and becomes castration resistant reflecting human PCa progression.

In order to enhance transgene expression, the LPB-Tag/LADY transgenic mouse model was developed, expressing only the large T antigen, regulated by the large probasin promoter (LPB; 11.5 kb/+28 bp). This model aimed at optimizing the expression of the transgene (Kasper et al., 1998). In the LADY model, PCa started as small foci of hyperplasia, followed by proliferative overgrowth, dysplasia, HGPIN, and finally neuroendocrine prostate carcinoma. However, while these mice show local invasion, only one of seven LPB-Tag mouse lines (12T-10) develops metastases in the lymph nodes, liver and lung at 6 months of age (Masumori et al., 2001).

While the LADY and TRAMP models offered several advantages for prostate cancer research, such as their reproducibility and high penetrant progression to carcinoma, they also had significant drawbacks. First, tumorigenesis is induced by a viral protein that is not involved in human prostate carcinogenesis (Grabowska et al., 2014). An additional notable limitation is the rapid progression observed in these models, which does not fully mirror the comparatively slower progression typically observed in human prostate cancer. Consequently, the

development of large primary tumors often necessitates euthanizing mice due to concerns about their quality of life before metastatic progression can be adequately assessed. Lastly and importantly, both PCa tumor models exhibit a neuroendocrine (NE) origin of the carcinoma. As previously mentioned, NE tumors are very rare in human PCa patients (only ~1% of patients) (Masumori et al., 2001). Thus, neither the TRAMP nor the LADY models of prostate cancer accurately recapitulate the natural history of prostatic adenocarcinoma in the early stages but may be valuable models for the rarer neuroendocrine carcinoma of the prostate.

Additional mouse models were inspired by the frequent overexpression or amplification of the transcription factor c-Myc in prostate cancer. For example, researchers have generated several transgenic mouse lines, including C3(1)-c-Myc, ARR2PB-Myc, probasin-Lo-Myc, and Hi-Myc, to overexpress c-Myc (Ellwood-Yen et al., 2003; Zhang et al., 2000). C3(1)-c-Myc transgenic mice develop LGPINs that do not progress to adenocarcinoma. In contrast, the Hi-Myc mice develop PINs as early as 2 weeks and adenocarcinoma tumors are observed in all mice by 6 months of age. The other models develop PINs that progress to adenocarcinoma rather than neuroendocrine tumors, but do not metastasize. Additionally, transgenic mouse models have been created, overexpressing growth factors such as FGFR1, referred to as JOCK1, which is implicated in prostate cancer initiation or progression (Freeman et al., 2003). This model exhibits epithelial hyperplasia, then PIN and eventually progresses to adenocarcinoma. The PB-FGFR1 model represents a good model for early stages of PCa but fails to recapitulate more aggressive aspects of the disease. In general, the phenotypes of these mice are less aggressive than those of the SV40 models, but have the important advantage that they tend not to develop neuroendocrine tumors (Irshad and Abate-Shen, 2013).

2.1.2 Whole-body knockout

Traditional knockout models, also known as whole-body knockout models, offer another approach to investigate the roles of key genes in prostate cancer (PCa). In these models, tumor suppressor genes, or critical regions of DNA necessary for their function, are deleted. Initially, these models were instrumental in identifying genes that are embryonically lethal.

The PTEN$^{-/-}$ mouse model was developed to study PCa, as *Pten* gene is strongly correlated with primary and advanced PCa patients. Of note, it was from the construction of this whole-body knockout PTEN$^{-/-}$ mice, that PTEN was found to be essential for early embryonic development, as no homozygous knockouts were viable. In contrast, heterozygous PTEN$^{+/-}$ mice survived to maturity, and developed a broad range of neoplastic lesions, including prostatic intraepithelial neoplasia (PIN), lymphomas, dysplastic intestinal polyps, and endometrial complex atypical hyperplasia (Cristofano et al., 1998; Podsypanina et al., 1999). In the same line, since Nkx3.1 plays a critical role in urogenital development and function and is often lost in the early stages of PCa in humans, the Nkx3.1$^{-/-}$ knockout mouse was developed. However, *Nkx3.1* depletion alone was not sufficient to induce PCa or HGPIN in mice (Bhatia-Gaur et al., 1999; Kim et al., 2002). On the contrary, mice that were simultaneously heterozygous KO for the *Nkx3.1* and *Pten* genes (Nkx3.1$^{+/-}$;PTEN$^{+/-}$) showed extensive hyperproliferative multifocal lesions, indicating the presence of HGPIN and adenocarcinoma.

In addition, lymph node metastasis and castration resistance were later reported in this double knockout (Abate-Shen et al., 2003).

2.1.3 Conditional knockout with spatial specificity

Due to the health problems afflicting the heterozygous $PTEN^{+/-}$ mice occurring in many organs and the embryonic lethality of homozygous $PTEN^{-/-}$ KO mice, subsequent studies have focused on organ-specific deletion of *Pten* gene. This became feasible thanks to the discovery of the CRE/LoxP system applied in genetic engineering (Sternberg and Hamilton, 1981). Its inception traces back over 40 years ago when Nat L. Sternberg unearthed the Cyclization Recombinase "Cre", along with its distinct crossover locus of X-over of P1 "LoxP", during investigations into the preservation of bacteriophage P1 as a stable plasmid. Cre-mediated recombination aid in both cyclizing the DNA of invading phages and resolving multimers of prophage formed through generalized recombination. The principle of this system in GEMMs is based on the function of the CRE recombinase, which targets and excises the LoxP sequences introduced in the exon of the gene that needs to be depleted. The revolution of this system comes with the basis that the CRE recombinase is expressed only in the tissue of interest under the control of a cell-specific promoter. Therefore, the deletion of the gene of interest is tissue specific.

For a prostate specific depletion, the probasin promoter was initially used. In the Pb-Cre lines, the Cre expression was higher in the ventral lobe, but excision was occurring in all lobes. Moreover, Cre was found to be expressed mainly by the basal and stromal cells of the prostate, rather than the epithelial ones that are the starting point of human PCa, and it was also ectopically expressed at low levels in the bladder and seminal vesicles (Maddison et al., 2000; Wu et al., 2001). Interestingly, the PB-CRE/Trp53 ($Trp53pc^{-/-}$) mouse line, in which p53 is invalidated in the prostate driven by the PB promoter, does not develop prostate cancer, but in contrast, the double depletion of *Pten* and *p53* in the PB-CRE4/PTEN/Trp53 ($PTEN/Trp53pc^{-/-}$) mouse line leads to the formation of HGPIN and invasive adenocarcinoma faster than the loss of PTEN alone, indicating that p53 loss accelerates the tumor progression initiated by PTEN loss. These mice however, do not develop metastases (Chen et al., 2005). Finally, mice in which Pten, p53 and Smad4 are invalidated in the prostate (PB-CRE4), develop aggressive prostate tumors, with some of them (12%) progressing to bone metastases (Ding et al., 2012). To explore the function of the androgen receptor (AR) in prostatic epithelial cells during cancer development, the AR was depleted in the prostatic epithelium of PB-CRE4/$PTEN^{L2/L2}$ mice. Proliferation of PTEN/AR-null cancer cells was enhanced by inhibition of AKT, suggesting an interplay between the AR and PI3K signaling pathways (Mulholland et al., 2011). Similarly, the ARR2PBi-Cre mouse line was constructed, expressing CRE under the control of the ARR2PB promoter/enhancer regions (Jin et al., 2003). While this mouse line exhibited efficient CRE recombination only in the epithelial cells, like human PCa, it was still ectopically expressed in seminal vesicles and ductus deference organs.

To resolve these issues of ectopic expression and cell type specificity, the 6-kb fragment of the human PSA promoter was used (Cleutjens et al., 1997). Interestingly, the generated transgenic PSA-Cre mouse lines show restricted recombination only in the luminal epithelial cells of the mature prostate, with no ectopic expression observed, compared to

probasin-based transgenic Cre lines that is expressed mainly the basal and stromal prostatic cells (Abdulkadir et al., 2002; Ma et al., 2005). The luminal specific depletion of the gene of interest, thus brings the PSA-models one step closer to human PCa, which also has a luminal origin. The success of the PSA-Cre mice led to the generation of numerous mouse lines in the scope of studying the effects of loss of function of various proteins specifically in the prostate, including PTEN, p53, mTOR and Nkx3.1. Notably, the PSA-CRE/Pten mouse line develops HGPINs that progress to invasive adenocarcinomas with lymph node metastasis (Wang et al., 2003).

Despite the fact that most models use targeted gene invalidation to induce prostate cancer in mice, the onset of prostatic intraepithelial neoplasia (PIN) occurs in young animals shortly after birth, while the prostate is still immature, and progresses rapidly. This contrasts with human prostate cancer, which typically occurs later in life (>65 years old men) and progresses over many years, often decades. Consequently, a major limitation of Cre technology is that crucial genes are invalidated in prostate cells before the organ is fully mature. Therefore, for an accurate phenocopy of sporadic prostate cancer, mutations should be induced in a restricted subset of prostate cells following puberty.

2.1.4 Conditional knockout with spatial & temporal specificity

To overcome the lack of temporal control in the GEMMs, the fusion of Cre recombinase with the binding domains of mutated nuclear receptors was developed (Metzger, 1999). The so-called ligand-controlled recombinases have revolutionized the use of mouse models in oncology, bringing them one step closer to the human disease characteristics. The most widely utilized chimeric recombinase for introducing spatio-temporally controlled targeted somatic mutations in mice is the Cre-ER^{T2} recombinase. This recombinase is a fusion protein comprising CRE and a mutated human estrogen receptor (ER). Its activity is selectively induced by the synthetic ligand Tamoxifen, but not by its natural ligand, estradiol. Therefore, the fusion protein translocates to the nucleus only after treatment of these transgenic mice with tamoxifen and leads to the excision of the chromosomally integrated gene flanked by loxP sites in tissues where the promoter drives the Cre-ER^{T2} expression. No excision occurs in untreated animals (Metzger and Chambon, 2001). Several prostate cancer models utilize Cre-ER^{T2} technology, with various promoters driving CRE expression, as listed in ***Table 1***. This includes the PSA-CreER^{T2} model used in my PhD thesis.

While ARR2PB-CreER^{T2} mice induce high efficiency recombination in luminal cells across all prostate lobes, PSA-Cre-ER^{T2} mice exhibit high recombination efficiency in luminal cells specifically in the DLP and VP lobes (>up to 80%) and lower recombination efficiency in the AP lobes (10–60%). This lobe specificity observed in PSA-Cre-ER^{T2} mice, makes them more representative of human PCa features, as PCa predominantly initiates in the DLP lobes which correspond to the peripheral zone in humans, where most adenocarcinomas occur.

Table 1. *Mouse lines expressing tamoxifen dependent Cre recombinases in prostatic epithelial cells. Adapted from (Parisotto and Metzger, 2013).*

Mouse line	Chimeric Cre recombinase	Transcriptional regulatory elements	Cre recombinase activity	References
PSA-Cre-ER^{T2}	Cre-ER^{T2}	PSA (6 kb)	Luminal cells: DLP, VP > AP	(Ratnacaram et al., 2008)
ARR$_2$PB-Cre-ER^{T2}	Cre-ER^{T2}	Probasin ARR$_2$PB	Luminal cells: AP, DLP, VP	(Luchman et al., 2008)
Nkx3.1-Cre-ER^{T2}	Cre-ER^{T2}	Nkx3.1 (KI)	Luminal cells & 10% basal cells	(Wang et al., 2009)

2.1.4.1 Mouse model PSA-CreER^{T2}/PTEN$^{L2/L2}$

To investigate the effects of PTEN loss in luminal epithelial cells of the prostate of adult mice, the team of D. Metzger generated the PSA-CreER^{T2}/PTEN$^{L2/L2}$ mouse model. In this model, ablation of the exons 4 and 5 of *Pten* was triggered by administration of Tamoxifen (Tam) to adult PSA-Cre-ER^{T2} mice with PTEN L2 alleles (***Figure 9A***) as described in (Ratnacaram et al., 2008).

While no Cre recombinase activity was observed in adult PSA-Cre-ER^{T2}/PTEN$^{L2/L2}$ mice in the absence of Tam treatment, administration of Tam (1mg/day for 5 days) induced Cre-mediated recombination selectively in prostatic epithelial cells with the highest efficiency in the DLP lobes. Subsequently, all mutant mice, called PTEN$^{(i)pe-/-}$, developed prostatic intraepithelial neoplasia (PIN) in DLP lobes within 2–3 months post Tamoxifen-induced Cre-ERT2-mediated bi-allelic *Pten* ablation (mouse aged 4-5 months), progressing to adenocarcinoma within 8–10 months (mouse aged 10-12 months) in the dorso-lateral lobes exclusively. Notably, no distant metastases were observed up to 20 months after PTEN ablation (mouse aged 22 months) (***Figure 9B***) (Ratnacaram et al., 2008).

The absence of PTEN protein expression in the PINs of these mice indicates that loss of PTEN function favors uncontrolled cell proliferation. Thus, Cre-ERT2-mediated ablation of *Pten* in luminal cells of adult prostate DLP lobes closely mimics early events in human prostate cancer development. This model is useful both for exploring the cellular mechanisms underlying PTEN loss in prostate cancer development and progression, and for developing and validating preventive and therapeutic approaches in preclinical settings as the tumor kinetics are highly reproducible.

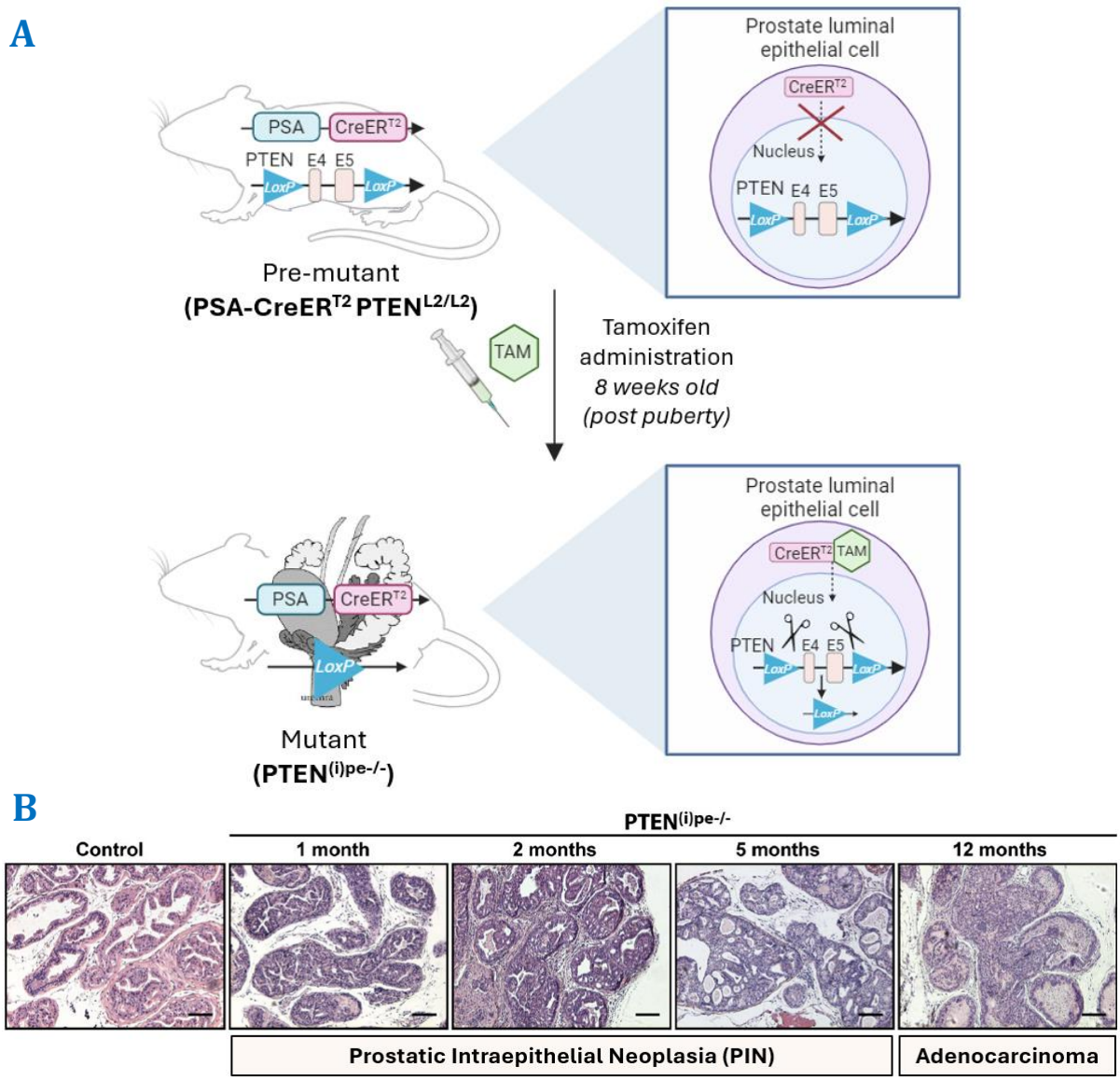

Figure 9. A) Generation of PTEN$^{(i)pe-/-}$ mice. *The pre-mutant PSA-CreER^{T2}/PTEN$^{L2/L2}$ mice bear the Pten alleles flanked by LoxP sites in the exon 4 & 5 and the Tamoxifen-dependent CreER^{T2} recombinase under the control of the PSA promoter. Following tamoxifen injection after puberty, the Pten gene is electively ablated in prostatic luminal epithelial cells in the mutant PTEN$^{(i)pe-/-}$ mice.* ***B) Histological analysis of prostate from PTEN$^{(i)pe-/-}$ mice following staining with H/E.*** *Timepoints shown from 1 to 12 months after treatment with Tamoxifen (Tam) at the age of 8 weeks. Adapted figure from (Parisotto et al., 2018).*

Interestingly, the team of D. Metzger observed that *Pten* ablation stimulates the proliferation of prostatic epithelial cells to form PINs within 1 month, followed by a progressive growth arrest with characteristics of cell senescence (Parisotto et al., 2018a). Oncogene-induced senescence (OIS), acts as a tumor-suppressive mechanism by permanently halting cell proliferation and promoting immune surveillance of premalignant lesions, thus providing a barrier against cell transformation (Courtois-Cox et al., 2008). Indeed, senescent cells are associated with cell cycle arrest and inhibition of cell proliferation. Hence, inducing cellular senescence of cancer cells is considered a potentially effective strategy against cancer (Calcinotto et al., 2019; Xiao et al., 2023).

2.1.4.2 Mouse model PSA-CreER^{T2}/PTEN$^{L2/L2}$/P53$^{L2/L2}$

Between 1 and 3 months following Tam injection, prostate luminal cells of PTEN$^{(i)pe-/-}$ exhibited high proliferation rate to generate PINs, then became senescent and harbored stabilized P53 (Parisotto et al., 2018a). Administration of Tamoxifen to 8-week-old PSA-CreER^{T2} mice bearing LoxP-flanked PTEN and p53 alleles allows to ablate both PTEN and p53 in prostatic luminal epithelial cells from the DLP lobes at adulthood. Comparison of the tumor kinetics of the two mouse models showed that PIN lesions in the DLP were similar in PTEN/p53$^{(i)pe-/-}$ and PTEN$^{(i)pe-/-}$ mice at 1 and 2 months, but were more severe in PTEN/p53$^{(i)pe-/-}$ mice than in PTEN$^{(i)pe-/-}$ mice at 5 and 6 months, sometimes resulting in loss of prostate epithelium architecture (***Figure 10***). This indicated that p53 ablation does not affect the early stimulation of PTEN-null prostatic luminal epithelial cell proliferation and PIN formation, but does impair their subsequent growth arrest (Parisotto et al., 2018a). Interestingly, unlike PTEN$^{(i)pe-/-}$ mice, the PTEN/p53$^{(i)pe-/-}$ mice developed metastasis located in the bones and the liver (D. Metzger, personal communication).

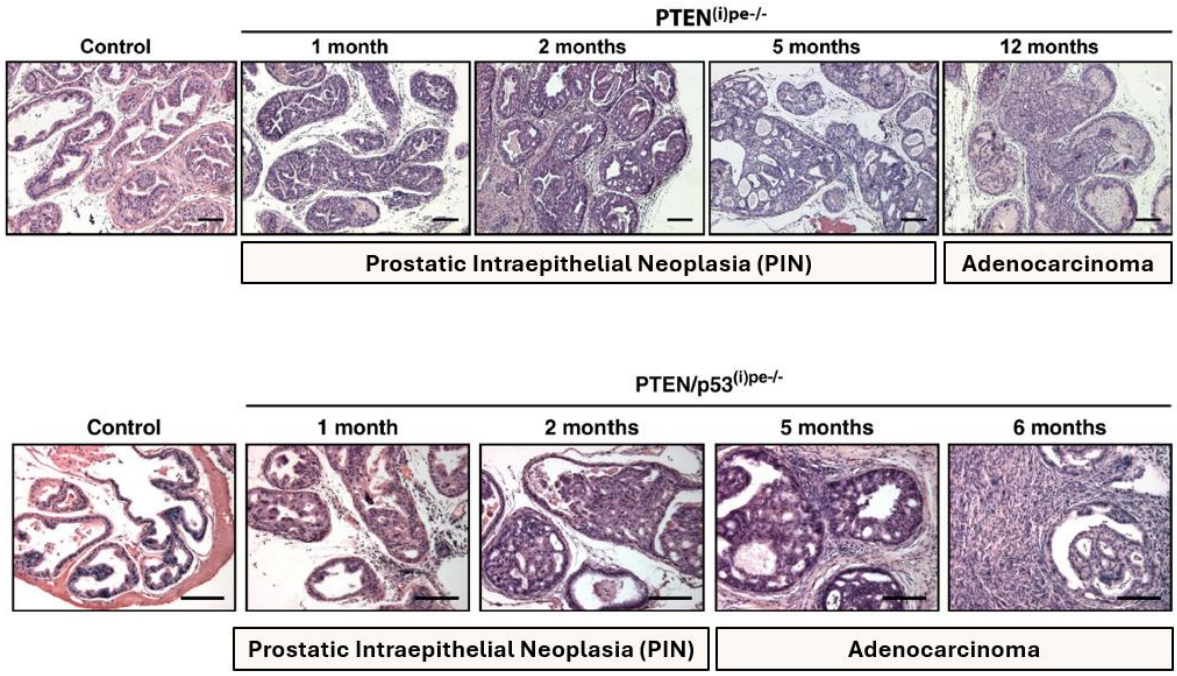

Figure 10. Comparative prostate tumor kinetics from PTEN$^{(i)pe-/-}$ (top) and PTEN/p53$^{(i)pe-/-}$ (bottom) mice following treatment with Tamoxifen at the age of 8 weeks. *Representative views of DLP sections stained with H/E, of PTEN $^{(i)pe-/-}$ and control mice sacrificed at 1, 2, 5 and 12 mo after gene ablation and of DLP sections of PTEN/p53$^{(i)pe-/-}$ and control mice sacrificed at 1, 2, and 5 months after gene ablation. Adapted figure from (Parisotto et al., 2018).*

~Chapter 3~

Immunity in healthy prostate & prostate cancer

Chapter 3: Immunity in healthy prostate and prostate cancer

3.1 Interplay of innate and adaptive immunity

The immune system is the body's defense against infections and diseases and consist of two interconnected branches: the innate immune system and the adaptive immune system (Chaplin, 2010). These systems comprise different cell types, each with unique functions, that work collaboratively to combat diseases and maintain overall health. The immune responses are orchestrated by leukocytes, that arise from progenitor cells in the bone marrow, a process called hematopoiesis. More precisely, pluripotent hematopoietic stem cells (HSCs) reside as rare cells in the bone marrow of adult mammals and differentiate into progenitors that become progressively restricted to multiple or single lineages. HSCs are defined by their ability to restore the entire blood system of a patient receiving a bone marrow transplant. HSCs give rise to the common lymphoid progenitor (CLP) and common myeloid progenitor (CMP) cells, which further differentiate into a variety of cell types (Orkin, 2000). The myeloid lineage consists primarily of cells belonging to the innate immune system, while the lymphoid lineages are essential components of the adaptive immune system (***Figure 11***).

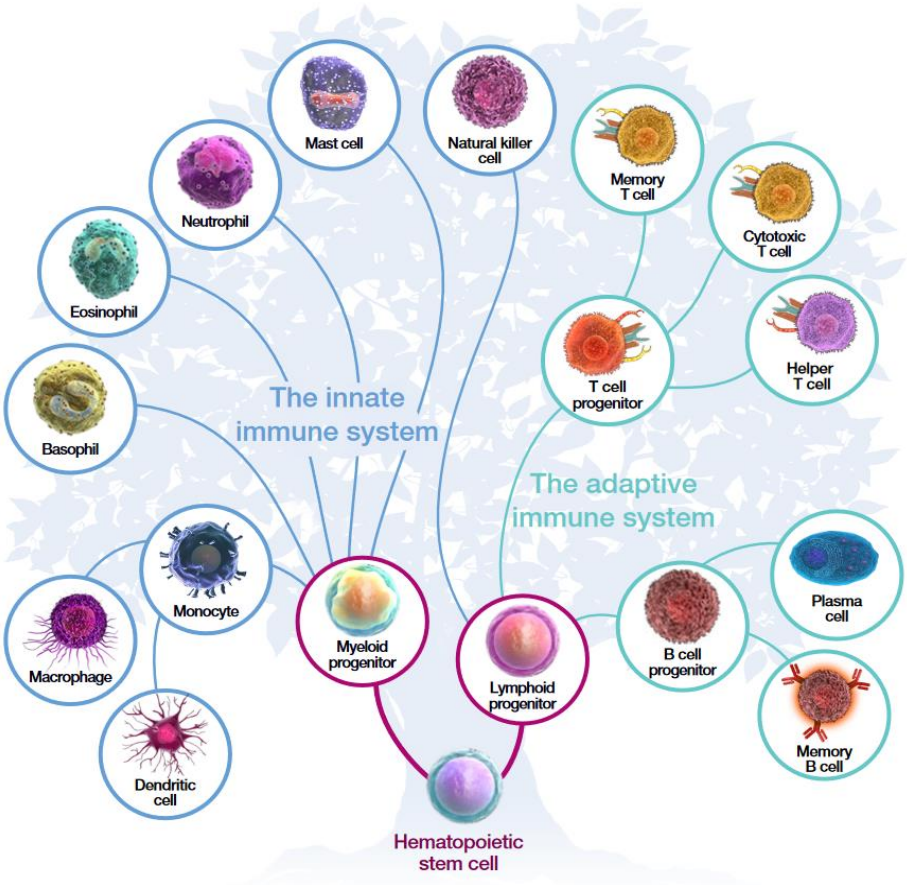

Figure 11. Cells of the innate and adaptive immune system. *Source figure from (Peprotech Inc, 2021, n.d.).*

Most immune cells are found in the bone marrow and the lymphatic system, and account for 40% and 39% of all immune cells, respectively. Immune cells are also found in the blood and in all tissues and organs. Interestingly, a recent quantitative meta-analysis study revealed that the average person's healthy immune system comprises approximately 1.8 trillion immune cells, weighing a total of about 1.2 kg. Lymphocytes constitute 40% of the total immune cells and 15% of the total immune mass. Neutrophils contribute to similar proportions. Macrophages make up only about 10% of the total immune cells, but their large size makes them responsible for nearly 50% of the total immune cell mass (Sender et al., 2023) (***Figure 12***).

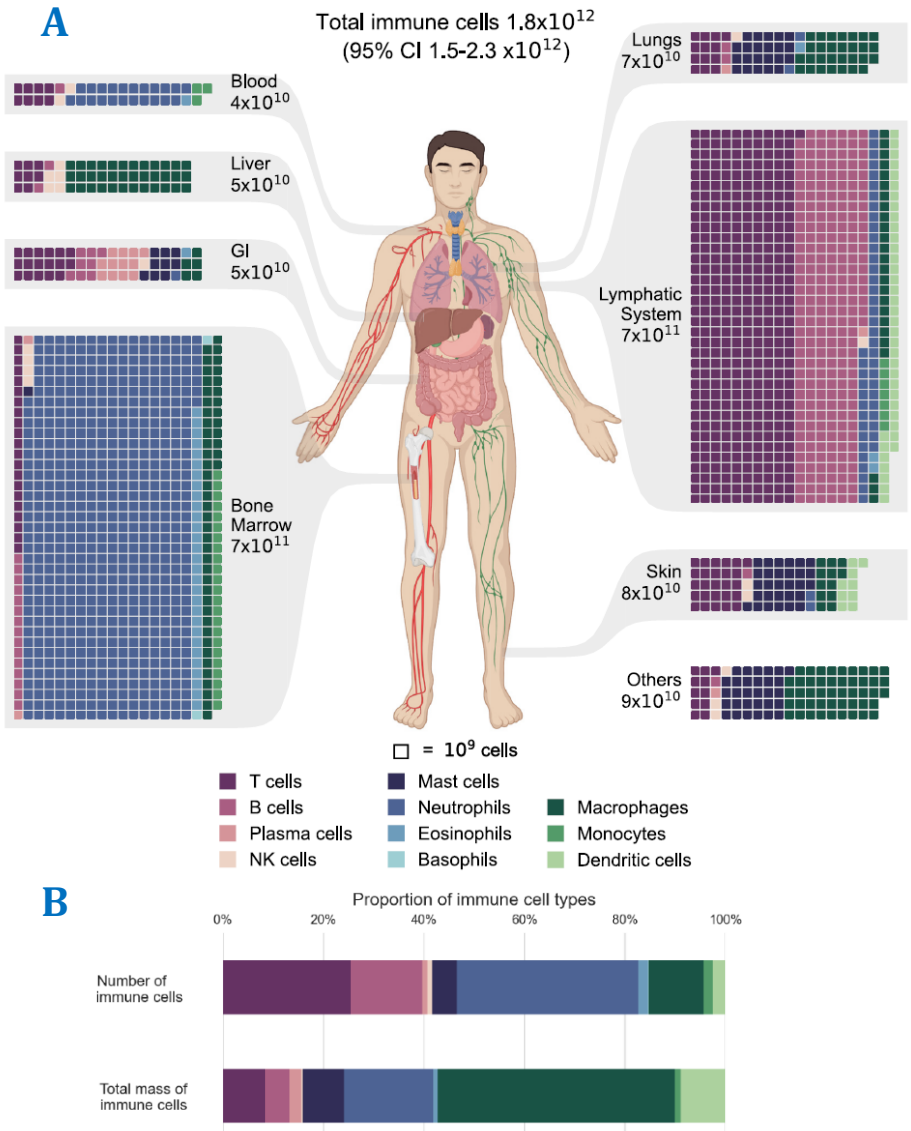

Figure 12. A. The distribution of immune cells in the human body. *Estimates of immune cell populations by cell type and tissue grouped by primary tissues and systems. The tissues are displayed via a chart of the human body. A waffle chart depicts the distribution of immune cells in each tissue, with each square representing a population of 10^9 cells. To facilitate the presentation, the populations were rounded to multiples of 10^9. The total population of each tissue is shown with one significant digit. Throughout all the figures, cell types are color-coded for ease of reference. GI = gastrointestinal tract. Other tissues and organs include the brain, heart, adipose tissue, skeletal muscles, kidneys, etc.* ***B. The proportion of immune cell types in the body by number and mass.*** *Source figure adapted from (Sender et al., 2023).*

Innate immunity corresponds to the first line of host defense against infection and represents a universal and ancient mechanism that augments protection of anatomical and physiological barriers. It responds rapidly (within few hours) in a non-specific way, relying on the recognition of conserved microbial components shared by large groups of pathogens (bacteria, viruses, fungi). These include the pathogen- or damage-associated molecular patterns (PAMPs or DAMPs). Subsequent binding of these molecular structures to pattern recognition receptors (PRRs), such as Toll- and NOD-like receptors (TLRs and NLRs), enables the immune system to distinguish the infectious non-self antigens from the non-infectious self-antigens and trigger intracellular signaling cascades that activate classical innate immune responses, such as phagocytosis and cytokine production (Janeway and Medzhitov, 2002). Innate immune cells include scavenger cells, such as macrophages and dendritic cells (DC), as well as effector cells, such as neutrophils, eosinophils, basophils, mast cells and natural killer cells (NK). The latter, although they have a lymphoid origin, are part of the innate immunity and belong to a newly identified family called innate lymphoid cells (ILCs). In addition to all these cellular components, innate immunity also includes a large arsenal of humoral elements such as complement proteins, LPS binding protein, complement-reactive protein and other acute phase reactants, anti-microbial peptides and mannose-binding lectin (Turvey and Broide, 2010). Innate elements play a dual role: not only are they crucial for detecting and eliminating harmful foreign antigens, but they are also vital for maintaining normal tissue homeostasis. This includes the recognition and repair of damaged tissues, as well as the elimination of senescent or apoptotic cells. Modern genome sequencing has revealed that many of these defense systems are conserved across animal phyla, reflecting not only their remarkable efficacy but also their versatility (Litman and Cooper, 2007).

On the other hand, the adaptive immunity represents the second line of defense. Although delayed as compared to innate immunity, it is more sophisticated as it relies on the engagement of pathogen-specific receptors. The term adaptive is applied because lymphocytes rapidly adapt to specific situations (e.g., to a specific type of microbial infection) and generate specialized cells, cytokines, antibodies, and long-lasting immune memory. In contrast to the limited variability of innate receptors, the adaptive immune system possesses an incredibly diverse repertoire of receptors, generated randomly by clonal somatic gene-segment rearrangement, and can recognize any possible antigen. Therefore, after the first encounter with a pathogen, it takes up to five days for clonal expansion of these rare antigen-specific T and B cells to occur, bearing the specific T cell receptor (TCR) or B cell receptor (BCR; immunoglobulin; Ig) respectively. This expansion is necessary for the adaptive immune response to become sufficiently robust to clear the pathogen (Chaplin, 2010). The humoral adaptive immune elements include the immunoglobulins secreted by B lymphocytes, known as antibodies. A hallmark of the adaptive immune response is its life-long memory, in which antigen-specific memory lymphocytes are generated to enhance and accelerate the response upon a second exposure to the same antigen. It is worth mentioning that the innate immune system also exhibits memory traits, based on epigenetic reprogramming of innate cells, lasting

up to one year, a property referred to as 'trained immunity' (Dagenais et al., 2023; Netea et al., 2020). The innate immune system activates the adaptive immune system, primarily through antigen presenting dendritic cells (DCs). Although the innate and adaptive immune responses differ fundamentally in their mechanisms of action, their synergy is essential for a fully effective immune response.

3.2 Role of immunity in cancer pathogenesis

Whenever an abnormal cell growth initiates, progressing toward cancer development, the body's immune system is committed to its elimination. The concept of the immune system controlling carcinogenesis dates back to 1909, proposed by Paul Ehrlich. This initial hypothesis, suggesting the involvement of the immune system in the recognition and elimination of malignant neoplastic cells, was later introduced as "cancer immunosurveillance" by Frank Macfarlane Burnet and Thomas Lewis (Burnet, 1970; Thomas, 1982). The interaction between tumors and immunity hinges on a delicate balance that determines whether a tumor progresses or is eliminated, known as immunoediting.

Cancer immunoediting is a dynamic process comprising three phases: elimination, equilibrium, and escape (Lasek, 2022). Elimination represents the classical concept of cancer immunosurveillance, where the innate and adaptive immune arms cooperate to identify and destroy the transformed cells. Equilibrium is the period of immune-mediated latency following incomplete tumor destruction during the elimination phase. Escape refers to the final outgrowth of tumors that evade the immunological restraints of the equilibrium phase, corresponding to the clinical manifestation of tumors, and is highlighted as one of the main hallmarks of cancer (Hanahan and Weinberg, 2011).

Various immune cells and mechanisms interact with a tumor in distinct ways, often exhibiting ambivalence towards tumor progression or elimination. The innate immune compartment plays a crucial role in regulating T cell immunosurveillance in cancer. This multistep process, called the cancer-immunity cycle, begins when DCs as professional antigen presenting cells (APCs), uptake neoantigens derived from apoptotic and necroptotic tumor cells, and cross-present them to naïve T cells (Chang and Beatty, 2020). Subsequently the naïve T cells are primed and activated into antigen-specific T cells, infiltrate the tumor microenvironment and eliminate tumor cells (***Figure 13***). However, any of these steps can fail, leading to tumor escape. Tumor cells can evade immune cells by a plethora of mechanisms, including inefficient presentation of tumor neoantigens by DCs, lack of costimulatory signaling, reduced expression of major histocompatibility complex (MHC) molecules on neoplastic cells, upregulation of BCL-2 and other anti-apoptotic molecules leading to resistance to apoptosis, and suppression of T cell mediated cytotoxicity through PDL-1 expression on neoplastic cells and tumor-infiltrating cells (Jhunjhunwala et al., 2021; Sun et al., 2018).

Thus, while the immune system initially limits the growth of heterogeneous tumors consisting of unstable and rapidly mutating cells, it may reach an asymptotic point which follows the Darwinian evolution theory of the fittest: although many of the original tumor cells

are eliminated, new variants emerge with additional mutations that enhance their resistance to immune attack. Ultimately, the ongoing interaction between immunity and cancer during the equilibrium phase leads to new populations of tumor cells that have been selected for survival in a host with a competent immune system. Nevertheless, it is worth mentioning that in some cases, the immune system effectively eliminates the tumor. Therefore, during the latent phase of equilibrium, a tumor may undergo one of the three possible outcomes: (a) eventual elimination by the immune system, or (b) sustained equilibrium maintained by the cellular and molecular mechanisms of immunity, or (c) evasion of immune surveillance leading to progression to the final escape phase of immunoediting. In particular, the first two phases of the cancer immunoediting process present potential objectives for immunotherapy: either eliminating the tumor or achieving long-term control of cancer in equilibrium (Dunn et al., 2004).

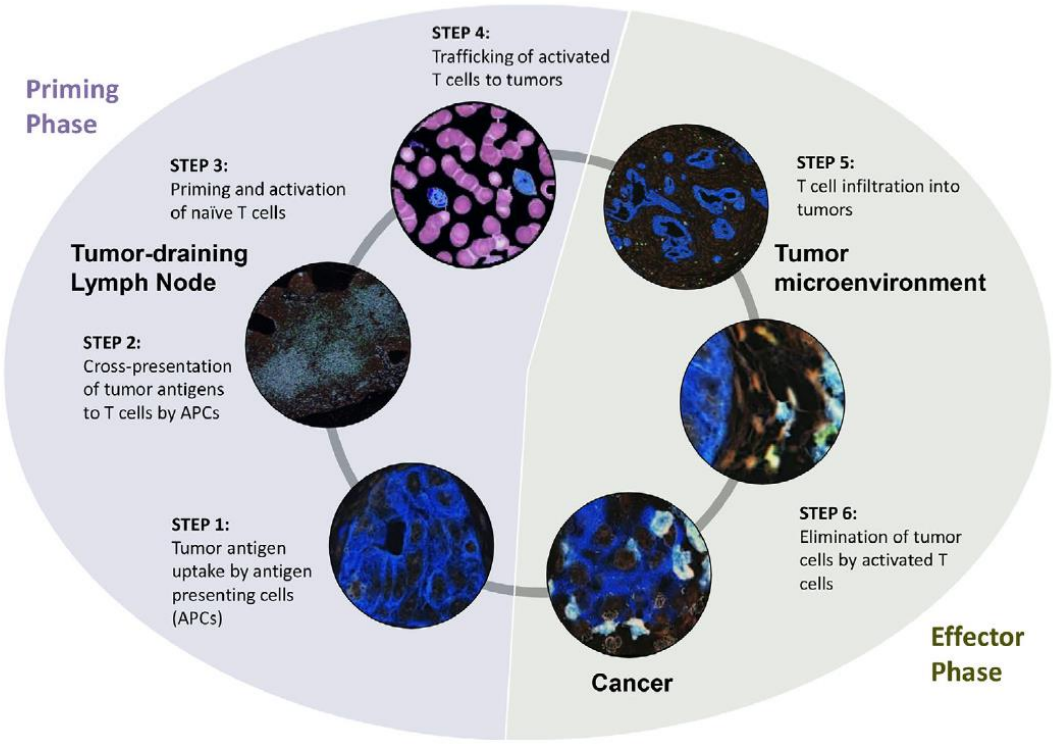

Figure 13. Adaptive immunity in cancer is defined by priming and effector phases. *T cell immunosurveillance in cancer is dependent on steps 1–4 that support T cell priming and activation (priming phase) and steps 5–6 which involve T cell effector activity (effector phase). Source figure from (Chang and Beatty, 2020).*

3.3 A focus on Neutrophils in health & cancer

Granulocytes, characterized by cytoplasmic granules and polymorphonuclear nuclei, include eosinophils, basophils, mast cells and neutrophils. Eosinophils are primarily involved in the defense against parasites, as their numbers increase during parasitic infections. The

production of eosinophils from the bone marrow and their survival in peripheral tissues are promoted by the cytokine IL-5, which makes them prominent cells in most allergic reactions. Basophils and mast cells are morphologically similar cells that represent distinct lineages. They are characterized by the expression of the surface marker FcεRI, and are key mediators of hypersensitivity responses to parasites by releasing histamine. Importantly, mast cells and, more prominently, basophils can release substantial amounts of IL-4, suggesting that they can play important roles in triggering allergic immune responses. Neutrophils dominate the innate immune response as they comprise about 60%-70% of all leukocytes. They are usually the first immune cells to be recruited to sites of infection and respond rapidly to inflammatory cues from infectious or damaged areas outside the blood system. In the following sections I will focus on the heterogeneity and function of neutrophils and their emerging role as key players in various cancer, including PCa.

3.3.1 Properties & functions

Neutrophils are produced during hematopoiesis in the bone marrow, with a production rate of approximately $1*10^{11}$ cells per day for an adult human, which can increase up to 10^{12} during infection (Borregaard, 2010). Neutrophil homeostasis is maintained by a balance of neutrophil production, release from the bone marrow, and clearance from the blood stream. Under physiological conditions less than 2% of the total body of mature neutrophils is in the bloodstream. The retention and release of neutrophils from the bone marrow is tightly regulated by a balance between CXCR4, which favors retention, and CXCR2, which favors release (Eash et al., 2010). When neutrophils need to be mobilized, ligands for CXCR2, including CXCL1, CXCL2, CXCL5 and CXCL8 (in humans only) are expressed outside the bone marrow. Finally, upregulation of the cell surface chemokine receptor CXCR4 allows 'aged' neutrophils to return to the bone marrow, liver, and spleen via the chemokine CXCL12/SDF-1α (Martin et al., 2003).

Neutrophils have the shortest lifespan of body cells, typically surviving in the circulation for an average of 7 hours in healthy humans and 8-10 hours in healthy mice (Hidalgo et al., 2019). Although their name is derived from their preferential uptake of pH neutral dyes, their role in inflammation and pathology is anything but neutral. Neutrophils are essential phagocytes and crucial for fighting bacterial and fungal infections. They eliminate pathogens through three main mechanisms: (i) fusion with lysosomes within the phagosome, releasing cytotoxic proteins, peptides, and enzymes into the phagolysosome (Cowland and Borregaard, 2016), (ii) activation of a membrane-bound NADPH-oxidase, leading to the production of superoxide anions (O2–) that are subsequently converted into hydrogen peroxide (H2O2) and other reactive oxygen species (ROS) (Roos et al., 2003) and (iii) extracellular formation of web-like chromatin structures known as neutrophil extracellular traps (NETs) that degrade virulence factors and kill bacteria (Brinkmann et al., 2004).

The first two mechanisms have been described long ago and occur both within the phagolysosome and extracellularly where the granules fuse with the plasma membrane, allowing degranulation and activating NADPH oxidase. The importance of these processes is

evident in severe immunodeficiencies observed in humans, such as chronic granulomatous disease (CGD), which is characterized by genetic defects in the multicomponent NADPH oxidase system, and Chédiak–Higashi syndrome, in which there is a deficiency of granules. The third mechanism, known as NETosis, was reported 20 years ago, and consists of neutrophils trapping microorganisms in webs of DNA, neutralizing and killing them to prevent their dissemination. NET formation is triggered by innate immune receptors, that activate downstream intracellular mediators, including reactive oxygen species (ROS) generated by NADPH oxidase or mitochondria. These ROS, in turn, activate enzymes such as myeloperoxidase (MPO), neutrophil elastase (NE), and protein-arginine deaminase type 4 (PAD4), facilitating chromatin decondensation (Papayannopoulos, 2018).

3.3.2 Implication in cancer

Neutrophils are involved in the development of numerous inflammatory conditions. These range from acute lung injury or sepsis to chronic inflammation observed in diseases such as chronic obstructive pulmonary disease (COPD) and various types of inflammatory arthritis as well as cancer. Individuals with neutrophil deficiency are highly susceptible to microbial infections. Conversely, excessive activation and improper recruitment of neutrophils can lead to severe inflammation and tissue damage, making them a "double-edged sword" in immune responses.

The role of neutrophils in cancer has often been overlooked compared to other immune cells such as macrophages. However, recent studies are increasingly focusing on the role of neutrophils in cancer. One reason that these cells have received less attention in the past compared to other immune cells may be their short lifespan, which was thought to be insufficient to influence tumor progression. However, this view is being re-considered, as studies suggest that tumor associated neutrophils have prolonged lifespan and can survive for several days in tumorous tissue, suggesting that the tumor microenvironment facilitates their survival (Mittmann et al., 2021).

The origin of neutrophils in cancers where significant numbers of neutrophils have been observed, has also been investigated. Some studies have shown that emergency granulopoiesis takes place over steady state granulopoiesis to rapidly increase neutrophil production. In tumor-bearing mice and humans with pancreatic or colon cancer, and likely other tumor types, the spleen serves as an alternative site for neutrophil production (Cortez-Retamozo et al., 2012). Additional studies using nuclear staining of circulating neutrophils from mammary and lung tumor models have shown the existence of ring like, banded and segmented nuclei (Sagiv et al., 2015). This suggests that differentiation at inflammatory sites or in tumors may prime immature neutrophils for functions they would not ordinarily perform. In our study we examined the phenotype and morphology of neutrophils to determine whether neutrophils in the $PTEN^{(i)-/-}$-induced murine prostate cancer model have an immature or mature profile.

3.3.3 Attraction to the tumor site

Interestingly, it was previously thought that neutrophils were solely involved in the acute phase of inflammation, primarily as pathogen eliminators. However, it is now known that neutrophils play a broader role in shaping the immune environment by interacting with macrophages, DCs, and cells of the adaptive immune system through direct cell-to-cell contact or by releasing soluble mediators (Mantovani et al., 2011). Tumor cells frequently exhibit constitutive production of numerous inflammatory chemokines, including CXC-chemokines that attract neutrophils such as CXCL8 (IL-8) that has been associated with increased tumor cell proliferation, invasion and migration, angiogenesis, and immunosuppression in prostate cancer and other cancers **(*Figure 14*)** (Maxwell et al., 2014; Tobin et al., 2019; Xiong et al., 2022). Besides tumor cells, the immune components themselves can also call the neutrophils to the cancer site. For example, activated regulatory T (Treg) or Th17 cells, can release CXCL8, which strongly attracts neutrophils (Fridlender et al., 2009; Pelletier et al., 2010). Pelletier and colleagues, provided the first evidence that human neutrophils and Th17 cells, once activated, can directly recruit each other, via the release of specific chemokine (Pelletier et al., 2010). More specifically, various Th17 cell-derived cytokines, such as IL-17, interferon-γ (IFNγ), tumor necrosis factor (TNF), CXCL8 and granulocyte-macrophage colony-stimulating factor (GM-CSF), promote the recruitment, activation, and prolonged survival of neutrophils at sites of inflammation.

Factors	Source	Responder	Outcome
CXCL1, CXCL2, CXCL5 and CXCL8	• Megakaryocyte • Endothelial cell • Cancer cell	Neutrophil	Neutrophil release from bone marrow in homeostasis and cancer; recruitment to tumours
G-CSF	• Fibroblast • Cancer cell	Neutrophil	Granulopoiesis in homeostasis and cancer; neutrophil polarization and immunosuppression
GM-CSF	Cancer cell	• Neutrophil • Monocyte	Granulopoiesis in homeostasis and cancer; neutrophil polarization and immunosuppression
IL-1β	• Macrophage • Dendritic cell	• $CD4^+$ T cell • γδ T cell	IL-17- and G-CSF-mediated granulopoiesis in homeostasis and cancer
IL-17	• $CD4^+$ T cell • γδ T cell	• Fibroblast • Bone marrow stromal cell	G-CSF-mediated granulopoiesis in homeostasis and cancer
IL-23	• Macrophage • Dendritic cell	• $CD4^+$ T cell • γδ T cell	IL-17- and G-CSF-mediated granulopoiesis in homeostasis and cancer
iNOS and ARG1	• Neutrophil • Monocyte	• T cells • NK cell	Suppression of antitumour immunity
TGFβ	• Neutrophil • B_{reg} cell	• T cells • NK cell • Neutrophil	Immunosuppression in tumour microenvironment and metastasis
TNF	• Endothelial cell • Cancer cell	• CD4 T cell • Neutrophil • Endothelial cell	IL-17- and G-CSF-mediated granulopoiesis in homeostasis; neutrophil recruitment to tumours; MET upregulation in neutrophils
THPO	Unknown	Megakaryocyte	CXCR2 ligand-dependent release of neutrophils from bone marrow in homeostasis

Figure 14. Bidirectional communication between neutrophils and other immune cells in homeostasis and cancer *as summarized in the review of (Coffelt et al., 2016). [ARG1, arginase 1; CXCL, C-X-C ligand; G-CSF, granulocyte-colony stimulating factor; GMCSF, granulocyte-macrophage-colony stimulating factor; IL, interleukin; iNOS, inducible nitric oxide synthase; TGFβ, transforming growth factor β; TNF, tumour necrosis factor; THPO, thrombopoietin].*

3.3.4 Heterogeneity and plasticity in cancer

Recent studies and the development of new genetic tools have provided the cancer research community with novel insights on the properties of tumor associated neutrophils (TANs). These discoveries highlight the profound influence of neutrophils in supporting tumor initiation (eg, ROS, proteases), proliferation (eg, neutrophil elastase (NE)), angiogenesis (eg, matrix metalloproteinase 9 (MMP-9), VEGF), immune evasion (eg, arginase-1), and metastasis (eg, NETs) (Bergers et al., 2000; Cools-Lartigue et al., 2013). The complex roles of neutrophils in cancer extend beyond promoting or preventing tumor progression and can be explained by various polarization states. Recent data have highlighted the plasticity of TANs, showing that they can be polarized towards distinct phenotypes in response to environmental cues. (Fridlender et al., 2009) proposed that TANs can be polarized towards an 'N1' or an 'N2' phenotype, analogous to the M1 and M2 macrophages. They showed that blocking TGF-β in lung adenocarcinoma and mesothelioma murine cancer models, not only slowed tumor growth by activating $CD8^+$ T-cells and macrophages, but also increased neutrophil-attracting chemokines. This led to an influx of $CD11b^+/Ly6G^+$ TANs that were hypersegmented and more cytotoxic to tumor cells and had higher pro-inflammatory cytokine levels. Depletion of these neutrophils (anti-Ly6G, clone 1A8) after TGF-β blockade attenuates the anti-tumor effects and reduces $CD8^+$ T-cell activation. In contrast, depletion of neutrophils in tumors without TGF-β blockade, slows tumor growth and activates intra-tumoral $CD8^+$ T-cells. This suggests that TGF-β promotes pro-tumoral TAN (N2), in the tumor microenvironment, whereas TGF-β inhibition recruits anti-tumoral TAN (N1) characterized by enhanced tumor cytotoxicity and immunostimulatory profile *in vitro* (i.e. higher expression of TNF, CCL3 and ICAM1 and lower expression of arginase 1). Previous studies in colon adenocarcinoma also indicated antitumoral neutrophil activity *in vitro* and *in vivo* (Colombo et al., 1991).

In contrast, the pro-metastatic profile of TANs was demonstrated in a rat mammary adenocarcinoma model, where co-injection of cancer cells with neutrophils derived from tumor-bearing rats significantly enhanced metastasis, unlike to co-injection with neutrophils from healthy rats (Welch et al., 1989). The complexity of neutrophil-based immunosuppressive mechanisms was further highlighted by recent evidence showing that neutrophil extracellular traps (NETs) released in the tumor microenvironment protect cancer cells from cytotoxic immune cells and also promote T cell exhaustion (Kaltenmeier et al., 2021). This phenomenon was observed in both transplantable tumor models and a spontaneous pancreatic adenocarcinoma mouse model (Teijeira et al., 2020; Zhang et al., 2020), and more recently in patients with prostate adenocarcinoma (Zheng et al., 2024).

These observations highlight the significant influence of the tumor microenvironment on the functional properties of neutrophils. Given the diverse phenotypes and functions of neutrophils in tumor biology, it is becoming increasingly clear that the definition of a ubiquitous and distinct function for tumor-associated neutrophils is no longer valid. Instead, identifying neutrophils' heterogeneity and targeting neutrophils with pro-tumoral activity in personalized treatments, could greatly benefit the tumor immunology field.

3.3.5 Clinical aspect of neutrophils in cancer

In addition to studies in mice and *in vitro*, numerous clinical studies have shown that a high neutrophil-to-lymphocyte ratio (NLR) in the blood of patients, is a poor prognostic indicator for several malignancies, including prostate cancer. For instance, a meta-analysis involving over 40.000 patients with solid tumors showed that a high NLR is associated with worse overall survival (OS), and was more pronounced in metastatic diseases than non-metastatic diseases (Templeton et al., 2014a). Castration-resistant prostate cancer patients also exhibited elevated NLR, which was associated with lower response rates to treatments with abiraterone or docetaxel (chemotherapy) (Leibowitz-Amit et al., 2014; Templeton et al., 2014b). Conversely, a decline of NLR during treatment with cabazitaxel (chemotherapy) has been associated with longer overall survival (Lorente et al., 2015).

The mechanisms underlying the relationship between high NLR levels and adverse survival outcomes, are not yet fully understood. This neutrophilic state could be due to a tumor burden, an ongoing chronic inflammatory process, or excessive production of granulocyte macrophage colony-stimulating factor (GM-CSF). Despite the multifaceted and sometimes opposing roles of neutrophils in cancer highlighted by experimental studies, the bulk of clinical evidence evaluating systemic neutrophil score (NLR) supports the notion that neutrophils generally promote, rather than inhibit, cancer progression. Therefore, the NLR has been proposed as a biomarker to guide treatment decisions for personalized approach to cancer therapy. Furthermore, clinically, an increase of the NLR during treatment is interpreted as an indication of recurrence or progression of the disease, while a drop in the value indicates a positive response to the applied treatment.

3.3.6 Resolving the Myeloid Derived Suppressor Cells (MDSCs) nomenclature

The relationship between neutrophils and myeloid-derived suppressor cells (MDSCs) adds further complexity to the picture of neutrophil subtypes. Elevated levels of immature MDSCs are common in many cancers including prostate cancer, (Brusa et al., 2013; Khaled et al., 2014). The MDCS nomenclature, introduced in 2007 by (Gabrilovich et al., 2007), describes a heterogeneous population of myeloid progenitors and precursors induced by tumors as a mechanism to evade immune surveillance These cells include monocytes and neutrophils, that express key factors involved in MDSC-mediated immune suppression including arginase (ARG1), inducible NOS (iNOS), TGF-β, IL-10, and COX2 among others (Marvel and Gabrilovich, 2015).

In preclinical models, MDSCs are phenotypically characterized by the co-expression of myeloid lineage differentiation antigens, CD11b and Gr-1 (clone RB6-8C5). Gr1 binds to two antigens, Ly6C and Ly6G, identifying two major cellular subsets in tumor-bearing mice: $CD11b^{+}Gr1^{high}$ granulocytic or polymorphonuclear (G/PMN)-MDSCs and $CD11b^{+}Gr1^{low}$ monocytic (M)-MDSCs. However, specific Ly6G (clone 1A8) and Ly6C antibodies allow the precise identification of neutrophils and monocytes respectively and their counterparts' infiltrating the tumors. Due to the shared markers and morphological similarity between G/PMN-MDSCs and neutrophils, there is ongoing controversy about their relationship and distinction. Although immaturity is often attributed to G/PMN-MDSCs compared to fully differentiated neutrophils, Gr1 and Ly6G recognize both mature and immature cells, making it technically difficult to distinguish them based on these markers alone. Furthermore, not all $CD11b^{+}Gr1^{+}$ cells in tumor-bearing mice exhibit immunosuppressive properties, which argues against generalizing all these cells as MDSCs. Consequently, (Di Mitri et al., 2014) characterized $Gr1^{+}$ MDSC infiltration in prostate tumors of the Pb-Cre4 driven $PTEN^{-/-}$ mouse model, and found that these cells antagonize PTEN-induced senescence of prostatic cancer cells via IL-1RA secretion, and promote cancer progression to adenocarcinoma. Since many studies on TANs refer to $Gr1^{+}$MDSCs, these data must be interpreted with caution.

In cancer patients, MDSCs express the common myeloid markers CD33 or CD11b and do not show expression of CD3, CD14, CD19, CD57 and/or HLA-DR. Initially, human MDSCs were defined as $HLA\text{-}DR^{-}CD33^{+}$ or $CD14^{-}CD11b^{+}$ cells, both of which exhibit T cell suppressive activity and are classified as a subset of $CD11b^{+}CD14^{-}$ cells with polymorphonuclear granulocyte morphology (G/PMN-MDSCs), which are distinct from mononuclear $CD11b^{+}CD14^{+}$ monocytes (M-MDSCs) (Almand et al., 2001). Studies have highlighted the presence of MDSCs in prostate cancer patients. Chi and colleagues observed elevated levels of circulating PMN-MDSCs, defined as $CD33^{+}CD11b^{+}HLA\text{-}DR^{-}CD14^{-}$, in prostate cancer patients. The percentage of MDSCs increased with clinical stage and served as a negative prognostic indicator for survival. Additionally, patients with prostate cancer exhibited higher serum levels of the pro-inflammatory cytokines IL-8 and IL-6, which correlated with a high number of MDSCs in the blood circulation, thus, likely contributing to the accumulation of MDSCs (Chi et al., 2014).

Recent single-cell RNA-seq studies have further characterized MDSCs in tumors. The study by (Alshetaiwi et al., 2020) confirmed that breast cancer associated PMN-MDSCs and M-MDSCs isolated from tumor bearing hosts have distinct gene signatures of neutrophils and monocytes, respectively, and identified CD84 as a new marker for MDSCs. In the same line, (Veglia et al., 2021a) have demonstrated the coexistence of classical PMNs and immune suppressive PMN-MDSCs in mice and humans and identified CD14 to distinguish PMN-MDSC in mice. They showed that while $CD14^{int}$ PMN-MDSCs gradually replace classical PMNs in spleens, the $CD14^{high}$ PMN-MDSCs appear early in tumors, with potent suppressive properties. In humans, the gene signature of tumor PMNs was strongly associated with a negative clinical outcome in patients with signature of T cell infiltration. Although markers such as CD84 and CD14 were proposed to distinguish G/PMN-MDSCs from neutrophils, they have not been

extensively tested across all cancer types, and these cells share many transcriptional similarities with mature neutrophils (Xie et al., 2020).

The MDSC nomenclature is self-limiting, as assigning a name based on one function, such as immunosuppression, implies that G/PMN-MDSCs exist predominantly for one purpose (Quail et al., 2022). Neutrophils, however, exhibit both pro-angiogenic and immunosuppressive capabilities as well as antitumoral activity. Hence, in the absence of compelling evidence that clearly separate neutrophils from G/PMN-MDSCs, it may be more reasonable to consider G/PMN-MDSCs as a subset of neutrophils with immunosuppressive properties. Therefore, this view, shared by others (Quail et al., 2022), suggests abandoning the restrictive term MDSCs in favor of a more comprehensive view of myeloid biology that encompasses both cellular and functional heterogeneity. Consequently, in our analysis the MDSC nomenclature will not be used for the identification of neutrophil clusters in our murine prostate cancer model.

3.4 A focus on Macrophages in health & cancer

In the late 19th century, Ilya Metchnikoff discovered a more than 500-million-years evolutionary conserved immune cell population that could phagocytose (Tauber, 2003). He named them macrophages as they appeared to be “large eaters” (from Greek μακρός (makrós) = large, φαγεῖν (phagein) = to eat) and he was awarded the Nobel Prize in Physiology or Medicine in 1908 for his discovery of the phagocyte cells (Schmalstieg and Goldman, 2008). In vertebrates, macrophages are found in all tissues throughout the body and play essential roles in maintaining tissue homeostasis as well as responding to diseases. They can arise either from embryonic precursors or from blood circulating monocytes in adults and different tissues harbor a mixture of embryonically derived and adult-derived macrophages. It remains however uncertain whether macrophages of different origins can perform similar functions or whether they have distinct roles under normal conditions.

3.4.1 Understanding their origins

Understanding the origins, developmental pathways, and homeostatic processes of tissue-resident macrophages is essential for the development of strategies to modulate macrophage functions at specific sites. The ontogeny of macrophages has been a subject of debate for decades dating back to the 1970s/80s. Historically, it was assumed that tissue-resident macrophages were constantly renewed by monocytes circulating in the bloodstream, which originated from progenitor cells in the adult bone marrow (BM). This concept was fundamental to the "mononuclear phagocyte system" (MPS) defined by Van Furth and colleagues in the 1970s, which includes BM promonocytes and their precursors, monocytes in the peripheral blood, and tissue macrophages (van Furth et al., 1972). BM promonocytes were considered to be the progenitors of blood-circulating monocytes, which were thought to be constantly recruited into the tissue to differentiate into resident macrophages. This assumption was challenged when some studies showed that microglia (the brain tissue-

resident macrophages) and alveolar macrophages (the lung tissue-resident macrophages) were independent of the HSC-derived blood monocytes (De Groot et al., 1992; Tarling et al., 1987). With the development of fate-mapping mouse models, recent studies have dramatically changed our understanding of MPS. It is now clear that the contribution of circulating monocytes to macrophage populations is mainly restricted to a few specific tissues, such as the gut, dermis, and heart, each of which has its own turnover rate in the steady state. However, most tissue-resident macrophage populations originate from embryonic precursors that settle in tissues before birth and persist locally throughout adulthood, with minimal input from BM-derived precursors (Ginhoux and Guilliams, 2016; Hashimoto et al., 2013; Yona et al., 2013).

In mammals, hematopoiesis takes place successively in the yolk sac, an area surrounding the dorsal aorta termed the aorta-gonad mesonephros (AGM) region, in the fetal liver, and finally in the bone marrow. Macrophages are first observed and expand in the extraembryonic yolk sac during what is termed primitive hematopoiesis in early gestation (embryonic day 6.5 [E6.5]–E8.5). At this developmental stage, macrophages are the only type of "white blood cells" that are generated, as specialized progenitor cells in the yolk sac differentiate exclusively into macrophages and red blood cells. Following this (E8.5–E10.5), definitive hematopoietic stem cells (HSCs) originate from the aorta-gonad-mesonephros and generate all immune cell lineages. From E10.5 onwards, these HSCs relocate to the fetal liver, which becomes the principal hematopoietic organ for the rest of embryonic development. It is only during the perinatal period that the conventional bone marrow HSCs take over the role of the primary hematopoietic site and generate the full range of immune cell lineages (Orkin and Zon, 2008).

Subsequently, macrophages are now generally categorized into two classes: tissue-resident macrophages (RTMs), originating from yolk sac & fetal liver, and infiltrating macrophages, originating from bone-marrow derived monocytes (Park et al., 2022). RTMs include splenic red-pulp macrophages, lung alveolar macrophages, epidermal Langerhans cells (LCs), brain microglia, liver Kupffer cells (KCs), large peritoneal macrophages, and F4/80^{bright} pancreatic, kidney, cardiac and testis macrophages (Hume et al., 1984; Morris et al., 1991; Perdiguero and Geissmann, 2016). These macrophages usually located in specific tissues and play a wide range of roles in development and homeostasis. Equipped with long dendrites or pseudopods and extensive endolysosomal machinery, the RTMs across tissues present specific functions, but also share common functions, such as the clearance of cell-associated materials and foreign bodies, safeguarding the neuronal net, preserving the vascular tone and integrity, and mounting the first line defense against pathogens as reviewed by (Park et al., 2022). This remarkable diversity of functions emphasizes the sessility and long-term residence of these cells in tissues. In contrast, infiltrating macrophages are mainly observed in response to pathological conditions. It is now known that classical monocytes, also referred to as "inflammatory" or Ly6C^{high} monocytes, serve as the source of infiltrating macrophages in pathological context, including cancer (Qian et al., 2011).

A complication in identifying the macrophage origin was that primitive yolk-sac-derived macrophages exhibit differences in transcription factor usage and surface-marker expression compared to fetal HSC-derived macrophages. For instance, the yolk-sac-derived macrophages exhibit the distinct $CD45^{+}CX_3CR1^{hi}F4/80^{hi}CD11b^{lo}$ expression profile, compared to the HSC-derived macrophages which express $CD45^{+}CX_3CR1^{+}F4/80^{low}CD11b^{high}$. Additionally, the $F4/80^{low}CD11b^{high}$ (HSC-derived) macrophages rely entirely on the transcription factor MYB, while the $F4/80^{hi}CD11b^{lo}$ (yolk-sac-derived) macrophages develop independently of MYB (Schulz et al., 2012). In addition, many adult RTMs originating from embryonic development alter their cell-surface marker expression upon maturation, making it difficult to accurately identify macrophage ontogeny. For example, the fate-mapping study by (Yona et al., 2013) using the conditional CX_3CR1 promoter driven-Cre recombinase to label macrophages, showed that Kupffer cells, lung alveolar, splenic, and peritoneal macrophages, are established prior to birth and while they express CX_3CR1 during development, they lose this expression after birth. Importantly, it was shown that they maintain during adulthood, independently of replenishment by blood monocytes.

Although all tissues are populated with fetal macrophages at birth, these cells can be replaced by HSC-derived progenitors to varying degrees over time, in a site-specific manner, as reviewed by (Ginhoux and Guilliams, 2016; Park et al., 2022). The contribution of adult precursor cell to certain tissue-resident macrophages and their continuous turnover during adulthood, was first demonstrated by parabiosis and bone-marrow chimera experiments. For instance, our laboratory has previously shown that the replacement of tissue macrophages in the dermis, at adulthood, was dependent on the recruitment of $Ly6C^{hi}$ monocytes after they exit the BM using the chemokine receptor CCR2. This was evidenced by the significant reduction of macrophage populations in mice lacking CCR2 and their reconstitution almost exclusively from wild-type BM-derived cells in WT:$Ccr2^{-/-}$ competitive chimeras (Tamoutounour et al., 2013). Similar observations were made for intestinal and pancreatic macrophages (Bain et al., 2014a; Calderon et al., 2015). Additionally, using diphtheria toxin (DT)–mediated ablation of tissue-resident macrophages and monocyte-derived cells in the $CD64^{DTR}$ mice (Baranska et al., 2018) to investigate the kinetics of reconstitution of monocytes and macrophage populations in the adult skin and intestine, they demonstrated that all the mo-DC and macrophage subsets present prior DT treatment can be readily depleted and reconstituted in normal ratios and numbers, probably from HSCs, and with kinetics consistent with their expected precursor-product relationship.

It is worth noting that most the studies investigating the origin of macrophage have been performed in young mice, aged from 0-10 weeks old. However, a crucial parameter that is often overlooked is the duration of residence within tissues during aging, which likely affects the degree of macrophage maturation and phenotype. For instance, at birth, the gut macrophage population consists exclusively of fetal macrophages. However, during the first three months of postnatal life, circulating monocytes are recruited and gradually replace the fetal-derived macrophages. By this time, fetal-derived macrophages are reduced to only 20%–30% of the total macrophage population in the tissue (Bain et al., 2014a). Interestingly, the

expression of Tim4 in macrophages is associated with long-term residence. A subpopulation of long-lived gut macrophages, which persist for several months, expresses Tim4 and shows only minor replacement by monocyte-derived cells (Shaw et al., 2018). Other studies indicate that Tim4 could serve as a marker for long-term resident macrophages, particularly in the liver (Scott et al., 2016). To clarify the monocytic origin of macrophages, (Liu et al., 2019) generated the fate-mapping Ms4a3^{Cre}-Rosa^{TdT} mice that traced monocytes and granulocytes, but not lymphocytes or conventional dendritic cells. This model permitted the assessment of monocyte derived cells in the pool of RTMs. They showed that in mice aged6 weeks and 8 months, monocytes contributed least to Tim4^{+} macrophages compared to Tim4^{-} mac in colon and small intestine. At 6 weeks, 13.1% of Tim-4^{+} macrophages were tdTomato-labeled, while at 8 months, this increased to 67.0%. The Tim4^{-} macrophages also showed increased tdTomato labeling over time. These findings indicate that Tim4 is not a completely reliable marker for tracing embryonic origin, as the long-lived Tim4^{+} gut macrophages comprise a mixture of embryonic and adult-derived cells, with the latter increasing with age. Additionally, this demonstrates that tissues contain a heterogeneous population of resident tissue macrophages (RTMs), ranging from recently recruited monocyte-derived macrophages, differentiated just hours earlier, to macrophages that resided for several months, alongside embryonic-derived macrophages that have been present before birth (***Figure 15***).

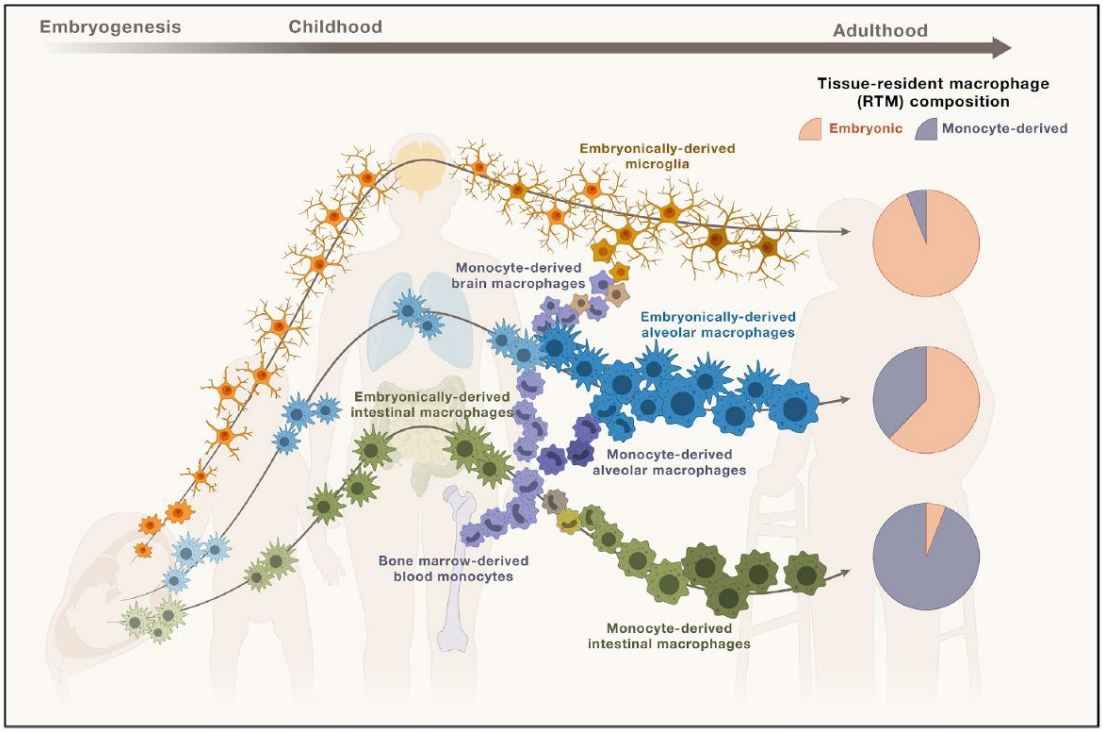

Figure 15. The ontological composition of tissue-resident macrophage (RTM) populations varies depending on the tissue and the age. *Illustration of the generation and development of these RTM populations during fetal development and post-birth, based on the widely accepted paradigm that all RTMs are derived from embryonic phagocytes. Microglia self-maintain in the brain through interactions with glial cells, such as astrocytes. They persist*

throughout aging with minimal contribution from peripheral monocytes, which rarely cross the blood-brain barrier to infiltrate the brain parenchyma under steady-state conditions. Alveolar macrophages in the lungs preserve their pool of embryonically derived cells during homeostasis. However, unlike brain-resident microglia, alveolar macrophages increasingly consist of tissue-infiltrating monocytes as aging progresses. Therefore, a significant fraction of alveolar macrophages can be derived from monocytes. Intestinal lamina propria macrophages are an exception among RTMs, as they are largely comprised of monocyte-derived cells. The high turnover rate of macrophages in the gut necessitates continuous input from blood monocytes. Source figure from (Park et al., 2022).

3.4.2 Impact of the environmental niche

The location and homeostatic functions of tissue-resident macrophages are regulated by specific "niches" in the tissue that control macrophage population size and imprint their tissue-specific identity. The niche as described by (Guilliams et al., 2020) is thought to provide a physical foundation or scaffold for the macrophage, to supply with trophic factors (such as CSF-1) and cytokines (such as IL-34) produced by neighboring cells that enable macrophage self-maintenance, to imprint the tissue-specific identity of the resident macrophage through the expression of key transcription factors and to ensure that macrophages, in turn, benefit their niche. Subsequently, the tissue residency of the macrophages determines to some extent their distinct phenotype and functions. For instance, in the lungs, heart, adipose tissue, and dermis, (Chakarov et al., 2019) showed that there are two macrophage subsets with specific subtissular locations: the nerve-associated ($CX_3CR1^+MHCII^{hi}$) macrophages located close to nerves, and the perivascular ($LYVE\text{-}1^+$) macrophages located in close proximity to blood vessels. These subsets of macrophages originate from embryonic progenitors but are gradually replaced by monocyte-derived cells in adulthood and are conserved across species.

Colony-stimulating factor 1 (CSF-1) is critical for the survival, proliferation, and differentiation of mononuclear phagocytic cells and is the major regulator of mononuclear phagocyte production *in vivo* (Cecchini et al., 1994). These effects are mediated by a high-affinity receptor tyrosine kinase (CSF-1R), encoded by the c-fms proto-oncogene (Sherr et al., 1985). CSF-1R is expressed on various cells including primitive multipotent hematopoietic cells, mononuclear phagocyte progenitor cells, monoblasts, promonocytes, monocytes, tissue macrophages, osteoclasts, B cells, smooth muscle cells, and neurons. CSF-1R is essential for the development, survival, recruitment, and proliferation of most macrophages as shown in $Csf1r^{-/-}$ mice (Dai et al., 2002). Fibroblasts produce membrane-bound CSF-1 to facilitate physical interactions with macrophages and ensure their survival. Considering also that fibroblasts are ECM-producing cells, the proteoglycan CSF1-isoform may preferentially bind to the ECM around the fibroblast, promoting macrophage-fibroblast proximity. Thus, the survival and nurture of the niche itself benefits from nurturing the macrophages (Zhou et al., 2018).

Since tissue macrophages in adult mice remain dependent on CSF1R, they can be depleted by treatment with an inhibitory anti-CSF1R antibody. Interestingly, CSF1R blockade reduced the numbers of tumor-associated macrophages in syngeneic tumor models,

suggesting that these cells are tissue resident macrophages (MacDonald et al., 2010). Conversely, it had no effect on inflammatory monocyte recruitment in models, including lipopolysaccharide-induced lung inflammation, wound healing, peritonitis, and severe acute graft-versus-host disease. Investigation of the molecular basis for myeloid-restricted transcriptional regulation of Csf1r, revealed a conserved super-enhancer within the second intron of Csf1r, called the fms-intronic regulatory element (FIRE), which contains binding sites for numerous macrophage-expressed transcription factors and is necessary and sufficient to direct macrophage-specific transcription (Hume et al., 2017). Deletion of the FIRE locus, selectively affects RTMs in the brain, skin, kidney, peritoneal, and heart in the $Csf1r^{\Delta FIRE/\Delta FIRE}$ mice but does not affect the development of CSF1R-dependent macrophages in other locations such as the dermis, liver, spleen and bone (Rojo et al., 2019).

While the heterogeneity and origin of macrophages, as well as their dependence on CSF-1R and FIRE enhancer have been extensively studied for many organs in steady state and pathological conditions, little is known about the myeloid compartment in prostate tissue. As part of my PhD project, building on the lab's expertise in unraveling the heterogeneity, origin and functions of myeloid cells in skin (Baranska et al., 2018; Malissen et al., 2014; Tamoutounour et al., 2013), we investigated the myeloid compartment in healthy prostate and upon cancer progression using state-of-the-art single-cell approaches.

3.4.3 Macrophages in cancer

In the context of cancer, tumor cells secrete various cytokines, such as CSF-1, and recruit monocytes and macrophages, called tumor associated macrophages (TAMs). TAMs exhibit phenotypic and functional differences from macrophages in healthy tissues. Understanding their behavior and heterogeneity is crucial for deciphering disease pathogenesis.

3.4.3.1 Macrophage polarization: the M1/M2 paradigm

25 years ago, Charlie Mills introduced the paradigm of M1/M2 macrophage polarization (Mills et al., 2017), inspired by the Th1/Th2 polarization concept previously introduced by Mosmann and Coffman. M1 macrophages (or "classically activated" macrophages) are pro-inflammatory and characterized by the upregulation of inducible nitric oxide synthase (iNOS), leading to the production of reactive oxygen species (ROS) and reactive nitrogen species (RNS). This activation promotes glycolysis, fatty acid synthesis (FAS), and the pentose phosphate pathway (PPP), while simultaneously suppressing the tricarboxylic acid cycle (TCA) and mitochondrial oxidative phosphorylation (OXPHOS). These metabolic shifts enhance the inflammatory response and phagocytosis. In contrast, M2 (or "alternatively activated") macrophages are anti-inflammatory, by upregulating arginase-1 (Arg-1) to produce ornithine and urea, which boosts OXPHOS, FAS, and glutamine metabolism, while suppressing PPP (Liu et al., 2021). M2 macrophages support tumor growth by promoting

angiogenesis and metastasis through the secretion of metalloproteinases and inhibiting antitumor immunity through the release immunosuppressive cytokines (Mantovani et al., 2006). The M1 profile generally provides protection against bacterial and viral infections and has an anti-tumoral function, whereas the anti-inflammatory M2 phenotype is associated with tumor promotion, neoangiogenesis, immunosuppression and low overall patient survival (Murray et al., 2014) (***Figure 16***).

The M1/M2 nomenclature has been widely used, and many studies have evaluated TAM functions based on this paradigm in various tumors, including prostate cancer, at both preclinical and clinical levels. For instance, in sections of nude mouse xenografts of seven common human PCa cell lines, more than 94% of TAMs exhibited an M2-like phenotype, with few M1-polarized macrophages distributed in the periphery. Additionally, a strong positive spatial relationship was found between macrophages, vasculature, and PSMA expression, with the fastest-growing tumors associated with the highest macrophage densities, while the slowest-growing tumors had focal tumor-infiltrating macrophage densities (Copeland et al., 2019). Interestingly, (Hu et al., 2015) analyzed TAMs in prostate tissue from 42 patients with prostate adenocarcinoma, who were followed up for 5 years. Immunofluorescent analysis showed that the mean number of total TAMs ($CD68^+$) and the M2 subset ($CD68^+CD206^+$) in prostate tissues of PCa patients with metastases was significantly higher than in patients without metastases. Moreover, the number and percentage of M2 TAMs correlated positively with tumor grade and elevated serum prostate-specific antigen (PSA) levels. These findings suggest that M2 macrophages may be implicated in the metastatic process of PCa, although the underlying mechanisms need to be further investigated.

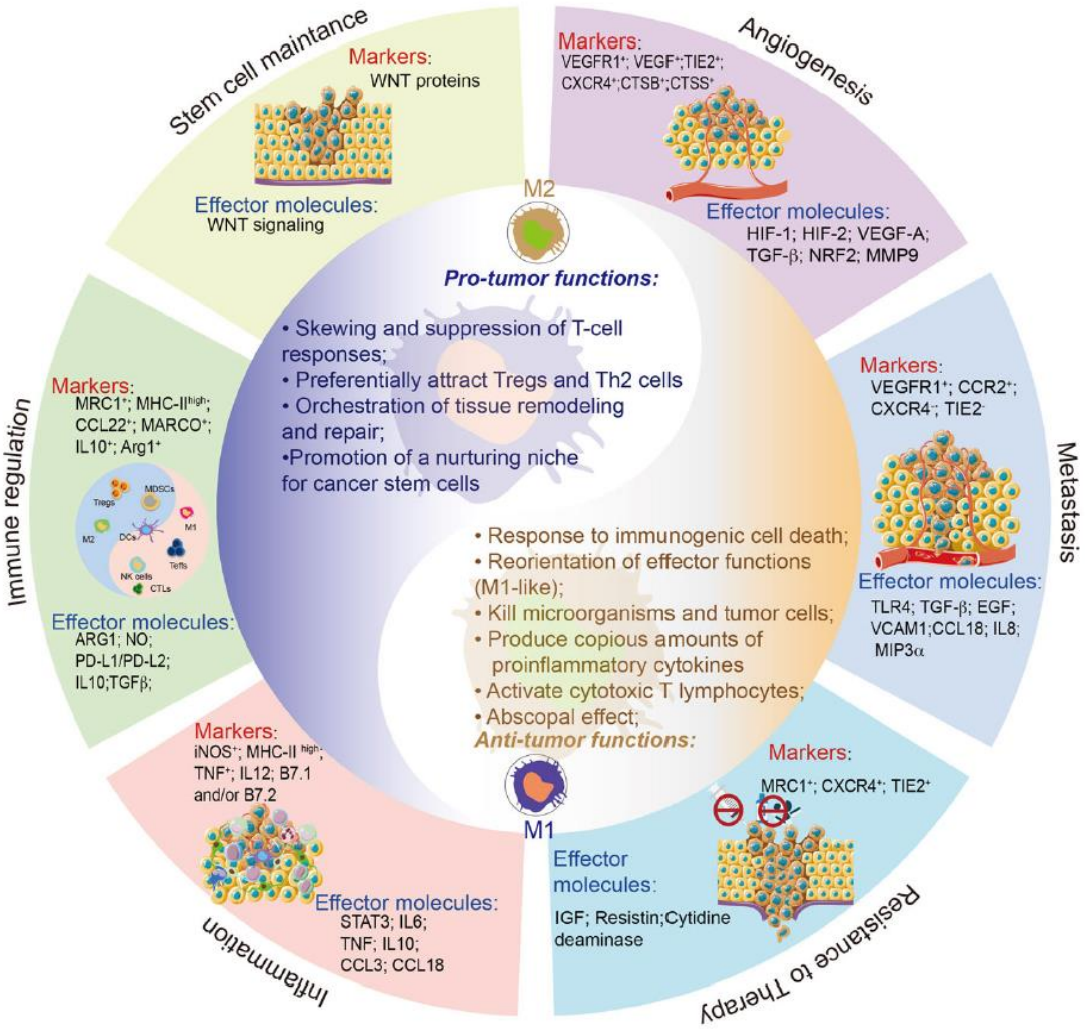

Figure 16. The yin and yang of TAMs in response to cancer immunotherapy. *Macrophages play dual roles in coordinating immune responses. They can either inhibit (left-hand side) or enhance (right-hand side) the effectiveness of cancer immunotherapy strategies. The two macrophage subtypes are known as M1 and M2. M1 macrophages, or 'killer' macrophages, were previously called classically activated macrophages. In contrast, M2 macrophages, or 'repair' macrophages, are referred to as alternatively activated macrophages. M2 macrophages are involved in constructive processes such as wound healing and tissue repair. They also inhibit immune surveillance by producing immunosuppressive cytokines. This differential polarization is influenced by various stimuli that alter the macrophages' differentiated state. Currently, TAMs are thought to promote cancer initiation and progression by stimulating tumor-associated angiogenesis, promoting tumor cell metastasis, invasion, and intravasation, contributing to chemotherapeutic resistance, and suppressing the antitumor immune response. Source figure from (Li et al., 2019).*

In a large PCa cohort study from (Zarif et al., 2019), 192 prostate cancer samples were processed and determined that the mannose receptor (CD206), an endocytic receptor characteristic of M2 macrophages, was N-glycosylated on the cell surface of human M2 macrophages and highly expressed in CRPC samples compared to benign normal-appearing

epithelial regions. These cells also co-expressed CD163, another marker related to the M2 phenotype. Patients with higher M2-TAM influx exhibited enhanced resistance to immunotherapy and nearly doubled mortality rates. More recently, (Kane et al., 2023) reported that prostate stereotactic body radiotherapy (SBRT), a neoadjuvant method to radical prostatectomy, amazedly alters the immune microenvironment within PCa. Multiplex immune-fluorescence revealed a 5.61-fold increase of $CD163^{+}$ macrophages density 2 weeks after SBRT. This was the first report to quantify infiltrating immune cells in situ within prostate tumors to determine local effects of SBRT in patients. These findings raise key questions about whether these myeloid subsets impair the anti-tumor immune response and how they could be effectively targeted.

However, the binary classification M1/M2 is too simplistic to explain the complex macrophage phenotypes and activation states present in various tissues. This may even lead to the erroneous assumption that there are only "two types of macrophages", overlooking the diversity of macrophages across species, tissues and pathological conditions. Subsequently, we might consider that using of only 2-3 markers to define macrophages is not sufficient to demonstrate their diversity and functions.

The study by (De Groot et al., 2021) characterized the TAMs beyond the M1/M2 paradigm in the two commonly used PCa GEEMs: the Hi-Myc and TRAMP models. In both models, macrophages adopt a more pro-tumoral phenotype in tumors of higher histological grade and older prostate tissue, although macrophage density differs between the two models: Hi-Myc tumors exhibit increased macrophage density ($CD11b^{+}F4/80^{+}CD206^{+}$), whereas TRAMP tumors show decreased macrophage density compared to age-matched wild-type mice. Additionally prostate macrophages in both models exhibited higher pro-tumoral (*Cd206*, *Arg1*, *Il10*, *Vegfa*, and *Pdl1*) and lower anti-tumoral (*Tnf*, *Il1b*, *Il12b, Cd80,* and *Cd86*) macrophage gene expression compared to age-matched WT mice. They concluded that, Hi-Myc model better mirrors patient tumors based on the macrophage density and the adenocarcinoma cancer type, compared to TRAMP model which develops neuroendocrine tumors and has lower macrophage density. Nevertheless, still the Hi-Myc model, does not fully recapitulate human prostate cancer as the tumor is initiated from birth and progressing fast, with the PIN stage as early as 2 weeks and adenocarcinoma at 6 months. Examination of the myeloid composition in the TME during cancer progression in more representative models of human prostate cancer, such as the tamoxifen-induced $PTEN^{(i)pe-/-}$, which mimics the slow progression of tumor formation in adult mice (3 months for PIN stage, 9 months for adenocarcinoma), would provide further insights into the characterization of TAMs in prostate cancer.

3.4.3.2 Macrophage heterogeneity in the single cell era

Recent advances in cytometry and single-cell RNA sequencing have greatly expanded our understanding of macrophage marker biology. Consequently, the identification of macrophage phenotypes using specific markers and the investigation of their origin and metabolic relationships have become essential in macrophage research. In neoplasia and

other inflammatory diseases, there is a substantial recruitment of Ly6C^{high} monocytes (Movahedi et al., 2010) which exhibit high plasticity and can be phenotypically polarized by cues from the surrounding microenvironment leading to the development of distinct subsets of monocyte-derived macrophages (mo-macs) (Olingy et al., 2019). This recruitment of monocyte-derived macrophages (mo-macs) during disease progression is influenced by several factors, including the presence of disease-specific alarmins and, the absence of steady-state tissue signals that promote the homeostatic differentiation of monocytes into monocyte-derived tissue-resident macrophages (RTMs). Consequently, mo-macs have a distinct transcriptomic signature when compared to their tissue-resident counterparts. Further research is needed to fully investigate the functional contributions of these molecular programs to disease progression.

A recent study on non-small cell lung cancer (NSCLC) by (Casanova-Acebes et al., 2021) used sc-RNA sequencing analysis to identify two distinct macrophage clusters enriched in human and mouse lung tumors: the alveolar RTMs expressing the genes *Pparg, Mrc1, Marco, Siglecf, Cd2, Siglec1, Stmn1, Tuba1b* and monocyte-derived macrophages (mo-macs) expressing the genes *C1q, Mafb, Arg1, Mgl2, Trem2, Apoe, Spp1, Gpnmb*. Using lineage tracing to assess their spatial and temporal distribution in the TME, the authors observed that during the early stages of tumor formation, alveolar RTMs accumulated close to tumor cells, promoting epithelial-mesenchymal transition in tumor cells and activating regulatory T cells and fibroblasts. However, as the tumor progressed, these tissue-resident macrophages reorganized to the periphery of tumors, and were replaced by a massive accumulation of mo-macs. The profile of tumor-infiltrating mo-macs has been analyzed in various cancers (***Figure 17***).

In a comprehensive pan-cancer analysis of single myeloid cells from 210 patients across 15 human cancer types, SPP1^{+} TAMs were identified in 8 tumor types including breast, pancreas, lung, colon, uterine, ovarian, nasopharyngeal, thyroid cancers. These TAMs preferentially expressed genes involved in angiogenesis. Conversely, C1QC^{+} TAMs exhibited significant higher phagocytosis levels (S. Cheng et al., 2021). One year later, the study by (Nalio Ramos et al., 2022) described two discrete APOE^{+} populations of TAMs in human and mouse breast cancer tumors: (a) TREM2^{+} macrophages expressing triggering receptor expressed by myeloid cells-2 (*Trem2*) and osteopontin (*Spp1*) genes, (b) FOLR2^{+} macrophages expressing folate receptor 2 (*Folr2*), hyaluronan receptor (*Lyve1*), and CD206/mannose receptor (*Mrc1*) genes. Trem2^{+} TAMs were scarcely present in healthy breast tissues but increased with tumor progression, while FOLR2^{+} macrophages were tissue-resident macrophages (RTMs) found in healthy mammary glands prior to cancer development. FOLR2^{+} macrophages localized in the perivascular areas of the tumor stroma, interacting with CD8^{+} T cells and efficiently priming effector CD8^{+} T cells *ex vivo*. Interestingly, their density in tumors correlates positively with better patient survival. Thus, this study highlights the specific role of tumor-associated macrophage subsets, and paves the way for subset-targeted therapeutic interventions in macrophage-based cancer therapies.

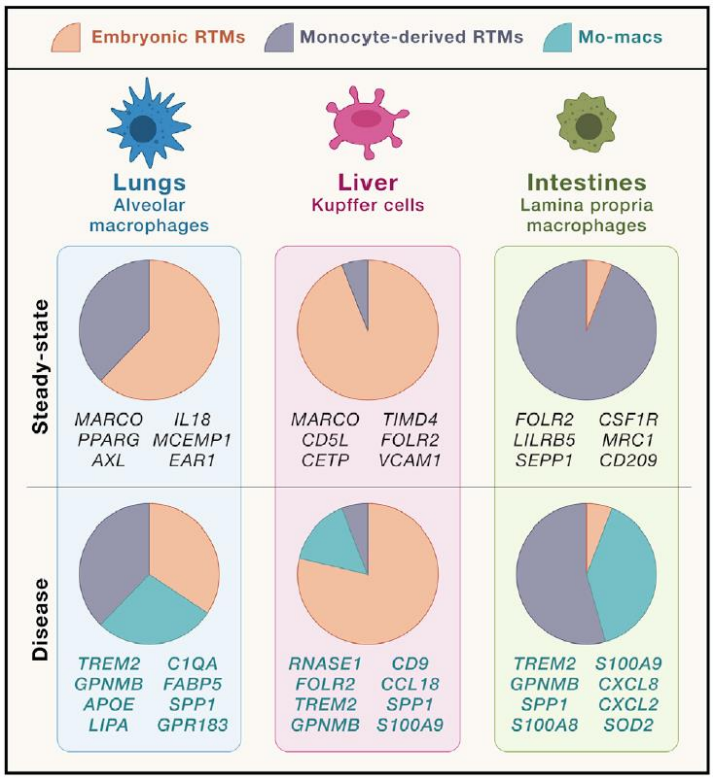

Figure 17. Transcriptional differences that discriminate disease associated mo-macs from RTMs. *Source figure from (Park et al., 2022).*

In a related study, (Sharma et al., 2020) identified two TAM populations in hepatocellular carcinoma (HCC), characterized by the markers FOLR2 and SPP1 for TAM1 and TAM2 respectively. RNA velocity analysis suggested that the FOLR2^{+} TAM1 population has a monocyte origin (mo-mac) and the SPP1^{+} TAM2 are RTMs. This finding is in contrast to the study by (Nalio Ramos et al., 2022). Additionally, the FOLR2^{+} TAM1 displayed more immunosuppressive interactions with Tregs compared to the SPP1^{+} TAM2 subpopulation, expressing higher levels of immunomodulatory chemokines such as CXCL12 and CXCL16 as well as CD86. These results suggest that FOLR2^{+} TAM1 may promote the immunosuppressive microenvironment in HCC. Moreover, TREM2 deficiency in mice with HCC enhanced tumor growth, suggesting that the TREM2 program functions as a tissue-dependent molecular network with both pathogenic and protective potential (Esparza-Baquer et al., 2021).

Recent studies have also focused on the lipid-associated TREM2 molecular program. TREM2, which has been extensively studied in microglia for its role in neurodegenerative pathologies such as Alzheimer's disease (Ulland and Colonna, 2018), has emerged as a characteristic marker of the mo-macs in various tumor types. The study by (Katzenelenbogen et al., 2020) used intracellular protein immunodetection followed by scRNA-seq (IN-seq) in MCA205 fibrosarcoma tumor-bearing mice, identifying two Arg1^{+}TREM2^{+} macrophages: (a) TAMs expressing *C1qa, Spp1, Cx3Cr1, Apoe,* and (b) Monocytic regulatory cells (named Mreg) expressing *Gpnmb, Il7r, Hilpda, Vegfa, Hmox1, Clec4d.* Genetic ablation of TREM2 in mice resulted in a significant decrease in the Mreg population and an increase in immune reactivity towards the tumor, characterized by a reduction in dysfunctional CD8^{+} T cells and an increase in NK and cytotoxic T cells. In line with these findings, (Molgora et al., 2020) showed that Trem2$^{-/-}$ mice exhibit greater resistance to tumor growth than wild-type mice in 3 cancer

types (MCA induced sarcoma, MC38 colorectal cancer, and mammary tumor). Furthermore, treatment with anti-TREM2 monoclonal antibody (mAb) inhibited tumor growth and promoted regression when combined with anti-PD-1 therapy. Single-cell RNA sequencing revealed that both TREM2 deletion and anti-TREM2 treatment were associated with a reduction in $MRC1^+$ and $CX3CR1^+$ macrophages in the tumor infiltrate. This was accompanied by an expansion of myeloid subsets expressing immunostimulatory molecules, which enhanced T cell responses. These data are consistent with observations in other cancers including prostate, gastric, renal and brain cancers, where elevated TREM-2 levels in tumor tissues correlate with poor prognosis (X. Cheng et al., 2021; Wang et al., 2016; Xiong et al., 2022; Zhang et al., 2018). Collectively, these findings highlight the role of TREM2 in regulating the suppressive nature of myeloid cells within the TME, and underscore the potential of targeting TREM2 signaling as an effective strategy to reactivate immune responses against tumors.

3.4.3.3 Commonly used markers to identify macrophages in mouse tissue

As mentioned above, elucidating the origin, heterogeneity and functions of macrophages based on their common surface markers is a major challenge. However, with the recent advances in myeloid research, we now have access to a repertoire of markers that help us decipher their heterogeneity in both health and cancer. In particular, a recent study by (Leach et al., 2020) on the transcriptome profiling of mononuclear cells in the lung, blood, LN and spleen in both human and mouse has provided a valuable resource of determinant marker genes to distinguish monocytes, macrophages and DCs across species. Below is a summary of pan-macrophage and subset-specific markers to discriminate macrophage populations in murine tissue (***Table 2***).

Table 2. Macrophage markers

Marker	Structure & Function	Expression	Reference
CD11b	Integrin alpha M (ITGAM) is member of the β2-integrin family. Involved in cell adhesion, chemotaxis, transmigration & phagocytosis.	Common myeloid cell marker. Expressed by monocytes, granulocytes, NK cells and most macrophages.	(Bednarczyk et al., 2020; Gordon et al., 2014)
F4/80	Member of EGF-TM7 family. Encoded by the *Adgre1* gene is dispensable for murine macrophage development and participates in the retention of macrophages in specific areas.	Common mononuclear phagocytic system marker. High expression by macrophages. Dim expression by monocytes, osteoclasts, macrophages of T cell areas and marginal zone, lung alveolar macrophages, cDC2 & eosinophils.	(Austyn and Gordon, 1981; Hume et al., 2002; P. R. Taylor et al., 2005)

MHCII	Major histocompatibility complex class II is indispensable for antigen presentation, and mediator of apoptosis.	Expressed by professional antigen presenting cells (e.g. macrophages & DCs). Upregulated in differentiating monocytes.	(Bain et al., 2014a; Reith et al., 2005; Tamoutounour et al., 2013)
IBA1	Ionized calcium-binding adapter molecule 1 is an actin-cross-linking protein participating in cell movement and phagocytosis.	Pan-macrophage marker Specifically expressed in macrophages/microglia. Not expressed by alveolar macrophages.	(Sasaki et al., 2001; Zhang et al., 2021)
CSF-1R	Colony stimulating factor 1 receptor (tyrosine kinase). Known also as CD115. Important controlling the development of most tissue macrophages, osteoclasts, microglia, Langerhans cells and Paneth cells of small intestine. Promotes monocyte commitment, survival, proliferation & chemotaxis of macrophages.	Highly expressed by monocytes and tissue macrophages, osteoclasts, microglia and Paneth cells. Dim expression by hematopoietic stem cells (HSCs) and DCs. Expressed also by non-immune cells (oocytes, epithelial cells, neural cells). CSF1R signaling in cancer is associated with immunosuppressive microenvironment.	(Cannarile et al., 2017; Mossadegh-Keller et al., 2013; Stanley and Chitu, 2014)
CD64	Fc gamma receptor I plays central role in macrophage antigen-dependent cellular cytotoxicity (ADCC) and clearance of immune complexes.	High affinity Fcγ receptor constitutively expressed on monocytes, macrophages and activated neutrophils. Distinguishes macrophages from DCs. Upregulated in M1-like macrophages.	(Akinrinmade et al., 2017; Hui et al., 2023; Tamoutounour et al., 2012)
CD88	Complement component 5a receptor 1 (C5AR1) functions as complement receptor and modulates inflammatory responses, obesity, development and cancers.	Expressed broadly by macrophages, neutrophils. Also, by monocytes, astrocytes & microglia. Distinguishes macrophages from DCs	(Leach et al., 2020; Markiewski et al., 2008)
CD11c	Integrin alpha X is involved in phagocytosis, leukocyte migration, and cytokine production by monocytes/ macrophages as well as induction of T cell proliferation by Langerhans cells. Favorable	Highly expressed by DCs. Expressed also by specific macrophage populations (eg alveolar Mf) and also by subsets of B, T, NK cells. Upregulated in M1-like macrophages	(Sadhu et al., 2007; Shin et al., 2021; Tang et al., 2021; Wang et al., 2023)

	prognosis for patients with CD11c-positive macrophages.		
SIRPα	Signal regulatory protein α (CD172a) acts as inhibitory receptor and interacts with the transmembrane protein CD47, also called the "don't eat me" signal, by negatively controlling the effector function of innate immune cells such as host cell phagocytosis. CD47 is expressed by cancer cells, including PCa, to avoid being phagocytosed.	Expressed broadly in the surface of macrophages and also in other myeloid cells, such as cDC2/DN DCs, monocytes, granulocytes & hematopoietic stem cells. It is also expressed in neurons.	(Barclay and Brown, 2006; Barclay and Van Den Berg, 2014; Dizman and Buchbinder, 2021)
CX3CR1	Fractalkine receptor is member of G-protein coupled receptor (GPCR). Involved in chemotaxis of immune cells and regulates macrophage function at sites of inflammation. CX3CR1 signaling enhances hypoxia and metastasis in PCa.	Highly expressed by monocytes, macrophages DCs, T cells and NK cells. Detectable in macrophages during development. Expressed also by non-immune cells (endothelial, epithelial, myocytes, astrocytes & cancer cells).	(Burgess et al., 2019; Liu et al., 2018; Schulz et al., 2012; Tang et al., 2016)
TIM-4	T-cell immunoglobulin and mucin domain 4. Maintains homeostasis by immune-regulation and transmits “eat me” signal to phagocytes to initiates efferocytosis.	Expressed by professional antigen presenting cells (macrophages & DCs). Specifically expressed by long-lived adipose tissue resident mac, Kuppfer cells. Expressed also by peritoneal B1 and NKT cells, stromal cells of lymph nodes and tumor cells.	(Blériot and Ginhoux, 2019; Wang et al., 2022)
FOLR2	Folate receptor beta is implicated in receptor-mediated endocytosis via high affinity binding of folic acid (vitamin B9). Presence of FOLR2 macrophages has positive correlation with T cell infiltration and better prognosis in breast cancer.	Expressed by tissue resident yolk sac-derived macrophages in healthy and malignant tissue and by proinflammatory monocytes in blood. Overexpressed in tumor-associated macrophages (TAMs). Residing in perivascular niches in tumor stroma.	(Nalio Ramos et al., 2022; Samaniego et al., 2020; Shen et al., 2014)

LYVE-1	Lymphatic vessel endothelial hyaluronan receptor 1 is linked with lymph angiogenesis. Associated also with tumor metastasis.	Marker of lymphatic endothelial cells. Expressed by specific macrophage subset (perivascular macrophages) in mouse brain, heart, eyes, adipose tissue, dermis, lung.	(Chakarov et al., 2019; Kieu et al., 2022; Siret et al., 2022)
CCR2	C-C chemokine receptor type 2 mediates monocyte chemotaxis, migration and scavenging. Required for monocyte egress from bone marrow but not for their extravasation from circulation to tissues.	Constitutively expressed by monocytes and downregulated upon their differentiation to macrophages. Under inflammation can be expressed by NK and T cells.	(Kurihara et al., 1997; Shroka et al., 2023; Tamoutounour et al., 2013)
CD206	Mannose receptor: required for clearance of mannose and is involved in endocytosis, cell adhesion and antigen uptake. Elevated levels are associated with poor prognosis in solid malignancies including PCa	Expressed by RTMs (perivascular microglia, Kupffer cells, lamina propria, dermal, peritoneal and alveolar macrophages), immature DCs. Also, by liver endothelial cells, dermal fibroblasts & keratinocytes. Upregulated in M2-like macrophages in humans and mouse.	(Debacker et al., 2021; Hu et al., 2015; Moseman et al., 2013; P. Taylor et al., 2005)
TREM2	Triggering receptor expressed on myeloid cells 2. Associated with Alzheimer's disease and with poor prognosis in various cancers.	Expressed on macrophages, immature monocyte-derived dendritic cells, osteoclasts, and microglia.	(X. Cheng et al., 2021; Katzenelenbogen et al., 2020; Molgora et al., 2020; Nalio Ramos et al., 2022; Ulland and Colonna, 2018)

3.5 Lymphoid cells in cancer

Traditionally, T lymphocytes, particularly $CD8^+$ cytotoxic T cells (CTLs) are considered the primary effector cells anti-tumor immune responses. These MHC class I restricted cells are activated by specific tumor-associated antigens (TAA), and subsequently produce perforin, granzymes, and cytokines that selectively kill tumor cells while sparing non-malignant cells. A subset of $CD4^+$ T helper (Th) cells is essential for providing the cytokine support required for CTL expansion and function. NK cells, which are not restricted to MHC and do not need prior

sensitization to antigens, also play a pivotal role in recognizing and eliminating tumor cells by releasing perforin, granzymes, and cytokines. These lymphocytes mediate cellular anti-tumor immunity. The contributions of NK cells to anti-tumor immunity have been largely considered in the context of antibody-dependent cytotoxicity (ADCC) during cancer therapy with antibodies (Vivier et al., 2024). B cells, upon antigen-specific activation, become antibody-producing plasma cells and mediate humoral anti-tumor immunity. The presence of B cells, which often form follicular-like structures in the tumor microenvironment (TME), is considered as a potential prognostic biomarker. It is now clear, that the cooperative interactions between these immune cells are essential for an effective anti-tumor response.

T cell priming, the process that generates effector and memory T cells, has been extensively studied in response to infectious agents, and similar fundamental principles likely apply to cancer. Naive T cells, which can undergo priming in tumor-draining lymph nodes or tertiary lymphoid structures within solid tumors, produce both effector and memory T cells. These cells give rise to terminally differentiated effector-like cytotoxic T cells, which can reside in various locations such as blood, lymphoid organs, tissues, or tumors. Prolonged exposure to an antigen leads T cells to upregulate activation markers, including negative regulators like PD-1, leading to the emergence of effector T cells exhibiting increasing levels of functional exhaustion (***Figure 18***) (Chen and Mellman, 2017).

T-cell exhaustion was first observed during chronic lymphocytic choriomeningitis virus (LCMV) infection in mice and later observed in human cancers. In the tumor microenvironment, exhausted T cells overexpressed inhibitory receptors including programmed cell death protein 1 (PD-1), lymphocyte activation gene 3 protein (LAG-3), T-cell immunoglobulin domain and mucin domain protein 3 (TIM-3), cytotoxic T lymphocyte antigen-4 (CTLA-4), band T lymphocyte attenuator (BTLA) and T-cell immunoglobulin and immunoreceptor tyrosine-based inhibitory motif domain (TIGIT) (Jin et al., 2010). They are also characterized by reduced effector cytokine production such as interferon-γ (IFN-γ), granzyme B (GzmB), interleukin-2 (IL-2) and tumor necrosis factor-α (TNF-α). Exhausted $CD8^+$ T cells also exhibit diminished cytolytic activity, leading to the failure of cancer elimination. Indeed, it is well-described that $CD8^+$ CTLs are significantly reduced in tumor tissue from patients with localized prostate cancer and exhibit an exhausted phenotype (Japp et al., 2015; Sfanos et al., 2009). Furthermore, human prostatic adenocarcinomas are infiltrated by terminally differentiated cytotoxic T lymphocytes that are, however, in an unresponsive state (Bronte et al., 2005). Restoring these exhausted T cells has proven to be a promising strategy for cancer treatment, and has led to significant breakthroughs in cancer immunotherapy (Jiang et al., 2015).

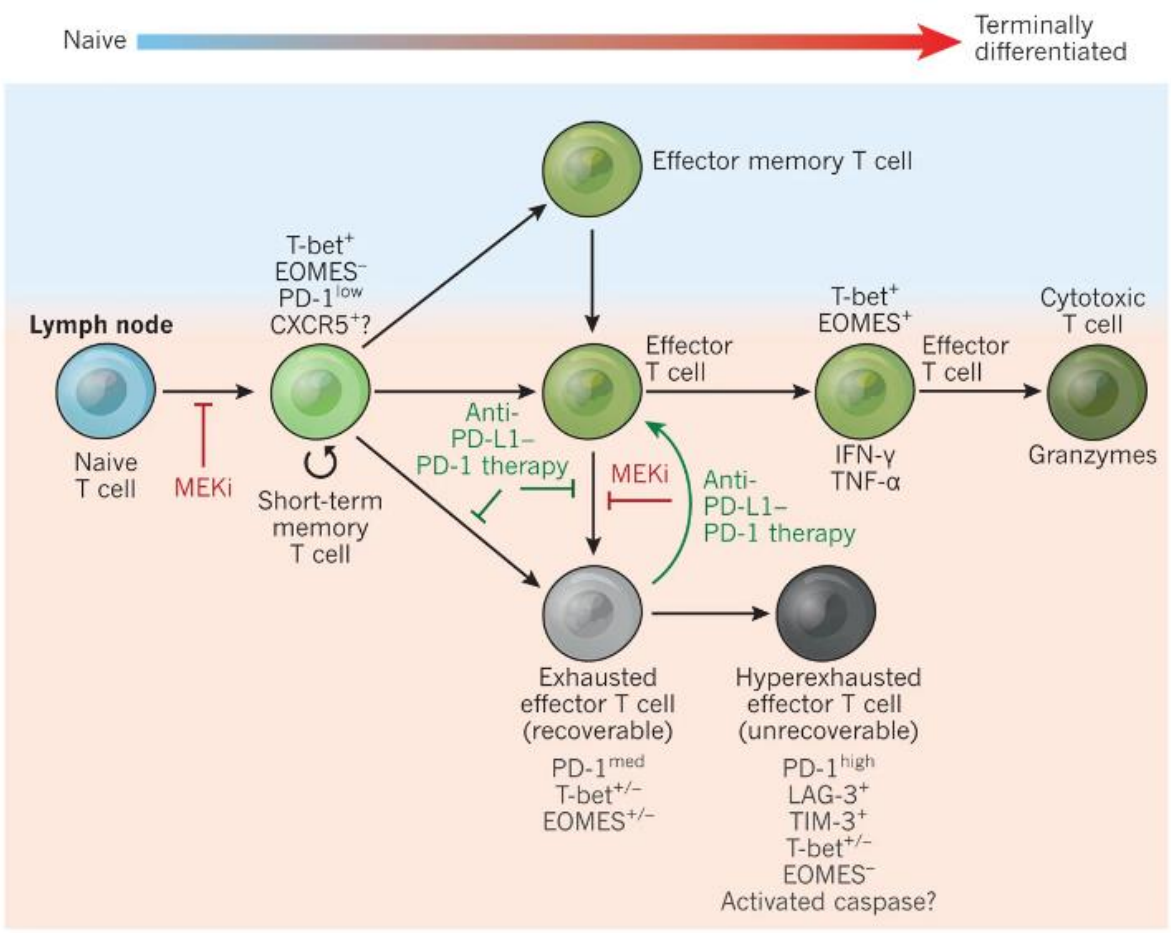

Figure 18. The development of various CD8-expressing T cell populations, including effector T cells, memory T cells, and exhausted T cells, is illustrated, with the expression of relevant proteins indicated for each stage. *Initially, naive CD8$^+$ T cells typically reside in lymph nodes and the spleen. Upon exposure to and activation by an antigen, these cells can differentiate into short-term memory T cells, which have the capacity to proliferate and differentiate further into effector T cells, effector memory T cells, central memory T cells (not depicted here), and cytotoxic T cells. However, with chronic antigen exposure, effector T cells may gradually become exhausted. Notably, only freshly exhausted cells expressing relatively low levels of PD-1 (PD-1^{med}) may be recoverable upon treatment with anti-PD-L1/PD-1 therapies, while 'hyperexhausted' effector T cells expressing high levels of PD-1 (PD-1^{high}) along with other activation markers (e.g., LAG-3, TIM-3, or TIGIT) may be irreversibly exhausted. Hyperexhausted effector T cells may represent T cells that are committed to a pathway of TCR-induced apoptosis due to chronic TCR stimulation. Treatment with anti-PD-L1/PD-1 or inhibitors of the mitogen-activated protein kinase pathway (MEKi) may mitigate T-cell exhaustion by attenuating the strength of the TCR signal. Key proteins involved in this process include EOMES (eomesodermin) and TNF (tumor necrosis factor). Figure source adapted from (Chen and Mellman, 2017).*

3.6 Elements of an immunosuppressive tumor microenvironment

The development and progression of prostate cancer are closely linked to persistent inflammation triggered by cellular and genomic damage caused by prostatitis. This chronic inflammation within the prostate leads to restructuring of the extracellular matrix and initiates epithelial mesenchymal transition, both pivotal processes in the development and progression of the disease (Cai et al., 2019). Lymphocytes, including natural killer cells, $CD8^+$ T cells, and $CD4^+$ helper T cells, as well as proinflammatory macrophages and DCs, contribute to anti-tumor immune responses. However, tumors are usually infiltrated with cells that appear to have an immunosuppressive function. This is often due to chronic inflammation and results from chemotactic factors released by tumor cells. The best-known immunosuppressive cells, such as $Foxp3^+$ regulatory T cells, the heterogeneous $Gr1^+$ MDSCs, and M2 macrophages, as well as the cancer cells themselves, secrete various mediators that effectively hinder immune responses. Key mediators that have also been associated with poor prognosis in various solid tumors including prostate cancer, include indoleamine 2,3-dioxygenase (IDO) (Vidotto et al., 2019; Zhai et al., 2020), arginase-1 (Grzywa et al., 2020; Matos et al., 2021), cyclooxygenase-2 (COX-2) (Brizzolara et al., 2017; Hashemi Goradel et al., 2019), and cytokines such as TGF-β, IL-10, and VEGF (Huijbers et al., 2022; Yu and Ho, 2019).

To date, only a few studies have shown the expression and/or activity of Arg1 and Arg2 in malignant prostatic cells, which appear to be influenced by androgens. Both isoforms have been detected in both androgen-dependent and androgen-independent prostate cancer cells, with androgen-dependent cells tending to exhibit higher Arg2 activity compared to androgen-independent prostate cancer cell lines (Mumenthaler et al., 2008). In androgen-dependent cells, both Arg1 and Arg2 expression is associated with activation of immunosuppressive pathways and stimulation of proliferation in a androgen receptor dependent manner (Gannon et al., 2010). Additionally, inhibition of COX-2 may be a good way to achieve therapeutic results in prostate cancer as administration of COX-2 inhibitors reduce the risk of cancer by approximately 68% (Brizzolara et al., 2017). Moreover, studies suggest that the immunosuppressive nature of the tumor microenvironment may also be due to a combination of factors, including hypoxia, low pH, restricted nutrient availability such as glucose deprivation and abundance of tumor cell-derived metabolites like citrate, lactate and fatty acids. This imbalance has been shown to impair the differentiation, proliferation, and function of effector tumor-infiltrating T lymphocytes (Liu et al., 2022; Philippe and Hubert, 2016). Since $CD8^+$ T cells are the primary mediators of anticancer immunity, modulation of the $CD8^+$ T cell response is central to immunotherapy to treat cancer.

3.6.1 Association of PTEN deficiency with an immunosuppressive TME

Interestingly, in addition to its role in PCa biology, PTEN also influences the composition of the inflammatory tumor microenvironment (Cetintas and Batada, 2020). Functionally intact PTEN is associated with the activation of pro-inflammatory IFN-I and NF-kB signaling pathways. Studies using oncolytic viruses have shown that loss of PTEN plays a critical

role in mediating innate antiviral immunity (Li et al., 2016). PTEN-deficient cancer cells exhibit reduced type I interferon responses and increased susceptibility to viral infections. These alterations in interferon regulation pathways by PTEN likely contribute to pro-tumorigenic effects and impact the innate immunity. Consequently, PTEN-deficient tumor cells may be more susceptible to IFN-sensitive oncolytic viruses, which has important implications for future oncolytic therapy trials targeting PTEN-deficient prostate cancers (Champion et al., 2016).

Moreover, loss of PTEN in melanoma has been shown to reduce T cell recruitment and function in tumors, promote immune resistance and lead to poorer outcomes in anti-PD-1 immunotherapy. This has been demonstrated both clinically, by analyzing independent cohorts of melanoma clinical samples, and preclinically, where PTEN loss induced *in vivo* the expression of immunosuppressive cytokines, in particular CCR2 and VEGF (Peng et al., 2016). Consistent with this finding, PTEN-deficient PCa tumors from patients exhibit higher $Foxp3^{+}$ Treg cell infiltration in both the stroma and tumor parenchyma, especially in patients with metastasis, and overexpress the IDO1 protein. This phenotype is associated with an immunosuppressive state and resistance to immunotherapy (Vidotto et al., 2019). Additionally, *in vitro* and *in vivo* studies using the TRAMP prostate mouse model have shown that PTEN loss in prostate cancer cells results in progressive dysregulation of the transcription factors NF-κB and STAT1, leading to increased production of the angiogenic CXC chemokines, CXCL12 and CXCL8 (Shen and Lentsch, 2004). Furthermore, *in vitro* studies with murine prostate epithelial cells and human prostate cancer cell lines have demonstrated that PTEN loss, via Akt1 activation, drives the expression of CXCR4 and CXCL12 (Conley-LaComb et al., 2013). *In vitro* analyses of prostate cancer cell lines and prostatic tissue demonstrated, that PTEN inactivation was also associated with the expression and secretion of the pro-inflammatory chemokine CXCL8 (Maxwell et al., 2014). Loss of PTEN function concomitantly increases the expression of CXCL8 receptors (CXCR1 and CXCR2), with the elevated autocrine CXCL8 signaling sustaining the viability of PTEN-deficient prostate cancer cells.

Collectively, evidence indicate that PTEN-deficient tumors across various cancer types are characterized by reduced levels of cytotoxic T cells, helper T cells and NK cells, as well as elevated pro-oncogenic inflammatory cytokines such as CCL2 and increased levels of immunosuppressive cells such as Tregs and MDSCs (***Figure 19***). The mechanism linking PTEN deficiency to immunosuppression may occur either indirectly, through dysregulation of the PI3K/Akt pathway and DNA damage, or directly due to the inability of PTEN deficient cells to activate the interferon signaling pathway. The PTEN controls the nuclear import of interferon regulatory factor 3 (IRF3), a key transcription factor for IFN production. Thus, PTEN deficiency results in a lack of IFN production and subsequently to a failure in the recruitment of cytotoxic leukocytes and the activation of T cell responses, which are crucial for tumor regression (Cetintas and Batada, 2020; Vidotto et al., 2020). In summary, alterations in PTEN and its interplay with other genes in mouse models of prostate cancer collectively influence immune-cell content and the expression of immunosuppressive markers in the TME.

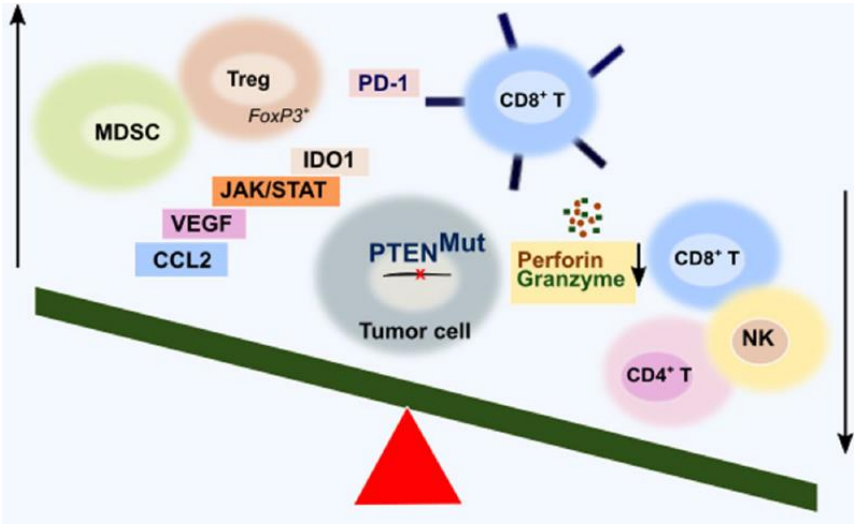

Figure 19. Immunosuppressive traits of PTEN mutant tumors. *PTEN-deficient tumors are characterized by infiltration of myeloid-derived suppressor cells (MDSCs) and regulatory T cells (Tregs). Activation of the JAK/STAT pathway, increased expression of IDO1 protein, upregulation of PD-1 receptors, and elevated levels of inhibitory cytokines are observed. Additionally, infiltration of CD4+, CD8+, and NK cells is reduced, and cytotoxic T lymphocytes show diminished lytic activity due to depletion of granzyme and perforin. Source figure from (Cetintas and Batada, 2020).*

3.7 Treatment landscape of PCa

Since prostate cancer covers a broad spectrum from indolent to very aggressive disease, there are different treatments that can be used depending on the stage of the diagnosis. Since one of the first observations on PCa patients was the increase of androgen receptor molecules on the cell surface of the tumor cells, androgen deprivation therapy (ADT) was the first therapeutic approach to show successful temporal regression. It is usually carried out chemically by administration of a leuteinizing-hormone-releasing hormone (LHRH) agonist, such as leuprolide acetate or zoledronic acid. Reports indicate that following the initiation of ADT, there is a short-term increase in the number of naïve T cells and Th-1 cells, along with a decrease in the number of regulatory T cells (Kissick et al., 2014; Page et al., 2006).

Currently, the recommended combination of treatment following early-stage PCa detection includes active surveillance, external radiotherapy, brachytherapy, radical prostatectomy and/or hormone therapy (ADT). Although these treatments are efficient in 70-80% of cases, they are usually accompanied by complicated side effects that can greatly impact the patient's quality of life (e.g. asthenia, urinary incontinence, erectile dysfunction) (Korfage et al., 2005). Additionally, besides the immunostimulatory benefits of standard ADT in PCa, patients will eventually relapse. For metastatic tumors on the lymph nodes or other sites, clinical trials are currently carried out with various second-generation AR antagonists (Abiraterone acetate, Enzalutamide, Apalutamide, Darolutamide) administered either as

single agents or together with other drugs and have been shown to prolong survival in early-stage patients. Chemotherapy with docetaxel, abiraterone and cabazitaxel drugs is also applied (Parker et al., 2015).

Despite the very high response rate to AR targeting interventions in metastatic PCa patients, treatment with ADT can induce changes in tumor cells that allow them to grow in androgen-depleted conditions. These changes can include tumors acquiring gene amplifications of the AR (Visakorpi et al., 1995), mutations arising in the AR (Eisermann et al., 2013), activation of the AR occurring independently of androgen (Lyons et al., 2008), tumors upregulation of steroidogenic enzymes (Pfeiffer et al., 2011) including de novo intratumoral androgen synthesis from androstenedione and DHEA (Cai et al., 2011), and persistent occupation of AR on DNA binding sites independent of ligand (Decker et al., 2012). Subsequently, nearly all advanced castration-sensitive PCa patients, relapse to metastatic Castration Resistant Prostate Cancer (mCRPC), which is hallmarked by high morbidity and mortality (Grabowska et al., 2014). The median life expectancy of CRPC patients is 16 to 18 months, and second-line therapies are able to increase the median overall survival by only a few months.

The latest approved drugs for mCRPC include the radium-223 dichloride to reduce bone metastases, the vaccine Sipuleucel-T immunotherapy, the taxane-based chemotherapy, the PSMA-targeting approaches, and the PARP inhibitors (Olaparib, Rucaparib) (***Figure 20***) (Gillette et al., 2023; Nevedomskaya et al., 2018). As life expectancy has increased significantly in the last decades it is expected that the male population with prostate cancer will increase accordingly. There is therefore an urgent need, to find new approaches to manage or cure the disease.

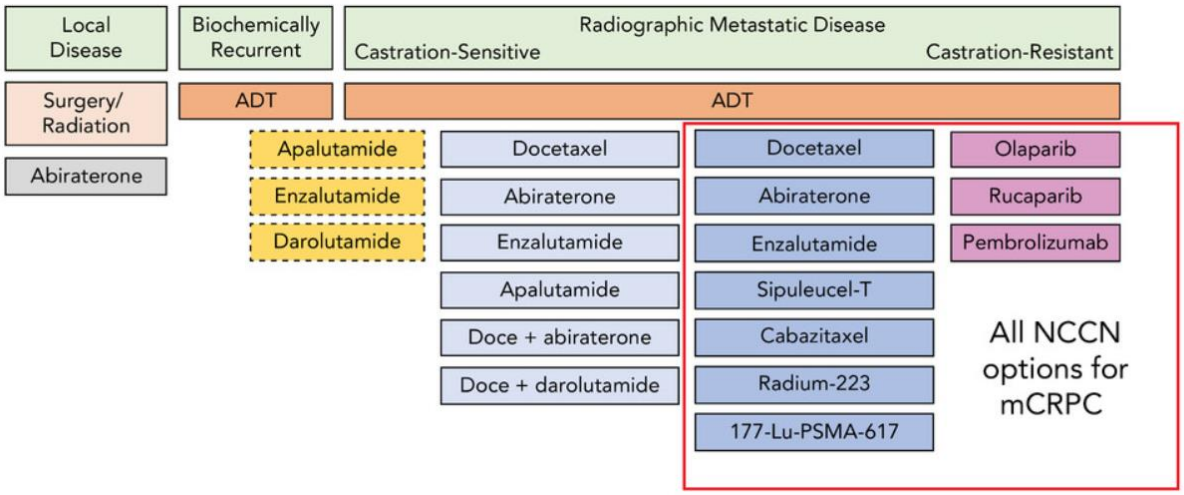

Figure 20. Treatment landscape for advanced prostate cancer based on National Comprehensive Cancer Network (NCCN) Clinical Practice Guidelines in Oncology 2023. *Abbreviations: ADT, androgen deprivation therapy; Doce, docetaxel; mCRPC, metastatic castration-resistant prostate cancer; NCCN, National Comprehensive Cancer Network. Adapted from (Ajmera et al., 2023).*

3.7.1 A focus on immunotherapy

Despite the proven survival benefit, current treatments for prostate cancer patients are noncurative, they are associated with toxicities and yield a median survival of approximately 3 years among patients with mCRPC (Francini et al., 2019). In this regard, therapeutic strategies leveraging the immune system against tumor cells have made significant progress over the past decade and are increasingly becoming a critical component of combination therapies for the treatment of patients with advanced solid tumors. However, past studies have shown that immunotherapy for prostate cancer has modest efficacy on patients (Von Amsberg et al., 2022). Nevertheless, various approaches to immunotherapy have been explored in PCa patients based on an initial set of potential PCa antigens such as PSA (***Figure 21***).

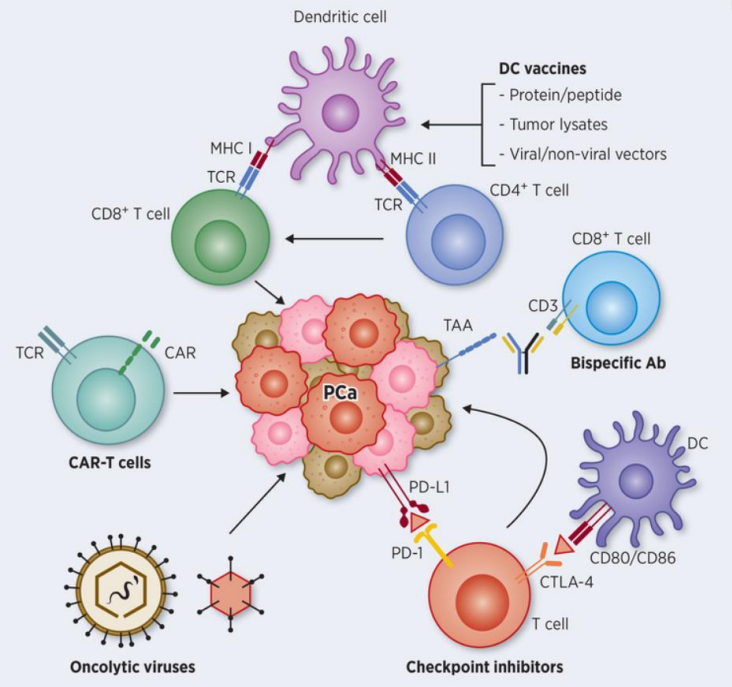

Figure 21. Major immunotherapy pathways targeting PCa. *Source figure from (Cha et al., 2020).*

3.7.2 Vaccine-based immunotherapy

A major challenge in oncology is the pronounced tumor heterogeneity across cancer types, but also among patients with the same cancer type, each exhibiting unique phenotypic characteristics. To overcome this problem, the concept of precision medicine has emerged by tailoring treatments to individual patients (Hoeben et al., 2021). This approach is now implemented in various cancers including breast, melanoma, oral and prostate cancers (Hawkey et al., 2023).

Several personalized vaccines are currently being evaluated in clinical trials as part of personalized treatment. Somatic mutations in cancer can generate cancer-specific neo-epitopes (tumor associated antigens or TAA), recognized as foreign entities by autologous T-

cells, making them ideal targets for cancer vaccines. Although each cancer exhibits distinct mutations, some neo-antigens are shared across different cancers (Ott et al., 2018). The goal of therapeutic vaccines is to enhance the host's immune system response against cancer cells.

Sipuleucel-T, the first personalized therapeutic prostate cancer vaccine, received FDA approval on April 2010 (Provenge; Dendreon Inc) (Drake, 2010). This vaccine is produced by *ex vivo* activation of autologous peripheral-blood mononuclear cells with a recombinant fusion protein comprising a common prostate cancer antigen, the prostatic acid phosphatase (PAP), and granulocyte-macrophage colony-stimulating factor (GM-CSF) as adjuvant. The process involves leukapheresis to enrich monocytes, followed by incubation with the immunogen fused protein. After intravenous administration, these autologous monocytes mature into functional antigen-presenting cells (APCs), and subsequently activate PAP-specific $CD4^+$ and $CD8^+$ T cells, which then migrate to the tumor sites, and trigger an anti-tumor response (***Figure 22***).

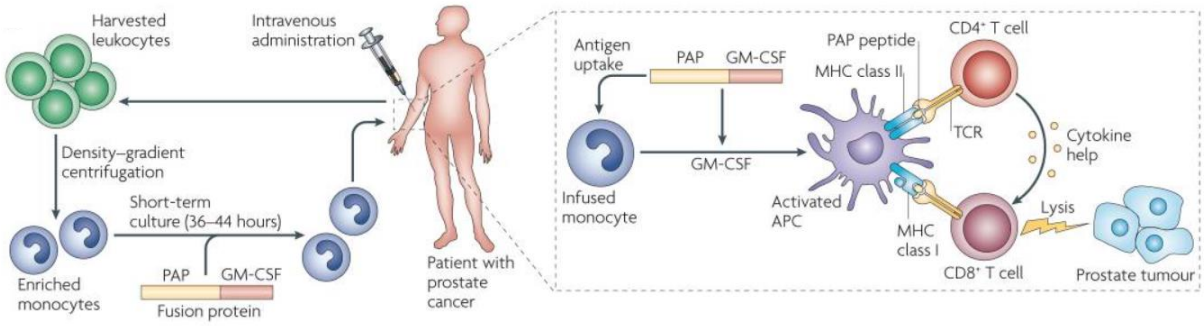

Figure 22. Sipuleucel-T immunotherapy. *T cell activation follows a two-step process. Initially the antigen is taken up by the antigen-presenting cells (APCs), digested internally, associated with a major histocompatibility complex (MHC) molecule, and then presented on the APC's surface. The second step involves binding of costimulatory molecules on the APC and T cell. Abbreviations: PAP = prostatic acid phosphatase; GM-CSF = granulocyte-macrophage colony-stimulating factor. Adapted from (Drake, 2010).*

Sipuleucel-T is used for metastatic castration-resistant prostate cancer and was validated in a randomized, double-blind, placebo-controlled phase III trial (Immunotherapy for Prostate Adenocarcinoma Treatment - IMPACT: NCT00065442). This trial showed that patients administered with Sipuleucel-T exhibited prolonged survival (by 4.1 months) compared to those who received a placebo, and a 22% reduction of relative mortality risk (Kantoff et al., 2010). Additionally, patients treated with Sipuleucel-T exhibited higher antigen-specific T cell proliferation and IFNγ secretion compared to control patients (Sheikh et al., 2013). Despite FDA approval, approval in Europe was withdrawn at the request of the marketing authorization holder, limiting its clinical application. However, ongoing studies combining Sipuleucel-T with AR-targeting agents (Hafron et al., 2022), atezolizumab (Dorff et al., 2021), or radio-223 (Marshall et al., 2021) in patients with mCRPC are promising.

Other PCa vaccines have followed, such as, GVAX (BioSante), which was synthesized from two prostate cancer cell lines, LNCaP and PC-3 transfected with a human GM-CSF gene.

However, GVAX failed in two phase III clinical trials applied as monotherapy or in combination with docetaxel (VITAL-1; VITAL-2) (Arlen et al., 2009). Similarly, the Poxvirus-based vector vaccine ProstVac VF–TRICOM (Bavarian Nordic), did not improve the Overall Survival (OS) on the phase III clinical trial and was not approved by the FDA and the EMA (Gulley et al., 2019). The mRNA vaccine CV9104, encoding 6 prostate specific antigens (PSA, PSMA, PSCA, STEAP1, PAP, MUC1) also failed to improve OS in mildly or asymptomatic mCRPC compared to standard therapy (Stenzl et al., 2017). Thus, Sipuleucel-T remains the only FDA-approved vaccine against PCa.

3.7.3 Immune Checkpoint Inhibitors (ICI) as monotherapy

Immune Checkpoint Inhibitor therapy, known as ICIs, includes antibodies targeting the cytotoxic T lymphocyte-associated protein 4 (CTLA-4) and the programmed death 1/programmed death ligand 1 (PD-1/PD-L1). ICIs have revolutionized oncology by enabling the immune system to trigger an antitumor responses, significantly prolonging survival in various cancers, including melanoma, lung, urothelial, lymphoma, cervical, gastrointestinal, breast and renal-cell carcinoma (Bellmunt et al., 2017; Ellis et al., 2017; Hodi et al., 2010; Motzer et al., 2015; Rosenberg et al., 2016). The emphasis on immune checkpoint inhibitors has also led to numerous trials in PCa, and in particularly in metastatic patients, but unfortunately, ICI monotherapy has shown limited efficacy in mCRPC (Beer et al., 2017; Hansen et al., 2018; Kwon et al., 2014; Topalian et al., 2012).

3.7.3.1 CTLA-4

CTLA-4, or cytotoxic T-lymphocyte-associated protein 4, is a costimulatory molecule expressed on activated T cells, and inhibits their functions. Ipilimumab (MDX-010; Bristol-Myers Squibb/Medarex) and tremelimumab (CP-675206; Pfizer) block CTLA-4. Studies in animal models have demonstrated that blocking CTLA-4 with antibodies can boost antitumor immunity. The effectiveness of CTLA-4 blockade has been studied across various malignancies, with the most comprehensive and outstanding data emerging from trials involving patients with melanoma. CTLA-4 blockade has shown an approximate 10% objective response rate. Notably, in advanced melanoma patients treated with ipilimumab, some individuals have survived for up to ten years (Schadendorf et al., 2015). However, as anticipated from findings in mice, CTLA-4 blockade is associated with 25–35% incidence of clinically significant immune-related toxicity (Lipson and Drake, 2011).

Preclinical studies combining CTLA-4 blockade with GM-CSF showed promising results and a phase I clinical study on 17 mCRPC patients combining a CTLA-4 specific antibody (ipilimumab) with GM-CSF was developed to stimulate an endogenous antitumor immune response (Fong et al., 2009). However, a phase III clinical trial with ipilimumab monotherapy was discontinued, because no benefit in the median OS (Overall Survival) was demonstrated

in chemotherapy-naïve patients with minimally symptomatic mCRPC compared to the placebo group (Beer et al., 2017).

3.7.3.2 PD-1 / PD-L1

Programmed death-1 (PD-1) and anti-programmed death-ligand 1 (PD-L1) are type I transmembrane glycoproteins transcribed by PDCD1 (located on chromosome 2) and CD274 genes (located on chromosome 9) respectively. PD-1, which is expressed on activated T cells, B cells, natural killer (NK) cells, and monocytes, interacts with PD-L1, which is found on both immune and non-immune cells (Patsoukis et al., 2020; Sun et al., 2018). PD-1 is a negative costimulatory receptor playing a critical role in maintaining T cell immune homeostasis and peripheral tolerance, preventing T cell hyperactivation and autoimmune responses. When PD-1, binds to its ligands PD-L1 and PD-L2, it inhibits the function of cytotoxic effector T cells, and thus suppresses the antitumor immune response. Additionally, other immune or stromal cells within the tumor microenvironment may also contribute to immunosuppression. Tumor cells expressing PD-L1 evade the T cell antitumor response through anergy, or apoptosis of effector T cells (Francisco et al., 2010; Muenst et al., 2016). PD-1 and PD-L1 inhibitors counteract these effects by blocking their respective targets, thereby reducing the ability of cancer cells to evade antitumor immunity (Xiong et al., 2021).

Several preclinical studies have investigated the expression of PD-1/PD-L1 in prostate cancer specimens to evaluate the potential rationale for treatment with checkpoint inhibitors in these patients. On the one hand, one study showed that the ICI ligands (PD-1, PD-L1/2 & CTLA-4) are amplified in patients with mCRPC who exhibited resistance to enzalutamide (AR antagonist), indicating that tumor resistance to enzalutamide correlates with increased expression of PD-L1 (Bishop et al., 2015). On the other hand, many other studies have shown that PCa has a relatively low expression level of PD-L1 (Baas et al., 2017; Martin et al., 2015; Massari et al., 2016). However, the evaluation methods for PD-L1 expression vary from one study to another, and the contradictory results obtained so far call into question the reliability of PD-L1 as a biomarker for guiding ICI treatment decision.

A systematic analysis of the literature review explains that the ERK/MEK, Akt-mTOR, NF-kB, and JAK/STAT signaling pathways upregulate PD-L1 expression, while inhibitors of these pathways have opposite effects (Palicelli et al., 2021). Additionally, altering the status of PD-L1 in prostate cancer cells has different effects in human and mouse PC-cell lines. When PD-L1 is downregulated, inhibited, or blocked, there is a notable reduction in both chemoresistance and tumor cell migration. Interestingly, co-culturing prostate cancer cells with NK cells, $CD8^+$ T cells, or chimeric antigen receptor T cells (CAR-T cells) shows an enhancement in immune cells cytotoxic activity when PD-L1 is downregulated, inhibited, or blocked. Conversely, the upregulation or activation of PD-L1 leads to opposite effects (Palicelli et al., 2021). Furthermore *in vivo* resistance to radiotherapy was found to correlate with increased expression of PD-1 in infiltrating $CD45^+/CD8^+$ T cells in a subcutaneously injected murine prostate tumor model (Philippou et al., 2020). While PD-L1 blockade appears

promising for PCa treatment in murine studies, ICI inhibitors of the PD-1/PD-L1 pathway have limited antitumor effect in human trials.

Atezolizumab, a monoclonal antibody against PD-L1, is well tolerated and effective in multiple cancers, but its safety and efficacy in mCRPC patients was only recently evaluated in a phase I clinical trial. The results indicated a similar safety profile to other tumor types as the drug was well tolerated by patients, but the median Overall survival is noy yet defined (Petrylak et al., 2021).

Pembrolizumab, a humanized monoclonal antibody of PD-1, intervenes in the PD-1/PD-L1 pathway by binding to PD-1 and blocking its interaction with PD-L1 and PD-L2 (Pardoll, 2012). Recently approved by the US FDA, pembrolizumab, is indicated for the treatment of microsatellite instability-high (MSI-H) or mismatch repair-deficient (dMMR) metastatic castration-resistant prostate cancer (mCRPC) following disease progression on one or more systemic therapies (Marcus et al., 2019). Additionally, monotherapy with pembrolizumab, has recently shown promising therapeutic efficacy, but only in a very specifically selected group of mCRPC patients (Antonarakis et al., 2020).

3.7.3.3 ICI in combination with other treatments

Given the modest results of ICI as monotherapy in patients with mCRPC, current research is focusing on the combination of therapies (Rebuzzi et al., 2022). Several clinical trials are currently exploring the combination of immune checkpoint inhibitors with standard treatments for patients with metastatic castration-resistant prostate cancer. The randomized IMbassador 250 trial, comparing atezolizumab (anti-PDL1) with enzalutamide (androgen inhibitor) or enzalutamide alone on 759 patients with mCRPC showed no survival benefit of the combined molecules (Powles et al., 2022). However, immune biomarker analysis suggested better response to treatment in the few patients (2%) with higher PD-L1 expression and $CD8^+$ T cell infiltration, while the majority of patients (98%) had low PD-L1 expression and low $CD8^+$ T cell infiltration, suggesting that patient selection may be required for a beneficial response to ICI therapies. The randomized double-blind phase III KEYNOTE-641 clinical trial (NCT03834493), initiated on July 2019 and evaluating the efficacy and therapeutic safety of the pembrolizumab (anti-PD1) and enzalutamide combination vs. enzalutamide plus placebo on patients with mCRPC is showing promising results (Graff et al., 2021).

Other combinatorial therapeutic approaches in ongoing PCa trials include nivolumab, another humanized monoclonal antibody of PD-1, approved on 2015 by the FDA for the metastatic non-small cell lung cancer (Kazandjian et al., 2016). Examples of these trials are: the Rad2Nivo trial (NCT04109729), which investigates the combination of nivolumab with radium-223, and the phase III Checkmate 7DX trial (NCT04100018), which assesses the combination of nivolumab with docetaxel (chemotherapy). The latter trial is based on the recent findings that docetaxel-based chemo-hormonal therapy is able to reprogram the tumor microenvironment by enhancing the DNA-cGAS/STING-IFN signaling pathway, leading to increased T cell infiltration and PD1 upregulation, thereby sensitizing mouse tumors to the anti-PD1 blockade (Ma et al., 2022). However, we should keep in mind, that it still remains

challenging to discriminate the actual impact of a single drug in such combinations without a comparator arm.

As an alternative strategy, other ongoing clinical trials for mCRPC adopt combinations of immune checkpoint inhibitors. Combination clinical trials in mCRPC patients of Sipuleucel-T with either ipilimumab (anti-CTLA4) (NCT01420965) or pidilizumab (anti-PD1) & cyclophosphamide (chemotherapy) (NCT01832870), have been unfortunately terminated due to drug supply issues, without any result reported. However, promising were the results of a follow-up study 2.5 years after the end of a randomized phase III trial comparing ipilimumab with placebo in 799 mCRPC patients following radiotherapy who had progressed on docetaxel therapy. While the primary analysis did not show statistically significant differences in terms of OS in the two treatment arms (Kwon et al., 2014), after long follow-up the survival favored the group of men who received ipilimumab, with overall survival rates being two to three times higher at 3 years and beyond (Fizazi et al., 2020). This suggests that longer follow-up of the patients received immunotherapy may be needed to better understand the efficacy of the treatment.

3.7.4 Myeloid targeting treatments

In tumors, CSF1 signaling promotes the survival of macrophages and their polarization into an ARG1, CD206, and IL-10 positive anti-inflammatory phenotype, while simultaneously inhibiting a NOS2 and IL-12 positive pro-inflammatory phenotype (Priceman et al., 2010). Inhibition of CSF1R or CSF1 typically results in reduced accumulation of TAMs, impaired vascularization, and enhanced infiltration of cytotoxic $CD8^+$ T cells (Cannarile et al., 2017; Pyonteck et al., 2013). Therefore, it is perhaps unsurprising that blocking CSF1R enhances antitumor T cell responses and promotes regression of pancreatic tumors and melanoma during checkpoint blockade (Zhu et al., 2014).

In prostate cancer, both in patients and preclinical models, androgen deprivation therapy induces the production of macrophage attracting cytokines, CSF-1 in particular. Inhibition of the CSF-1R tyrosine kinase had synergistic antitumor effect with androgen inhibition (Escamilla et al., 2015; Nonomura et al., 2011). Recently, a phase I clinical study (NCT00757757) evaluated the immunological and clinical activity, as well as the safety profile of CSF1R inhibition with the mAb LY3022855 in patients with advanced metastatic castration-resistant prostate cancer (mCRPC) or refractory metastatic breast cancer (MBC) (Autio et al., 2020). The treatment was well tolerated, with circulating CSF-1 levels increasing across dose cohorts, and a trend for increased immune activating genes was observed in patients with clinical benefit. The study highlighted that targeting tumor-associated macrophages earlier in the disease course may be much more beneficial.

Cytokines, especially interleukins, represent alternative promising prognostic targets in various human cancers, including prostate cancer. The goal is to direct the host's immune system against cancer cells. Elevated circulating levels of interleukin 6 (IL-6) and 8 (IL-8) have been associated to unfavorable outcomes in patients with metastatic prostate cancer

(Drachenberg et al., 1999; Harshman et al., 2020). The C-X-C motif chemokine receptor 2 (CXCR2), also known as IL-8RB, is a receptor for IL-8 primarily expressed in granulocytes and macrophage progenitor cells (Han et al., 2019). Through its ligand interactions, CXCR2 enables potent chemotaxis, which contributes to tumor progression, angiogenesis, invasion, metastasis, and chemoresistance. Consequently, CXCR2 is considered a marker of poor prognosis in various tumor types. Indeed, CXCR2 blockade has been reported to reprogram tumor-associated macrophages (TAMs) and suppress tumor growth in mouse models of pancreatic ductal adenocarcinoma (PDAC) and also to increase the efficacy of anti-PD-1 inhibitors by increasing T-cell infiltration (Steele et al., 2016). Similarly, inhibition of CXCR2 in a lung cancer mouse model decreased tumor-associated neutrophils, increased anti-tumor T cell activity through enhanced $CD8^+$ T cell activation and increased the therapeutic effect of cisplatin treatment (Y. Cheng et al., 2021).

Recently, (Di Mitri et al., 2019) showed that CXCR2 blockade in prostate cancer triggers TAMs re-education, leading to tumor inhibition. CXCR2-KO monocytes infused in $Pten^{pc-/-}$; $Trp53^{pc-/-}$ tumor-bearing mice differentiate into TNFα-releasing pro-inflammatory macrophages that induce senescence in tumor cells. PTEN-null tumors show higher sensitivity to TNF-α-induced senescence because TNFR1 is upregulated. Previously, the same group had used CXCR2 blockade to prevent the recruitment of $CD11b^+$ $Gr1^+$ myeloid cells in $PTEN^{-/-}$ prostate tumors. They showed that the total number of $CD11b^+$ $Gr1^+$ cells was significantly decreased in the treated $PTEN^{-/-}$ mice at 11.7%, versus 23.3% in the untreated $PTEN^{-/-}$ mice but was not completely blockade or as low as in the steady-state non treated WT mice (5% infiltration). Additionally, since the Gr1 marker stains both $Ly6G^+$ & $Ly6C^+$ cells, it remains unclear whether the $Ly6G^+$ neutrophil infiltration at the tumor site is impaired. Last but not least, a multi-centric phase I/II proof of concept clinical trial, with the CXCR2 antagonist AZD5069 in combination with the AR antagonist enzalutamide in patients with mCRPC is currently ongoing (NCT03177187).

3.7.5 Adoptive Cellular Therapy

Adoptive cellular therapy (ACT) is a promising approach for a personalized immunotherapy in cancer, in which patient's own T cells are genetically modified before being reinfused to the patients. In the context of prostate cancer treatment, particularly in cases of metastasis or advanced disease, various ACT methods have been developed and are tested. These include engineered T cell receptors, tumor-infiltrating lymphocytes, and chimeric antigen receptor (CAR) T cells (Perica et al., 2015).

Among these engineered T cells, CAR-T cells have shown the most significant therapeutic potential. CAR-T cells are engineered in the laboratory to express a specific CAR gene, which targets antigens using a single-chain variable fragment (scFv) derived from antibodies. After infusion into the patient, the CAR-T cells trigger an inflammatory response that leads to the destruction of tumor cells expressing the targeted antigen (Titov et al., 2020). CAR-T cells are employed in patients with prostate cancer to target prostate-specific membrane antigen (PSMA), a type II transmembrane glycoprotein that is specifically

upregulated in prostate cancer cells. Encouragingly, the results of the phase I clinical trial, of the PSMA-directed/TGFβ-insensitive CAR-T cell therapy in patients with mCRPC passed the safety control (Narayan et al., 2021). Nevertheless, future clinical investigations should be done to assess the anti-tumor efficacy of this treatment. Despite this potential, CAR-T cell therapy has shown so far a better clinical response in hematological malignancies than in solid tumors, including PCa (Mehrabadi et al., 2022). Besides CAR-T cells, recent experiments focusing on tumor-infiltrating lymphocytes (TILs) in prostate cancer have demonstrated the potential to expand TILs that exhibit reactivity against PCa. In a particular study, 28 cultures of TILs derived from PCa were successfully extracted and expanded *in vitro* capable of producing high levels of IFNγ in response to stimuli (Yunger et al., 2019).

Bi-specific antibodies, directed against both CD3 on T cells and tumor-associated antigens (TAA), represent a promising novel approach for the treatment of hormone-refractory prostate cancer (CRPC). These antibodies work by recruiting cytotoxic T cells to cancer cells, potentially enhancing the immune response against the tumor. In this context, diverse combinations of bispecific conjugates have been explored, which have led to encouraging results (Baeuerle and Reinhardt, 2009). Particularly the a site-specific bispecific antibody incorporating moieties of PSMA and anti-CD3 Fab, has shown potent activity in both *in vitro* studies and *in vivo* xenograft PCa models (Kim et al., 2013). While bispecific antibodies were rather inefficient in clinical trials until recently, it was not until 2019 that a phase I study of a PSMA-targeted bi-specific T cell agent (pasotuxizumab) in mCRPC showed a dose-dependent antitumor activity, with two patients showing a durable response for over one year (Hummel et al., 2019). This is the first clinical study to showi that Bispecific T cell Engager (BiTE) immunotherapy can be effectives in solid tumors. Since then, more studies are focusing on the use of bispecific antibodies as a potential therapeutic treatment for mCRPC such as the study testing BiTE molecule with an extended half-life (Deegen et al., 2021).

Although these findings are promising, challenges remain for CAR-T cell therapy, TILs and bispecific antibodies, primarily due to the immunosuppressive nature of the tumor microenvironment in PCa, which limits the efficacy of adoptive immunotherapy. To date, despite intensive efforts, the sipuleucel-T vaccine is the only immunotherapeutic agent that has achieved a significant survival benefit for mCRPC. We believe that a better understanding of the characteristics of the tumor immune infiltrates is crucial for the development of more effective treatments. As part of my PhD, we have therefore unraveled the heterogeneity and properties of immune cells at a single-cell-level in the preclinical $PTEN^{(i)pe-/-}$ model, uncovering new potential targets for a more successful immunotherapeutic strategy.

Thesis Objectives

Prostate cancer (PCa) is the most diagnosed cancer and the second leading cause of cancer-related death among men of western societies. Despite the therapeutic advancements made in recent years, advanced PCa remains incurable. While the immune system's ability to control tumor cells has been revolutionized by therapies that target T cell inhibitory checkpoint signaling pathways, numerous trials in PCa have yielded disappointing results thus far, compared to other cancers, especially with immune checkpoint inhibitors (ICI) monotherapies. This resistance could be explained by scarce tumor-infiltrating T cells but can also be the consequence of tumor-specific immunosuppressive microenvironment. Indeed, the prostate TME presents numerous other immunosuppressive traits, potentially undermining the effectiveness of immunotherapeutic approaches utilizing ICI.

Hence, it is imperative to understand the composition, phenotypic states, and functions of intratumoral immune cells within the tumor immune microenvironment in order to develop appropriate immunotherapeutic strategies and improve PCa treatment. This is the aim of my PhD research using the innovative pre-clinical inducible PTEN$^{(i)pe-/-}$ mouse model that faithfully recapitulates the features and staging of human PCa progression from neoplasia to adenocarcinoma stages (3- & 5-months post-Tamoxifen for early & advanced prostatic intraepithelial neoplasia [PIN] stages, and 9- & 12-months post-Tamoxifen for adenocarcinoma & advanced adenocarcinoma stages respectively). My PhD work is divided in 4 main axes (***Figure 23***):

-Resolving the immune heterogeneity at a single cell level: The objective of this axis is to perform longitudinal characterization of the myeloid and lymphoid heterogeneity present in healthy murine prostate and recruited upon prostate cancer development in PTEN$^{(i)pe--}$ mice. A combination of state-of-the-art techniques will make it feasible:

- Multiparametric flow cytometric analysis: designing specific panels for identifying the myeloid cells [Neutrophils, Eosinophils, dendritic cell subsets (cDC1, cDC2), monocytes, macrophages] and the lymphoid cells [B lymphocytes, T lymphocytes (CD4$^+$, CD8$^+$, gd T), NK cells]
- Use of reporter mouse models for in-depth immunophenotyping: Zbtb46-GFP for cDC, CX3CR1-GFP, Slco2b1-hCD2 for macrophages.
- scRNA-sequencing analysis from sorted prostate immune cells (CD45$^+$ cells from DLV prostates of PTEN$^{(i)pe-/-}$ mice at PIN and adenocarcinoma stages and of age-matched controls)
- Confocal microscopy: revealing their localization within the prostate gland and explore if the immune changes during cancer progression will be visible at specific areas within the prostate TME.

-Assessing the origin and renewal of myeloid cells: we aspire to explore, for the first time, the origin and renewal of prostate resident macrophages using various strategies, including

complete and protected bone-marrow chimeras, CD64^{DTR} and CCR2$^{-/-}$ mice to determine if they are replaced by monocytes, like gut macrophages, or self-renew, like Langerhans cells, and additionally, investigate their dependence on CSF-1 using anti-CSF1R treatment.

-Exploring the functional role of prostate immune cells:

- ❖ Based on the scRNAseq signature of the identified immune populations and the expression changes in the PCa condition, we aim at deciphering their functions and their interactions using bioinformatic tools and databases
- ❖ Performing *ex vivo* functional assays, to determine their potential anti-tumoral or immunosuppressive role within the prostate tumor microenvironment and their phagocytic properties.

-Evaluating the response to novel immunotherapy: Ultimately, our goal is to test and propose a novel immunotherapeutic approach for prostate cancer. Given that previous studies showed that myeloid-derived suppressor cells (MDSCs) are recruited in PCa, once we determine through our study whether these cells are neutrophils or monocytes with immunosuppressive functions, we will be able to target them specifically. We aim on combining depleting strategies against pro-tumoral myeloid cells with conventional immune checkpoint inhibitor (ICI) treatments, such as anti-PD1. In response to immunotherapy, we will study the changes within the immune infiltrate and determine if the therapies are able to induce anti-tumoral cytotoxic responses.

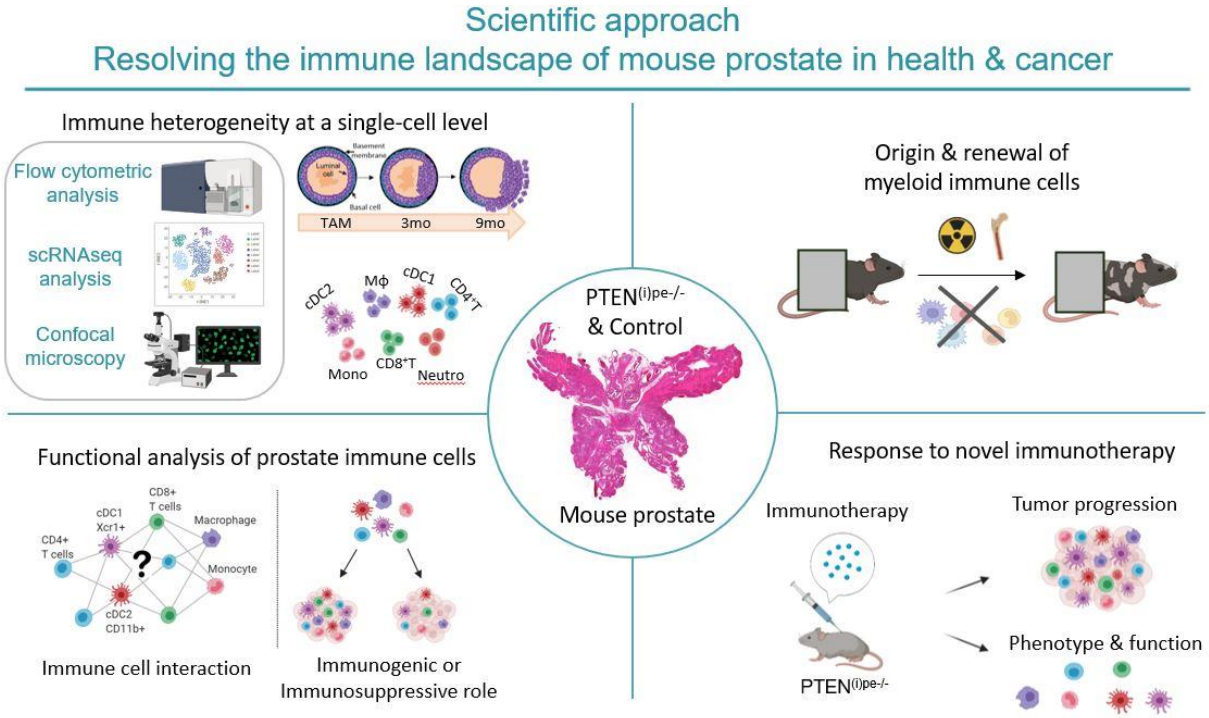

Figure 23. Graphical abstract recapitulating the objectives of my PhD study.

Results: Scientific Article

Scientific Article

In the following section I will present the results of my PhD thesis in a format of scientific article in preparation for publication:

Despoina Pervizou, Joanna De Chiara, Lionel Spinelli, Lionel Chasson, Frédéric Fiore, Marc Bajénoff, Bernard Malissen, Daniel Metzger, Gilles Laverny and Sandrine Henri. Trem2^{+} tumor-associated macrophages (Trem2^{+} TAM) and interferon-stimulated gene-tumor associated neutrophils (ISG-TANs) infiltrate precancerous lesions in the PTEN$^{(i)pe-/-}$ mouse model of prostate cancer. In preparation (2024).

Trem2^{+} tumor-associated macrophages (Trem2^{+} TAM) and interferon-stimulated gene-tumor associated neutrophils (ISG-TANs) infiltrate precancerous lesions in the PTEN$^{(i)pe-/-}$ mouse model of prostate cancer

Despoina Pervizou[1], Joanna De Chiara[1], Lionel Spinelli[1], Lionel Chasson[1], Frédéric Fiore[2], Marc Bajénoff[1], Bernard Malissen[1,2], Daniel Metzger[3,4,5,6], Gilles Laverny[3,4,5,6] and Sandrine Henri[1,7]

[1]Centre d'Immunologie de Marseille-Luminy, Aix Marseille Université, INSERM, CNRS UMR, 13288 Marseille, France.
[2]Centre d'Immunophénomique, Aix Marseille Université, INSERM, CNRS, 13288 Marseille, France
[3]Institut de Génétique et de Biologie Moléculaire et Cellulaire, Illkirch, France.
[4]Centre National de la Recherche Scientifique (CNRS), UMR7104, Illkirch, France.
[5]Institut National de la Santé et de la Recherche Médicale (INSERM), U1258, Illkirch, France.
[6]Université de Strasbourg, Strasbourg, France.
[7]Present address is INSERM, Centre d'Etude des Pathologies Respiratoires (CEPR), UMR 1100, Université de Tours, Tours, France

Running title: Prostate cancer, PTEN$^{(i)pe-/-}$ murine model, Trem2^{+} tumor-associated-macrophages (TAM), distinct states of tumor-associated-neutrophils (TAN), exhausted CD8^{+} T cells

Corresponding author: Sandrine Henri, Centre d'Immunologie de Marseille-Luminy, Case 906, 13288 Marseille Cedex 9, France

Email: sandrine.henri@inserm.fr

ABSTRACT

The early alterations in the composition of the immune cell compartment, during the development of prostate cancer (PCa), remain poorly characterized. In this study, we conducted a longitudinal analysis of $CD45^+$ cells infiltrating the murine prostate in health and cancer, using single-cell RNA-sequencing, reporter mouse models, flow cytometry and confocal microscopy approaches. Our findings reveal profound changes in the immune cell landscape from the prostatic intraepithelial neoplasia (PIN) stage to the adenocarcinoma stage in the $PTEN^{(i)pe-/-}$ PCa mouse model, which mirrors human PCa features. Notably, the myeloid-dominant immune cells exhibit an immunosuppressive signature already at the neoplastic stage. During PCa progression, neutrophils emerge as the predominant immune cell population, resolving into eight distinct states, with ISG- and a dcTRAIL-R1-states prevailing in the PIN and adenocarcinoma stages, respectively. This suggests reprogramming and functional diversification of neutrophils during tumor evolution. Additionally, the PIN stage is characterized by the presence of exhausted $CD8^+$ T cells and $Trem2^+$ tumor-associated-macrophages. The latter displays strong metabolic and immunosuppressive signatures that are likely mediated by the MIF/HIF1A-signaling axis.

INTRODUCTION

The prostate, an integral component of the male reproductive system, encircles the urethra and, functions as an exocrine gland, collaborating with the testes and epididymis to produce seminal fluid. Unlike the human prostate, which is uni-lobular and divided into distinct zones, the mouse prostate is organized into individual lobes and undergoes development through a series of sequential events. In mice, these events include the pre-bud stage from the urogenital sinus (UGS) and initial budding at embryonic day (E) 13-15 and E16-18 respectively. This is followed by bud elongation (ventral, dorsal, lateral and anterior) and branching morphogenesis from day 1 to 40 post-birth, and subsequently by ductal canalization and differentiation of luminal and basal epithelial cells from day 3 to 50 post-birth (Cunha et al., 2018; Joseph et al., 2021; Timms, 2008). Prostate development thus initiates in the embryo and continues postnatally throughout puberty until reaching adulthood, and is regulated predominantly by dihydrotestosterone (DTH) mainly produced by the testes.

Prostate cancer (PCa) is the most prevalent malignant visceral neoplasm and the second leading cause of cancer-related mortality in males of Western societies, particularly among those over 65 years old (Siegel et al., 2024). PCa originates from the malignant transformation of prostatic luminal epithelial cells, frequently deriving from a mutation in the well-described tumor suppressor gene Phosphatase and TENsin homolog deleted on chromosome 10 (*PTEN*). *PTEN* ranks as the second most commonly inactivated gene across cancer types, with significant alterations observed in uterine, glioblastoma, prostate, lung and melanoma cancer (Luongo et al., 2019). The progression of human PCa occurs slowly through a series of defined stages, starting from precancerous lesions known as prostatic intraepithelial neoplasia (PIN), progressing over decades to adenocarcinoma, and eventually leading to castration-resistant metastatic cancer. In humans, prostate adenocarcinoma predominantly arises in the peripheral zone, analogous to the dorsolateral (DL) lobes in mice. The study of prostate cancer pathogenesis, particularly in precancerous lesions, and the development of new therapies have been hindered by the absence of mouse models that accurately recapitulate the features of human PCa. These include the spatio-temporal controlled deletion of tumor suppressor genes at adulthood, the tumor localization within the DL lobes and the slow progression of precancerous lesions to malignant tumors.

The $PTEN^{(i)pe-/-}$ mice, in which *PTEN* is selectively ablated in prostatic luminal epithelial cells (PECs) at adulthood via the tamoxifen (Tam)-dependent Cre-ERT2 system, stimulates PEC proliferation, leading to the formation of PIN in prostate DL lobes within one month (Ratnacaram et al., 2008). This initial phase of active proliferation is followed by a gradual growth arrest lasting 7 months, characterized by features of cellular senescence and senescence-associated secretory phenotype (SASP) (Abu El Maaty et al., 2021; Parisotto et al., 2018). Moreover, a shift of luminal cell phenotype is observed, along with an induced stromal reaction indicated by the remodeling of the stromal extracellular matrix (ECM) (Abu El Maaty et al., 2021). The rapid proliferation of PECs following *PTEN* deletion induces also hypoxia, characterized by high levels of the hypoxia-inducible factor HIF1A and SASP components, that

are identified as key drivers of malignant progression in prostatic lesions (Abu El Maaty et al., 2022). Eventually, between eight to twelve months post-*PTEN* deletion, the senescent hypoxic PIN lesions progress to invasive adenocarcinoma (Ratnacaram et al., 2008). Therefore, the pre-clinical PTEN$^{(i)pe-/-}$ prostate cancer mouse model accurately reproduces the key features of human PCa (Abu El Maaty et al., 2021; Abu El Maaty et al., 2022).

Studies in cancers of different etiologies have emphasized the crucial role of the tumor immune microenvironment in tumor progression and response to therapy. The ability of the immune system to control tumor cells was successfully harnessed using therapies targeting T cell inhibitory checkpoint signaling pathways (Chamoto et al., 2023; Sharma et al., 2023). However, the effectiveness of immunotherapy on prostate cancer remains under debate and is often considered as a 'cold tumor' based on the low CD8$^+$ T cell infiltration. This underlines the necessity of identifying immunotherapy targets beyond T cells. Moreover, while many therapeutic strategies were successful in preclinical models, they often fail in human trials. This discrepancy likely arises from the need of a better characterization of the immune tumor environment in pre-clinical mouse models that can accurately recapitulate the tissue-specific and slow developing nature of human prostate cancer, such as the PTEN$^{(i)pe-/-}$ model.

So far, there is limited information on the composition of the tissue-resident immune cell compartment in PTEN$^{(i)pe-/-}$ prostate. It has been shown that luminal HIF1A promotes an immunosuppressive SASP, characterized by elevated levels of myeloid-derived suppressive cell (MDSC)-recruiting factors, including CXCL5 and CX3CL1 (Abu El Maaty et al., 2022). Gr1$^+$ cells, also known as MDSCs, were detected in the PTEN$^{(i)pe-/-}$ prostate at 2 months post *PTEN* deletion and were reduced in PTEN/HIF1A$^{(i)pe-/-}$ prostates (Abu El Maaty et al., 2021; Parisotto et al., 2018).

Thus, here we utilized the strict temporal control of PTEN ablation in PECs in the PTEN$^{(i)pe-/-}$ mouse model, characterized by a slow tumor progression and recapitulating prostate carcinogenesis in humans, to conduct a longitudinal study of the immune infiltrate in the dorsolateral lobes of mouse prostates from early neoplasia to advanced adenocarcinoma. Using high resolution protein and RNA analysis at a single cell level, we found that Trem2$^+$ tumor-associated macrophages (TAM) with MIF/HIF1A-mediated immunosuppressive features and PD-1^{hi}Tim3$^+$ exhausted CD8$^+$ T cells are present from the precancerous stage (PIN). Moreover, we observed a massive infiltration of heterogeneous neutrophils from the PIN stage dominating the tumor immune microenvironment and suggesting evidence of neutrophil reprogramming within the prostate during the progression towards the adenocarcinoma stage.

RESULTS

Heterogeneity of immune cells residing in prostate tissue

PTEN$^{(i)pe-/-}$ mice were obtained upon crossing the LoxP-flanked PTEN mice (PTEN$^{L2/L2}$) with the PSA-Cre-ER^{T2} mice that express the tamoxifen-dependent Cre-ER^{T2} recombinase selectively in prostatic luminal epithelial cells (Ratnacaram et al., 2008). Tamoxifen administration in adult PTEN$^{(i)pe-/-}$ mice and age-matched littermate controls induced the inactivation of the *Pten* gene from the prostatic luminal epithelial cells of the DL lobes, thereby initiating the slow-paced prostate cancer development that recapitulates the staging and features of human prostate cancer. We initially conducted longitudinal flow cytometry analysis to obtain a comprehensive overview of the distribution of the major immune cell lineages from the preneoplastic stage (1 month post tam) to the advanced adenocarcinoma stage (13 months post tam) (**Figure 1A**) (Ratnacaram et al., 2008). Few minutes prior sacrifice, mice were injected intravenously with fluorescent anti-CD45.2 antibodies to facilitate blood/tissue partitioning. This procedure ensured exclusion of cells present in the vasculature, enabling the study of immune cells specifically within the prostate parenchyma. Given that the development of prostate cancer in PTEN$^{(i)pe-/-}$ mice is associated with an increase of both prostate weight (**Sup Figure 1A**) and infiltration of CD45$^+$ tissue-resident immune cells (**Sup Figure 1B-C**), cell counts were normalized per 1mg of prostate. Normalized data indicated that CD45$^+$ tissue-resident immune cells are significantly increased from PIN stage at 3 months post tam injection and further accumulate at the adenocarcinoma stage, 9-13 months post tam injection (**Figure 1B**). All major immune cell lineages are present within CD45$^+$ tissue-resident immune cells including CD5$^+$ T and CD19$^+$MHCII$^+$ B lymphocytes, CD161c$^+$ NK cells, CD11b$^+$Ly-6G$^+$ neutrophils, MHCII$^+$F4/80$^-$ and MHCII$^+$F4/80$^+$ mononuclear phagocytes (MNPs) (**Figure 1C-D** and **Sup Figure 1D**). Upon PTEN inactivation in prostate luminal cells, a profound shift in the immune composition was observed, highlighted by a substantial infiltration of neutrophils from 3 months post tam treatment (**Figure 1C**, **1E**, **1F** and **Sup Figure 1D**). Additionally, the development of prostate cancer in PTEN$^{(i)pe-/-}$ mice was associated with increased infiltration of MHCII$^+$F4/80$^+$ MNPs, and T lymphocytes, though to a lesser extent than neutrophils (**Figure 1F**). Following PTEN inactivation the increase in immune cell infiltration was detected exclusively in the dorsolateral-ventral (DLV) lobes and not in the anterior prostate lobes (**Sup Figure 1E**). This finding aligns with the tumorigenic pattern in PTEN$^{(i)pe-/-}$ mice, where tumor lesions predominantly develop in dorsolateral prostate lobes, which are considered analogous to the peripheral zone of the human prostate, where adenocarcinoma commonly arises (Ratnacaram et al., 2008). Confocal microscopy analysis of DLP tissue sections revealed Ly6G$^+$ neutrophil accumulation in the lumen and tumorous epithelium, while Iba1$^+$ macrophages and CD3$^+$ T cells predominantly localize in the stroma (**Figure 1G**).

To characterize the immune landscape of mouse prostate at steady-state, PIN and adenocarcinoma stages at high resolution, we implemented a droplet-based single-cell RNA-sequencing (scRNA-seq) on fluorescence-activated cell sorting (FACS)-enriched tissue resident

$CD45^+$ immune cells freshly isolated from DLV prostate lobes. Given our findings demonstrating that neutrophils are the prevalent population within the leukocyte infiltrates from PIN to adenocarcinoma in the $PTEN^{(i)pe-/-}$prostate, neutrophils were sorted separately from the rest $CD45^+$ immune resident cells on the $PTEN^{(i)pe-/-}$ samples. Eventually cells were mixed again at a ratio of 30% neutrophils to 70% of $CD45^+$ non neutrophil immune cells before the droplet step, allowing to improve the yield of non-neutrophil immune cells (**Figure 2A** and **Sup Figure 2A**). We included 8 independent samples encompassing 2 replicates of $Pten^{L2/L2}$ control mice at 3 months and 9 months post tamoxifen, and 2 replicates of $PTEN^{(i)pe-/-}$ mice at 3 months and 9 months post tamoxifen (PIN and adenocarcinoma stage respectively). Following the integration of the 8 single-cell datasets, the QC steps indicated first that a substantial number of cells from $PTEN^{(i)pe-/-}$ samples had low ribosome counts and correspond to neutrophils. Therefore, no filtering threshold was applied on ribosome counts to allow their detection prior to unsupervised analysis. Following quality control filtration, we applied Seurat at a resolution of 0.1 to analyze 36,175 prostatic immune cells, resulting in the identification of 14 clusters (**Figure 2B**). Analysis of the top genes expressed by each cluster and module scoring from published data of human prostate cancer immune signature (Hirz et al., 2023) revealed the presence of four mononuclear phagocyte (MNP) clusters, including two dendritic cell (DCs) clusters (Clusters 8, 11) and two macrophage clusters (Clusters 0, 3), six lymphoid clusters including two T cells clusters (Clusters 1, 7), one natural killer (NK) cluster (Cluster 4), three B lymphocyte clusters (Clusters 5, 6, 12), and one neutrophil cluster (Cluster 2), as well as three non-immune clusters (Clusters 9, 10, 13) corresponding respectively to epithelial cells, endothelial cells and fibroblasts contaminants from the sorting (**Figure 2 B-C** and **Sup Figure 2B**).

To reliably identify the different immune cell subsets present in prostate tissue, we next performed independent re-clustering on the MNPs (Clusters 0, 3, 8, 11), the T and NK cells (Clusters 1, 4, 7), the B lymphocytes (Clusters 5, 6, 12), and the neutrophils (cluster 2).

scRNAseq and reporter mouse models allowed to decipher the MNP compartment in steady-state prostate

The four MNPs clusters were pooled and subjected to unsupervised re-clustering with additional removal of doublets and contaminating cells (epithelial cells, T lymphocytes and neutrophils). At a resolution 0.8, the UMAP visualization elucidates the intricate myeloid landscape within steady-state control prostates and reveals 18 distinct clusters (**Figure 3A**). Analysis of the top genes expressed by each cluster and module scoring from published data in other organs (Chakarov et al., 2019; Dick et al., 2022; Dwyer et al., 2016; Liu et al., 2023) allowed us to identify six clusters of DCs, ten clusters of macrophages, one cluster of monocyte and one cluster of rare mast cells, constituting 26%, 70%, 4% and 0.4%, respectively, of the total 4,712 myeloid cells analyzed (**Figure 3B** and **Sup Figure 3A**). Mast cells were characterized by the expression of *Cma1*, *Tpsb2*, *Fcer1a* genes (**Figure 3B**) (Tauber et al., 2023). The type 1 conventional dendritic cells (cDC1) are dependent on the transcription

factors Batf3 and Irf8 for their development and are specialized in cross-presenting exogenous antigens to $CD8^+$ T cells. The canonical cDC1 genes *Xcr1*, *Clec9a*, *Wdfy4* were expressed by three clusters, labelled cDC1_1, cDC1_2 and cDC1_3, confirming the presence of cDC1 in prostate tissue with an heterogeneity that could correspond to different states of activation. cDC1_3 cluster also expresses high levels of *Hist1h1b*, *Pclaf*, *Top2a*, *Stmn1* and *Mki67* genes, suggesting it could correspond to cDC1 proliferating precursors (**Figure 3 A-B**). The type 2 conventional dendritic cells (cDC2) are dependent on the transcription factors Irf4 and Zeb2 for their development and are involved in driving $CD4^+$ T cell responses. The cluster characterized by the expression of the *Cd209a* gene corresponds to cDC2 cells, which are also found in prostate tissue (**Figure 3A-B**). The plasmacytoid dendritic cells (pDC) are dependent on the transcription factors Tcf4 and Irf7 for their development and are primarily involved in antiviral defense through the production of large amounts of type I interferons. pDCs were also found in prostate tissue and correspond to the cluster expressing *Grm8*, *Ly6d*, *Siglech*, *Plac8* and *Ly6c2* genes (**Figure 3A-B**). Prostate tissue also contains a specific mature cluster ($CCR7^+$DC) characterized by the expression of *Ccr7*, *Fscn1* and *Mreg* genes (**Figure 3A-B**) (Ardouin et al., 2016; Maier et al., 2020). Regarding their prevalence, among the total 1,232 DC cells analyzed, the prostate gland at steady-state harbors slightly more cDC2 (49%) compared to cDC1 (43%) and fewer $CCR7^+$ mature DC (8%), while pDC are very rare (1%).

Circulating monocytes which are transiting through the blood stream, can also be recruited into tissues. In prostate tissue, the monocyte cluster is characterized by *Plac8*, *Ly6c2* and *Ccr2* gene expression (**Figure 3A-B**). The prostate harbors also a population of $Lyz1^+$ myeloid cells, which express *Ccr2*, *Lyz1*, *Ear2* and *Fn1* genes, constituting 8% of the total prostate MNPs at steady-state (**Figure 3A-B**).

As indicated above, macrophages are the dominant MNPs found in prostate tissue. While resident macrophages were studied in details in many tissues such as skin, lung, liver, brain, intestine (Park et al., 2022) and many exocrine glands such as mammary gland, pancreas, salivary gland or testis (Bijnen and Bajenoff, 2021), little is known about the complexity of macrophages residing in prostate (Tuong et al., 2021). Moreover, there is growing evidence that diverse resident-tissue macrophage (RTM) subpopulations coexist within tissues with unique tissue-specific subsets, such as, Langerhans cells in the skin, alveolar macrophages in the lung, Kupffer cells in the liver or microglia in the brain. Furthermore, multi-organ conserved RTMs subsets exhibit unique anatomical location, such as the $Lyve1^{hi}$ perivascular macrophages (PVMs) located in tight contact with blood endothelial cells (Chakarov et al., 2019; Zhao et al., 2024), or the $Cx3cr1^{hi}$ ductal macrophages located in the epithelium of exocrine glands (Bijnen and Bajenoff, 2021; Dawson et al., 2020). Transcriptomic analysis of steady-state prostate RTMs allowed us to delineate two main macrophage clusters the $Cx3cr1^+$ Mac, expressing *Cx3cr1*, *Mmp12* and *Ccl4* genes, and the $Tim4^+FolR2^+$ Mac, expressing *Ccl8*, *Lyve1*, *FolR2*, *Timd4* and *Mrc1* genes (**Figure 3A-B**), constituting 35% and 23% respectively of the total 2,879 macrophages analyzed. Interestingly, the $Cx3cr1^+$ Mac cluster exhibits low expression of *Itgam* (CD11b) and high level of *Itgax* (CD11c) (**Figure 3C**). Six additional minor macrophages clusters were identified, each

constituting less than 8 % of the total macrophage population. Some of these clusters share gene signatures with the main macrophage clusters and with Lyz1$^+$ myeloid cells. For instance, Tim4$^-$FolR2$^+$ Mac share gene expression with both Tim4$^+$FolR2$^+$ Mac and Lyz1$^+$ Mac. Similarly, the Mac_2 cluster shares gene expression with Cx3cr1$^+$ Mac, while the Mac_3 and Mac_4 clusters share gene expression with Tim4$^+$FolR2$^+$ Mac, specifically expressing *Ccl8*, *Lyve1*, *FolR2*, *Timd4*, *Mrc1* and *St18*, *Samd4*, *Plekhg5*. This suggests that these clusters may represent different activation states of the main macrophage clusters and Lyz1$^+$ myeloid cells. Additionally, the minor Trem2$^+$ Mac exhibits higher expression of *Ccl12*, *Apoe*, *Trem2* genes, while the Mac_4 cluster shows increased expression of the *Cd209g* gene (**Figure 3A-B**). Altogether, the scRNAseq analysis focusing on myeloid cells uncovers the high heterogeneity of the myeloid landscape within steady-state control prostates.

Subsequently, we performed flow cytometry analysis using cell surface markers to detect the myeloid subsets of DCs, monocytes and macrophages. Tissue resident myeloid cells from prostate were pre-gated as CD45$^+$ Non-B-T-NK-Neutrophils-Eosinophils (using Siglec-F) and then divided into CD11b$^+$ and CD11b$^-$ populations. The CD11b$^-$ population was further analyzed using XCR1 versus CD11c to identify XCR1$^+$CD11c$^+$ cells corresponding to cDC1 (**Figure 3D**). Within the XCR1$^-$CD11b$^-$ cells, we identified CD11c$^+$MHCII$^+$ cells, that also expressed the macrophage marker F4/80, suggesting they could correspond to the Cx3cr1$^+$ Mac cluster found by scRNAseq and were called CD11b$^-$ macrophages (**Figure 3D**). Conversely, the CD11b$^+$ population was further analyzed using CD64 versus CD88 to identify the CD64$^-$CD88$^-$ cells and the CD64$^+$CD88$^+$ cells. The CD64$^+$CD88$^+$ cells correspond to macrophages and were further subdivided into Tim4$^-$ and Tim4$^+$ macrophage subsets (**Figure 3D**). The CD64$^-$CD88$^-$ cells were further analyzed using MHCII versus Ly6C, allowing us to identify Ly6C$^+$MHCII$^-$ cells (P1) and Ly6C$^+$MHCII$^+$ cells (P2), corresponding to classical and activated monocytes respectively, as well as Ly6C$^-$MHCII$^+$ cells (P3), which likely contain cDC2 and monocyte-derived cells (**Figure 3D**) (Tamoutounour et al., 2013).

To confirm the identity of the different myeloid subsets gated above, we used reporter mouse models and additional surface markers. Zbtb46, a transcription factor specifically expressed in conventional DC (cDC) (Satpathy et al., 2012), was used in *Zbtb46*$^{GFP/+}$ mouse model to distinguish cDC among the other MNP subsets. High levels of Zbtb46-GFP were detected in all XCR1$^+$CD11c$^+$ cells and in 50% of P3 cells, confirming that the XCR1$^+$CD11c$^+$ are cDC1 and that P3 cells include cDC2 cells (**Figure 3E**). Furthermore, the solute carrier organic anion transporter family member 2B1 (*Slco2b1*) is highly expressed at the mRNA level in various tissue macrophages including those in the dermis, spleen, brain, lung and gut (Chakarov et al., 2019; Tamoutounour et al., 2013). To utilize this marker for macrophage tracking in tissues, we generated a mouse model expressing the *hCD2* gene under the control of *Slco2b1* promoter, enabling the detection of macrophages using an anti-hCD2 fluorescent antibody. The expression of F4/80 and Slco2b1 by the Tim4$^-$ and Tim4$^+$ macrophages as well as CD11b$^-$ macrophages confirmed their macrophage identity (**Figure 3E**). Additionally, Tim4$^+$ macrophages express high levels of Lyve-1, FolR2 and CD206, similar to the PVMs described in the literature (**Figure 3E**) (Chakarov et al., 2019). CX3CR1, a chemokine receptor expressed

by myeloid cells, is an additional key marker for macrophage subset identification, as demonstrated by high GFP expression in *CX3CR1* $^{GFP/+}$ mouse model (Jung et al., 2000). This marker identifies ductal macrophages located in the epithelium of exocrine glands (Bijnen and Bajenoff, 2021). Tim4^{-} macrophages in prostate tissue found to express CX3CR1 and a fraction of these cells also express Lyve-1 and FolR2, with the latter corresponding to the Tim4^{-}FolR2^{+} Mac cluster as identified by the scRNAseq (**Figure 3E**). Additionally, similar to the scRNAseq data, the CD11b^{-} macrophages express high level of CX3CR1 but do not express Lyve1, FolR2 or CD206 (**Figure 3E**).

The DC-SIGN (Dendritic Cell-Specific Intercellular adhesion molecule 3 (ICAM-3)-Grabbing Nonintegrin) marker, encoded by the *CD209a* gene, was used to further subdivide the P3 subset into DC-SIGN^{-}CD11c^{+} cells and DC-SIGN^{+}CD11c^{+} cells (**Figure 3F**). The latter, which also express Zbtb46-GFP, corresponds to cDC2 (**Figure 3F**). DC-SIGN^{-}CD11c^{+} cells are heterogeneous and can be divided in Zbtb46-GFP expressing cDC2 and Lyz^{+} cells (**Figure 3F**). Thus, our FACS gating strategy allows the detection of both cDC2 and Lyz^{+} cell subsets that were identified by scRNAseq (**Figure 3A**).

Although FACS analysis did not enable the detection of rare cell subsets such as mast cells and pDC, it confirmed the presence of the main MNP subsets in murine prostate tissue. These include three main macrophage subsets (Tim4^{+}FolR2^{+} Mf, Tim4^{-} Mf and CD11b^{-}CX3CR1^{+} Mf), cDC1 and cDC2, monocytes and Lyz^{+} cells. The analysis also validated that macrophages are the dominant myeloid cells found in physiological prostate tissue (**Figure 3G**).

Developmental origin, turn-over and location of macrophage subsets residing in healthy murine prostate

Tissue-resident macrophages are often considered long lived cells, originating from early stages of embryogenesis, capable of maintaining themselves locally and independently of circulating precursors (e.g., alveolar macrophages, Kupffer cells, microglia, Langerhans cells). Alternatively, some can be replaced by monocytes generated in the bone marrow, as seen in intestine (Ginhoux and Guilliams, 2016; Hoeffel and Ginhoux, 2015; Park et al., 2022). To determine the turn-over rate of the three resident macrophage subsets in the prostate and estimate the contribution of circulating monocytes, we generated various bone marrow (BM) chimera animals. Initially, we aimed at clearing the tissue niche with full-body irradiation of adult CD45.2 WT males, resulting in the complete replacement of blood and prostate Ly6C^{hi} monocytes from CD45.1^{+} WT donor cells (**Sup Figure 4A-C**). Moreover, 85% of Tim4^{-} Mf and 70% of Tim4^{+} Mf were replaced by CD45.1^{+} WT donor cells, compared to only 47% of the CD11b^{-} Mf (**Figure 4A,B**, **Sup Figure 4D**). This suggested that following complete irradiation the Tim4^{+} and Tim4^{-} Mac subsets are predominantly replaced by circulating precursors, whereas the CD11b^{-} Mac might be maintained through *in situ* proliferation independently of BM-derived cells. To circumvent the effect of irradiation on tissue prostate, we implemented an irradiation strategy using shielded conditions, protecting the prostate and back limbs (**Figure 4A**). As a result, monocytes from circulation and prostate, as well as Tim4^{-} Mf exhibited

lower chimerism (37%, 50% and 30% of donor cells respectively), compared to fully irradiated animals (**Figure 4B, Sup Figure 4B,C**). This suggests that circulating precursors contribute to the renewal of tissue resident monocytes and, to a lesser extent, of Tim4^{-} Mf. Nonetheless, under protected irradiation, the Tim4^{+} and CD11b^{-} Mf remain predominantly of host origin (5% and 1.8% of donor cells respectively), confirming their slow turn-over and maintenance *in situ* independently of circulating precursors (**Figure 4B**, **Sup Figure 4D**).

CCR2, a C-C chemokine receptor 2 expressed by monocytes, facilitates their exit from the BM (Serbina and Pamer, 2006). *Ccr2*$^{-/-}$ mice exhibit a significantly reduced number of monocytes in both blood and prostate (**Sup Figure 4E**), and while the number of Tim4^{-} prostate resident mac is slightly reduced (not significant), the Tim4^{+} and CD11b^{-} Mac populations remain unaffected (**Figure 4C**). This indicates that in *Ccr2*$^{-/-}$ mice, the prostate is predominantly populated by macrophages of prenatal origin that self-maintain without significant contribution from adult monopoiesis for the Tim4^{+} and CD11b^{-} Mf populations and with minimal input for the Tim4^{-} Mf. Furthermore, the generation of competitive BM chimera following full body irradiation and reconstitution with CD45.1xCD45.2 WT + CD45.1 *Ccr2*$^{-/-}$ or CD45.1xCD45.2 WT + CD45.1 WT mixed BM, confirmed that macrophages can be replaced by BM donor cells and derived from blood monocytes in a CCR2-dependent manner (**Sup Figure 4F,G**).

Additionally, we used the CD64^{dtr} mouse model, previously described by our group (Baranska et al., 2018) to induce diphtheria toxin (DT)-mediated ablation of tissue resident macrophages, monocytes, and monocyte-derived cells. CD64^{dtr} mice were treated with DT twice, 24h apart and the resident macrophages in the prostate were analyzed at various time points after the last DT injection to determine the reconstitution dynamics of the different resident tissue macrophage subsets. While all prostate RTM subsets were ablated within 24h following the final DT injection, the reconstitution patterns of these subsets varied significantly (**Figure 4D-E and Sup Figure 4H**). Notably, higher numbers of Tim4^{-}FolR2^{-} Mac were detected at day 3 post-DT (**Figure 4D-E**), suggesting a rebound of cells and increased myelopoiesis following DT treatment, as previously observed in circulating monocytes (Baranska et al., 2018). Interestingly, while CD11b^{+} macrophages in non-DT-treated prostates comprise mainly Tim4^{-}FolR2^{-} and Tim4^{+}FolR2^{+} Mf, a Tim4^{-}FolR2^{+} intermediate state was detected from day 7 post-DT depletion, suggesting a precursor-product relationship between newly recruited Tim4^{-}FolR2^{-} Mf and Tim4^{+}FolR2^{+} Mf (**Figure 4D-E**). The complete replenishment of Tim4^{-}FolR2^{-} and Tim4^{+}FolR2^{+} Mac was observed from day 3 and day 7 post-DT treatment respectively, both of which were influenced by the transient rebound (**Figure 4D-E**). In contrast, CD11b^{-} Mf exhibited no rebound and demonstrated a prolonged reconstitution kinetics, achieving full restoration by day 45 post-DT treatment (**Figure 4E and Sup Figure 4H**). These findings suggest that monocyte-derived differentiation supports the reconstitution of Tim4^{-} and Tim4^{+} Macs, while *in situ* proliferation from monocytes or precursors not depleted by DT contributes to the generation of CD11b^{-} Mac.

Tissue-resident macrophage development and survival depend on supportive stromal cells expressing factors such as colony-stimulating factor 1 (CSF1) (Dai et al., 2002; Sherr et al.,

1985), treatment with anti-CSF1R deprives RTMs of their survival signals, leading to their depletion (MacDonald et al., 2010). In this study, following anti-CSF1R treatment we observed that prostatic Tim4^{+}, Tim4^{-} and CD11b^{-} Mf subsets were depleted (**Figure 4F**), confirming their macrophage identity and dependency on CSF1-producing cells for survival. Furthermore, it has been well reported that deletion of the super-enhancer *fms*-intronic regulatory element (FIRE) within the Csf1r locus results in the depletion of resident macrophages in skin, kidney, heart, peritoneum, and microglia, but not in vasculature-associated macrophages (PVMs) (Rojo et al., 2019). Interestingly, FACS analysis revealed that prostates from Csf1R$^{\Delta FIRE/\Delta FIRE}$ lacked Tim4^{-} and CD11b^{-} Mf subsets, whereas Tim4^{+} Mf were unaffected (**Figure 4G**), suggesting they may represent prostate PVMs. Subsequent confocal analysis of DLP tissue from control Csf1R$^{\Delta FIRE/+}$ prostate sections stained with CD31 (blood vessel marker), Iba1 (pan macrophage marker) and Tim4, demonstrated that Iba1^{+}Tim4^{-} mac were predominantly located in the epithelium, while Iba1^{+}Tim4^{+} mac were found in the stroma and in close proximity to CD31^{+} blood vessels (**Figure 4H**). In contrast, in the Csf1R$^{\Delta FIRE/\Delta FIRE}$ prostate sections, only the Iba1^{+}Tim4^{+} mac associated with CD31^{+} blood vessels were detected, with the other macrophage populations being depleted (**Figure 4H**). To further confirm the identity of Tim4^{+} macrophages as PVMs, we conducted an *in vivo* scavenging assay. Both FACS and confocal analyses indicated that the perivascular Tim4^{+} Mf were highly efficient at internalizing intravenously injected FITC-labelled dextran (**Figure 4I-J**), which also correlates with their high expression of the mannose receptor CD206 (**Figure 3D**). Additionally, the greater phagocytic capacity of Tim4^{+} Mf over the Tim4^{-} and CD11b^{-} Mf, was also demonstrated *in vitro* using fluorescent microspheres (**Sup Figure 4I-J**).

Trem2^{+} tumor-associated-macrophages accumulate early during prostate cancer development

Previously, we demonstrated a significant increase in the total population of MHCII^{+}F4/80^{+} macrophages in the prostate of PTEN$^{(i)pe-/-}$ mice following tamoxifen-induced PTEN gene invalidation, predominantly localized within the stroma of the DLV lobes (**Figure 1F-G**). Applying the myeloid cell gating strategy depicted in **Figure 3D**, we investigated the distribution of the various MNP subsets in the prostates of PTEN$^{(i)pe-/-}$ mice from the preneoplastic stage (1 month post tam) to advanced adenocarcinoma stage (13 months post tam). Notably, the Tim4^{-} Mf subset and CD11b^{+}CD64^{-}CD88^{-}, encompassing monocytes and cDC2 cells, exhibited significant increases from 3 months post gene invalidation, while the Tim4^{+} Mf and cDC1 remained stable (**Figure 5A**). To further characterize the myeloid cell populations in PTEN$^{(i)pe-/-}$ mice, we analyzed the scRNAseq dataset, comparing 4,712 from control prostates to 5,610 from PTEN$^{(i)pe-/-}$ prostates comprising both timepoints (**Figure 5B**). This analysis revealed an increase in monocytes (cluster 6) and Tim4^{-}FolR2^{+} Mac (cluster 1), along with the emergence of a tumor-associated-macrophage (TAM) subset (cluster 4) expressing the triggering receptor expressed on myeloid cells 2 (Trem2) in PTEN$^{(i)pe-/-}$ mice compared to controls (**Figure 5B-C**, **Sup Figure 5A**). Analysis of the top genes expressed by Trem2^{+} TAM (*Spp1*, *Gpnmb*, *Cxcl10*, *Rsad2*, *Bglap*) and module scoring based on tumor-

associated macrophage gene signatures from published data (Casanova-Acebes et al., 2021; Giraud et al., 2024a; Katzenelenbogen et al., 2020; Nalio Ramos et al., 2022), suggested that these correspond to the immunosuppressive TAMs found in various tumor microenvironments (**Figure 5D**, **Sup Figure 5B-C**). On the contrary, the cluster 1 (Tim4^{-}FolR2^{+} Macs) along with cluster 3 (Tim4^{+}FolR2^{+} Macs) RTMs that pre-exist in healthy prostates, displayed high scoring with the gene signature of FolR2^{+} RTMs found in human and murine breast cancer, located in perivascular areas of the tumor and bearing anti-tumoral potential by effectively priming CD8^{+} T cells *ex vivo* (Nalio Ramos et al., 2022).

Both cluster 1 and cluster 4 macrophages were included in the Tim4^{-} Mac subset analyzed by FACS in **Figure 5A**. Incorporating the FolR2 and Trem2 markers in the FACS staining panel resulted in a higher resolution analysis of the macrophages subsets. Notably, few Trem2^{+} macrophages were identified within the Tim4^{-}FolR2^{+} Mf, although not significantly increased in PTEN$^{(i)pe-/-}$ mice at PIN stage (**Figure 5E-F**). In contrast, Trem2^{-}Tim4^{-}FolR2^{+} Macs were significantly increased in PTEN$^{(i)pe-/-}$ mice corresponding to cluster 1 found in the scRNAseq dataset (**Figure 5E-F**). Additionally, within the Tim4^{-}FolR2^{-} Macs, there was a substantial and significant increase in both Trem2^{-} and Trem2^{+} macrophage subsets at the PIN stage (3 months post tam) (**Figure 5E-F**), with the latter corresponding to Trem2^{+} TAM (cluster 4) found in the scRNAseq dataset and detected from the PIN stage (**Sup Figure 5D**). Differential gene expression analysis (DEG) comparing PTEN$^{(i)pe-/-}$ over control samples revealed enrichment for leukocyte and granulocyte chemotaxis and migration among various MNP clusters, suggesting that in Pten$^{(i)pe-/-}$ mice, these subsets contribute to their own recruitment as well as the recruitment of neutrophils and lymphocytes in the prostate tumor microenvironment (**Figure 5G**). DEG analysis also indicated enrichment for the regulation of phagocytosis by various MNP clusters (**Figure 5G**) and extracellular matrix (ECM) remodeling with high expression levels of various cathepsins, including *Ctsd* and *Ctss,* and matrix metalloproteinase *Mmp9* (**Figure 5H**). Various MNP clusters also exhibit a hypoxia pathway signature with expression of *Hif1a* and Hif1a-target genes (*Eno1*, *Gapdh*, *Ldha*) (**Figure 5H**). Interestingly, *in vivo* scavenging assay demonstrated that Iba1^{+}CD206^{+} macrophages in the stroma of PTEN$^{(i)pe-/-}$ prostates exhibit high efficiency at internalizing intravenously injected FITC-labelled dextran (**Figure 5I** and **Sup Figure 5E**). FACS analysis further indicated a significant increase of dextran-positive Tim4^{+}Trem2^{-} and Tim4^{-}Trem2^{-} macrophages in PTEN$^{(i)pe-/-}$ prostates compared to Trem2^{+} TAM that did not show any uptake of FITC-labelled dextran (**Figure 5J** and **Sup Figure 5F**). Nonetheless, Trem2^{+} TAMs (cluster 4) harbor a strong metabolic signature (*Apoe*, *Eno1*, *Gapdh*, *Ldha*) and Gene Ontology (GO) analysis and KEGG pathway database interrogation for Trem2^{+} TAM indicated enrichment for various metabolic processes including purine metabolism, generation of metabolites and ATP, oxidative phosphorylation and ROS formation, suggesting hypoxia, the Warburg effect, and immunosuppressive function (**Figure 5K**). Interestingly, Trem2^{+} TAMs express high level of the *Mif* gene, encoding for the macrophage migration inhibitory factor (**Figure 5H**), involved in various protumoral pathways (Mora Barthelmess et al., 2023; Noe and Mitchell, 2020). However, the substantial number of cells needed for *in vitro* assay to evaluate the

immunosuppressive function of intratumoral immune cells, combined with the limited yield of Trem2$^+$ TAMs due to the small size of the murine prostate, prevents us from conducting *in vitro* immunosuppressive assays with Trem2$^+$ TAMs isolated at the PIN stage of mouse prostate cancer.

PIN stage PCa is infiltrated by exhausted-like CD8$^+$ T cells

We next focused our analysis on the T and NK cells identified in the scRNAseq dataset. Clusters 1, 4 and 7 described in **Figure 2** were isolated and reclustered, yielding to 19 clusters (**Figure 6A**). Based on their top gene signature and module scoring from published data (Daniel et al., 2022; Giraud et al., 2024b; Magen et al., 2019), we identified five NK cell clusters (Clusters 0, 4, 8, 12, 17), five CD8$^+$ T cell clusters (clusters 1, 3, 5, 16, 18), five CD4$^+$ T cell clusters (clusters 6, 7, 10, 11, 13) including Tregs (Cluster 13, expressing *Foxp3*, *Ctla4* and *Tnfrsf4*), and four clusters comprising γδ T cells (cluster 2), ILCs (clusters 9, 15) and senescent cells (cluster 14) (**Figure 6A-B**, **Sup Figure 6A**). Among these clusters, two CD8$^+$ T cell clusters (clusters 3 and 16) were significantly increased in PTEN$^{(i)pe-/-}$ mice as compared to control, whereas one NK cluster (cluster 8) and one CD4$^+$ T cell cluster (cluster 11) were significantly reduced (**Figure 6C**, **Sup Figure 6B**). Interestingly, cluster 3 exhibited an increase expression of *Pdcd1* and *Lag3* genes in PTEN$^{(i)pe-/-}$ mice, suggesting an exhausted phenotype (**Figure 6D**). Subsequently, we performed flow cytometry analysis using cell surface markers to detect the T lymphocyte subsets including CD4$^+$, CD8$^+$ and γδ T cells (**Sup Figure 6C**). Applying the gating strategy depicted in **Sup Figure 6C**, we assessed the distribution of the various T cell subsets in the prostates of PTEN$^{(i)pe-/-}$ mice from the preneoplastic stage (1 month post tam) to advanced PIN stage (5 months post tam). While the number of γδ T cells was unchanged during PCa development, CD4$^+$ and CD8$^+$ T cells exhibited significant increases from 3 months post gene invalidation (**Sup Figure 6D**). Incorporating the PD-1 and Tim3 markers in the FACS staining panel enabled the identification of PD-1^{high}Tim3$^+$ and PD-1^{high}Tim3$^-$ within CD8$^+$ T cells which were significantly increased in PTEN$^{(i)pe-/-}$ mice from 2- and 3-months post tam respectively (**Figure 6E**), supporting the observations from scRNAseq data. DEG analysis comparing PTEN$^{(i)pe-/-}$ versus control revealed enrichment for apoptotic pathways for cluster 3 associated with an exhausted phenotype (**Figure 6F**). Moreover, DEG analysis comparing PTEN$^{(i)pe-/-}$ over the control indicated enrichment for leukocyte chemotaxis and migration among various T and NK clusters suggesting that in PTEN$^{(i)pe-/-}$ mice, these subsets contribute to their own recruitment as well as the recruitment of neutrophils and MNPs in the prostate tumor microenvironment (**Figure 6G**).

Furthermore, the B lymphocytes (Clusters 5, 6, 12) described in **Figure 2** were isolated and reclustered, yielding to three main clusters corresponding to plasma (cluster 0), naive (cluster 1) and mature (cluster 2) B cells and two minor clusters with strong IgG signature (Clusters 3, 4) (**Sup Figure 6E-F**). The distribution of the B cell clusters was unchanged in PTEN$^{(i)pe-/-}$ mice as compared to control (**Sup Figure 6F-G**) and DEG analysis comparing

PTEN$^{(i)pe-/-}$ over the control revealed enrichment for leukocyte chemotaxis and migration (**Sup Figure 6I**).

Neutrophils massively invade precancerous lesions and harbor distinct activation states

Last, we concentrated on tumor-associated neutrophils (TANs) frequently identified as PMN-MDSCs (Akkari et al., 2024; Veglia et al., 2021). Various murine models of cancers have documented MDSC or neutrophil expansion in primary tumors as well as bone marrow, blood, and spleen (Alshetaiwi et al., 2020; Casbon et al., 2015; Cortez-Retamozo et al., 2012). In PTEN$^{(i)pe-/-}$ mice, neutrophil prevalence was observed in the prostate from the PIN stage with sustained and exponential recruitment into late adenocarcinoma (**Figure 1 C-F, Sup Figure 7A**). Notably, neutrophil counts were unchanged in blood and spleen, suggesting significant recruitment from the circulation into the prostate tissue, rather than systemic neutrophilia (**Sup Figure 7A**). Hematoxylin-eosin stained cytospin revealed that the infiltrating neutrophils were mature, exhibiting multi-lobed and hypersegmented nuclei (**Figure 7A**) (Hidalgo et al., 2019). Additionally, neutrophils from both prostate and blood of PTEN$^{(i)pe-/-}$ mice expressed similar levels of CD101, indicating a mature phenotype, while CXCR2 expression was downregulated in prostate TANs implying restricted recirculation to the BM (**Figure 7B**). Unlike other tumor models, TANs in PTEN$^{(i)pe-/-}$ mice did not express CD84 or Trem2 (**Sup Figure 7D**) (Alshetaiwi et al., 2020; Bancaro et al., 2023). scRNAseq of PTEN$^{(i)pe-/-}$ prostate identified a neutrophil cluster, cluster 2 (**Figure 2B-C**), expressing *S100a9*, *Ptgs2*, *Cd274*, *Arg2*, *Il1b*, *Il1rn*, suggestive of immunosuppressive functions (**Figures 2C, 7C**). S100A9 and PD-L1 expression by TANs were confirmed by confocal microscopy and FACS respectively (**Sup Figure 7C-D**). TANs sorted from PTEN$^{(i)pe-/-}$ PINs were effective in suppressing the proliferation of CD8$^+$ T cells *ex vivo*, contrasting with bulk CD11b$^+$ sorted macrophages which did not impair the proliferation of CD8$^+$ T cells *ex vivo* (**Figure 7D-E**, **Sup Figure 7E-F**).

While neutrophils have been conventionally perceived as a homogeneous and transient population, recent studies have highlighted the heterogeneity of TANs, characterized by distinct cell states that could explain the controversies on their opposing pro- and anti-tumoral functions depending on the tumor context (Blaisdell et al., 2015; Gungabeesoon et al., 2023; Ng et al., 2024; Veglia et al., 2021; Wu et al., 2024; Xie et al., 2020; Zilionis et al., 2019). To explore the diversity of neutrophil infiltrating PTEN$^{(i)pe-/-}$ prostate, the cluster 2 from **Figure 2** was isolated and reclustered, revealing eight distinct clusters, N0-N7 (**Figure 7F-G**). Cluster N3, predominant within the few neutrophils found in control prostate, shares a signature with steady-state mature blood neutrophils and early tumor stage, while cluster N5 harbors a signature matching late tumor stage (**Figure 7F-G**, **Sup Figure 7G-H**), as described in the literature (Ng et al., 2024; Veglia et al., 2021; Xie et al., 2020). Interestingly, clusters N0 and N2 were detected primarily at the PIN stage while clusters N5 and N7 were more prominent at the adenocarcinoma stage (**Figure 7H-I**). The differential distribution of these clusters between the PIN and adenocarcinoma stages suggests that tumor-infiltrating

neutrophils exhibit plasticity, adopting distinct states and likely following diverse developmental trajectories. Notably, velocity analysis suggested a differentiation pathway from cluster N3 towards cluster N2 at 3 months PIN stage, and from cluster N3 to cluster N5 at 9-mo adenocarcinoma stage, (**Sup Figure 7J**). All clusters harbor functions related to leukocyte migration and chemotaxis, indicative of their potential involvement in self-recruitment but also in the recruitment of MNPs and lymphocytes (**Figure 7J**). Interestingly, N0 exhibited an interferon-stimulated gene (ISG) signature, expressing high levels of *Cxcl10*, *Gbp5*, *Gbp2*, *Ifit1*, *Ifit2* and *Ifit3* (**Figure 7G**) and, recently described in the literature on other tumor types (Gungabeesoon et al., 2023; Wu et al., 2024; Xie et al., 2020)(**Sup Figure 7G**). N0 also expresses high level of cathepsin S (*Ctss*), which could promote pericellular proteolysis and ECM alterations, allowing tumor cell and leukocyte migration to the TME and high level of PD-L1 (CD274) suggestive of immunosuppressive functions (**Sup Figure 7K**). BP GO and KEGG pathway analysis confirmed that cluster 0 was associated with active immune response involved in antiviral immunity, TNF signaling pathway, phagosome, apoptosis and necroptosis (**Figure 7J-K**). N2, which prevails at the PIN stage, exhibits an immunosuppressive signature with *Il1b* and alarmins *S100a8* and *S100a9* gene expression. BP GO and KEGG analysis for N2 highlighted enrichment in the regulation of actin cytoskeleton, leukocytes transendothelial migration, VEGF and chemokine signaling pathways and neutrophil extracellular trap (NET) formation (**Figure 7G, 7J-K** and **Sup Figure 7K**). Notably, N5, which is significantly increased at the adenocarcinoma stage, expresses *Ccl6*, *Hif1a* genes, and Hif1a-target genes (*Eno1*, *Gapdh*, *Ldha*), as well as the gene *Tnfrsf23*, coding for the protein dcTRAIL-R1 (**Figure 7G** and **Sup Figure 7K**). Recent investigations have identified dcTRAIL-R1 as a hallmark of terminally differentiated intratumoral neutrophils, exhibiting prolonged lifespan and localizing to hypoxic-glycolytic niches within tumors, where they can exert pro-angiogenic functions (Ng et al., 2024). Moreover, BP GO terms and KEGG analysis indicated that N5 is associated to leukocyte migration, cytokine response, efferocytosis and ferroptosis (**Figure 7J**-**K**). The N7 cluster showed high expression of mitochondrial genes *mt-Atp6*, *mt-Co1*, *mt-Co2*, *mt-Co3,* coding respectively for the ATP synthase F0 subunit 6, cytochrome c oxidase subunits 1, 2 and 3, indicatives of significant metabolic activity. Moreover, BP GO and KEGG analysis for N7 highlighted enrichment in mRNA metabolic processes, efferocytosis and necroptosis (**Figure 7G** and **7J-K**). Thus, here we described an evident neutrophil heterogeneity at the transcriptomic level. However, the absence of specific surface marker for each cluster prevents us from distinguishing the different populations and states by flow cytometry and further assessing their functions *ex vivo*. We attempted to study their functions *in vivo* using murinized anti-Ly-6G mediated depletion (Olofsen et al., 2022). Since a consecutive one-month depletion could not be maintained (**Sup Figure 7L-N**), we performed one-week treatment combining anti-Ly-6G with anti-Csf1R and anti-PD-1, and followed the IFN-γ and TNF-α production by intratumoral $CD8^+$ T cells (**Sup Figure 7O-Q**). The numbers of IFN-γ^+TNF-α^- and IFN-γ^+TNF-α^+ $CD8^+$ T cells from $PTEN^{(i)pe-/-}$ prostates were similar across the different treatments and did not enhance a cytotoxic phenotype (**Sup Figure 7Q**). Altogether, we found

that during prostate cancer progression, neutrophils resolved in eight different states with dominant protumoral functions.

DISCUSSION

Our study aims to provide a comprehensive resource on the immune cells present in mouse prostate tissue at steady-state and to elucidate changes in the immune infiltrate pattern during prostate cancer initiation and progression. We employed the PTEN$^{(i)pe-/-}$ prostate cancer model, known for faithfully recapitulating human PCa features (Ratnacaram et al., 2008), enabling temporal deletion of tumor suppressor gene *Pten* in adult mice, via tamoxifen-induced Cre-ERT2 activation (injected at 8-week old). This model develops lesions in the dorsolateral lobes, analogous to the peripheral zone of the human prostate, where PCa commonly arises and exhibits a slow progression from prostatic intraepithelial neoplastic (PIN) precancerous lesions to malignant adenocarcinoma tumors over 3 to 9 months post-induction, mirroring human disease progression (Ratnacaram et al., 2008).

To investigate the cellular origins of benign prostatic hyperplasia (BPH) and prostate cancer, epithelial and stromal cells were extensively studied in both human and mouse prostates, while the immune compartment remain largely unexplored (Chen et al., 2021; Crowley et al., 2020; Henry et al., 2018; Karthaus et al., 2020).

Given the emerging evidence on the trophic functions of tissue-resident macrophages in various endocrine and exocrine glands (Bijnen and Bajenoff, 2021), and our prior research on skin macrophages (Baranska et al., 2018; Malissen et al., 2014; Tamoutounour et al., 2013), we sought to elucidate macrophage heterogeneity in the murine prostate. Distinct macrophages were described in various tissues and glands, differing in their origin and importantly in their location within the niche. They comprise duct-, acini-, perivascular-, nerve-, endocrine cell- and stem cell-associated macrophages (Bijnen and Bajenoff, 2021; Park et al., 2022). Using flow cytometry, confocal analysis and scRNAseq, we characterized three primary macrophage subsets in the prostate, Tim4^{+}, Tim4^{-} and CD11b^{-} macrophages. Prostatic Tim4^{+} macrophages correspond to perivascular macrophages, expressing Tim4, FolR2 and Lyve-1, exhibiting high scavenging capacity of blood-borne ligand (intravenously injected dextran) and colocalizing with CD31^{+} endothelial cells (Chakarov et al., 2019). CD11b^{-} macrophages, expressing high level of CX3CR1 and presenting long dendrites in between epithelial cells, resemble to ductal CX3CR1^{+} macrophages described in murine mammary gland (Dawson et al., 2020). Due to the lack of specific markers, the precise location of Tim4^{-} macrophages in prostate tissue remains unclear and their heterogeneity suggested by the scRNAseq dataset should be further disentangle.

Another critical attribute of tissue-resident macrophages is their origin, self-maintenance and renewal (Ginhoux and Guilliams, 2016; Guilliams et al., 2020). Sequential waves of hematopoiesis generate distinct macrophage types, named after their origin as yolk sac-, fetal-liver or bone-marrow derived macrophages. Depending on their tissue location,

those macrophages of different precursors can exhibit varying homeostatic turnover, self-proliferation *in situ* or gradual replacement over time by monocytes originating from hematopoietic stem cell precursors (Park et al., 2022). For instance, microglia and Langerhans cells originate from primitive macrophages in the yolk sac that invade the brain parenchyma and the epidermis respectively, and persist through adulthood, while intestinal lamina propria macrophages undergo frequent turnover and are largely derived from monocytes (Park et al., 2022). Nonetheless, none of this was yet explored on the prostate tissue. Approaches to determine tissue-resident macrophage origin and turn-over include reporter mouse models, parabiotic experiments or bone-marrow chimera models. In our study, prostate-protected BM chimera showed that both Tim4^{+} and CD11b^{-} macrophages remain of host origin in prostate tissue, indicating an embryonic origin and self-renewal. On the contrary, the partial replacement of Tim4^{-} macrophages by donor BM-derived cells suggests heterogeneity within this subset, comprising both slow-renewing cells and monocyte-derived macrophages akin to lamina propria macrophages. Moreover, our findings demonstrated that all macrophage subsets depend on Csf-1 for their survival as administration of anti-Csf1R antibody resulted in their depletion. However, Tim4^{+} macrophages associated to the blood vasculature were independent of the FIRE super-enhancer of the Csf1r locus (Rojo et al., 2019). Further research would be required to elucidate the respective prenatal origin of the various macrophage subsets and to identify their specific Csf1-producing niche (Guilliams et al., 2020).

Tumorigenesis involves complex biological events, with immune cells playing a pivotal role in the formation of tumor microenvironment. In the PTEN$^{(i)pe-/-}$ model, loss of *Pten* induces senescence and hypoxia likely influencing immune cells infiltration (Abu El Maaty et al., 2022; Parisotto et al., 2018). The hypoxia-inducible factor 1, HIF1a, reprograms luminal cell metabolism by upregulating glycolytic enzymes and lactate production, and remodels the tumor micro-environment through immunosuppressive chemokines such as CXCL5 and CXCL3. These chemokines recruit MDSCs, which have been implicated in prostate cancer progression (Adekoya and Richardson, 2020; Begley et al., 2008; Husain et al., 2013a; Husain et al., 2013b; Li et al., 2020). Inhibition of HIF1a, either genetically or pharmacologically with PX-478, impairs prostatic epithelial cell proliferation, enhances cytotoxic lymphocyte and NK cell infiltration, reduces Gr1^{+} MDSC infiltration, and induces apoptosis in PINs (Abu El Maaty et al., 2022). The hypoxia-activated prodrug TH-302 demonstrates cytotoxicity under hypoxia and has shown efficacy in various cancer models, both as a monotherapy or in combination with chemo-, radio- or immunotherapy (Li et al., 2021). For instance, in Pb-Cre4, PTEN$^{pc-/-}$ Smad4$^{pc-/-}$ TRAMP-C2 mice, which develop aggressive prostate adenocarcinoma, the combination of TH-302 hypoxia-prodrug and CTLA-4 and PD-1 checkpoint blockade extends survival (Jayaprakash et al., 2018). Our study revealed that in PTEN$^{(i)pe-/-}$ prostates, the primary change in the mononuclear phagocyte compartment already from the PIN stage is the recruitment of Trem2^{+} TAMs. Trem2 expression in human PCa is associated with poor prognosis (Gao et al., 2023) and recent studies in other cancer types have shown that Trem2^{+} TAMs are critical mediators of immune suppression in the tumor microenvironment, making Trem2 a promising target to enhance antitumoral immune responses. For example,

combination of anti-Trem2 and anti-PD-1 treatment, in an anti-PD-1 resistant colon carcinoma model (CT26), induced tumor rejection in 20–60% of mice and increased activated $CD8^+$ T cell infiltration. Moreover, $Trem2^{-/-}$ mice exhibit significant expansion of natural killer (NK) and cytotoxic T cell populations (Binnewies et al., 2021; Katzenelenbogen et al., 2020; Molgora et al., 2023; Yalcin et al., 2024). In $PTEN^{(i)pe-/-}$ prostate, Trem2 expression is restricted to macrophages, while $Trem2^+$ immunosuppressive neutrophils have been detected in the probasin-mediated aggressive prostate adenocarcinoma (Bancaro et al., 2023). Subsequently, we could consider targeting the suggested immunosuppressive Trem2 macrophages using anti-Trem2 antibody, in combination with anti-PD1 in order to rewire the exhausted $CD8^+$ T cells within the $PTEN^{(i)pe-/-}$ PIN lesions.

Moreover, in our model, $Trem2^+$ TAM express high levels of macrophage migration inhibitory factor (MIF), as indicated by scRNAseq analysis. MIF is a known contributor to the intratumoral recruitment of TAMs, MDSCs and neutrophils, reducing $CD8^+$ T cells and NK cytotoxicity, and promoting angiogenesis (Noe and Mitchell, 2020). This suggests that in $PTEN^{(i)pe-/-}$ prostates, $Trem2^+$ TAMs exert immunosuppressive activity through MIF. Furthermore, in hypoxic tissues such as the tumor microenvironment, MIF and HIF1A synergistically increase lactate production and the senescence-associated secretory phenotype (SASP), promoting the Warburg effect and stabilization of P53 observed in senescence (Mora Barthelmess et al., 2023; Noe and Mitchell, 2020; Yan et al., 2024). MIF also regulates $CD11b^+Gr\text{-}1^+$ myeloid cell migration, differentiation, and proangiogenic function (Zhu et al., 2014). Thus, $Trem2^+$ TAMs could sustain tumor progression and senescence observed in $PTEN^{(i)pe-/-}$ prostates through the MIF/HIF1a axis (Abu El Maaty et al., 2022; Parisotto et al., 2018). Targeting MIF has improved the therapeutic efficacy of immune checkpoint blockade (ICB) in triple-negative breast cancer, increasing intratumoral cytolytic $CD8^+$ T cells and pro-inflammatory macrophages, while decreasing Tregs and tumor-associated neutrophils (Yan et al., 2024). Therefore, combining anti-Trem2 and anti-PD1 treatments or targeting the MIF/HIF1A axis in $Trem2^+$ TAMs, using anti-MIF antagonist, neutralizing anti-MIF antibodies or nanobodies (Sumaiya et al., 2022), stands a promising strategy to control tumor progression in the $PTEN^{(i)pe-/-}$ model.

In $PTEN^{(i)pe-/-}$ prostates, the prominent change observed from the PIN stage is the massive infiltration of neutrophils. Neutrophils, generated in the bone marrow from hematopoietic stem cells (HSCs), differentiate into mature neutrophils, enter the bloodstream and then reach tissues (Overbeeke et al., 2022). Inflammation and certain cancers are associated with accelerated granulopoiesis and induction of neutrophilia (Raskov et al., 2022; Veglia et al., 2021). Research on tumor-associated neutrophils has been hindered by the use of the Gr1 marker to describe the myeloid-derived suppressor cells (MDSC), which include neutrophil and monocyte lineages with potent immunosuppressive activity (Akkari et al., 2024). $Gr1^+$ myeloid cells (Parisotto et al., 2018) or $S100a8^+$ MDSCs (Abu El Maaty et al., 2022) were observed in the prostate of $PTEN^{(i)pe-/-}$ model. As Gr1 recognizes both Ly-6C and Ly-6G, markers commonly used to distinguish monocytes and neutrophils respectively, we avoided using the Gr1 antibody and the MDSCs nomenclature, favoring the monocyte, macrophage

and neutrophil nomenclature instead. Until recently, neutrophils in blood and tissues were considered terminally differentiated cells with defined functions and limited plasticity. This understanding is nowadays being challenged by evidence that neutrophils constitute a heterogeneous population, with reprogramming potential (Gungabeesoon et al., 2023; Ng et al., 2024; Veglia et al., 2021; Wu et al., 2024; Xie et al., 2020; Zilionis et al., 2019). A recent study showed distinct neutrophils states in the tumor microenvironment of orthotopic pancreatic ductal adenocarcinoma (PDAC), undergoing reprogramming to a terminal stage expressing dcTRAIL-R1 and VEGFα while localizing in hypoxic-glycolytic niches where they exert pro-angiogenic, immunosuppressive and pro-tumoral functions (Ng et al., 2024). In $PTEN^{(i)pe-/-}$ prostate, neutrophils resolve in eight different states, with dcTRAIL-R1-expressing neutrophils (N5) primarily detected at the prostatic adenocarcinoma stage, suggesting reprogramming along tumor progression, potentially regulated by the hypoxic microenvironment (Abu El Maaty et al., 2022). Additionally, N5 neutrophils exhibit high expression of Ccl6, suggesting involvement in TME remodeling and sustaining an immunosuppressive environment, as shown recently in lung during breast cancer metastasis (McGinnis et al., 2024).

Neutrophils in the blood are rapidly mobilized to tissues in response to infection or injury. The study by Xie and colleagues showed that in physiological conditions, mature blood neutrophils are divided into three distinct states, including a distinct ISG-expressing population that expands during bacterial infection (Xie et al., 2020). However, thus far, there is no consensus on the nomenclature of the emerging complexity of neutrophil differentiation and activation states in tumors (Jaillon et al., 2020). A recent study generated a neutrophil map across various human cancer types, describing ten distinct states, including an $IFIT1^{+}ISG15^{+}$ subset (Wu et al., 2024). This ISG-expressing subset showed high PD-L1 expression, indicative of an immunosuppressive role (Wu et al., 2024). Moreover, another study recently underscored that efficient immunotherapy with anti-CD40 correlates with ISG-expressing neutrophil infiltration, exhibiting high cytotoxic potential and anti-tumor activity (Gungabeesoon et al., 2023). These neutrophils expressed elevated levels of CXCL10, similar to tumoricidal neutrophils described in mice after TGFβ neutralization (Shaul et al., 2016). Increased levels of CXCL10 are associated with tumor infiltration by effector $CD4^{+}$, $CD8^{+}$, and natural killer cells coinciding with reduced tumor growth and indicative of immunotherapy response in metastatic melanoma (Antonicelli et al., 2011; Reschke et al., 2021). Hoch *et al.* demonstrated that CXCL9 and CXCL10 co-localize with $LAG3^{+}$ T cells expressing CCL4 or CXCL13, contributing to a "hot" $CD8^{+}$ T cell inflamed tumor microenvironment (Hoch et al., 2022). In $PTEN^{(i)pe-/-}$ prostate, the most prominent neutrophil state N0 at the early PIN stage, exhibits an ISG-signature, characterized by high CXCL10 expression, as well as high PDL-1 expression. We can thus, hypothesize that early infiltrating neutrophils (N0) may have anti-tumoral properties, similar to (Gungabeesoon et al., 2023), but they are rapidly reprogrammed towards an immunosuppressive state during prostate progression, ultimately exhibiting dcTRAIL-R1 expression. This reprogramming could be modulated by $Trem2^{+}$ TAMs, and tumor cells via the MIF1/HIF1A axis. Further studies on neutrophil reprogramming in

PTEN$^{(i)pe-/-}$ prostate, particularly with anti-CD40 and anti-PD-L1 treatment, could determine if maintaining or enhancing the ISG state stalls prostate tumor progression.

The validation of innovative immunotherapies in clinical trials for prostate cancer has been hampered by the lack of pre-clinical mouse models recapitulating the genetic alterations, immunological and clinical features of human cancers. Our study provides valuable insights on key immune cells infiltrating the prostate tumors, including exhausted CD8$^+$ T cells (Chen and Mellman, 2017), Trem2$^+$ TAM (Katzenelenbogen et al., 2020), dcTRAIL-R1$^+$ TANs (Ng et al., 2024) and ISG-TANs (Gungabeesoon et al., 2023), as potential targets for mono- or combination therapy. Additionally, our analysis of the immune compartment during prostate cancer development reveals convergent alterations in the tumor microenvironment through the HIF1a/MIF/Ccl6 axis from the PIN stage to adenocarcinoma progression, highlighting that the immune compartment is mobilized very early in tumor formation from the precancerous stage of prostatic intraepithelial neoplasia and is susceptible on reprogramming based on the tumor environmental cues. Notably, the TME exhibits immunosuppressive and pro-tumoral characteristics from the PIN stage. Therefore, early diagnosis and treatment hold greater potential for effectively reprogramming the immune compartment to target tumor cells. A combinatory approach that would reprogram protumoral neutrophils (e.g., using anti-CD40) and Trem2$^+$ TAMs (via anti-Trem2 or modulation of the MIF axis using anti-MIF) and rewire exhausted CD8$^+$ T cells (with anti-PD1) from the PIN stage could induce a critical switch in the immune microenvironment converting “cold” prostate tumors into “hot” tumors, characterized by infiltration of cytotoxic cells. Furthermore, integrating this myeloid-targeting immunotherapeutic strategy with standard treatments, such as androgen deprivation therapy or chemotherapy, could enhance the overall efficacy of prostate cancer treatment.

Thus, our dataset provides a critical resource for the development of novel immunotherapies against prostate cancer.

ACKNOWLEDGEMENTS

We thank the flow cytometry, imaging, bioinformatics, and genomics platforms for their technical support and the biological resource units for the breeding of animals (CIML, CIPHE); Kateryna Len and Darya Yanushko for discussions and technical help at IGBMC; Hugues Lelouard and David Hume for discussions and providing mouse models; Pierre Milpied for discussions and help for the scRNAseq experiments; Pierre Golstein for discussions and the critical reading of the manuscript. scRNAseq experiments were performed at the Plateforme GenomEast (Strasbourg, France; http:// www .igbmc .fr/ technologies/ 5/ team/ 54/) and the Genomics platform of CIML. Bioinformatic analysis was performed in Computational Biology, Biostatistics & Modeling platform (GB2M) of CIML.

FUNDING

This work was supported by the French National Cancer Institute (INCA) to D.M. G.L. and S.H (INCA2019-191 ; PLBIO23-177); the Fondation ARC pour la recherche sur le cancer

(PJA20191209674) and the INCA, Région Sud, the Institute for Cancer Immunology (ICI) and Canceropôle to S.H (2023-01Kpole). The Ministère de l'Enseignement supérieur et de la Recherche and the Fondation pour la Recherche Médicale (FRM) to D.P. ; ANR-10-INBS-04-01 France Bio Imaging to CIML Imagim platform; and the Centre d'Immunologie de Marseille Luminy, which receives its core funding from Aix Marseille University, CNRS, and INSERM.

AUTHOR CONTRIBUTIONS

D.P., G.L., D.M. and S.H. conceived the project. D.P., J.D.C. and S.H. designed and performed the experiments and analyzed the data. G.L. supervised the scRNAseq experiments. L.S. realized the bioinformatic analysis on the scRNAseq dataset. L.C. performed the prostate tissue sections and histology experiments; F.F. and B.M. designed the Slco2b1-IRES-cre-hCD2 mice; M.B. performed fluorescent microscopy analysis and provided mouse models; D.P. and S.H wrote the manuscript. B.M., G.L. and D.M. edited the manuscript.

COMPETING INTERESTS

The authors declare no competing financial interests.

MATERIALS AND METHODS

Mice

CD64^{dtr}, CCR2$^{-/-}$, CX3CR1$^{GFP/WT}$, Zbtb46^{GFP} and CSF1R$^{\Delta FIRE}$ mice were previously described (Baranska et al., 2018; Boring et al., 1997; Faust et al., 2000; Jung et al., 2000; Rojo et al., 2019; Satpathy et al., 2012). Generation of *Slco2b1-IRES-iCre-P2A-hCD2t* is described below. PTEN$^{(i)pe-/-}$ male mice as well as sex-matched PTEN$^{L2/L2}$ control littermates (all on a C57BL/6 genetic background) were generated as described (Ratnacaram et al., 2008). Briefly, mice carrying one copy of the PSA-Cre-ER^{T2} transgene, expressing the Tam-inducible Cre-ER^{T2} recombinase in prostate epithelium under the control of the human PSA promoter, were crossed with mice carrying LoxP-flanked (floxed) alleles of PTEN (L2 allele) to generate PSA-Cre-ER$^{T2(tg/0)}$/PTEN$^{L2/L2}$ (tg, transgenic) and PSA-Cre-ER$^{T2(0/0)}$/PTEN$^{L2/L2}$ mice. Gene ablation was induced by intraperitoneal injection of Tam performed daily for 5 days (1 mg/mouse) to 8- to 10-week-old mice, to generate the transgenic PTEN$^{(i)pe-/-}$ (pe, prostate epithelium; (i), induced) and the respective control PTEN$^{L2/L2}$ mice that did not bear the PSA-Cre-ER^{T2} transgene.

Mice were housed under specific pathogen-free conditions in temperature- and humidity-controlled animal facility with a 12h light/dark cycle. Animals were euthanized with carbon dioxide or cervical dislocation, and tissues were immediately collected, weighed processed for single-cell or histological analysis. *In vivo* procedures were handled in accordance with national and European laws for laboratory animal welfare and experimentation, and protocols approved by the Marseille Ethical Committee for Animal Experimentation and French Animal Ethics Committee (approval APAFIS #25240-2020042716503331 v5 and n° #46078-2023112412266817 v4).

Generation of *Slco2b1-IRES-iCre-P2A-hCD2t* mice

A targeting construct was designed to introduce an IRES-iCre-P2A-hCD2t cassette in the 3' untranslated region of the *Slco2b1* gene, 30 bp downstream of the stop codon. IRES corresponds to an internal ribosomal entry site, iCre to a sequence coding for a codon-improved Cre recombinase, P2A to the sequence coding for a self-cleaving 2A peptide, and hCD2t, to a sequence coding for the human CD2 (Ai et al., 2006). JM8.F6 C57BL/6N ES cells (Pettitt et al., 2009) were electroporated with the targeting vector. After selection in G418, ES cell clones were screened for proper homologous recombination by PCR and Southern blot. Properly recombined embryonic stem cells were injected into Balb/CNRj blastocysts. Following germline transmission, excision of the frt-neo^{r}-frt cassette was achieved through crossing with mice expressing the FLP recombinase (Rodriguez et al., 2000). Two pairs of primers were used to distinguish the WT and edited *Slco2b1* alleles. The first pair (sense 5'-TCAGCAGACAGTCCTTACCC-3' and antisense 5'- ACCGTCAACCTCCTGGAATC-3') amplified a 682 bp band in case of the wild-type *Slco2b1* allele, whereas the second pair (sense 5'-CTCATCATTGGCATATGTGG-3' and antisense 5'- ACCGTCAACCTCCTGGAATC-3') amplified a 295 bp band in the case of the Slco2b1- IRES-iCre-P2A-hCD2t allele.

Cell isolation from tissues

To distinguish circulating cells from tissue resident cells, mice were injected intravenously with 3µg of anti CD45.2-FITC for 3 minutes before euthanasia. Prostates were collected and weighted either as a whole or after the DLV (dorsal-lateral-ventral) lobe isolation. They were minced and incubated under regular manual mixing for 20 min at RT, in 2% FCS RPMI medium containing 1mg/ml DNAse I (Sigma) and 7 mg/ml collagenase II (Worthington). The enzymatic reaction was stopped by adding 60µL of 0.5M EDTA. The cellular suspension was passed through a 5ml syringe with 20G needles for complete tissue dissociation. The single cell solution was filtered through a 70µm cell strainer and centrifuged. The pellet was resuspended in FACS buffer (PBS-5mM EDTA- 2% FCS) and was re-filtered through a 30µm cell stainers (Miltenyi) solution prior to antibody staining.

Spleens were collected and dissociated by mechanical disruption in RPMI medium containing 2% FCS. Red blood cells were lysed using RBC lysis buffer (eBioscience) for 5 min at RT. Single cell suspensions were filtered through a 70 µm cell strainer, centrifuged and resuspended in FACS buffer prior to antibody staining.

Analysis of Blood cells

Blood was collected in EDTA-containing tubes and stained with the appropriate antibody mix in PBS-5mM EDTA solution for 30 min at RT at dark. Red blood cells were lysed with BD FACS Lysing Solution (Becton Dickinson) and the absolute numbers were estimated using CountBright^{TM} absolute count microbeads for flow cytometry (Invitrogen) and normalized by 1µl of blood volume.

***In vivo* depletion of CD64^{+} cells using the CD64^{DTR} mice**

CD64dtr mice were injected intraperitoneally twice and 24 h apart with 1µg DT (Calbiochem, EMD Millipore) in PBS as previously described in (Baranska et al., 2018).

***In vivo* uptake of dextran**

200µM of Dextran-FITC with average mol wt 40,000 (fluorescent Isothiocyanate-dextrane, 250MG FD40-250MG Merck/Sigma-Aldrich) were administered i.v. in a 100 µl volume. The recipient mice were sacrificed after 1 h and the blood and prostates were collected for flow cytometry (blood and prostate) or confocal microscopy (prostate).

***In vivo* treatments**

Adult tumor bearing PTEN$^{(i)pe-/-}$mice at 2 months post tamoxifen were treated i.p. with 100µg murinized anti-Ly-6G (clone 1A8, Vivopurex, Cat# AB00295-2.0-VXL), three times per week for four weeks as described by (Olofsen et al., 2022). Blood was collected prior to the treatment and every 7 days, just before a treatment injection, in order to follow neutrophil counts by facs. Prostate and blood were collected 24h after the last treatment injection and subsequently analyzed by FACS.

In another experimental set-up, tumor bearing PTEN$^{(i)pe-/-}$mice at 3 months post tamoxifen were treated i.p. with a combination of 100µg murinized anti-Ly6G (clone 1A8, Vivopurex, Cat# AB00295-2.0-VXL), and 500µg of murinized rat anti-CSF1R (clone AFS98, Biolegened, Ultra-LEAF™ Purified anti-mouse CD115, Cat # 135542) and 100µg of murinized rat anti-PD1 (clone RMP1-14, BioX Cell, Cat # BE0146) at days 0,3,5,7 of treatment. Alternatively, mice were treated with Rat IgG2a, κ Isotype control (Biolegend, Ultra-LEAF™ Purified, Cat # 400566). Blood was collected prior to the treatment at d0, and at d8 (24h after the last treatment injection), prostate and blood were collected for further facs analysis of the immune compartment.

Chimeras

Complete bone-marrow (BM) chimeras: 8-week-old male C57BL/6J (CD45.2) recipient mice were lethally irradiated twice (4G), 4 h apart, and then transplanted i.v. with 2×10^6 BM cells. BM cells were obtained from femurs and tibias of male C57BL/6J (CD45.1).

Competitive BM chimeras: 8-week-old male C57BL/6J (CD45.2) recipient mice were lethally irradiated twice (4G), 4 h apart. They were transplanted with a 1 to 1 mixture of BM cells isolated either from WT (CD45.1) and WT (CD45.1/CD45.2) or from WT (CD45.1) and CCR2$^{-/-}$ (CD45.1/CD45.2) mice.

Protected BM chimeras: Anesthetized 8-week-old male C57BL/6J (CD45.2) recipient mice were placed into a 6mm thick lead cylinder to selectively expose their upper body to irradiation and protect their lower body including the prostate. Mice were then irradiated (8Gy) and transplanted i.v. with 3×10^7 BM cells. BM cells were obtained from femurs and tibias of male C57BL/6J (CD45.1).

For all chimeric conditions, 8 weeks after reconstitution, the level of reconstitution was determined by facs analysis in blood and prostate. Chimeras were kept on antibiotic-containing water (0.2% Bactrim, Roche) during the whole experiment.

***Ex vivo* phagocytosis assay**

Prostate single cell suspension was incubated at 37°C, 5% CO2, under gentle shaking in culture medium (RPMI-1640 supplemented with 10% fetal calf serum (FCS), 1% GM-CSF, 10% M-CSF, 1% penicillin/streptomycin, 10 mM HEPES, 1 mM glutamine, 1 mM non-essential amino-acids, and 50 µM 2-ME) and in presence of 0.5 µM Fluoresbrite Bright Blue microspheres (Polysciences, Cat# 18339-10). As a control, an identical sample was incubated at 4˚C. After 1h incubation, the phagocytosis was halted by adding 2mL of ice-cold PBS. Cells were washed 2 times and proceed to facs staining.

***Ex vivo* suppressive assay**

CD8$^+$ T cells were isolated from spleen of control PTEN$^{L2/L2}$ mice using the Dynabeads® Untouched™ Mouse CD8 Cells kit (Invitrogen, Cat# 11417D) and following the manufacture's protocol. Isolated CD8$^+$ T cells are stained with Cell Trace Violet (CTV) according to manufacturer's instructions and they were cultured (1 x 10^4 CD8$^+$ T cells/well) with activating

a-CD3/CD28 beads at a stable ratio 1:1 (Dynabeads™ CD3/CD28 Mouse T Activator for T Cell Expansion and Activation, Invitrogen, Cat# 11452D) in 96 well V-bottom plates in culture medium (RPMI-1640 supplemented with 10% fetal calf serum (FCS), 1% GM-CSF, 10% M-CSF, 1% penicillin/streptomycin, 10 mM HEPES, 1 mM glutamine, 1 mM non-essential amino-acids, and 50 µM 2-ME). Decreasing numbers of $CD45^+Ly6G^+CD11b^+$ neutrophils or $CD45^+CD11b^+CD64^+CD88^+$ macrophages sorted from tumor prostates of $PTEN^{(i)pe-/-}$mice at 3 months post tamoxifen (PIN stage), were added to the 1 x 10^4 $CD8^+$ T cells/well to have the following T cell: neutrophil or macrophage ratios, 1:1, 2:1, 4:1, 8:1 and 16:1. Negative controls included non-activated $CD8^+$ T cells, whereas positive controls were $CD8^+$ T cells cultured only with activating beads. Cells were collected after 48h and cell division was measured by assessing the relative CTV dilution by FACS.

Flow cytometry

For surface staining, single cell suspensions were preincubated with anti-Fc receptor antibody (clone 2.4G2) at 4°C for 15 min at dark. Cells were centrifuged and stained with appropriate fluorescent labeled monoclonal antibodies (***Table 3***) in Brilliant FACS Buffer (BD) at 4°C for 30 min at dark.

Cell viability was evaluated using DAPI (4',6-Diamidino-2-Phenylindole, Dihydrochloride) (Life Technologies) or Zombie UV™ Fixable Viability (Biolegend). For intracytoplasmic staining, cells were fixed and permeabilized using a Cytofix/Cytoperm™ fixation-permeabilization kit (BD Biosciences). For cytokines staining, 1 x 10^6 cells were activated for 4 h at 37° C in 0.5 ml of 1x Cell Stimulation Cocktail plus inhibitors (eBioscience).

Stained cell samples were analyzed on a LSR Fortessa or a FACSymphony Flow Cytometer equipped with FACSDiva software (BD Biosciences), and both instruments were validated prior to data acquisition using Flow Cytometry Calibration Particles (Spherotech, RQC-30-5A). Photomultiplier tube voltages were also adjusted to minimize fluorescence spillover. Single-stain controls were prepared with UltraComp eBeads (Thermo Fisher Scientific) following the manufacturer's instructions and were used to calculate a compensation matrix. To determine the positive staining for a given fluorophore-coupled antibody, Fluorescent Minus One (FMO) controls were performed, consisting of the full staining antibody mix except one antibody. Debris were removed based on forward and side scatter, dead cells were excluded using live/dead staining and doublets were excluded by plotting FSC-A versus FSC-H. Leukocytes were subsequently selected by plotting CD45 versus FSC-A. Immune cell heterogenous populations were identified with a multiplexed panel of antibodies directed at 25 cell surface markers, myeloid or lymphoid specific, and the resulting data set was exported for supervised analysis with either BD FACSDiva™ V9 Software or FlowJo™ V10.7 Software (BD Biosciences) or unsupervised analysis with OMIQ Software. Absolute numbers were estimated using CountBright™ absolute count microbeads for flow cytometry (Invitrogen) and normalized by the prostate weight.

For cell sorting, prostate single-cell suspension was pre-enriched using CD45 MicroBeads following manufacturer's protocol (Miltenyi, Cat # 130-052-301) in the AutoMacs separator

(Miltenyi). Subsequently, the enriched sample of $CD45^+$ prostate cells was stained as described above and the populations of interest were sorted on a FACSAria SORP (BD Biosciences).

Table 3. Fluorescent-labeled antibodies used for flow cytometry.

Marker	Clone	Fluorochrome	Company	Cat Number
CD101	Moushi101	PE-Cy7	Invitrogen	25-1011-82
CD115	MCSF-R	PE-Cy7	eBioscience	25-1152-82
CD11b	M1/70	BUV395	BD	563553
CD11c	N418	PE-Cy5	Biolegend	117316
CD161c	PK146	BUV737	BD	741715
CD182 (CXCR2)	SA044G4	PE	Biolegend	149304
CD19	1D3	BUV661	BD	612971
CD2 (human)	RPA-2.10	PE	eBioscience	12-0029-42
CD206	C068C2	BV785	Biolegend	141729
CD274 (PD-L1)	MIH5	SB600	Invitrogen	63-5982-82
CD279 (PD-1)	29F.1A12	G-610-20	Biolegend	135228
CD336 (TIM3)	RMT3-23	PE	Biolegend	566346
CD4	RMA-4	BV605	BD	563151
CD45	30-F11	BV605	BD	563053
CD45	30-F11	BV785	BD	564225
CD45.1	A20	BUV805	BD	741958
CD45.2	104	BV785	BD	563686
CD45.2	104	FITC	BD	553772
CD5	53-7.3	APC-Fire 750	Biolegend	100634
CD5	53-7.3	BUV737	BD	612809
CD5	53-7.3	BV421	BD	562739
CD64	X54-5/7.1	BV711	Biolegend	139311
CD84	Mcd84.7	PE	Biolegend	122805
CD88	20/70	BB630-P	BD	624294
CD8b	H35-17.2	BUV395	BD	740278
DC Sign	MMD3	PE	Biolegend	833004
F4/80	T45-2342	BB790-P	BD	624296
FolR2	FR-b	PE	Biolegend	153304
FolR2	FR-b	APC	Biolegend	153305
IFNg	XMG1,2	BV421	BD	563376
Ly-6C	AL-21	BV421	BD	562727
Ly-6G	1A8	PE-Cy7	BD	560601
Ly-6G	1A8	BV750	BD	747072
Lyve1	ALY7	eFluor660	eBioscience	50-0443-82
MHCII	M5-114.15.2	Alexa Fluor700	Biolegend	107622
CD161c	PK136	BB700	BD	566503
CD161c	PK136	APC-Cy7	Biolegend	108752
Siglec-F	E50-2440	PE-CF594	BD	562757
TCRb	H57-597	BV605	Biolegend	109241
TCRgd	GL3	PE-Cy5	Inviotrogen	15-5711-82

Tim4	RMT4-54	PE-Cy7	Biolegend	130010
Tim4	RMT4-54	Per CP-Cy5.5	eBioscience	46-5866-80
TNFa	MP6-XT22	BV650	BD	563943
TREM2	# 237920	APC	R&D usa	FAB17291A
XCR1	ZET	BV650	Biolegend	148220

Cell morphology

Sorted cells were spun onto Shandon Cytoslides with a Thermo Shandon Cytospin 4 cytofuge (4 min at 400g), fixed with methanol and stained with hematoxylin and eosin.

Confocal microscopy

The whole urogenital system was fixed in Antigen Fix (Microm Microtech) for 4h, washed in 0.1M phosphate buffer, then the prostate was isolated under binocular microscope and dehydrated overnight in 30% sucrose in 0.1M phosphate buffer. Prostates were frozen in Tissue-Tek OCT compound (Electron Microscopy Sciences, Hartfield, PA) and 25-µm sections were permeabilized with Tris buffer + 2% BSA. Unspecific binding was blocked with homemade buffer (Tris + 2% BSA + triton 1% + 1% FCS + 1% serum) for 30 min and sections were stained with the indicated antibodies for cell identification (***Table 4***) and DAPI for nuclei staining. Immunofluorescence confocal microscopy was performed using a Zeiss LSM 880 confocal microscope. Separate images were collected for each fluorochrome and merged to obtain a multicolor image. Final image processing was performed with Image J.

Table 4. Primary and secondary antibodies used for confocal microscopy.

Marker	Species	Clone	Fluorochrome	Company	Cat Number
Anti-goat	Donkey IgG	-	A647	Jackson immunoresearch	705-606-147
Anti-rabbit	Donkey IgG	-	A488	Jackson immunoresearch	711-546-152
Anti-rabbit	Donkey IgG	-	CF568	BIOTIUM	20098-1
Anti-Rat	Donkey IgG	-	Cy3	Jackson immunoresearch	712-166-153
Anti-Rat	Goat	-	A564	Invitrogen	A11081
CD206	Rat	C068C2	APC	Biolegend	141708
CD3	Rat	17A2	FITC	Biolegend	141708
CD31	Goat	PECAM-1	Pur	R&D Systems	AF3628-SP
CD326	Rat	G8.8	AF488	Biolegend	118210
Iba1	Rabbit	AIF1	Pur	Antibodies online	ABIN2857032
Ly-6G	Rat	1A8	APC	Biolegend	127614
Mrp14	Rat	2B10	Pur	Abcam	ab105472
Phalloidin	-	-	AF405	Invitrogen	A30104
Phalloidin	-	-	AF488	Invitrogen	A12379
Tim4	Goat	AF2826	Pur	R&D systems	AF2826

scRNA-seq

DLV lobes of mouse prostates were isolated and dissociated in single-cell suspension as described above. Prostate samples from three PTEN$^{(i)pe-/-}$ mice at 3months post tamoxifen were pooled. Similarly, five prostate samples from sex-matched PTEN$^{L2/L2}$ control littermates at 3months post-tamoxifen were also pooled. The same approach was applied for the 9months samples of PTEN$^{(i)pe-/-}$ and control mice respectively. This experimental procedure was repeated twice in order to generated duplicates for each timepoint and sample type to eliminate possible batch effects during the analysis. Next, samples were FACS-sorted using a BD FACSAriaTM Fusion flow cytometer. Cell viability was evaluated using DAPI (4',6-Diamidino-2-Phenylindole, Dihydrochloride). The control samples were sorted as bulk resident immune cells (CD45.2^{-}CD45^{+}). However, for the tumorous PTEN$^{(i)pe-/-}$ samples, the tissue resident neutrophils (CD45.2^{-}CD45^{+}CD11b^{+}Ly-6G^{+}) were sorted independently from the rest of the immune cells (CD45.2^{-}CD45^{+}CD11b^{+}Ly-6G^{-}). Post sorting, they were re-pooled in a ratio of 30% neutrophils to 70% of rest immune cells.

Trypan blue exclusion assay was used to determine cell number viability of each FACS-sorted sample using a Neubauer Chamber. Samples with a cell viability of >95% were processed with a Chromium Controller (10X Genomics, Leiden, The Netherlands). Sixteen thousand cells were loaded per well in nanoliter-scale Gel Beads-in Emulsion (GEMs). Single-cell 3' mRNA-seq libraries were generated according to "User guide Chromium Next GEM Single Cell 3 prime Reagent Kits v3.3 (Dual index) (10x Genomics, PN CG000315- Rev.D). Briefly, cells were partitioned into droplets with barcoded gel beads and reverse transcription master mix using Chromium Chip G. After complementary DNA (cDNA) synthesis and barcoding from poly-adenylated mRNA, GEMs were disrupted and pooled before amplification of cDNA by 11 polymerase chain reaction (PCR) cycles. Following enzymatic fragmentation and size selection of cDNA amplicons, sequencing libraries were constructed by adding Illumina P5 and P7 adapters (San Diego, USA) and i5 and i7 sample indexes by end repair, A-tailing, adaprot ligation, and 10 cycles of PCR amplification. Quality control and quantification of libraries was performed with a Bioanalyzer 2100 (Agilent Technologies, Santa Clara, CA). The generated libraries were sequenced on NextSeq2000 sequencer using a P3-type flow cell and 100-type cartridge.

Analysis of scRNA-seq datasets

The complete scRNA-seq dataset is composed of 16 datasets: 2 conditions x 2 time points (3 months/9 months) x 2 replicates (R1/R2) x 2 resequencing (Illumina RUN ID 144 and 188). To ensure a rigorous and traceable analysis, these datasets were analyzed through an iterative process.

a) Analysis of individual datasets

Each individual dataset was first independently analyzed to check for the cell quality and the cell heterogeneity using the following workflow.

mRNA FASTQ raw files were processed using Cell Ranger v6.0.1 (10X genomics Inc.) software with default parameters to perform alignment, filtering, barcode counting and unique

molecular identifier (UMI) counting. Reads were aligned to the mouse GRCm38/mm10 genome. Datasets were analyzed using the R package Seurat 4.9.9 (Hao et al., 2020). Quality control was performed to remove poor quality cells. Observing distribution of co-variables we fixed different thresholds for the number of UMIs (max 40000), number of features (max 6000), percentage of mitochondrial genes (max 10%). We did not fix any threshold for the percentage of ribosomal genes since we observed that good quality neutrophils cells have a low content in ribosomal genes. Cells outside the QC threshold ranges were removed. Identification of putative multiplets was performed using scDblFinder (v 1.12, (Germain et al., 2021)). However, since previous tests using multiple samples with HTO identification showed us that the result of automatic multiplet identification is not fully reliable, we decided to flag the identified multiplets but not to remove them at first sight. Instead, we traced them during the whole analysis and removed them only in the final datasets, when all evidence clearly identify them as multiplets.

Expression data were normalized using the NormalizeData function of the Seurat R package (logNormalize method and scale factor of 10000). We centered the expression data from these factors using the Seurat R package ScaleData function (centering true and scaling false). Feature selection was performed using the FindVariableFeatures Seurat R package function with the vst algorithm and 2000 genes selected. Principal component analysis (PCA) was run using Seurat RunPCA function on those 2000 most variable genes. UMAP dimensionality reduction was run using Seurat RunUMAP function on the first 30 principal components from PCA. Clustering was done with Seurat FindClusters based on the first 30 principal components from PCA dimensionality reduction. Best resolution for clustering was determined using the treeMap package (v2.4-4) and the analysis of the cluster's marker genes. Marker genes for each cluster were identified using Wilcoxon rank-sum test from Seurat FindAllMarkers with the log fold change threshold set to 0.1 and an adjusted FDR threshold at 0.001. Cell-cycle scores and cell phases were calculated using CellCycleScoring function with s.genes and g2m.genes from the Seurat package.

b) Analysis of merged datasets by time points

The pairs of re-sequenced samples were then combined together using 10x Genomics Cell Ranger in a single analysis to obtain a complete dataset for each combination of condition, time points and replicate. We then used the obtained count matrices to create merged datasets. We first combined separately the two conditions and two replicates datasets for each time points to obtain one dataset per time point. A complete analysis similar to the one performed for individual dataset was applied (for QC, the main filter was on the percentage of mitochondrial genes set to 10% for both datasets, cluster resolution was set to 0.1 and 0.4 for both datasets). After QC, we obtained 27535 and 8674 cells respectively for the 3 months and 9 months datasets. We observed that, in both datasets, the cells from the two conditions overlapped very well and we decided not to apply any integration algorithm. Heatmap of expression of genes across clusters was performed using the Heatmap function of the ComplexHeatmap (v2.10.0) (Gu et al., 2016) R package.

We then made an automatic cell type annotation using Azimuth (v 0.4.6). Since no reference specific to prostate was available, we used the human PBMC reference as proxy and convert the human genes to mouse genes using Babelgene (v 22.9). Cell were assigned to cell types using 3 levels of annotation. Cell type annotation was then refined through a manual curation of marker genes of clusters in order to identify specific subtypes and cell states.

Using this annotation, we defined 4 main cell types: B cells, T/NK cells, myeloids and neutrophils. Each of these groups was then extracted to create a separate dataset that was analyzed using a similar workflow as for the previous dataset. The new clusters obtained from the separate datasets were assigned to cell types using the newly identified marker genes. The differentially expressed genes (DEG) inside each cluster between cells of the two conditions were identified using the FindMarkers function of the Seurat package. Functional enrichment analysis of the DEG was performed using ClusterProfiler (v 4.6.2).

c) Analysis of global merged dataset

The analysis of the time points datasets allowed us to have a good understanding of the data at each time point. We decided to merge the dataset of all conditions, time points and replicates to generate a single complete dataset. A complete analysis similar to the one performed for individual dataset was applied (for QC, thresholds were number of UMIs max 70000, number of features max 8000, percentage of mitochondrial genes max 10%, cluster resolution was set to 0.1 and 0.4). After QC, we obtained 36175 cells. We observed that, in both datasets, the cells from the two conditions and two time points overlapped very well and we decided not to apply any integration algorithm. As before, Azimuth was used to roughly identify cell types and cell type annotation was refined through manual curation of identified marker genes of clusters.

Here again, using this annotation, we defined 3 main cell types: B cells, T/NK cells, myeloids and neutrophils. Each of these groups was then extracted to create a separate dataset that was analyzed using a similar workflow as for the previous dataset. Moreover, thanks to the increase in cell number, we were able to identify a few cell clusters that were identified as contaminants (Stroma, epithelial, blood vessel, adipocytes and basal cells). Finally, automatic multiplets identification allowed to flag cells that we identified as true multiplets considering gene expression and spatial position in UMAP. Contaminant and multiplets were removed from analysis.

The new clusters obtained from the separate datasets were assigned to cell type using the newly identified marker genes. The differentially expressed genes (DEG) inside each cluster between cells of the two conditions were identified using the FindMarkers function of the Seurat package. Functional enrichment analysis of the DEG was performed using ClusterProfiler (v 4.6.2). Statistical analysis of comparison of gene expression among time points or conditions through clusters was performed by a Kruskal-Wallis test followed by Dunn post-hoc tests. In each dataset, statistical analysis of the change of clusters cell number respect to change in condition and time points was performed using sccomp (v 1.5.6, (Mangiola et al., 2023)).

Cell trajectories analysis was first performed using Monocle 3 (Cao et al., 2019). Cells were clustered using the Monocle 3 cluster_cells function with a resolution set to 0.003. Trajectories were computed using the Monocle 3 learn_graph and order_cells function. Score of gene sets were computed using the AddModuleScore method of the Seurat package and plotted along the pseudotime. Since several datasets showed unconnected clusters, we split the dataset in several cluster groups for which valid trajectory hypothesis were possible. Analysis of gene expression or gene module score along pseudotime was performed using a LOESS regression with the ggplot package.
To confirm trajectories identified by Monocle, we also applied cell dynamic inference using RNA velocity method with velocyto.R (v 0.6). Maps of cell velocity vectors were compared to the trajectories from Monocle and divergent conclusions were not considered for analysis.

Data analysis
Data analysis was performed using the GraphPad Software Prism 10.

Figure 1

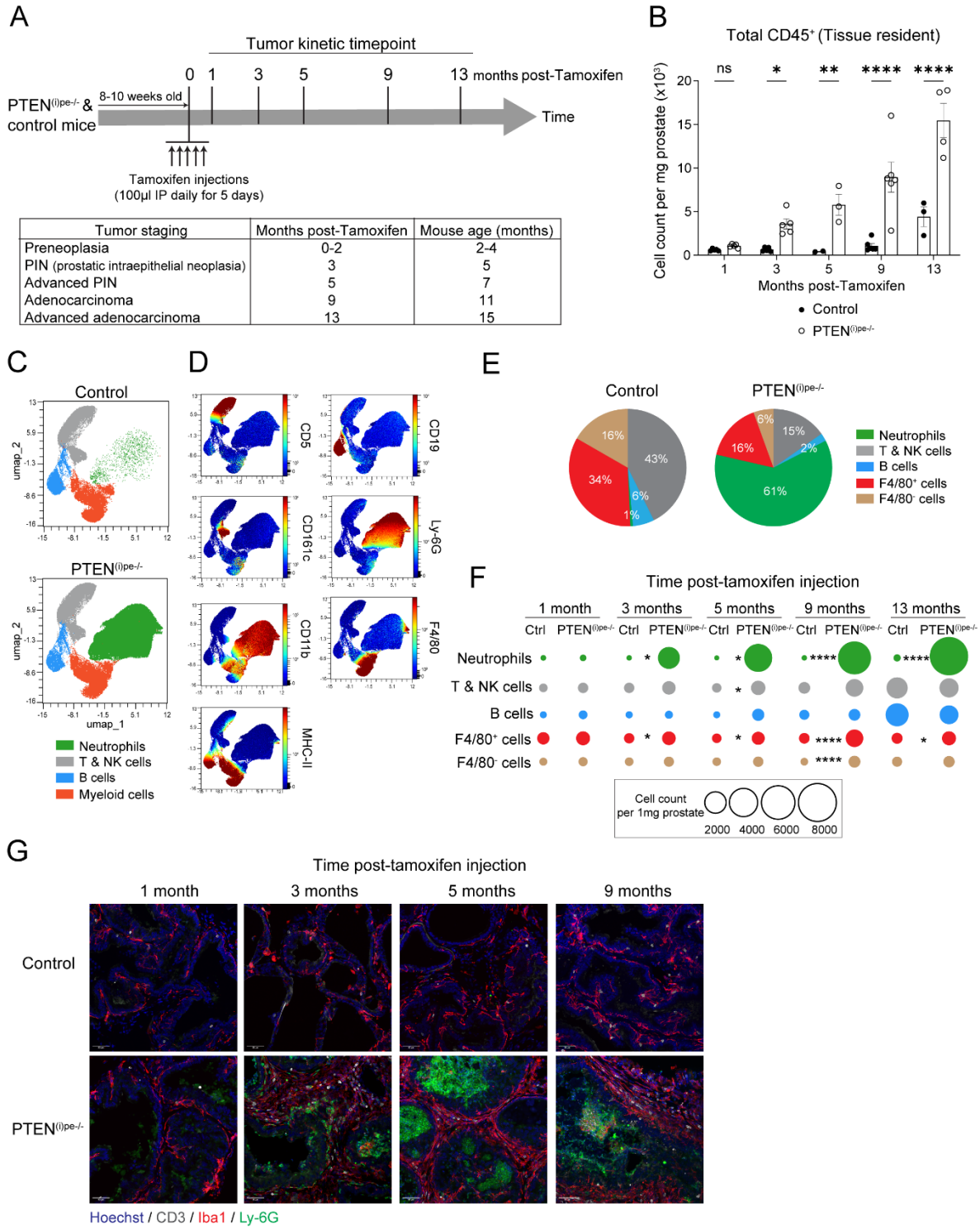

Tumor staging	Months post-Tamoxifen	Mouse age (months)
Preneoplasia	0-2	2-4
PIN (prostatic intraepithelial neoplasia)	3	5
Advanced PIN	5	7
Adenocarcinoma	9	11
Advanced adenocarcinoma	13	15

Figure 1. Longitudinal kinetic analysis of the immune cell infiltration in PTEN$^{(i)pe-/-}$ prostate from preneoplasia to advanced adenocarcinoma stage.

(A) Schematic representation of the spatio-temporal controlled prostate tumor induction indicating the tumor time points analyzed for the longitudinal kinetic study. Both PTEN$^{(i)pe-/-}$ and age-matched male littermate control mice (PTEN$^{L2/L2}$, not carrying CreER^{T2} transgene) are treated with 100µl tamoxifen i.p. for 5 consecutive days after they reach adulthood (8-10 weeks old). The first tamoxifen injection is considered as tumor time point 0. Prostate immune infiltration is assessed at the time points of 1, 3, 5, 9 and 13 months after tamoxifen administration, representing the tumor stages of Preneoplasia, Prostatic Intraepithelial Neoplasia (PIN), Advanced PIN, Adenocarcinoma, and Advanced Adenocarcinoma respectively. The age of the mice at each stage is also indicated.
(B) Quantification of total resident CD45$^+$ immune cells in the prostate of control mice (PTEN$^{L2/L2}$) and tumor bearing PTEN$^{(i)pe-/-}$ mice, determined by flow cytometry at different time points post-tamoxifen administration (1, 3, 5, 9 and 13 months). Counts were normalized per mg of prostate weight. The detailed gating strategy is shown in (**Sup Figure 1B**). Data are presented as mean ±SEM of n=3-6 and are representative of 5 independent experiments per time point with 3-6 animals per group. Statistically significant differences were calculated using two-way ANOVA followed by Sidak's multiple comparison test; ns, non-significant; *, P < 0.05; **, P < 0.01; ****, P < 0.0001.
(C) UMAP plot of unsupervised flow cytometry analysis of control (top) and tumor bearing PTEN$^{(i)pe-/-}$ (bottom) prostates at 3 months post-tamoxifen administration (PIN stage).
(D) Scatter plots (colored-continuous) of control and PTEN$^{(i)pe-/-}$ prostates, showing the expression of surface markers used for the unsupervised facs analysis and annotation, as presented in (C).
(E) Pie charts showing the frequencies of neutrophils, T-NK cells, B cells, F4/80$^+$ cells and F4/80$^-$ cells, detected by the supervised flow cytometry analysis, in the prostates of control and PTEN$^{(i)pe-/-}$ mice at 3 months post-tamoxifen administration. Detailed gating strategy is described in (**Sup Figure 1D**).
(F) Quantitative counts of neutrophils, T-NK cells, B cells, F4/80$^+$ cells and F4/80$^-$ cells, detected by the supervised flow cytometry analysis, in the prostates of control and PTEN$^{(i)pe-/-}$ mice, at different time points post-tamoxifen administration (1, 3, 5, 9 and 13 months) and after normalization per mg of prostate weight. The dot size is representative of the cell count. Data are presented as mean ±SEM of n=3-6 and are representative of 5 independent experiments per time point with 3-6 animals per group. Statistically significant differences were calculated using two-way ANOVA followed by Sidak's multiple comparisons test; *, P < 0.05; ****, P < 0.0001.
(G) Confocal microscopy analysis showing Hoechst (blue), CD3$^+$ T cells (white), Iba1$^+$ macrophages (red), and Ly-6G$^+$ neutrophils (green) in prostate tissue sections from control and tumor bearing PTEN$^{(i)pe-/-}$ mice, at different time points post-tamoxifen administration (1, 3, 5 and 9 months). Representative staining from the dorsal-lateral (DL) prostate lobes (scale bar of 50 µm).

Figure 2

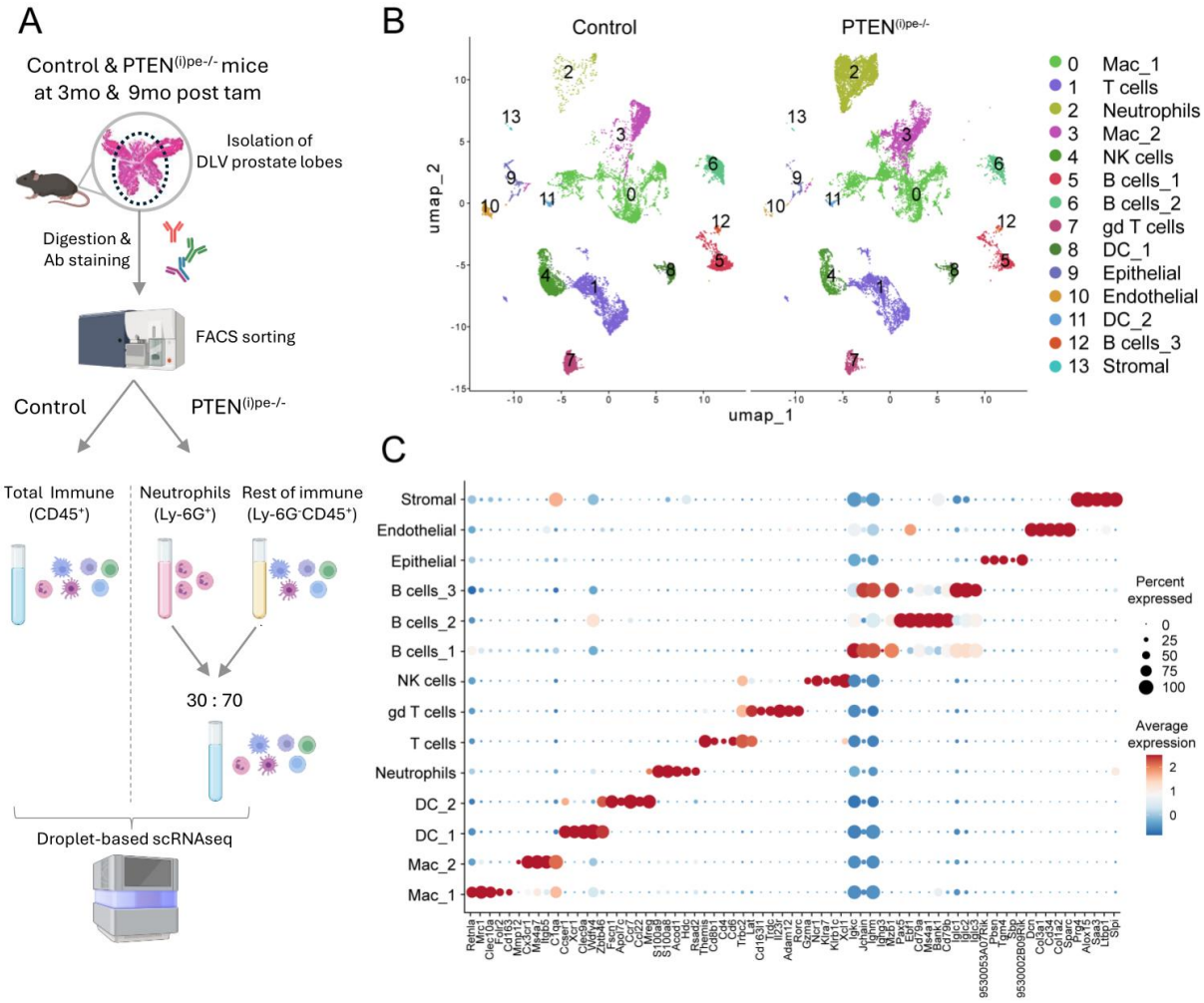
A
Control & PTEN(i)pe-/- mice
at 3mo & 9mo post tam
Isolation of
DLV prostate lobes
Digestion &
Ab staining
FACS sorting
Control
PTEN(i)pe-/-
Total Immune
(CD45+)
Neutrophils
(Ly-6G+)
Rest of immune
(Ly-6G-CD45+)
30 : 70
Droplet-based scRNAseq
B
Control
PTEN(i)pe-/-
umap_2
umap_1
0 Mac_1
1 T cells
2 Neutrophils
3 Mac_2
4 NK cells
5 B cells_1
6 B cells_2
7 gd T cells
8 DC_1
9 Epithelial
10 Endothelial
11 DC_2
12 B cells_3
13 Stromal
C
Stromal
Endothelial
Epithelial
B cells_3
B cells_2
B cells_1
NK cells
gd T cells
T cells
Neutrophils
DC_2
DC_1
Mac_2
Mac_1
Percent
expressed
0
25
50
75
100
Average
expression
2
1
0

Figure 2. Single cell RNA sequencing analysis of tissue resident CD45^{+} prostate immune cells in PTEN$^{(i)pe-/-}$ and control mice at 3- and 9-months post tamoxifen administration.

(A) Cells were extracted from DLV prostate lobes by enzymatic digestion. Prostate samples from three PTEN$^{(i)pe-/-}$ mice at 3 months post tamoxifen were pooled prior to sorting. Similarly, prostate samples from five sex-matched PTEN$^{L2/L2}$ control littermates at 3 months post-tamoxifen were also pooled prior to sorting. The same approach was applied for the 9 months samples from PTEN$^{(i)pe-/-}$ and control mice. Tissue resident CD45^{+} immune cells were sorted by fluorescence-activated cell sorting (FACS). As we had previously found that neutrophils were predominant within the leukocyte infiltrate from PIN to adenocarcinoma stage in PTEN$^{(i)pe-/-}$ prostates, neutrophils were sorted separately from the other CD45^{+} resident immune cells. The separated-sorted cells were then re-mixed at a ratio of 30% neutrophils with CD45^{+} non-neutrophil immune cells prior 10X Genomics Chromium System encapsulation and scRNA sequencing.
(B) Integrative analysis of scRNA-seq of the CD45^{+} prostate resident immune cells visualized with a UMAP embedding for control (left) and PTEN$^{(i)pe-/-}$ (right) samples comprising 2 replicates of 3 months and 9 months for each genotype. The color-coded cluster annotation is mentioned. The cell types assigned to the clusters was determined by identifying the marker genes of the clusters.
(C) Dot plot of the average expression level of the 5 top marker genes of each cluster identified in (B). The color of the dots represents the average of the normalized and scaled expression of the marker genes in each cell type, and their size indicates the percentage of cells expressing the marker genes in the cluster.

Figure 3

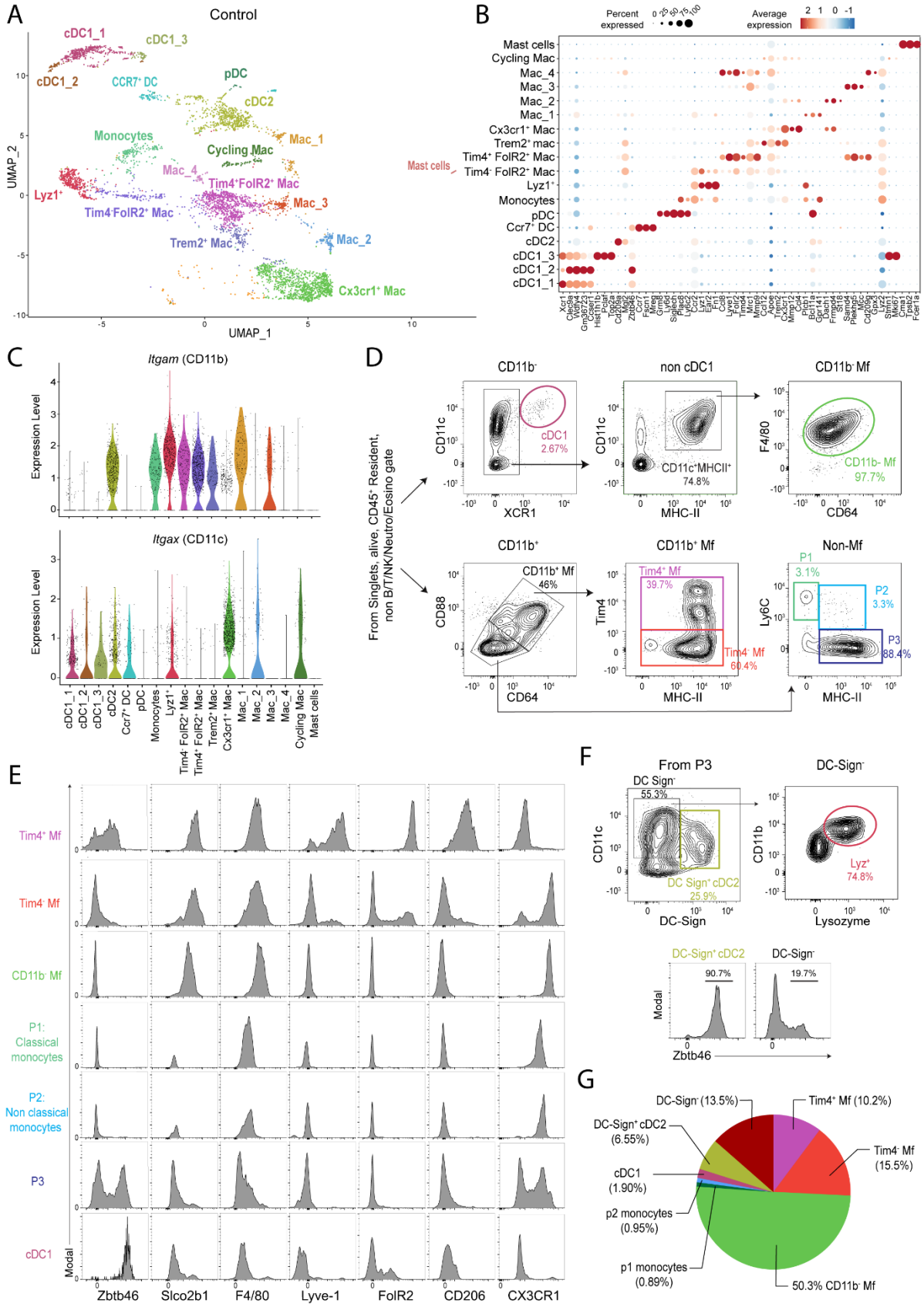
A
Control
cDC1_1
cDC1_3
cDC1_2
CCR7⁺ DC
pDC
cDC2
Monocytes
Mac_1
Cycling Mac
Mac_4
Tim4⁺FolR2⁺ Mac
Lyz1⁺
Mac_3
Tim4⁻FolR2⁺ Mac
Trem2⁺ Mac
Mac_2
Cx3cr1⁺ Mac
UMAP_1
UMAP_2
B
Percent expressed
Average expression
Mast cells
Cycling Mac
Mac_4
Mac_3
Mac_2
Mac_1
Cx3cr1⁺ Mac
Trem2⁺ mac
Tim4⁺ FolR2⁺ Mac
Tim4⁻ FolR2⁺ Mac
Lyz1⁺
Monocytes
pDC
Ccr7⁺ DC
cDC2
cDC1_3
cDC1_2
cDC1_1
C
Itgam (CD11b)
Itgax (CD11c)
Expression Level
cDC1_1
cDC1_2
cDC1_3
cDC2
Ccr7⁺ DC
pDC
Monocytes
Lyz1⁺
Tim4⁻ FolR2⁺ Mac
Tim4⁺ FolR2⁺ Mac
Trem2⁺ Mac
Cx3cr1⁺ Mac
Mac_1
Mac_2
Mac_3
Mac_4
Cycling Mac
Mast cells
D
From Singlets, alive, CD45⁺ Resident, non B/T/NK/Neutro/Eosino gate
CD11b⁻
non cDC1
CD11b⁻ Mf
CD11c
XCR1
cDC1
2.67%
MHC-II
CD11c⁺MHCII⁺
74.8%
F4/80
CD64
CD11b- Mf
97.7%
CD11b⁺
CD11b⁺ Mf
CD88
CD11b⁺ Mf
46%
CD64
CD11b⁺ Mf
Tim4⁺ Mf
39.7%
Tim4
Tim4⁻ Mf
60.4%
MHC-II
Non-Mf
Ly6C
P1
3.1%
P2
3.3%
P3
88.4%
MHC-II
E
Tim4⁺ Mf
Tim4⁻ Mf
CD11b⁻ Mf
P1: Classical monocytes
P2: Non classical monocytes
P3
cDC1
Modal
Zbtb46
Slco2b1
F4/80
Lyve-1
FolR2
CD206
CX3CR1
F
From P3
DC Sign⁻
55.3%
CD11c
DC Sign⁺ cDC2
25.9%
DC-Sign
DC-Sign⁻
CD11b
Lyz⁺
74.8%
Lysozyme
DC-Sign⁺ cDC2
90.7%
DC-Sign⁻
19.7%
Modal
Zbtb46
G
DC-Sign⁻ (13.5%)
Tim4⁺ Mf (10.2%)
DC-Sign⁺ cDC2 (6.55%)
Tim4⁻ Mf (15.5%)
cDC1 (1.90%)
p2 monocytes (0.95%)
p1 monocytes (0.89%)
50.3% CD11b⁻ Mf

Figure 3. Unraveling the myeloid cell heterogeneity in steady-state mouse prostate using transcriptomic and flow cytometric analysis.

(A) Integrative analysis on the myeloid clusters 0, 3, 8 and 11 of the scRNA-seq control samples comprising both timepoints from the general UMAP shown in **Figure 2B**, visualized with a UMAP embedding. The colors represent the recalculated clusters. Cell type annotation was performed using the new cluster marker genes.
(B) Dot plot of the average expression level of the 5 top marker genes of each cluster identified in (A). The color of the dots represents the average of the normalized and scaled expression of the marker genes in each cell type, and their size indicates the percentage of cells expressing the marker genes in the cluster.
(C) Violin plots of the transcript levels of *Itgam* and *Itgax* genes for each cluster from the control samples as annotated in (A).
(D) Representative myeloid gating strategy of flow cytometry analysis in adult (10 weeks old) C57BL/6J prostates. First doublets, dead cells and blood contaminants ($CD45.2^+$) were excluded. After removal of T, B, NK cell and neutrophils (gating as described in **Figure 1B, D**), tissue resident $CD45^+$ immune cells were analyzed. Eosinophils were also excluded using the markers CD11b and Siglec-F (not shown). Then, the $XCR1^+CD11c^+$ cDC1 cells were identified from the $CD11b^-$ cells. Within the $XCR1^-$ non-cDC1 gate, the $CD11c^+$MHC-II^+ population was identified and further gated as $CD64^+F4/80^+$ cells, that we named $CD11b^-$ macrophages. The $CD11b^+$ cells were plotted to identify the $CD11b^+CD64^+CD88^+$ macrophages, that were further separated into $Tim4^+$ and $Tim4^-$ macrophages using the Tim4 and MHC-II markers. From the $CD64^-CD88^-$ non-macrophage gate, three populations were distinguished based on the expression of Ly-6C and MHC-II: the P1 classical monocytes (Ly-$6C^{High}$MHC-II^-), the P2 non-classical/activated monocytes (Ly-$6C^{int\ to\ low}$MHC-II^+), and the P3 population (Ly-$6C^-$MHC-II^+).
(E) Histograms showing the protein expression of F4/80, Lyve-1, FolR2 and CD206 on the identified myeloid prostatic populations based on the gating strategy presented in (D). The following cell-reporter mouse models were also used: Zbtb46-GFP, Slco2b1-hCD2, CX3CR1-GFP.
(F) Gating strategy to identify cDC2 cells and Lyz^+ cells. DC-$Sign^+CD11c^+$ cDC2 cells were identified from the P3 population (Ly-$6C^-$MHC-II^+), based on the expression of DC-Sign and CD11c. From the DC-$Sign^-$ $CD11c^+$, the Lyz^+ cells were also identified, based on the intracellular marker Lysozyme. Histograms of Zbtb46 expression is shown for cDC2 and DC-$Sign^-CD11c^+$ populations.
(G) Pie chart showing the distribution the different color-coded myeloid cell subpopulations in the adult steady-state prostate (10 weeks old C57BL/6J) based on their frequency.

Figure 4

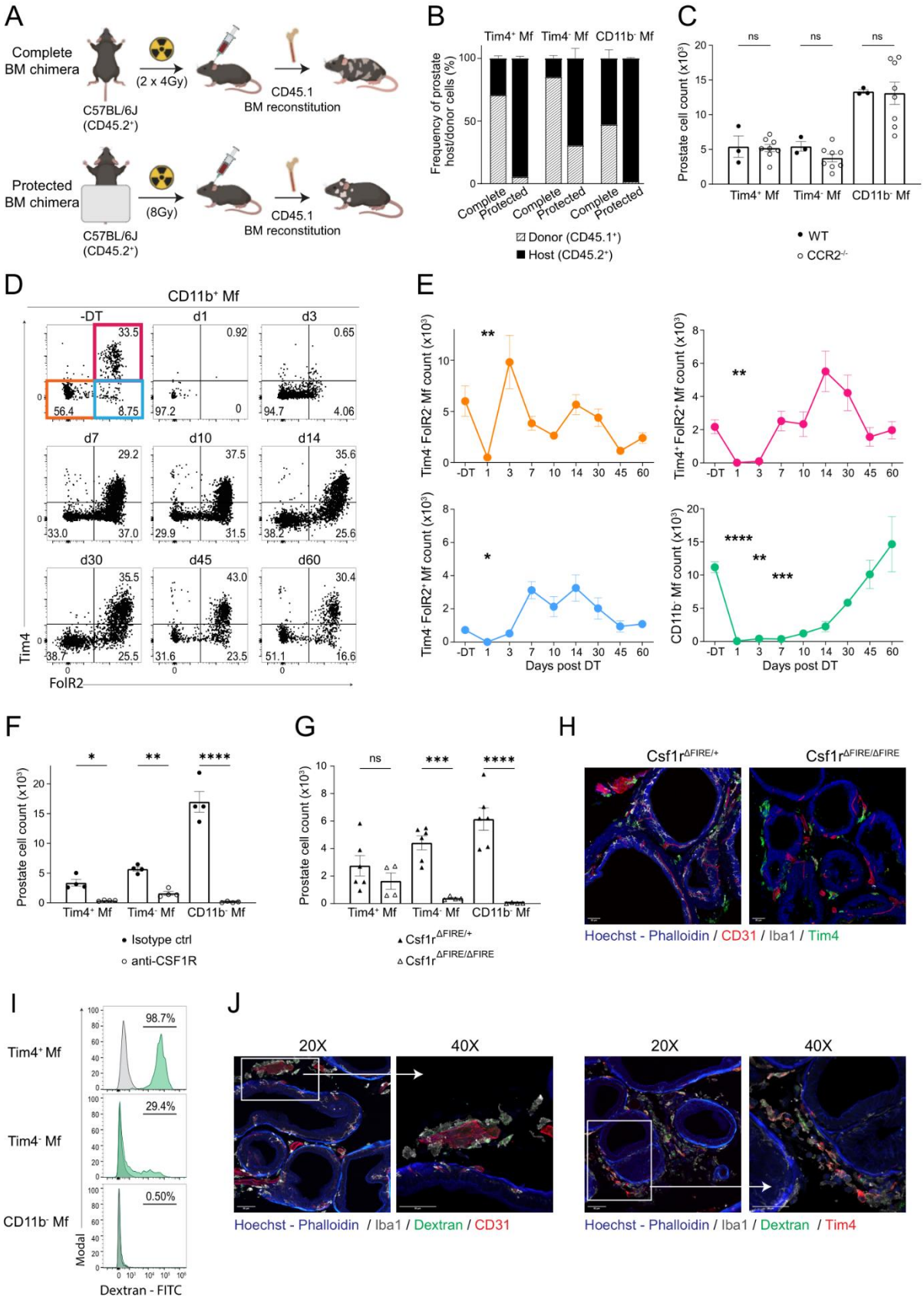
A
Complete BM chimera
(2 x 4Gy)
C57BL/6J (CD45.2+)
CD45.1 BM reconstitution
Protected BM chimera
(8Gy)
C57BL/6J (CD45.2+)
CD45.1 BM reconstitution
B
Tim4+ Mf
Tim4- Mf
CD11b- Mf
Frequency of prostate host/donor cells (%)
Complete
Protected
Donor (CD45.1+)
Host (CD45.2+)
C
ns
Prostate cell count (x10³)
Tim4+ Mf
Tim4- Mf
CD11b- Mf
WT
CCR2-/-
D
CD11b+ Mf
-DT
d1
d3
d7
d10
d14
d30
d45
d60
Tim4
FolR2
E
Tim4+ FolR2- Mf count (x10³)
Tim4+ FolR2+ Mf count (x10³)
Tim4- FolR2+ Mf count (x10³)
CD11b- Mf count (x10³)
Days post DT
F
Prostate cell count (x10³)
Tim4+ Mf
Tim4- Mf
CD11b- Mf
Isotype ctrl
anti-CSF1R
G
Prostate cell count (x10³)
Csf1r ΔFIRE/+
Csf1r ΔFIRE/ΔFIRE
H
Csf1r ΔFIRE/+
Csf1r ΔFIRE/ΔFIRE
Hoechst - Phalloidin / CD31 / Iba1 / Tim4
I
Tim4+ Mf
Tim4- Mf
CD11b- Mf
98.7%
29.4%
0.50%
Modal
Dextran - FITC
J
20X
40X
Hoechst - Phalloidin / Iba1 / Dextran / CD31
Hoechst - Phalloidin / Iba1 / Dextran / Tim4

Figure 4. Unraveling the ontogeny and turnover of prostate macrophages.

(A) 10 weeks old C57BL/6J (CD45.2) male mice were irradiated following two schemes: (top) complete BM chimera with 2 x 4Gy irradiations of the whole body, 4 hours apart, or (bottom) protected BM chimera with 1 x 8Gy shielded irradiation of upper-body, by placing a protective lead shield with only the head and front legs exposed. Following irradiation, all the mice were reconstituted by i.v. injection of CD45.1$^+$ WT BM cells. The reconstitution by donor immune cells in blood and prostate was analyzed 8 weeks later by facs analysis.
(B) BM chimerism is presented as the frequency of host (CD45.2$^+$) to donor (CD45.1$^+$) cells for the Tim4$^+$, Tim4$^-$ and CD11b$^-$ prostate macrophages in complete and protected BM chimeras (FACS gating strategy similar to **Figure 3D**). Data are presented as mean ±SEM of n=3-5 and are representative of 3 independent experiments.
(C) Absolute cell numbers of Tim4$^+$, Tim4$^-$ and CD11b$^-$ macrophages in prostates of 10 weeks old CCR2$^{-/-}$ and WT mice (FACS gating strategy similar to **Figure 3D**). Data are presented as mean ± SEM of n = 3-8, and statistical difference was calculated using an unpaired t-test; ****, P < 0.0001. Data are representative of 2 independent experiments.
(D) Replenishment kinetics of CD11b$^+$ macrophages in the prostate of CD64^{dtr} mice after diphtheria toxin (DT) treatment. CD64^{dtr} mice were untreated (-DT) or treated twice, 24h apart with i.p. injections of DT. Flow cytometry analysis was performed on untreated (-DT) and 1, 3, 7, 10, 14, 30, 45 and 60 days (d) after the last DT injection. CD11b$^+$ macrophage subsets were analyzed at the specific time points using Tim4 and FolR2 markers to define the percentage of Tim4$^-$FolR2$^-$ (orange gate), Tim4$^+$FolR2$^+$ (pink gate) and Tim4$^-$FolR2$^+$ (blue gate) macrophages in prostate.
(E) Quantification of the replenishment kinetics of Tim4$^-$FolR2$^-$ (orange), Tim4$^+$FolR2$^+$ (pink), Tim4$^-$FolR2$^+$ (blue) and CD11b$^-$ (green) macrophage subsets in CD64^{dtr} prostates (based on gating strategy on FACS plots in **Figure 4D** and **Supp Figure 4H**) showing untreated (-DT) and 1, 3, 7, 10, 14, 30, 45 and 60 days (d) after the last DT injection. Data are presented as mean ±SEM of n=3-14 and are a cumulative representation of 4 independent experiments with 3-5 animals per group. Statistically significant difference was calculated using Kruskal-Wallis one-way ANOVA followed by Dunn's multiple comparisons test; *, P < 0.05; **, P < 0.01; ***, P < 0.001; ****, P < 0.0001
(F) Counts of prostate macrophage subsets in adult steady-state mice (10 weeks old C57BL/6J) treated with rat IgG2a isotype control or anti-CSF1R antibody (FACS gating strategy similar to **Figure 3D**). Data are presented as mean ±SEM, are representative of 2 independent experiments with 4 animals /group.
(G) Counts of prostate macrophage subsets in adult (10 weeks old) Csf1r$^{\Delta FIRE/+}$ and Csf1r$^{\Delta FIRE/\Delta FIRE}$ mice (FACS gating strategy similar to **Figure 3D**). Data are presented as mean ±SEM and are a cumulative representation of 2 independent experiments with 2-4 animals per group. For F-G, the statistically significant difference was calculated using Ordinary one-way ANOVA followed by multiple comparisons test; *, P < 0.05; **, P < 0.01; P < 0.001; ****, P < 0.0001.
(H) Qualitative confocal microscopy analysis showing the staining of Hoechst-Phalloidin (blue), CD31$^+$ blood vessels (red), Iba1$^+$ Macrophages (white), and Tim4$^+$ macrophages (green) in prostate tissue sections from adult Csf1r$^{\Delta FIRE/+}$ and Csf1r$^{\Delta FIRE/\Delta FIRE}$ mice (10 weeks old). Representative staining from the dorsal-lateral (DL) prostate lobes (scale bar of 50 µm).
(I) Histograms showing *in vivo* dextran-FITC uptake by the different macrophage subsets in the prostate of adult steady-state mice (9 weeks old C57BL/6J), 1h after i.v. injection of dextran-FITC (FACS gating strategy similar to **Figure 3D**). Representative data (overlay) from treated (green) and non-treated (grey) mice. Frequency of the Dextran$^+$ gate is shown. Data are representative of 3 independent experiments with 3-5 animals per group.
(J) Qualitative confocal microscopy analysis of prostate tissue sections from adult steady-state mice (10 weeks old C57BL/6J). On the left: staining with Hoechst-Phalloidin (blue), CD31$^+$ blood vessels (red), Iba1$^+$ Macrophages (white) and dextran-FITC (green), at 20x and 40x magnification. On the right: staining with Hoechst-Phalloidin (blue), Tim4$^+$ macrophages (red), Iba1$^+$ Macrophages (white) and Dextran-FITC (green) at 20x and 40x magnification. Representative staining from the dorsal-lateral (DL) prostate lobes (scale bar of 50 µm).

Figure 5

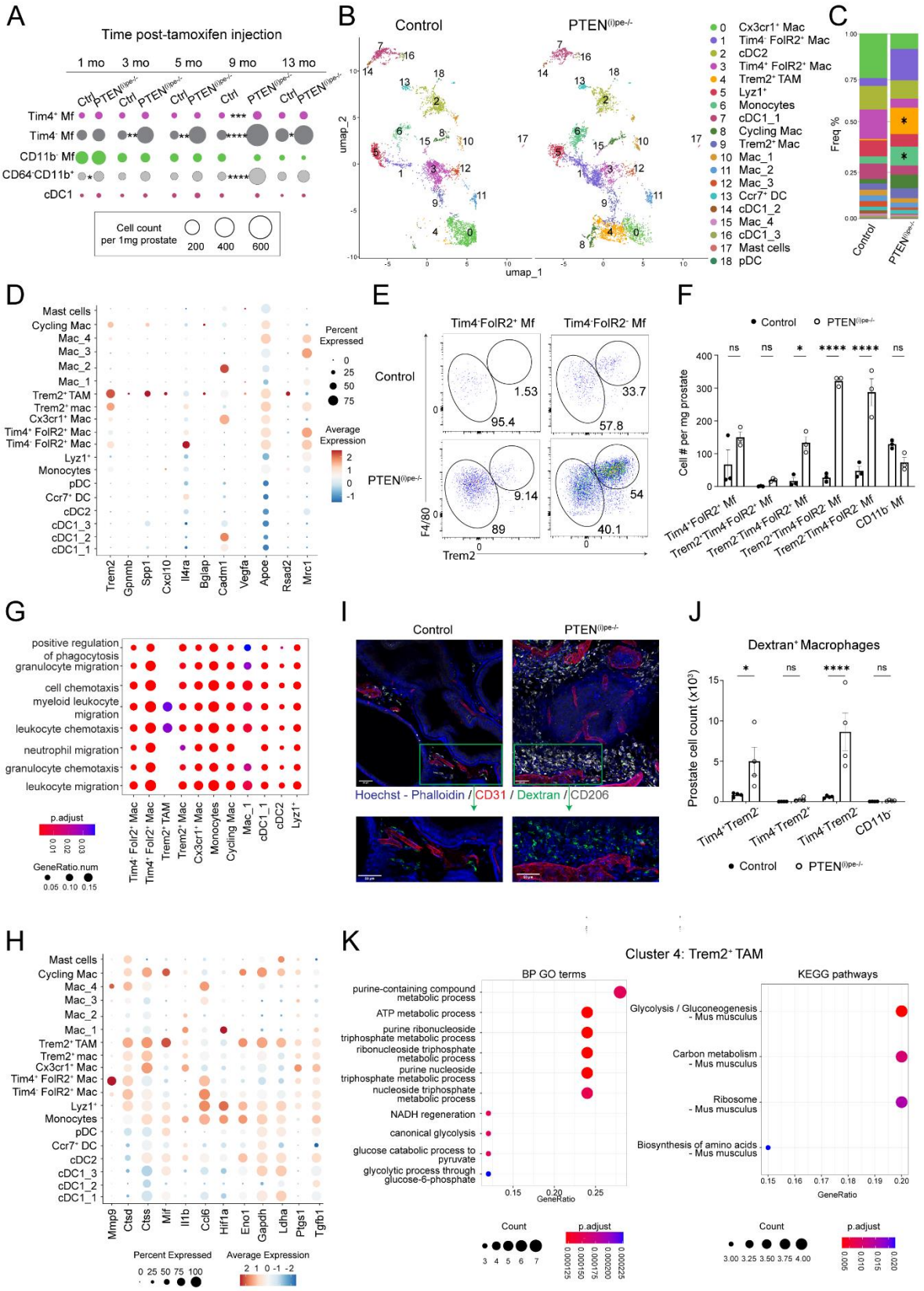
A
Time post-tamoxifen injection
1 mo
3 mo
5 mo
9 mo
13 mo
Ctrl
PTEN(i)pe-/-
Tim4+ Mf
Tim4- Mf
CD11b- Mf
CD64-CD11b+
cDC1
Cell count per 1mg prostate
200
400
600
B
Control
PTEN(i)pe-/-
umap_1
umap_2
0 Cx3cr1+ Mac
1 Tim4- FolR2+ Mac
2 cDC2
3 Tim4+ FolR2+ Mac
4 Trem2+ TAM
5 Lyz1+
6 Monocytes
7 cDC1_1
8 Cycling Mac
9 Trem2+ Mac
10 Mac_1
11 Mac_2
12 Mac_3
13 Ccr7+ DC
14 cDC1_2
15 Mac_4
16 cDC1_3
17 Mast cells
18 pDC
C
Freq %
Control
PTEN(i)pe-/-
D
Mast cells
Cycling Mac
Mac_4
Mac_3
Mac_2
Mac_1
Trem2+ TAM
Trem2+ mac
Cx3cr1+ Mac
Tim4+ FolR2+ Mac
Tim4- FolR2+ Mac
Lyz1+
Monocytes
pDC
Ccr7+ DC
cDC2
cDC1_3
cDC1_2
cDC1_1
Trem2
Gpnmb
Spp1
Cxcl10
Il4ra
Bglap
Cadm1
Vegfa
Apoe
Rsad2
Mrc1
Percent Expressed
Average Expression
E
Tim4-FolR2+ Mf
Tim4-FolR2- Mf
Control
PTEN(i)pe-/-
1.53
95.4
33.7
57.8
9.14
89
54
40.1
F4/80
Trem2
F
Control
PTEN(i)pe-/-
Cell # per mg prostate
ns
*
****
Tim4+FolR2+ Mf
Trem2-Tim4+FolR2+ Mf
Trem2+Tim4+FolR2+ Mf
Trem2-Tim4+FolR2- Mf
CD11b- Mf
G
positive regulation of phagocytosis granulocyte migration
cell chemotaxis
myeloid leukocyte migration
leukocyte chemotaxis
neutrophil migration
granulocyte chemotaxis
leukocyte migration
Tim4- Folr2+ Mac
Tim4+ Folr2+ Mac
Trem2+ TAM
Trem2+ Mac
Cx3cr1+ Mac
Monocytes
Cycling Mac
Mac_1
cDC1_1
cDC2
Lyz1+
p.adjust
GeneRatio.num
I
Control
PTEN(i)pe-/-
Hoechst - Phalloidin / CD31 / Dextran / CD206
J
Dextran+ Macrophages
Prostate cell count (x10³)
ns
****
Tim4+Trem2-
Tim4-Trem2+
Tim4-Trem2-
CD11b-
Control
PTEN(i)pe-/-
H
Mast cells
Cycling Mac
Mac_4
Mac_3
Mac_2
Mac_1
Trem2+ TAM
Trem2+ mac
Cx3cr1+ Mac
Tim4+ FolR2+ Mac
Tim4- FolR2+ Mac
Lyz1+
Monocytes
pDC
Ccr7+ DC
cDC2
cDC1_3
cDC1_2
cDC1_1
Mmp9
Ctsd
Ctss
Mif
Il1b
Ccl6
Hif1a
Eno1
Gapdh
Ldha
Ptgs1
Tgfb1
Percent Expressed
Average Expression
K
Cluster 4: Trem2+ TAM
BP GO terms
purine-containing compound metabolic process
ATP metabolic process
purine ribonucleoside triphosphate metabolic process
ribonucleoside triphosphate metabolic process
purine nucleoside triphosphate metabolic process
nucleoside triphosphate metabolic process
NADH regeneration
canonical glycolysis
glucose catabolic process to pyruvate
glycolytic process through glucose-6-phosphate
GeneRatio
KEGG pathways
Glycolysis / Gluconeogenesis - Mus musculus
Carbon metabolism - Mus musculus
Ribosome - Mus musculus
Biosynthesis of amino acids - Mus musculus
Count
p.adjust

Figure 5. Trem2^{+} tumor associated macrophages infiltrate the prostate of PTEN$^{(i)pe-/-}$ mice.

(A) Quantitative kinetic FACS analysis of the prostatic myeloid immune cells populations (Tim4^{+} Mf, Tim4^{-} Mf, CD11b^{-} Mf, CD64^{-}CD11b^{+} cells, cDC1) from control and tumor-bearing PTEN$^{(i)pe-/-}$ mice, examined at different time points post-tamoxifen administration (1, 3, 5, 9 and 13 months) and after normalization per mg of prostate weight (FACS gating strategy similar to **Figure 3D**). The dot size is representative of cell count. Data are presented as mean ±SEM of n=3-6 and they are representative of 5 independent experiments per timepoint with 3-6 animals per group. Statistical significance was calculated using mixed effects model followed by Sidak's multiple comparisons test; *, P < 0.05; **, P < 0.01; ***, P < 0.001; ****, P < 0.0001

(B) Integrative analysis of scRNA-seq of mononuclear phagocyte clusters (0, 3, 8, 11) of prostates from the general UMAP shown in **Figure 2B**, visualized with a UMAP embedding for control (left) and PTEN$^{(i)pe-/-}$ (right) samples comprising 2 replicates of 3 months and 9 months for each genotype. The colors represent the recalculated clusters. Cell type annotation was performed based on the marker genes of the new clusters.

(C) Stacked bar graph showing the fractional composition of cell number for different clusters within scRNA-seq for control and PTEN$^{(i)pe-/-}$ samples. The color code corresponds to the clusters shown in (B). Significance between the conditions for the different clusters is indicated by an asterisk, based on the statistical analysis presented in **Sup Figure 5A**.

(D) Dot plot of the average expression level of selected top marker genes of cluster 4 (Trem2^{+} TAM) as identified in (B). The color of the dots represents average of normalized and scaled expression of marker genes in each cell type, and their size indicates the percent of cells expressing the marker genes in the cluster

(E) Gating strategy to identify Trem2^{+} and Trem2^{-} populations within the Tim4^{-}FolR2^{+} and Tim4^{-}FolR2^{+} Mf subsets from control and PTEN$^{(i)pe-/-}$ prostates at PIN stage (3 months post tam).

(F) Quantification of the different macrophage populations from control and PTEN$^{(i)pe-/-}$ prostates at PIN stage (3 months post tam), based on the gating strategy shown in (E). Counts are normalized per mg of prostate. Data are presented as mean ±SEM of n=3 animals and are representative of 2 independent experiments. Statistical significance was calculated using ordinary two-way Anova followed by Sidak's multiple comparisons test; **, P < 0.01; ****, P < 0.0001

(G) Functional enrichment of the different myeloid clusters based on differential gene expression (DEG) of PTEN$^{(i)pe-/-}$ versus Control samples for several selected Gene Ontology (GO) Biological Process (BP) terms. Dot color represents the adjusted p-value of the test and dot size represents the ratio of DEG present in the GO BP term.

(H) Dot plot of the average expression level of selected marker genes for the myeloid clusters of PTEN$^{(i)pe-/-}$ samples as identified in (B). The color of the dots represents average of normalized and scaled expression of marker genes in each cell type, and their size indicates the percent of cells expressing the marker genes in the cluster.

(I) Qualitative confocal microscopy analysis of prostate tissue sections from control (left) and PTEN$^{(i)pe-/-}$ (right) prostates, at PIN stage (3 months post tam). Staining shows Hoechst-Phalloidin (blue), CD31^{+} blood vessels (red), CD206^{+} Macrophages (white) and Dextran-FITC (green). Representative staining from the dorsal-lateral (DL) prostate lobes (scale bar of 50µm).

(J) Quantification of the dextran^{+} prostate macrophage subsets at PIN stage (3 months post tam), based on the gating strategy shown in **Sup Figure 5E**. Data are presented as mean ±SEM of n=3-6 and are representative of 3 independent experiments with 3 animals per group. Statistical significance was calculated using ordinary two-way Anova followed by Sidak's multiple comparisons test; *, P < 0.05; ****, P < 0.0001

(K) Functional enrichment of cluster 4 (Trem2^{+} TAM) based on the expression of marker genes in PTEN$^{(i)pe-/-}$ prostates for top 10 Gene Ontology (GO) Biological Process (BP) terms (left) and selected pathways from the Kyoto Encyclopedia of Genes and Genomes (KEGG). Dot color represents the adjusted p-value of the test and dot size represents the count of genes present in the GO BP term and KEGG pathways respectively.

Figure 6

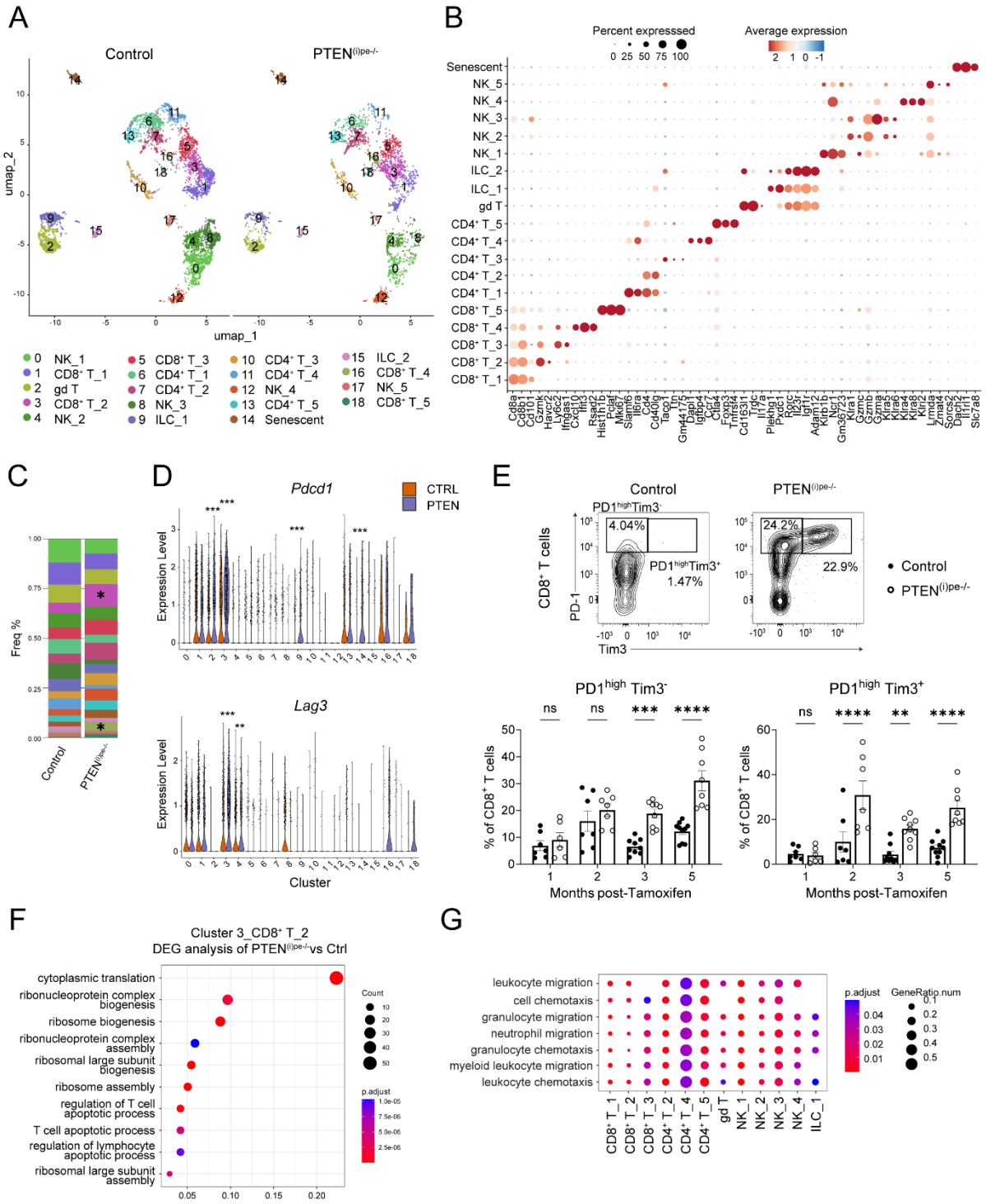
A
Control
PTEN(i)pe-/-
umap_2
umap_1
0 NK_1
1 CD8+ T_1
2 gd T
3 CD8+ T_2
4 NK_2
5 CD8+ T_3
6 CD4+ T_1
7 CD4+ T_2
8 NK_3
9 ILC_1
10 CD4+ T_3
11 CD4+ T_4
12 NK_4
13 CD4+ T_5
14 Senescent
15 ILC_2
16 CD8+ T_4
17 NK_5
18 CD8+ T_5
B
Percent expresssed
0 25 50 75 100
Average expression
2 1 0 -1
Senescent
NK_5
NK_4
NK_3
NK_2
NK_1
ILC_2
ILC_1
gd T
CD4+ T_5
CD4+ T_4
CD4+ T_3
CD4+ T_2
CD4+ T_1
CD8+ T_5
CD8+ T_4
CD8+ T_3
CD8+ T_2
CD8+ T_1
C
Freq %
Control
PTEN(i)pe-/-
D
Pdcd1
CTRL
PTEN
Expression Level
Lag3
Cluster
E
Control
PTEN(i)pe-/-
PD1highTim3-
4.04%
PD1highTim3+
1.47%
24.2%
22.9%
CD8+ T cells
PD-1
Tim3
Control
PTEN(i)pe-/-
PD1high Tim3-
PD1high Tim3+
% of CD8+ T cells
Months post-Tamoxifen
ns
***
****
**
F
Cluster 3_CD8+ T_2
DEG analysis of PTEN(i)pe-/-vs Ctrl
cytoplasmic translation
ribonucleoprotein complex biogenesis
ribosome biogenesis
ribonucleoprotein complex assembly
ribosomal large subunit biogenesis
ribosome assembly
regulation of T cell apoptotic process
T cell apoptotic process
regulation of lymphocyte apoptotic process
ribosomal large subunit assembly
Count
p.adjust
G
leukocyte migration
cell chemotaxis
granulocyte migration
neutrophil migration
granulocyte chemotaxis
myeloid leukocyte migration
leukocyte chemotaxis
p.adjust
GeneRatio.num
CD8+ T_1
CD8+ T_2
CD8+ T_3
CD4+ T_2
CD4+ T_4
CD4+ T_5
gd T
NK_1
NK_2
NK_3
NK_4
ILC_1

Figure 6. Exhausted CD8$^+$ T cells infiltrating the prostate of PTEN$^{(i)pe-/-}$ mice.

(A) Integrative analysis of scRNA-seq of T and NK clusters (1, 4, 7) from the general UMAP shown in **Figure 2B**, visualized using a UMAP embedding for control (left) and PTEN$^{(i)pe-/-}$ (right) samples comprising 2 replicates of 3 months and 9 months for each genotype. Colors represent the recalculated clusters. Cell type annotation was performed using marker genes of the new clusters.
(B) Dot plot of the average expression level of the 5 top marker genes of each cluster identified in (A). The color of the dots represents average of normalized and scaled expression of marker genes in each cell type, and their size indicates the percent of cells expressing the marker genes in the cluster.
(C) Stacked bar graph showing the fractional composition of cell number for different clusters within scRNA-seq for control and PTEN$^{(i)pe-/-}$ samples. The color code corresponds to the clusters shown in (A). Significance among the conditions in clusters is indicated by an asterisk, based on the statistical analysis presented in **Sup Figure 6B**.
(D) Violin plots of the expression levels of *Pdcd1* and *Lag3* genes for each cluster of control (orange) and PTEN$^{(i)pe-/-}$ (purple) samples as annotated in (A). Significance is calculated based on global Kruskal-Wallis test followed by Dunn's pairwise post-hoc tests between conditions in the same cluster.
(E) FACS gating strategy and quantification of PD1^{high}Tim3$^-$ and PD1^{high}Tim3$^-$ CD8$^+$ T cells in control and PTEN$^{(i)pe-/-}$ prostates of DLV lobes at 1-, 2-, 3- and 5-months post tamoxifen. Representative facs plots from 3 months post tamoxifen. Quantification is presented as frequency of CD8$^+$ T cells. Data are presented as mean ±SEM of n=6-10 animals and are a concatenation of 2 independent experiments at each time point. Statistical significance was calculated using mixed effects model followed by Tukey's multiple comparisons test; **, $P < 0.01$; ***, $P < 0.001$; ****, $P < 0.0001$
(F) Functional enrichment of cluster 3 (CD8$^+$ T_2) based on marker gene expression of PTEN$^{(i)pe-/-}$ samples for top 10 Gene Ontology (GO) Biological Process (BP) terms. Dot color represent the adjusted p-value of the test and dot size represent the count of genes present in the GO BP term.
(G) Functional enrichment of various lymphoid clusters based on differential gene expression (DEG) of PTEN$^{(i)pe-/-}$ versus Control samples for several selected Gene Ontology (GO) Biological Process (BP) terms. Dot color represents the adjusted p-value of the test and dot size represents the ratio of DEG present in the GO BP term.

Figure 7

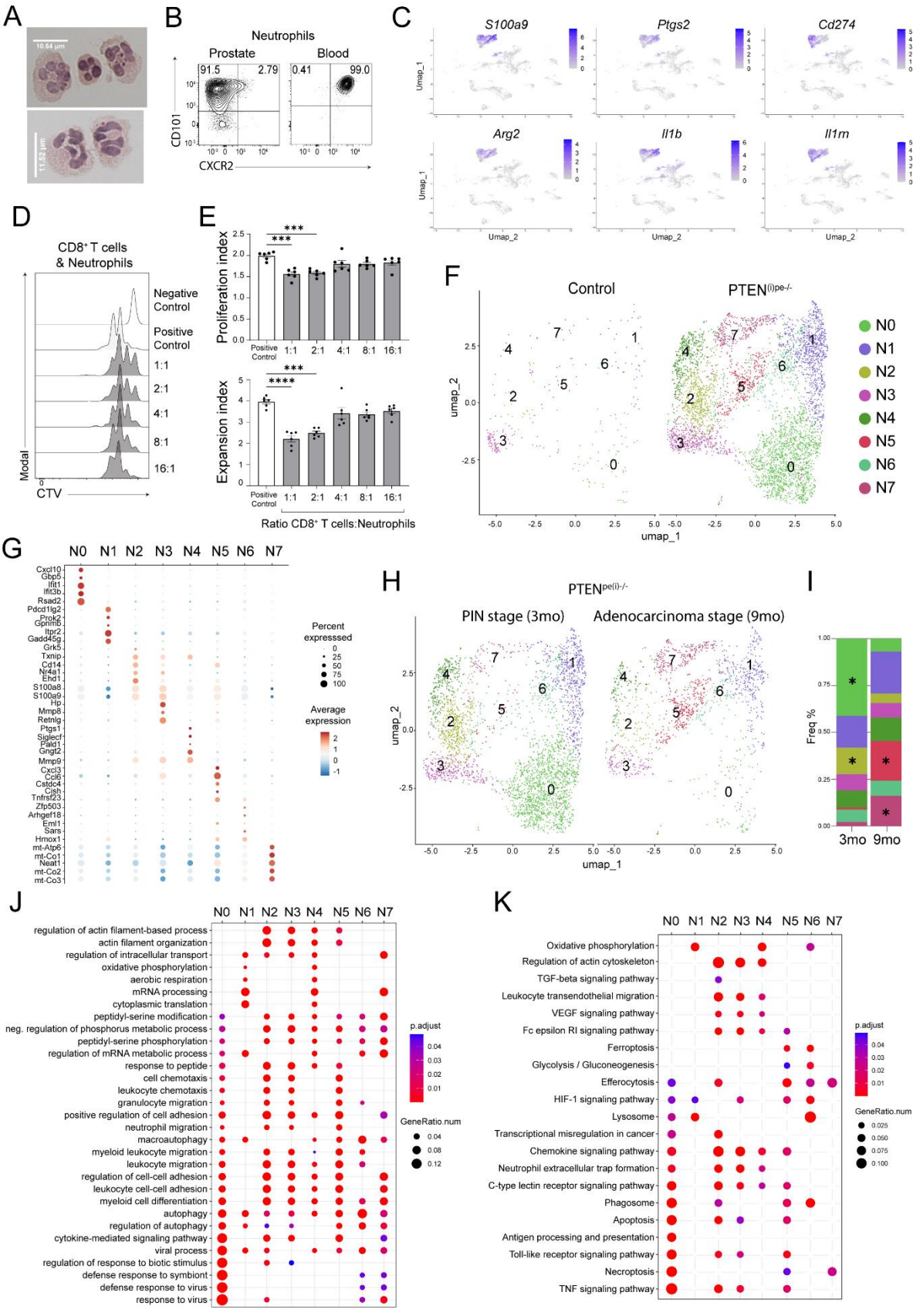
A
B
Neutrophils
Prostate
Blood
91.5
2.79
0.41
99.0
CD101
CXCR2
C
S100a9
Ptgs2
Cd274
Arg2
Il1b
Il1rn
Umap_1
Umap_2
D
CD8⁺ T cells
& Neutrophils
Negative Control
Positive Control
1:1
2:1
4:1
8:1
16:1
Modal
CTV
E
Proliferation index
Expansion index
Positive Control
1:1
2:1
4:1
8:1
16:1
Ratio CD8⁺ T cells:Neutrophils
F
Control
PTEN(i)pe-/-
N0
N1
N2
N3
N4
N5
N6
N7
umap_1
umap_2
G
N0 N1 N2 N3 N4 N5 N6 N7
Percent expressed
Average expression
H
PTENpe(i)-/-
PIN stage (3mo)
Adenocarcinoma stage (9mo)
I
Freq %
3mo
9mo
J
regulation of actin filament-based process
actin filament organization
regulation of intracellular transport
oxidative phosphorylation
aerobic respiration
mRNA processing
cytoplasmic translation
peptidyl-serine modification
neg. regulation of phosphorus metabolic process
peptidyl-serine phosphorylation
regulation of mRNA metabolic process
response to peptide
cell chemotaxis
leukocyte chemotaxis
granulocyte migration
positive regulation of cell adhesion
neutrophil migration
macroautophagy
myeloid leukocyte migration
leukocyte migration
regulation of cell-cell adhesion
leukocyte cell-cell adhesion
myeloid cell differentiation
autophagy
regulation of autophagy
cytokine-mediated signaling pathway
viral process
regulation of response to biotic stimulus
defense response to symbiont
defense response to virus
response to virus
p.adjust
GeneRatio.num
K
Oxidative phosphorylation
Regulation of actin cytoskeleton
TGF-beta signaling pathway
Leukocyte transendothelial migration
VEGF signaling pathway
Fc epsilon RI signaling pathway
Ferroptosis
Glycolysis / Gluconeogenesis
Efferocytosis
HIF-1 signaling pathway
Lysosome
Transcriptional misregulation in cancer
Chemokine signaling pathway
Neutrophil extracellular trap formation
C-type lectin receptor signaling pathway
Phagosome
Apoptosis
Antigen processing and presentation
Toll-like receptor signaling pathway
Necroptosis
TNF signaling pathway
p.adjust
GeneRatio.num

Figure 7. Distinct neutrophil states infiltrate the PIN and adenocarcinoma stages of PTEN$^{(i)pe-/-}$ prostate.

(A) Morphological characteristics of Ly-6G$^+$CD11b$^+$ neutrophils sorted from PTEN$^{(i)pe-/-}$ prostates at PIN stage (3 months post tamoxifen) and analyzed by hematoxylin and eosin staining after cytospin on glass slides. Two representative images are shown, and scale bars indicate the size of the sorted neutrophils.
(B) FACS showing the cell surface expression of the markers CD101 and CXCR2 by Ly-6G$^+$CD11b$^+$ neutrophils from prostate and blood of PTEN$^{(i)pe-/-}$ mice at PIN stage (3 months post tamoxifen).
(C) Feature plots show normalized expression of selected marker genes (*S100a9, Ptgs2, Cd274, Arg2, Il1b, Il1rn*) in the total CD45$^+$ immune cells presented in the UMAP in **Figure 2B** from PTEN$^{(i)pe-/-}$ samples including both time points.
(D) Cell Trace Violet (CTV) histograms for the *ex vivo* suppressive assay showing the proliferation of WT splenic CD8$^+$ T cells stimulated with anti-CD3 and anti-CD28 and co-cultured with Ly-6G$^+$CD11b$^+$ neutrophils sorted from prostate of PTEN$^{(i)pe-/-}$ mice at PIN stage (3 months post tamoxifen) at different ratios (CD8$^+$ T : Neutrophils). Negative control: non-stimulated CD8$^+$ T cells cultured alone. Positive control: CD8$^+$ T cells stimulated with anti-CD3 and anti-CD28 and cultured alone.
(E) Proliferation and expansion indexes of CD8$^+$ T cells based on the CTV histograms shown in (D). Data are presented as mean ±SEM of n=4 culture replicates for each condition and are representative of 2 independent experiments. Statistical significance was calculated using Kruskal Wallis test followed by Dunn's multiple comparisons test; ***, $P < 0.001$; ****, $P < 0.0001$
(F) Integrative analysis of scRNA-seq of the neutrophil cluster (2) from the general UMAP shown in **Figure 2B**, visualized using a UMAP embedding for control (left) and PTEN$^{(i)pe-/-}$ (right) samples comprising 2 replicates of 3 months and 9 months for each genotype. Colors represent the recalculated clusters. Cell type annotation was performed using the marker genes of the new clusters.
(G) Dot plot of the average expression level of the 5 top marker genes of each cluster identified in (F). The color of the dots represents average of normalized and scaled expression of marker genes in each cell type, and their size indicates the percent of cells expressing the marker genes in the cluster.
(H) Integrative analysis of scRNA-seq of the neutrophil clusters shown in F, visualized using a UMAP embedding for PTEN$^{(i)pe-/-}$ samples at 3 months PIN stage (left) and 9 months adenocarcinoma stage (right) comprising 2 replicates of each timepoint. Colors represent the recomputed clusters, similar to F-G.
(I) Stacked bar graph showing the fractional composition of cell number for different clusters within scRNA-seq of PTEN$^{(i)pe-/-}$ samples at PIN (3-mo) and adenocarcinoma (9-mo) stages. The color code corresponds to the clusters depicted in (F). Significance between the conditions in the clusters is indicated by an asterisk, based on the statistical analysis shown in **Sup Figure 7E**.
(J) Functional enrichment of the neutrophil clusters based on the expression of marker genes of each cluster for several selected Gene Ontology (GO) Biological Process (BP) terms. Dot color represents the adjusted p-value of the test and dot size represents the ratio of DEG present in the GO BP term.
(K) Functional enrichment of the neutrophil clusters based on the expression of marker genes of each cluster for several selected Kyoto Encyclopedia of Genes and Genomes (KEGG) pathways. Dot color represents the adjusted p-value of the test and dot size represents the ratio of DEG present in the GO BP term.

Supplementary Figure 1

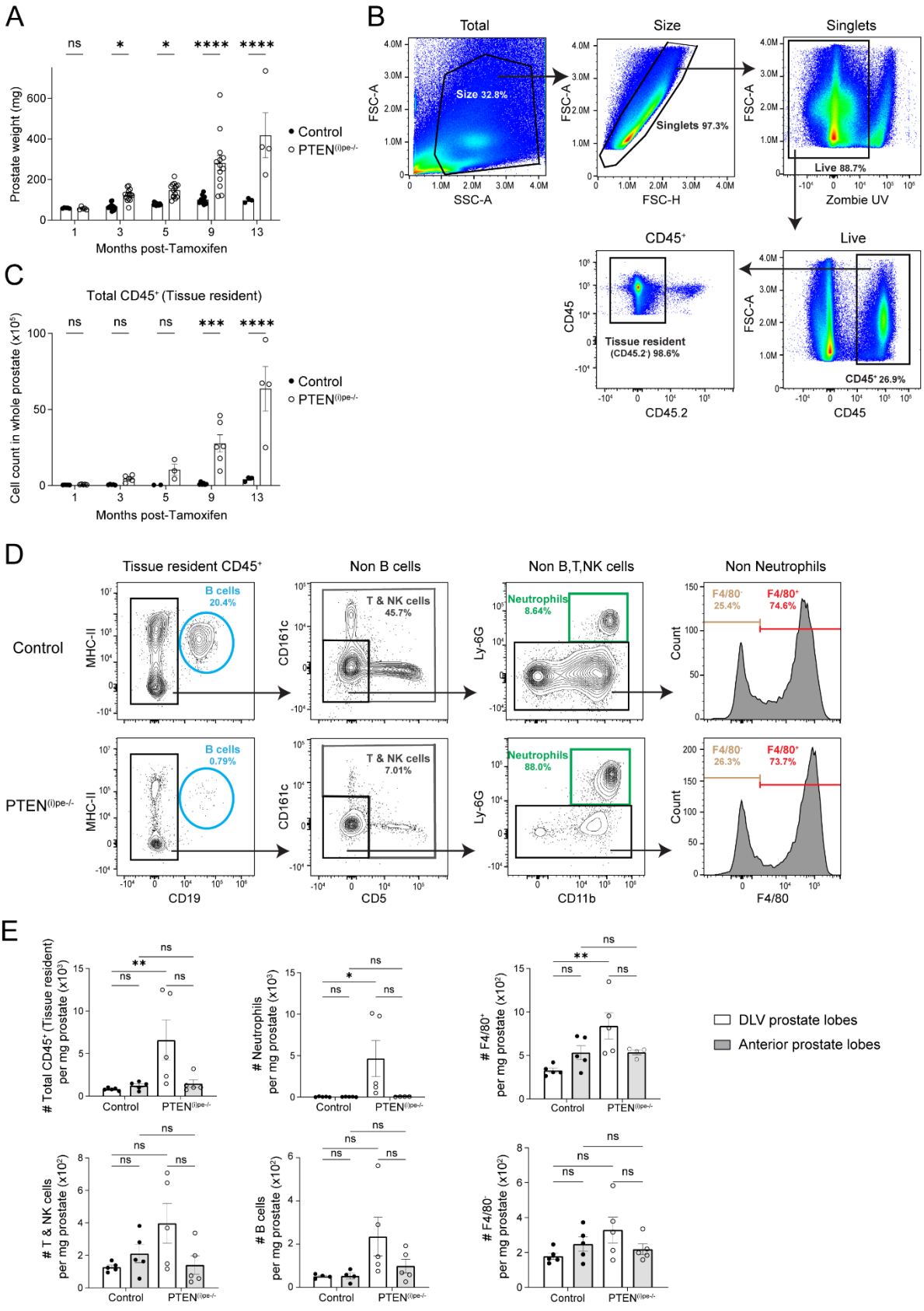

Sup Figure 1. Identification of the prostatic immune cell populations by supervised flow cytometric analysis.

(A) Prostate weight of control and tumor-bearing PTEN$^{(i)pe-/-}$ mice at different time points after tamoxifen administration (1, 3, 5, 9 and 13 months). Data are presented as mean ±SEM of n=4-15 and are cumulative of 4 independent experiments per time point with 1-5 animals per group. Statistically significant difference was calculated using two-way ANOVA followed by Tukey's multiple comparisons test; ns, non-significant; *, P < 0.05; ****, P < 0.0001.
(B) Representative gating strategy to identify resident immune cells in the prostate by flow cytometry. Total prostate cells were gated based on their size (FSC-A/SSC-A), excluding doublets and dead cells. From the live cells, the CD45.2$^+$ blood contaminants were excluded (*in vivo* i.v. staining prior to euthanasia), allowing to select the CD45$^+$ tissue resident immune cells.
(C) Total number of CD45$^+$ resident prostate immune cells from control and tumor-bearing PTEN$^{(i)pe-/-}$ prostate determined by flow cytometry at different time points post-tamoxifen administration (1, 3, 5, 9 and 13 months). Data are presented as mean ±SEM of n=3-6 and are representative of 4 independent experiments per time point with 3-6 animals per group. Statistical significance was calculated using two-way ANOVA and Tukey's multiple comparisons test; ns, non-significant; ***, P < 0.001; ****, P < 0.0001.
(D) Representative gating strategy to identify myeloid and lymphoid immune cells in prostate from control (top) and PTEN$^{(i)pe-/-}$ mice (bottom), at 3 months post-tamoxifen administration. Tissue resident CD45$^+$ cells were plotted with MHC-II and CD19 allowing to identify CD19$^+$MHC-II$^+$ B cells. From the non-B cell gate (MHC-II$^-$) the T and NK cells were identified as CD161c$^+$CD5$^+$. From the non-T and NK cell gate (CD161c$^-$CD5$^-$), the Ly-6G$^+$CD11b$^+$ neutrophils were selected and, from the non-neutrophil gate (Ly-6G$^-$) the F4/80$^+$ and F4/80$^-$ cells were identified.
(E) Quantitative facs analysis of the immune cell populations as identified in **Sup Figure 1 B and D**) in DLV lobes (dorsal-lateral-ventral) and anterior lobe in control and tumor-bearing PTEN$^{(i)pe-/-}$ mice at PIN stage (3months post tamoxifen). Counts are normalized per mg of prostate. Data are presented as mean ±SEM of n=5 and are representative of 2 independent experiments with 4-5 animals per group. Statistically significant difference was calculated using Kruskal-Wallis test followed by Dunn's multiple comparisons test; ns, non-significant; ***, P < 0.001; ****, P < 0.0001.

Supplementary Figure 2

A

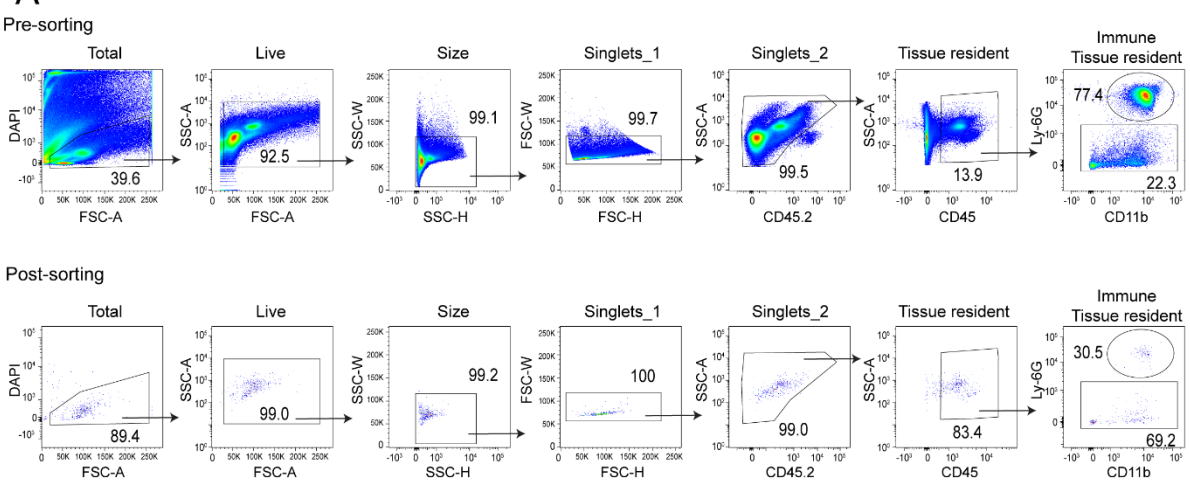

B

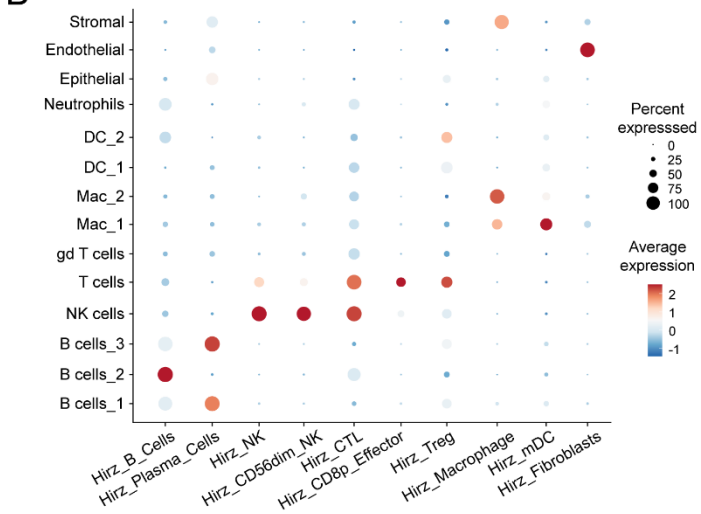

Sup Figure 2. Sorting strategy before scRNA sequencing and modules scoring.

(A) Representative FACS sorting strategy applied on PTEN$^{(i)pe-/-}$ samples at 3- and 9-months post tamoxifen and FACS analysis after remixing. Pre-sorting: From the total prostate cells, dead cells, doublets and blood contaminants (CD45.2^{+}) were successively excluded, then CD45^{+} resident immune cells were selected and Ly-6G^{+}CD11b^{+} neutrophils that comprised ~70% of the total immune cells were sorted independently from the rest non-neutrophils immune cells (Ly-6G^{-}). The 2 sorted populations were remixed in a ratio of 30% of Ly-6G^{+}CD11b. Post-sorting: The ratio was verified by recording by FACS the cell suspension after remixing. This approach was applied only for the PTEN$^{(i)pe-/-}$ samples at 3 months and 9 months timepoint, while the control samples were sorted as bulk CD45^{+} resident immune cells.
(B) Dot plot representing gene modules scores of the annotated clusters shown in **Figure 2B** using gene modules identified in human prostate cancer by (Hirz et al., 2023). The color represents average of scores in each cell type, and the size indicates the percentage of cells in the cluster with a positive score.

Supplementary Figure 3

A

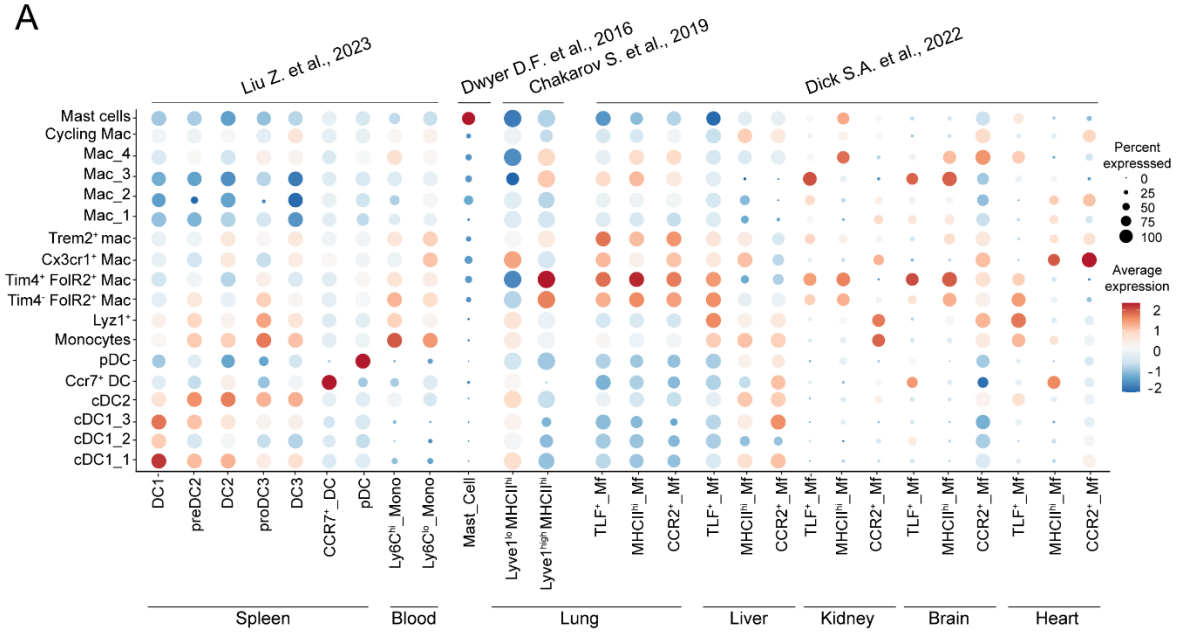

Sup Figure 3. Modules scoring analysis of the annotated myeloid clusters with published gene signatures.

(A) Dot plot representing gene modules scores of the annotated clusters shown in **Figure 3A** using gene modules identified in myeloid clusters in other tissues by (Chakarov et al., 2019; Dick et al., 2022; Dwyer et al., 2016; Liu et al., 2023). The color represents average of scores in each cell type, and the size indicates the percentage of cells in the cluster with a positive score.

Supplementary Figure 4

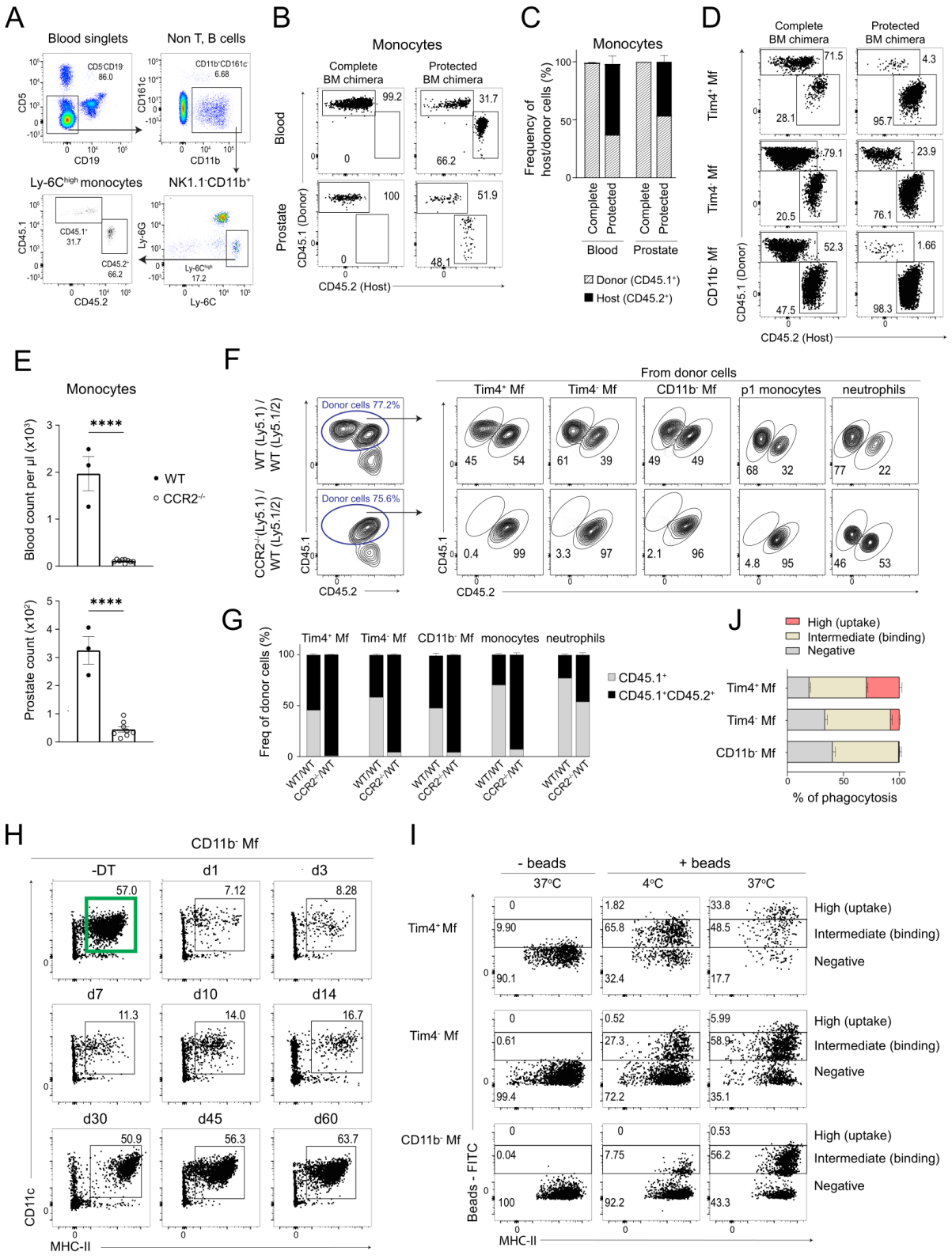

Sup Figure 4. Monocytes in blood and prostate and macrophage subsets in prostate.

(A) Gating strategy used to identify the Ly-6C^{high} monocytes in blood, 8 weeks post BM reconstitution of complete and protected BM chimera mice. After exclusion of CD5$^+$ T cells, CD19$^+$ B cells, CD161c$^+$ NK cells and Ly-6G$^+$ neutrophils, blood monocytes were identified as CD11b$^+$Ly-6C$^+$. BM chimerism was determined by the expression of CD45.1 and CD45.2 markers to distinguish CD45.2$^+$ host cells from CD45.1$^+$ donor cells.
(B) Representative FACS dot plots of CD45.2 and CD45.1 staining on monocytes from blood (gating shown in A) and prostate (gating shown in **Figure 3D**), at 8 weeks post BM reconstitution in complete and protected BM chimera mice. Frequencies of CD45.2$^+$ (host) cells and CD45.1$^+$ (donor) cells are shown.
(C) Bar plots showing the BM chimerism represented as a frequency of host/donor cells for blood and prostate monocytes (gating shown in B) in complete and protected BM chimera mice. Data are presented as mean ±SEM of n=3-5 and are representative of 3 independent experiments.
(D) Representative FACS dot plots of CD45.2 and CD45.1 staining on the three prostate macrophage subsets (gating shown in **Figure 3D**), at 8 weeks post BM reconstitution in complete and protected BM chimera mice. Frequencies of CD45.2$^+$ (host) cells and CD45.1$^+$ (donor) cells are shown.
(E) Monocyte numbers in blood and prostate of 10 weeks old CCR2$^{-/-}$ versus WT mice. Data are presented as mean ± SEM of n=3-8, and statistically significant difference was calculated using unpaired t-test; ****, $P < 0.0001$. They are representative of 2 independent experiments.
(F) Representative FACS dot plots of CD45.2 and CD45.1 staining on the three prostate macrophage subsets, p1 monocytes and neutrophils at 10 weeks post BM reconstitution in complete competitive BM chimera mice. CD45.1$^+$ (donor) cells were selected and frequencies of WT (Ly5.1) and WT (Ly5.1/2) or WT (Ly5.1) and CCR2$^{-/-}$ (Ly5.1/2) are shown.
(G) Bar plots showing the BM chimerism represented as a frequency of WT (Ly5.1) and WT (Ly5.1/2) or WT (Ly5.1) and CCR2$^{-/-}$ (Ly5.1/2) for prostate macrophage subsets, p1 monocytes and neutrophils (gating shown in F) in complete competitive BM chimera mice. Data are presented as mean ±SEM of n=3-5 and are representative of 2 independent experiments.
(H) Replenishment kinetics of CD11b$^-$ macrophages (green gate) in the prostate of CD64^{dtr} mice after diphtheria toxin (DT) treatment. CD64^{dtr} mice were untreated (-DT) or treated twice, 24h apart with i.p. injections of DT. Flow cytometry analysis was performed on untreated (-DT) and 1, 3, 7, 10, 14, 30, 45 and 60 days (d) after the last DT injection.
(I) Representative FACS dot plots of the *in vitro* phagocytosis assay of fluorescent beads by the three prostate macrophage subsets at 4°C and 37°C.
(J) Bar plots showing the percentage of phagocytosis based on the gating strategy shown in (I). Data are presented as mean ±SEM of n=3-5 and are representative of 2 independent experiments.

Supplementary Figure 5

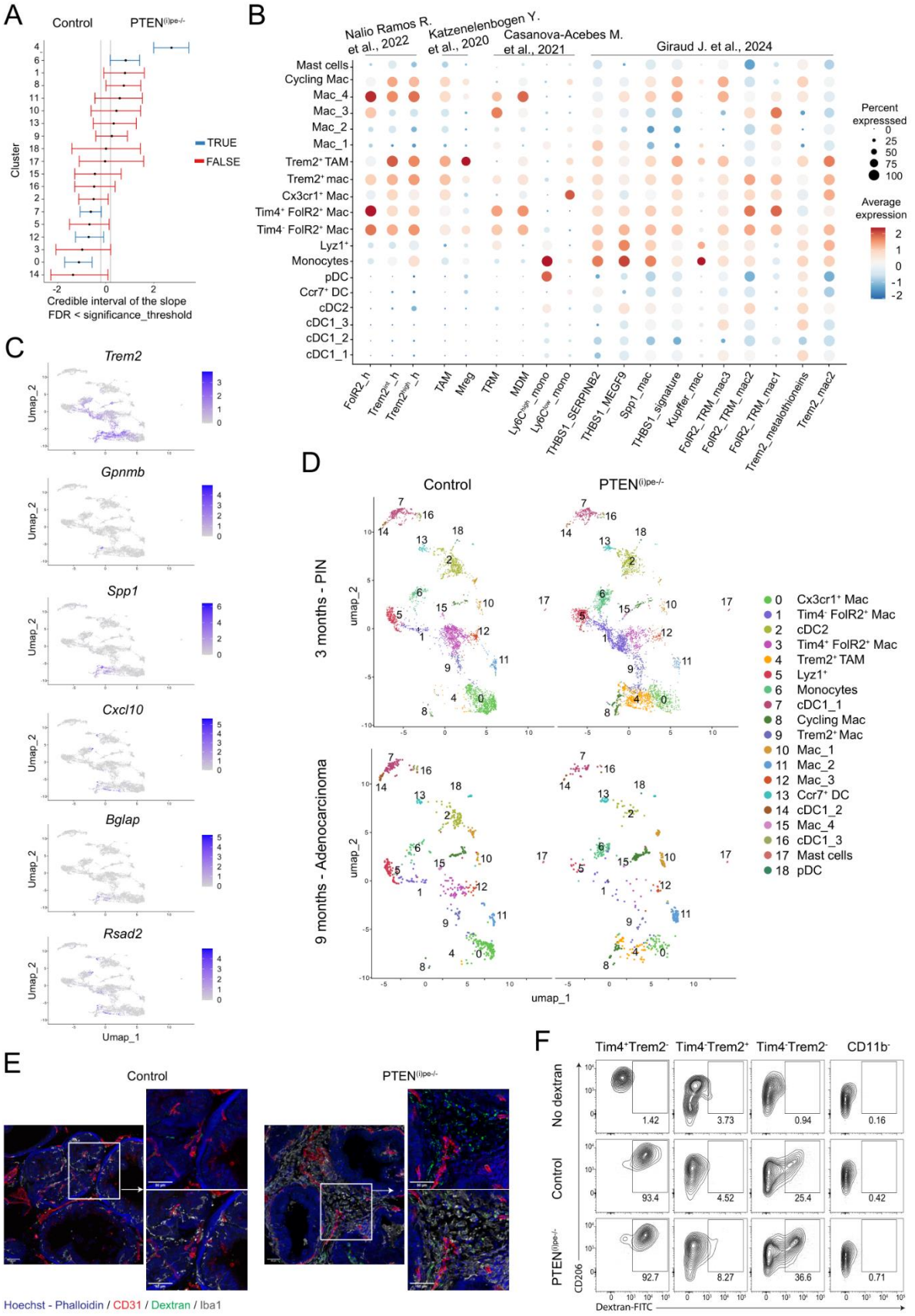

Sup Figure 5. Analysis of MNPs in prostate tumors.

(A) Statistical analysis of the MNP cluster composition ratio between Control (left) and PTEN$^{(i)pe-/-}$ (right) showing the credible interval of the slope. Significance (FDR < 0.05) is color coded by blue (true) and red (false).
(B) Dot plot representing the gene module scores of the annotated clusters shown in **Figure 5B** using gene modules identified in tumor-associated macrophage clusters in other tissues by (Casanova-Acebes et al., 2021; Giraud et al., 2024a; Katzenelenbogen et al., 2020; Nalio Ramos et al., 2022). The color represents average of scores in each cell type, and the size indicates the percent of cells in the cluster with positive score.
(C) Feature plots show the normalized expression of selected marker genes (*Trem2, Spp1, Gpnmb, Bglap, Cxcl10, Rsad2*) in the MNP UMAP representation from PTEN$^{(i)pe-/-}$ samples including both time points.
(D) UMAP integrative analysis of scRNA-seq MNP clusters presented in **Figure 5B**, showing separately the UMAP embeddings for 3 months (top) and 9 months (bottom) post-tamoxifen. At each timepoint the UMAP shows the control (left) and PTEN$^{(i)pe-/-}$ (right) samples encompassing 2 replicates for each genotype. Colors represent the recalculated MNP clusters. Cell type annotation is similar to **Figure 5B**.
(E) Qualitative confocal microscopy analysis of prostate tissue sections from control (left) and PTEN$^{(i)pe-/-}$ (right) prostates, at 3 months post tam. Staining shows Hoechst-Phalloidin (blue), CD31^{+} blood vessels (red), Iba^{+} Macrophages (white) and Dextran-FITC (green). Representative staining from the dorsal-lateral (DL) prostate lobes (scale bar of 50µm).
(F) FACS gating strategy showing the dextran^{+} cells within the macrophage subsets of control and PTEN$^{(i)pe-/-}$ prostates at PIN stage (3 months post tam) treated i.v. with dextran-FITC, as well as non-injected control mice.

Supplementary Figure 6

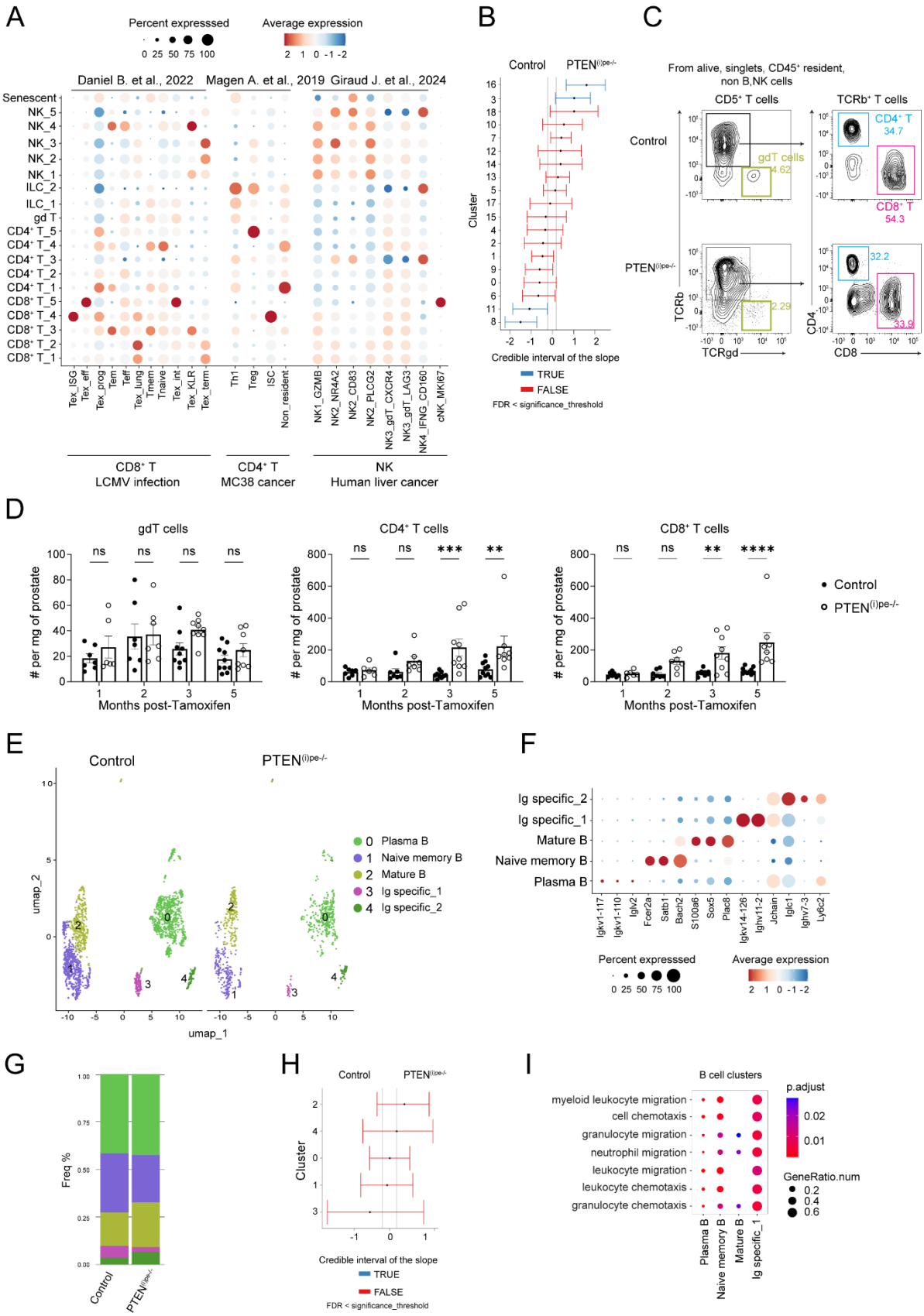

Sup Figure 6. Deciphering the T, B, NK cells in PTEN$^{(i)pe-/-}$ prostate.

(A) Dot plot representing gene modules scores of the annotated clusters shown in **Figure 6A** using gene modules identified in T and NK clusters in other tissues by (Daniel et al., 2022; Giraud et al., 2024a; Magen et al., 2019). The color represents average of scores in each cell type, and the size indicates the percent of cells in the cluster with positive score.
(B) Statistical analysis of the T and NK cell cluster composition ratio between Control (left) and PTEN$^{(i)pe-/-}$ (right) showing the credible interval of the slope. Significance (FDR < 0.05) is color coded by blue (true) and red (false).
(C) FACS gating strategy for the identification of T lymphocyte subsets. From alive, singlets, CD45$^+$ resident, non-B, NK cells (gating shown in **Sup Figure 1D**), the conventional T (TCRβ^+) and $\gamma\delta$T (TCR$\gamma\delta^+$) cells were identified. Within the conventional (TCRβ^+) T cells, the CD4$^+$ T cells and CD8$^+$ T cells were distinguished. Representative facs plots from 3 months post tamoxifen for control and PTEN$^{(i)pe-/-}$ prostates of DLV lobes.
(D) Quantification of $\gamma\delta$, CD4$^+$ and CD8$^+$ T cells in control and PTEN$^{(i)pe-/-}$ DLV lobes of prostates at 1-, 2-, 3- and 5-months post tamoxifen. Counts are normalized per mg of prostate. Data are presented as mean ±SEM of n=6-10 animals and are a concatenation of 2 independent experiments of each timepoint. Statistical significance was calculated using mixed effects model followed by Tukey's multiple comparisons test; **, P < 0.01; ***, P < 0.001; ****, P < 0.0001
(E) Integrative analysis of scRNA-seq of B clusters (5, 6, 12) from the general UMAP shown in **Figure 2B**, visualized using a UMAP embedding for control (left) and PTEN$^{(i)pe-/-}$ (right) samples comprising 2 replicates of 3 months and 9 months for each genotype. Colors represent the recalculated clusters. Cell type annotation was performed using the marker genes new clusters.
(F) Dot plot of the average expression level of the 5 top marker genes of each cluster identified in (E). The color of the dots represents average of normalized and scaled expression of marker genes in each cell type, and their size indicates the percent of cells expressing the marker genes in the cluster.
(G) Stacked bar plot showing the fractional composition of the different B cell clusters within scRNA-seq for control and PTEN$^{(i)pe-/-}$ samples. The color code corresponds to the B cell clusters depicted in (E).
(H) Statistical analysis of the B cell cluster composition ratio between Control (left) and PTEN$^{(i)pe-/-}$ (right) showing the credible interval of the slope. Significance (FDR < 0.05) is color coded by blue (true) and red (false).
(I) Functional enrichment of the different B cell clusters based on the differential gene expression (DEG) of PTEN$^{(i)pe-/-}$ versus Control samples for several selected Gene Ontology (GO) Biological Process (BP) terms. Dot color represents the adjusted p-value of the test and dot size represents the ratio of DEG present in the GO BP term.

Supplementary Figure 7

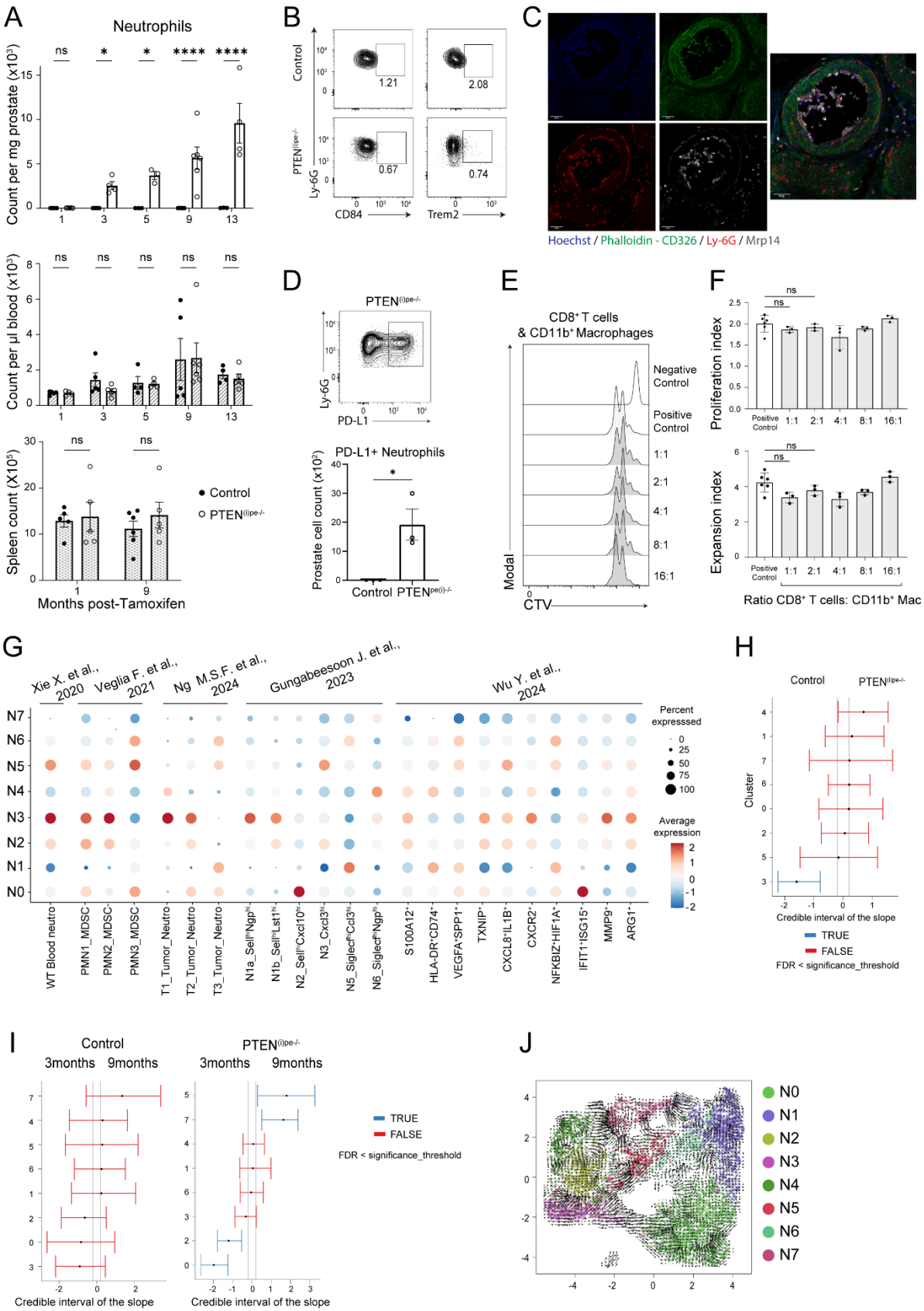

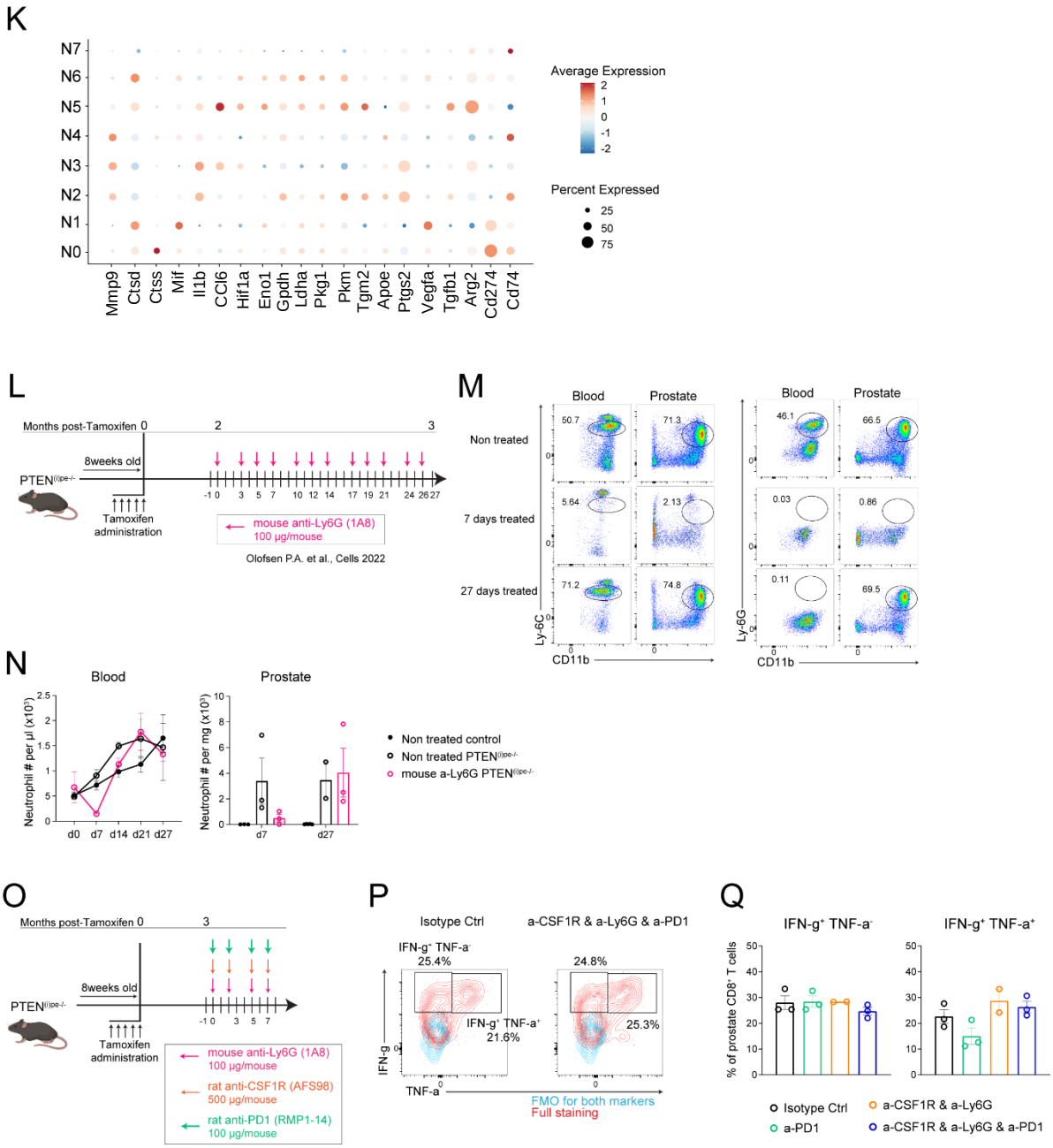
K
N7
N6
N5
N4
N3
N2
N1
N0
Mmp9 Ctsd Ctss Mif Il1b CCl6 Hif1a Eno1 Gpdh Ldha Pkg1 Pkm Tgm2 Apoe Ptgs2 Vegfa Tgfb1 Arg2 Cd274 Cd74
Average Expression
2
1
0
-1
-2
Percent Expressed
25
50
75
L
Months post-Tamoxifen 0
2
3
8weeks old
PTEN(l)pe-/-
-1 0 3 5 7 10 12 14 17 19 21 24 26 27
Tamoxifen administration
mouse anti-Ly6G (1A8) 100 µg/mouse
Olofsen P.A. et al., Cells 2022
M
Blood
Prostate
Non treated
7 days treated
27 days treated
50.7
71.3
5.64
2.13
71.2
74.8
46.1
66.5
0.03
0.86
0.11
69.5
Ly-6C
Ly-6G
CD11b
N
Blood
Prostate
Neutrophil # per µl (x10³)
Neutrophil # per mg (x10³)
d0 d7 d14 d21 d27
d7 d27
Non treated control
Non treated PTEN(l)pe-/-
mouse a-Ly6G PTEN(l)pe-/-
O
Months post-Tamoxifen 0
3
8weeks old
PTEN(l)pe-/-
-1 0 3 5 7
Tamoxifen administration
mouse anti-Ly6G (1A8) 100 µg/mouse
rat anti-CSF1R (AFS98) 500 µg/mouse
rat anti-PD1 (RMP1-14) 100 µg/mouse
P
Isotype Ctrl
a-CSF1R & a-Ly6G & a-PD1
IFN-g+ TNF-a-
25.4%
IFN-g+ TNF-a+
21.6%
24.8%
25.3%
IFN-g
TNF-a
FMO for both markers
Full staining
Q
IFN-g+ TNF-a-
IFN-g+ TNF-a+
% of prostate CD8+ T cells
Isotype Ctrl
a-PD1
a-CSF1R & a-Ly6G
a-CSF1R & a-Ly6G & a-PD1

Sup Figure 7. Deciphering tumor-associated neutrophils in PTEN$^{(i)pe-/-}$ prostate.

(A) Quantification of Ly-6G$^+$CD11b$^+$ neutrophils (FACS gating shown in **Sup Figure 1D**) in blood and prostate from control and tumor-bearing PTEN$^{(i)pe-/-}$ mice, at different time points post-tamoxifen administration: 1-, 3-, 5-, 9- and 13- months for prostate and blood, and in spleen at 1- and 9-months post-tam. Counts for prostate and blood have been normalized per mg of prostate and µl of blood respectively. Data are presented as mean ±SEM of n=4-6 and are representative of 5 independent experiments per time point with 3-6 animals per group. Statistically significant difference was calculated using mixed effects model followed by Tukey's multiple comparisons test; ns, non-significant; *, P < 0.05; ****, P < 0.0001.
(B) FACS staining showing the expression of CD84 and Trem2 markers on Ly-6G$^+$CD11b$^+$ neutrophils from control and PTEN$^{(i)pe-/-}$ prostate at 3 months post tamoxifen.
(C) Qualitative confocal microscopy analysis of prostate tissue sections from PTEN$^{(i)pe-/-}$ prostates at 3 months post tam. Staining shows Hoechst (blue), Phalloidin-CD326 (green), Ly-6G$^+$ (red) and S100A9/Mrp14$^+$ (white). Representative staining from the dorsal-lateral (DL) prostate lobes (scale bar of 50µm).
(D) FACS staining showing the expression (top) of PD-L1 marker on Ly-6G$^+$CD11b$^+$ neutrophils from PTEN$^{(i)pe-/-}$ prostates at 3 months post tamoxifen and counts of PD-L1$^+$Ly-6G$^+$CD11b$^+$ neutrophils (bottom) in control and PTEN$^{(i)pe-/-}$ prostates at 3 months post tamoxifen. Data are presented as mean ±SEM of n=3 and are representative of 3 independent experiments 3-5 animals per group. Statistically significant difference was calculated using unpaired t-test test; *, P < 0.05.
(E) Cell Trace Violet (CTV) histograms for the *ex vivo* suppressive assay showing the proliferation of WT splenic CD8$^+$ T cells stimulated with anti-CD3 and anti-CD28 and co-cultured with CD11b$^+$ macrophages sorted from prostate of PTEN$^{(i)pe-/-}$ mice at PIN stage (3 months post tamoxifen) at different ratios (CD8$^+$ T : macrophages). Negative control: non-stimulated CD8$^+$ T cells cultured alone. Positive control: CD8$^+$ T cells stimulated with anti-CD3 and anti-CD28 and cultured alone.
(F) Proliferation and expansion indexes of CD8$^+$ T cells based on the CTV histograms shown in (E). Data are presented as mean ±SEM of n=4 culture replicates for each condition and are representative of 2 independent experiments. Statistical significance was calculated using Kruskal Wallis test followed by Dunn's multiple comparisons test; ***, P < 0.001; ****, P < 0.0001
(G) Dot plot representing gene modules scores of the annotated clusters shown in Figure 7F using gene modules identified in tumor associated neutrophils in other tissues by (Gungabeesoon et al., 2023; Ng et al., 2024; Veglia et al., 2021; Wu et al., 2024; Xie et al., 2020). The color represents average of scores in each cell type, and the size indicates the percent of cells in the cluster with positive score.
(H) Statistical analysis of the neutrophil cluster composition ratio between Control (left) and PTEN$^{(i)pe-/-}$ (right) showing the credible interval of the slope. Significance (FDR < 0.05) is color coded by blue (true) and red (false).
(I) Statistical analysis of the B cell cluster composition ratio between 3 months and 9 months Controls (left) and between 3 months and 9 months PTEN$^{(i)pe-/-}$ (right) showing the credible interval of the slope. Significance (FDR < 0.05) is color coded by blue (true) and red (false).
(J) RNA velocity analysis in neutrophil clusters from integration of Control and PTEN$^{(i)pe-/-}$ samples of both time points.
(K) Dot plot of the average expression level of selected marker genes for the neutrophil clusters of PTEN$^{(i)pe-/-}$ samples as identified in **Figure 7F**. The color of the dots represents average of normalized and scaled expression of marker genes in each cell type, and their size indicates the percent of cells expressing the marker genes in the cluster.

(L) Treatment scheme for neutrophils depletion using murinized anti-Ly-6G. PTEN$^{(i)pe-/-}$ mice at 2 months post tamoxifen were treated with 100 µg of murinized anti-Ly-6G (clone 1A8) three times per week for four weeks as described by (Olofsen et al., 2022). Blood was collected before injection with the antibodies on days 0, 7, 14, 21 and 27.
(M) FACS plots to identify Ly-6C^{int}CD11b^{+} neutrophils using Ly-6C and CD11b markers on blood and prostate of PTEN$^{(i)pe-/-}$ non-treated or treated mice analyzed on days 7 and 27 of treatment.
(N) Quantification of the Ly-6C^{int}CD11b^{+} neutrophils in the blood and prostate of non-treated control mice, non-treated PTEN$^{(i)pe-/-}$mice and treated Pten$^{(i)pe-/-}$mice. Counts for prostate and blood were normalized per mg of prostate and µl of blood respectively. Data are presented as mean ±SEM of n=2-3 and are representative of 2 independent experiments per time point.
(O) Treatment scheme for combined therapy. PTEN$^{(i)pe-/-}$ mice at 3 months post tamoxifen were treated with 100 µg of murinized anti-Ly-6G (clone 1A8), 500 µg of murinized rat anti-CSF1R (clone AFS98) and 100µg of murinized rat anti-PD1 (clone RMP1-14) at day 0, 3, 5, 7.
(P) FACS contour plots showing IFN-γ and TNF-α production by CD8^{+} T cells from prostate of mice treated with the isotype control or with the combined triple therapy. Plots are presented as overlays of FMO (blue) and IFN-γ and TNF-α staining (red).
(Q) Bar plots showing the frequency of IFN-γ^{+}TNF-α^{-} and IFN-γ^{+}TNF-α^{+} CD8^{+} T cells in PTEN$^{(i)pe-/-}$ prostate of the different treated groups: Isotype control, anti-PD1 alone, anti-CSF1R + anti-Ly-6G, or anti-CSF1R + anti-Ly-6G + anti-PD1.

Supplementary Figure 8

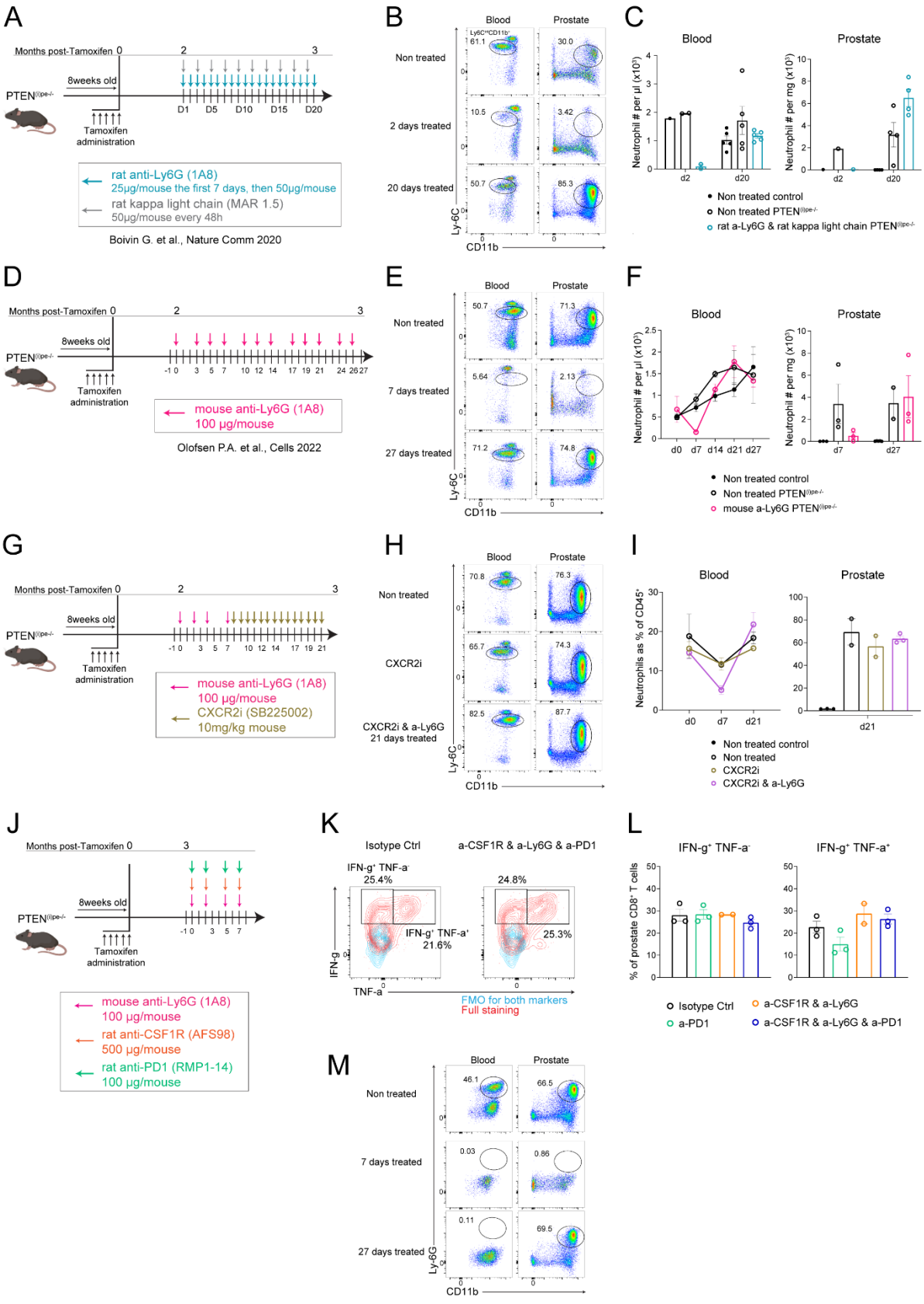

Sup Figure 8. In vivo neutrophil depletion approaches.

(A) Treatment scheme for neutrophils depletion using rat anti-Ly-6G and anti-rat kappa light chain. PTEN $^{(i)pe-/-}$ mice at 2 months post tamoxifen were treated for 20 days with anti-Ly-6G (clone 1A8) daily (25µg the first 7 days, and 50µg for the rest of treatment) and with anti-rat kappa light chain every 48hours (50µg/mouse) as described by (Boivin et al., 2020).
(B) Representative FACS plots of Ly-6C^{int}CD11b^{+} neutrophils using Ly-6C and CD11b markers in blood and prostate from non-treated and treated PTEN$^{(i)pe-/-}$ mice analyzed at days 2 and 20 of treatment described in (A).
(C) Quantification of the Ly-6C^{int}CD11b^{+} neutrophils in the blood and prostate of non-treated control mice, non-treated PTEN$^{(i)pe-/-}$mice and treated PTEN$^{(i)pe-/-}$mice as described in (A-B). Counts for prostate and blood were normalized per mg of prostate and µl of blood respectively. Data are presented as mean ±SEM of n=1-5.
(D) Treatment scheme for neutrophils depletion using murinized anti-Ly-6G. PTEN$^{(i)pe-/-}$ mice at 2 months post tamoxifen were treated with 100 µg of murinized anti-Ly-6G (clone 1A8) three times per week for four weeks as described by (Olofsen et al., 2022). Blood was collected before injection with the antibodies on days 0, 7, 14, 21, 27.
(E) Representative FACS plots of Ly-6C^{int}CD11b^{+} neutrophils using Ly-6C and CD11b markers on blood and prostate of PTEN$^{(i)pe-/-}$ non-treated or treated mice analyzed on days 7 and 27 of treatment described in (D).
(F) Quantification of Ly-6C^{int}CD11b^{+} neutrophils in the blood and prostate of non-treated control mice, non-treated PTEN$^{(i)pe-/-}$ and treated PTEN$^{(i)pe-/-}$mice as described in (D-E). Counts for prostate and blood were normalized per mg of prostate and µl of blood respectively. Data are presented as mean ±SEM of n=2-3 and are representative of 2 independent experiments per timepoint.
(G) Treatment scheme for neutrophil depletion and prevention from tissue homing. PTEN$^{(i)pe-/-}$ mice at 2 months post tamoxifen were treated with 100 µg of murinized anti-Ly-6G (clone 1A8) for 7 days every 48 hours. Then, mice were treated daily for 2 weeks with 10 mg/kg/mouse of CXCR2 inhibitor (SB225002).
(H) Representative FACS plots of Ly-6C^{int}CD11b^{+} neutrophils using Ly-6C and CD11b markers on blood and prostate of PTEN$^{(i)pe-/-}$ mice, non-treated, or treated with CXCR2i only, or with both anti-Ly6G and CXCR2i, and analyzed at the end of treatment described in (G).
(I) Quantification of Ly-6C^{int}CD11b^{+} neutrophils in the blood and prostate of different treated groups described in (G-H). Data are shown as frequency of the total CD45^{+} cells for prostate and blood and are presented as mean ±SEM of n=1-3.
(J) Treatment scheme for for combined therapy. PTEN$^{(i)pe-/-}$ mice at 3 months post tamoxifen were treated with 100 µg of murinized anti-Ly-6G (clone 1A8), 500 µg of murinized rat anti-CSF1R (clone AFS98) and 100µg of murinized rat anti-PD1 (clone RMP1-14) at day 0, 3, 5, 7.
(K) FACS contour plots showing IFN-γ and TNF-α production by CD8^{+} T cells from prostate of mice treated with the isotype control or with the combined triple therapy. Plots are presented as overlays of FMO (blue) and IFN-γ and TNF-α staining (red).
(L) Bar plots showing the frequency of IFN-γ^{+}TNF-α^{-} and IFN-γ^{+}TNF-α^{+} CD8^{+} T cells in PTEN$^{(i)pe-/-}$ prostate of the different treated groups: Isotype control, anti-PD1 alone, anti-CSF1R + anti-Ly-6G, or anti-CSF1R + anti-Ly-6G + anti-PD1.

Literature of research article

Abu El Maaty, M.A., E. Grelet, C. Keime, A.I. Rerra, J. Gantzer, C. Emprou, J. Terzic, R. Lutzing, J.M. Bornert, G. Laverny, and D. Metzger. 2021. Single-cell analyses unravel cell type-specific responses to a vitamin D analog in prostatic precancerous lesions. *Sci Adv* 7:

Abu El Maaty, M.A., J. Terzic, C. Keime, D. Rovito, R. Lutzing, D. Yanushko, M. Parisotto, E. Grelet, I.J. Namer, V. Lindner, G. Laverny, and D. Metzger. 2022. Hypoxia-mediated stabilization of HIF1A in prostatic intraepithelial neoplasia promotes cell plasticity and malignant progression. *Sci Adv* 8:eabo2295.

Adekoya, T.O., and R.M. Richardson. 2020. Cytokines and Chemokines as Mediators of Prostate Cancer Metastasis. *Int J Mol Sci* 21:

Ai, H.W., J.N. Henderson, S.J. Remington, and R.E. Campbell. 2006. Directed evolution of a monomeric, bright and photostable version of Clavularia cyan fluorescent protein: structural characterization and applications in fluorescence imaging. *Biochem J* 400:531-540.

Akkari, L., I. Amit, V. Bronte, Z.G. Fridlender, D.I. Gabrilovich, F. Ginhoux, C.C. Hedrick, and S. Ostrand-Rosenberg. 2024. Defining myeloid-derived suppressor cells. *Nat Rev Immunol*

Alshetaiwi, H., N. Pervolarakis, L.L. McIntyre, D. Ma, Q. Nguyen, J.A. Rath, K. Nee, G. Hernandez, K. Evans, L. Torosian, A. Silva, C. Walsh, and K. Kessenbrock. 2020. Defining the emergence of myeloid-derived suppressor cells in breast cancer using single-cell transcriptomics. *Sci Immunol* 5:

Antonicelli, F., J. Lorin, S. Kurdykowski, S.C. Gangloff, R. Le Naour, J.M. Sallenave, W. Hornebeck, F. Grange, and P. Bernard. 2011. CXCL10 reduces melanoma proliferation and invasiveness in vitro and in vivo. *Br J Dermatol* 164:720-728.

Ardouin, L., H. Luche, R. Chelbi, S. Carpentier, A. Shawket, F. Montanana Sanchis, C. Santa Maria, P. Grenot, Y. Alexandre, C. Gregoire, A. Fries, T.P. Vu Manh, S. Tamoutounour, K. Crozat, E. Tomasello, A. Jorquera, E. Fossum, B. Bogen, H. Azukizawa, M. Bajenoff, S. Henri, M. Dalod, and B. Malissen. 2016. Broad and Largely Concordant Molecular Changes Characterize Tolerogenic and Immunogenic Dendritic Cell Maturation in Thymus and Periphery. *Immunity* 45:305-318.

Bancaro, N., B. Cali, M. Troiani, A.R. Elia, R.A. Arzola, G. Attanasio, P. Lai, M. Crespo, B. Gurel, R. Pereira, C. Guo, S. Mosole, D. Brina, M. D'Ambrosio, E. Pasquini, C. Spataro, E. Zagato, A. Rinaldi, M. Pedotti, S. Di Lascio, F. Meani, M. Montopoli, M. Ferrari, A. Gallina, L. Varani, R. Pereira Mestre, M. Bolis, S. Gillessen Sommer, J. de Bono, A. Calcinotto, and A. Alimonti. 2023. Apolipoprotein E induces pathogenic senescent-like myeloid cells in prostate cancer. *Cancer Cell* 41:602-619 e611.

Baranska, A., A. Shawket, M. Jouve, M. Baratin, C. Malosse, O. Voluzan, T.P. Vu Manh, F. Fiore, M. Bajenoff, P. Benaroch, M. Dalod, M. Malissen, S. Henri, and B. Malissen. 2018. Unveiling skin macrophage dynamics explains both tattoo persistence and strenuous removal. *J Exp Med* 215:1115-1133.

Begley, L.A., S. Kasina, R. Mehra, S. Adsule, A.J. Admon, R.J. Lonigro, A.M. Chinnaiyan, and J.A. Macoska. 2008. CXCL5 promotes prostate cancer progression. *Neoplasia* 10:244-254.

Bijnen, M., and M. Bajenoff. 2021. Gland Macrophages: Reciprocal Control and Function within Their Niche. *Trends Immunol* 42:120-136.

Binnewies, M., J.L. Pollack, J. Rudolph, S. Dash, M. Abushawish, T. Lee, N.S. Jahchan, P. Canaday, E. Lu, M. Norng, S. Mankikar, V.M. Liu, X. Du, A. Chen, R. Mehta, R. Palmer, V. Juric, L. Liang, K.P. Baker, L. Reyno, M.F. Krummel, M. Streuli, and V. Sriram. 2021. Targeting TREM2 on tumor-associated macrophages enhances immunotherapy. *Cell Rep* 37:109844.

Blaisdell, A., A. Crequer, D. Columbus, T. Daikoku, K. Mittal, S.K. Dey, and A. Erlebacher. 2015. Neutrophils Oppose Uterine Epithelial Carcinogenesis via Debridement of Hypoxic Tumor Cells. *Cancer Cell* 28:785-799.

Boivin, G., J. Faget, P.B. Ancey, A. Gkasti, J. Mussard, C. Engblom, C. Pfirschke, C. Contat, J. Pascual, J. Vazquez, N. Bendriss-Vermare, C. Caux, M.C. Vozenin, M.J. Pittet, M. Gunzer, and E. Meylan. 2020. Durable and controlled depletion of neutrophils in mice. *Nat Commun* 11:2762.

Boring, L., J. Gosling, S.W. Chensue, S.L. Kunkel, R.V. Farese, Jr., H.E. Broxmeyer, and I.F. Charo. 1997. Impaired monocyte migration and reduced type 1 (Th1) cytokine responses in C-C chemokine receptor 2 knockout mice. *J Clin Invest* 100:2552-2561.

Cao, J., M. Spielmann, X. Qiu, X. Huang, D.M. Ibrahim, A.J. Hill, F. Zhang, S. Mundlos, L. Christiansen, F.J. Steemers, C. Trapnell, and J. Shendure. 2019. The single-cell transcriptional landscape of mammalian organogenesis. *Nature* 566:496-502.

Casanova-Acebes, M., E. Dalla, A.M. Leader, J. LeBerichel, J. Nikolic, B.M. Morales, M. Brown, C. Chang, L. Troncoso, S.T. Chen, A. Sastre-Perona, M.D. Park, A. Tabachnikova, M. Dhainaut, P. Hamon, B. Maier, C.M. Sawai, E. Agullo-Pascual, M. Schober, B.D. Brown, B. Reizis, T. Marron, E. Kenigsberg, C. Moussion, P. Benaroch, J.A. Aguirre-Ghiso, and M. Merad. 2021. Tissue-resident macrophages provide a pro-tumorigenic niche to early NSCLC cells. *Nature* 595:578-584.

Casbon, A.J., D. Reynaud, C. Park, E. Khuc, D.D. Gan, K. Schepers, E. Passegue, and Z. Werb. 2015. Invasive breast cancer reprograms early myeloid differentiation in the bone marrow to generate immunosuppressive neutrophils. *Proc Natl Acad Sci U S A* 112:E566-575.

Chakarov, S., H.Y. Lim, L. Tan, S.Y. Lim, P. See, J. Lum, X.M. Zhang, S. Foo, S. Nakamizo, K. Duan, W.T. Kong, R. Gentek, A. Balachander, D. Carbajo, C. Bleriot, B. Malleret, J.K.C. Tam, S. Baig, M. Shabeer, S.E.S. Toh, A. Schlitzer, A. Larbi, T. Marichal, B. Malissen, J. Chen, M. Poidinger, K. Kabashima, M. Bajenoff, L.G. Ng, V. Angeli, and F. Ginhoux. 2019. Two distinct interstitial macrophage populations coexist across tissues in specific subtissular niches. *Science* 363:

Chamoto, K., T. Yaguchi, M. Tajima, and T. Honjo. 2023. Insights from a 30-year journey: function, regulation and therapeutic modulation of PD1. *Nat Rev Immunol* 23:682-695.

Chen, D.S., and I. Mellman. 2017. Elements of cancer immunity and the cancer-immune set point. *Nature* 541:321-330.

Chen, S., G. Zhu, Y. Yang, F. Wang, Y.T. Xiao, N. Zhang, X. Bian, Y. Zhu, Y. Yu, F. Liu, K. Dong, J. Mariscal, Y. Liu, F. Soares, H. Loo Yau, B. Zhang, W. Chen, C. Wang, D. Chen, Q. Guo, Z. Yi, M. Liu, M. Fraser, D.D. De Carvalho, P.C. Boutros, D. Di Vizio, Z. Jiang, T. van der Kwast, A. Berlin, S. Wu, J. Wang, H.H. He, and S. Ren. 2021. Single-cell analysis reveals transcriptomic remodellings in distinct cell types that contribute to human prostate cancer progression. *Nat Cell Biol* 23:87-98.

Cortez-Retamozo, V., M. Etzrodt, and M.J. Pittet. 2012. Regulation of macrophage and dendritic cell responses by their lineage precursors. *J Innate Immun* 4:411-423.

Crowley, L., F. Cambuli, L. Aparicio, M. Shibata, B.D. Robinson, S. Xuan, W. Li, H. Hibshoosh, M. Loda, R. Rabadan, and M.M. Shen. 2020. A single-cell atlas of the mouse and human prostate reveals heterogeneity and conservation of epithelial progenitors. *Elife* 9:

Cunha, G.R., C.M. Vezina, D. Isaacson, W.A. Ricke, B.G. Timms, M. Cao, O. Franco, and L.S. Baskin. 2018. Development of the human prostate. *Differentiation* 103:24-45.

Dai, X.M., G.R. Ryan, A.J. Hapel, M.G. Dominguez, R.G. Russell, S. Kapp, V. Sylvestre, and E.R. Stanley. 2002. Targeted disruption of the mouse colony-stimulating factor 1 receptor gene results in osteopetrosis, mononuclear phagocyte deficiency, increased primitive progenitor cell frequencies, and reproductive defects. *Blood* 99:111-120.

Daniel, B., K.E. Yost, S. Hsiung, K. Sandor, Y. Xia, Y. Qi, K.J. Hiam-Galvez, M. Black, J.R. C, Q. Shi, S.L. Meier, J.A. Belk, J.R. Giles, E.J. Wherry, H.Y. Chang, T. Egawa, and A.T. Satpathy. 2022. Divergent clonal differentiation trajectories of T cell exhaustion. *Nat Immunol* 23:1614-1627.

Dawson, C.A., B. Pal, F. Vaillant, L.C. Gandolfo, Z. Liu, C. Bleriot, F. Ginhoux, G.K. Smyth, G.J. Lindeman, S.N. Mueller, A.C. Rios, and J.E. Visvader. 2020. Tissue-resident ductal macrophages survey the mammary epithelium and facilitate tissue remodelling. *Nat Cell Biol* 22:546-558.

Dick, S.A., A. Wong, H. Hamidzada, S. Nejat, R. Nechanitzky, S. Vohra, B. Mueller, R. Zaman, C. Kantores, L. Aronoff, A. Momen, D. Nechanitzky, W.Y. Li, P. Ramachandran, S.Q. Crome, B. Becher, M.I. Cybulsky, F. Billia, S. Keshavjee, S. Mital, C.S. Robbins, T.W. Mak, and S. Epelman. 2022. Three tissue resident macrophage subsets coexist across organs with conserved origins and life cycles. *Sci Immunol* 7:eabf7777.

Dwyer, D.F., N.A. Barrett, K.F. Austen, and C. Immunological Genome Project. 2016. Expression profiling of constitutive mast cells reveals a unique identity within the immune system. *Nat Immunol* 17:878-887.

Gao, H.T., Z. Yang, H. Sun, Y. Zhang, Z. Wang, W.Y. Liu, H.Z. Wen, C.B. Qu, and X.L. Wang. 2023. TREM2 as an independent predictor of poor prognosis promotes the migration via the PI3K/AKT axis in prostate cancer. *Am J Transl Res* 15:779-798.

Germain, P.L., A. Lun, C. Garcia Meixide, W. Macnair, and M.D. Robinson. 2021. Doublet identification in single-cell sequencing data using scDblFinder. *F1000Res* 10:979.

Ginhoux, F., and M. Guilliams. 2016. Tissue-Resident Macrophage Ontogeny and Homeostasis. *Immunity* 44:439-449.

Giraud, J., D. Chalopin, E. Ramel, T. Boyer, A. Zouine, M.A. Derieppe, N. Larmonier, O. Adotevi, B. Le Bail, J.F. Blanc, C. Laurent, L. Chiche, M. Derive, M. Nikolski, and M. Saleh. 2024a. THBS1(+) myeloid cells expand in SLD hepatocellular carcinoma and contribute to immunosuppression and unfavorable prognosis through TREM1. *Cell Rep* 43:113773.

Giraud, J.S., A. Jouinot, E. Pasmant, and C. Tlemsani. 2024b. NF1 mutations as biomarker of response to immune checkpoint blockades for lung adenocarcinoma patients. *NPJ Precis Oncol* 8:32.

Gu, Z., R. Eils, and M. Schlesner. 2016. Complex heatmaps reveal patterns and correlations in multidimensional genomic data. *Bioinformatics* 32:2847-2849.

Guilliams, M., G.R. Thierry, J. Bonnardel, and M. Bajenoff. 2020. Establishment and Maintenance of the Macrophage Niche. *Immunity* 52:434-451.

Gungabeesoon, J., N.A. Gort-Freitas, M. Kiss, E. Bolli, M. Messemaker, M. Siwicki, M. Hicham, R. Bill, P. Koch, C. Cianciaruso, F. Duval, C. Pfirschke, M. Mazzola, S. Peters, K. Homicsko, C. Garris, R. Weissleder, A.M. Klein, and M.J. Pittet. 2023. A neutrophil response linked to tumor control in immunotherapy. *Cell* 186:1448-1464 e1420.

Henry, G.H., A. Malewska, D.B. Joseph, V.S. Malladi, J. Lee, J. Torrealba, R.J. Mauck, J.C. Gahan, G.V. Raj, C.G. Roehrborn, G.C. Hon, M.P. MacConmara, J.C. Reese, R.C. Hutchinson, C.M. Vezina, and D.W. Strand. 2018. A Cellular Anatomy of the Normal Adult Human Prostate and Prostatic Urethra. *Cell Rep* 25:3530-3542 e3535.

Hidalgo, A., E.R. Chilvers, C. Summers, and L. Koenderman. 2019. The Neutrophil Life Cycle. *Trends Immunol* 40:584-597.

Hirz, T., S. Mei, H. Sarkar, Y. Kfoury, S. Wu, B.M. Verhoeven, A.O. Subtelny, D.V. Zlatev, M.W. Wszolek, K. Salari, E. Murray, F. Chen, E.Z. Macosko, C.L. Wu, D.T. Scadden, D.M. Dahl, N. Baryawno, P.J. Saylor, P.V. Kharchenko, and D.B. Sykes. 2023. Dissecting the immune suppressive human prostate tumor microenvironment via integrated single-cell and spatial transcriptomic analyses. *Nat Commun* 14:663.

Hoch, T., D. Schulz, N. Eling, J.M. Gomez, M.P. Levesque, and B. Bodenmiller. 2022. Multiplexed imaging mass cytometry of the chemokine milieus in melanoma characterizes features of the response to immunotherapy. *Sci Immunol* 7:eabk1692.

Hoeffel, G., and F. Ginhoux. 2015. Ontogeny of Tissue-Resident Macrophages. *Front Immunol* 6:486.

Husain, Z., Y. Huang, P. Seth, and V.P. Sukhatme. 2013a. Tumor-derived lactate modifies antitumor immune response: effect on myeloid-derived suppressor cells and NK cells. *J Immunol* 191:1486-1495.

Husain, Z., P. Seth, and V.P. Sukhatme. 2013b. Tumor-derived lactate and myeloid-derived suppressor cells: Linking metabolism to cancer immunology. *Oncoimmunology* 2:e26383.

Jaillon, S., A. Ponzetta, D. Di Mitri, A. Santoni, R. Bonecchi, and A. Mantovani. 2020. Neutrophil diversity and plasticity in tumour progression and therapy. *Nat Rev Cancer* 20:485-503.

Jayaprakash, P., M. Ai, A. Liu, P. Budhani, T. Bartkowiak, J. Sheng, C. Ager, C. Nicholas, A.R. Jaiswal, Y. Sun, K. Shah, S. Balasubramanyam, N. Li, G. Wang, J. Ning, A. Zal, T. Zal, and M.A. Curran. 2018. Targeted hypoxia reduction restores T cell infiltration and sensitizes prostate cancer to immunotherapy. *J Clin Invest* 128:5137-5149.

Joseph, D.B., A.E. Turco, C.M. Vezina, and D.W. Strand. 2021. Progenitors in prostate development and disease. *Dev Biol* 473:50-58.

Jung, S., J. Aliberti, P. Graemmel, M.J. Sunshine, G.W. Kreutzberg, A. Sher, and D.R. Littman. 2000. Analysis of fractalkine receptor CX(3)CR1 function by targeted deletion and green fluorescent protein reporter gene insertion. *Mol Cell Biol* 20:4106-4114.

Karthaus, W.R., M. Hofree, D. Choi, E.L. Linton, M. Turkekul, A. Bejnood, B. Carver, A. Gopalan, W. Abida, V. Laudone, M. Biton, O. Chaudhary, T. Xu, I. Masilionis, K. Manova, L. Mazutis, D. Pe'er,

A. Regev, and C.L. Sawyers. 2020. Regenerative potential of prostate luminal cells revealed by single-cell analysis. *Science* 368:497-505.

Katzenelenbogen, Y., F. Sheban, A. Yalin, I. Yofe, D. Svetlichnyy, D.A. Jaitin, C. Bornstein, A. Moshe, H. Keren-Shaul, M. Cohen, S.Y. Wang, B. Li, E. David, T.M. Salame, A. Weiner, and I. Amit. 2020. Coupled scRNA-Seq and Intracellular Protein Activity Reveal an Immunosuppressive Role of TREM2 in Cancer. *Cell* 182:872-885 e819.

Li, B.H., M.A. Garstka, and Z.F. Li. 2020. Chemokines and their receptors promoting the recruitment of myeloid-derived suppressor cells into the tumor. *Mol Immunol* 117:201-215.

Li, Y., L. Zhao, and X.F. Li. 2021. The Hypoxia-Activated Prodrug TH-302: Exploiting Hypoxia in Cancer Therapy. *Front Pharmacol* 12:636892.

Liu, Z., H. Wang, Z. Li, R.J. Dress, Y. Zhu, S. Zhang, D. De Feo, W.T. Kong, P. Cai, A. Shin, C. Piot, J. Yu, Y. Gu, M. Zhang, C. Gao, L. Chen, H. Wang, M. Vetillard, P. Guermonprez, I. Kwok, L.G. Ng, S. Chakarov, A. Schlitzer, B. Becher, C.A. Dutertre, B. Su, and F. Ginhoux. 2023. Dendritic cell type 3 arises from Ly6C(+) monocyte-dendritic cell progenitors. *Immunity* 56:1761-1777 e1766.

Luongo, F., F. Colonna, F. Calapa, S. Vitale, M.E. Fiori, and R. De Maria. 2019. PTEN Tumor-Suppressor: The Dam of Stemness in Cancer. *Cancers (Basel)* 11:

MacDonald, K.P., J.S. Palmer, S. Cronau, E. Seppanen, S. Olver, N.C. Raffelt, R. Kuns, A.R. Pettit, A. Clouston, B. Wainwright, D. Branstetter, J. Smith, R.J. Paxton, D.P. Cerretti, L. Bonham, G.R. Hill, and D.A. Hume. 2010. An antibody against the colony-stimulating factor 1 receptor depletes the resident subset of monocytes and tissue- and tumor-associated macrophages but does not inhibit inflammation. *Blood* 116:3955-3963.

Magen, A., J. Nie, T. Ciucci, S. Tamoutounour, Y. Zhao, M. Mehta, B. Tran, D.B. McGavern, S. Hannenhalli, and R. Bosselut. 2019. Single-Cell Profiling Defines Transcriptomic Signatures Specific to Tumor-Reactive versus Virus-Responsive CD4(+) T Cells. *Cell Rep* 29:3019-3032 e3016.

Maier, B., A.M. Leader, S.T. Chen, N. Tung, C. Chang, J. LeBerichel, A. Chudnovskiy, S. Maskey, L. Walker, J.P. Finnigan, M.E. Kirkling, B. Reizis, S. Ghosh, N.R. D'Amore, N. Bhardwaj, C.V. Rothlin, A. Wolf, R. Flores, T. Marron, A.H. Rahman, E. Kenigsberg, B.D. Brown, and M. Merad. 2020. A conserved dendritic-cell regulatory program limits antitumour immunity. *Nature* 580:257-262.

Malissen, B., S. Tamoutounour, and S. Henri. 2014. The origins and functions of dendritic cells and macrophages in the skin. *Nat Rev Immunol* 14:417-428.

Mangiola, S., A.J. Roth-Schulze, M. Trussart, E. Zozaya-Valdes, M. Ma, Z. Gao, A.F. Rubin, T.P. Speed, H. Shim, and A.T. Papenfuss. 2023. sccomp: Robust differential composition and variability analysis for single-cell data. *Proc Natl Acad Sci U S A* 120:e2203828120.

McGinnis, C.S., Z. Miao, D. Superville, W. Yao, A. Goga, N.E. Reticker-Flynn, J. Winkler, and A.T. Satpathy. 2024. The temporal progression of lung immune remodeling during breast cancer metastasis. *Cancer Cell* 42:1018-1031 e1016.

Molgora, M., Y.A. Liu, M. Colonna, and M. Cella. 2023. TREM2: A new player in the tumor microenvironment. *Semin Immunol* 67:101739.

Mora Barthelmess, R., B. Stijlemans, and J.A. Van Ginderachter. 2023. Hallmarks of Cancer Affected by the MIF Cytokine Family. *Cancers (Basel)* 15:

Nalio Ramos, R., Y. Missolo-Koussou, Y. Gerber-Ferder, C.P. Bromley, M. Bugatti, N.G. Nunez, J. Tosello Boari, W. Richer, L. Menger, J. Denizeau, C. Sedlik, P. Caudana, F. Kotsias, L.L. Niborski, S. Viel, M. Bohec, S. Lameiras, S. Baulande, L. Lesage, A. Nicolas, D. Meseure, A. Vincent-Salomon, F. Reyal, C.A. Dutertre, F. Ginhoux, L. Vimeux, E. Donnadieu, B. Buttard, J. Galon, S. Zelenay, W. Vermi, P. Guermonprez, E. Piaggio, and J. Helft. 2022. Tissue-resident FOLR2(+) macrophages associate with CD8(+) T cell infiltration in human breast cancer. *Cell* 185:1189-1207 e1125.

Ng, M.S.F., I. Kwok, L. Tan, C. Shi, D. Cerezo-Wallis, Y. Tan, K. Leong, G.F. Calvo, K. Yang, Y. Zhang, J. Jin, K.H. Liong, D. Wu, R. He, D. Liu, Y.C. Teh, C. Bleriot, N. Caronni, Z. Liu, K. Duan, V. Narang, I. Ballesteros, F. Moalli, M. Li, J. Chen, Y. Liu, L. Liu, J. Qi, Y. Liu, L. Jiang, B. Shen, H. Cheng, T. Cheng, V. Angeli, A. Sharma, Y.H. Loh, H.L. Tey, S.Z. Chong, M. Iannacone, R. Ostuni, A. Hidalgo, F. Ginhoux, and L.G. Ng. 2024. Deterministic reprogramming of neutrophils within tumors. *Science* 383:eadf6493.

Noe, J.T., and R.A. Mitchell. 2020. MIF-Dependent Control of Tumor Immunity. *Front Immunol* 11:609948.

Olofsen, P.A., M.C. Stip, J.H.M. Jansen, C. Chan, M. Nederend, R.G. Tieland, M. Tsioumpekou, and J.H.W. Leusen. 2022. Effective, Long-Term, Neutrophil Depletion Using a Murinized Anti-Ly-6G 1A8 Antibody. *Cells* 11:

Overbeeke, C., T. Tak, and L. Koenderman. 2022. The journey of neutropoiesis: how complex landscapes in bone marrow guide continuous neutrophil lineage determination. *Blood* 139:2285-2293.

Parisotto, M., E. Grelet, R. El Bizri, Y. Dai, J. Terzic, D. Eckert, L. Gargowitsch, J.M. Bornert, and D. Metzger. 2018. PTEN deletion in luminal cells of mature prostate induces replication stress and senescence in vivo. *J Exp Med* 215:1749-1763.

Park, M.D., A. Silvin, F. Ginhoux, and M. Merad. 2022. Macrophages in health and disease. *Cell* 185:4259-4279.

Pettitt, S.J., Q. Liang, X.Y. Rairdan, J.L. Moran, H.M. Prosser, D.R. Beier, K.C. Lloyd, A. Bradley, and W.C. Skarnes. 2009. Agouti C57BL/6N embryonic stem cells for mouse genetic resources. *Nat Methods* 6:493-495.

Raskov, H., A. Orhan, S. Gaggar, and I. Gogenur. 2022. Neutrophils and polymorphonuclear myeloid-derived suppressor cells: an emerging battleground in cancer therapy. *Oncogenesis* 11:22.

Ratnacaram, C.K., M. Teletin, M. Jiang, X. Meng, P. Chambon, and D. Metzger. 2008. Temporally controlled ablation of PTEN in adult mouse prostate epithelium generates a model of invasive prostatic adenocarcinoma. *Proc Natl Acad Sci U S A* 105:2521-2526.

Reschke, R., J. Yu, B. Flood, E.F. Higgs, K. Hatogai, and T.F. Gajewski. 2021. Immune cell and tumor cell-derived CXCL10 is indicative of immunotherapy response in metastatic melanoma. *J Immunother Cancer* 9:

Rodriguez, C.I., F. Buchholz, J. Galloway, R. Sequerra, J. Kasper, R. Ayala, A.F. Stewart, and S.M. Dymecki. 2000. High-efficiency deleter mice show that FLPe is an alternative to Cre-loxP. *Nat Genet* 25:139-140.

Rojo, R., A. Raper, D.D. Ozdemir, L. Lefevre, K. Grabert, E. Wollscheid-Lengeling, B. Bradford, M. Caruso, I. Gazova, A. Sanchez, Z.M. Lisowski, J. Alves, I. Molina-Gonzalez, H. Davtyan, R.J. Lodge, J.D. Glover, R. Wallace, D.A.D. Munro, E. David, I. Amit, V.E. Miron, J. Priller, S.J. Jenkins, G.E. Hardingham, M. Blurton-Jones, N.A. Mabbott, K.M. Summers, P. Hohenstein, D.A. Hume, and C. Pridans. 2019. Deletion of a Csf1r enhancer selectively impacts CSF1R expression and development of tissue macrophage populations. *Nat Commun* 10:3215.

Satpathy, A.T., W. Kc, J.C. Albring, B.T. Edelson, N.M. Kretzer, D. Bhattacharya, T.L. Murphy, and K.M. Murphy. 2012. Zbtb46 expression distinguishes classical dendritic cells and their committed progenitors from other immune lineages. *J Exp Med* 209:1135-1152.

Serbina, N.V., and E.G. Pamer. 2006. Monocyte emigration from bone marrow during bacterial infection requires signals mediated by chemokine receptor CCR2. *Nat Immunol* 7:311-317.

Sharma, P., S. Goswami, D. Raychaudhuri, B.A. Siddiqui, P. Singh, A. Nagarajan, J. Liu, S.K. Subudhi, C. Poon, K.L. Gant, S.M. Herbrich, S. Anandhan, S. Islam, M. Amit, G. Anandappa, and J.P. Allison. 2023. Immune checkpoint therapy-current perspectives and future directions. *Cell* 186:1652-1669.

Shaul, M.E., L. Levy, J. Sun, I. Mishalian, S. Singhal, V. Kapoor, W. Horng, G. Fridlender, S.M. Albelda, and Z.G. Fridlender. 2016. Tumor-associated neutrophils display a distinct N1 profile following TGFbeta modulation: A transcriptomics analysis of pro- vs. antitumor TANs. *Oncoimmunology* 5:e1232221.

Sherr, C.J., C.W. Rettenmier, R. Sacca, M.F. Roussel, A.T. Look, and E.R. Stanley. 1985. The c-fms proto-oncogene product is related to the receptor for the mononuclear phagocyte growth factor, CSF-1. *Cell* 41:665-676.

Siegel, R.L., A.N. Giaquinto, and A. Jemal. 2024. Cancer statistics, 2024. *CA Cancer J Clin* 74:12-49.

Sumaiya, K., D. Langford, K. Natarajaseenivasan, and S. Shanmughapriya. 2022. Macrophage migration inhibitory factor (MIF): A multifaceted cytokine regulated by genetic and physiological strategies. *Pharmacol Ther* 233:108024.

Tamoutounour, S., M. Guilliams, F. Montanana Sanchis, H. Liu, D. Terhorst, C. Malosse, E. Pollet, L. Ardouin, H. Luche, C. Sanchez, M. Dalod, B. Malissen, and S. Henri. 2013. Origins and functional specialization of macrophages and of conventional and monocyte-derived dendritic cells in mouse skin. *Immunity* 39:925-938.

Tauber, M., L. Basso, J. Martin, L. Bostan, M.M. Pinto, G.R. Thierry, R. Houmadi, N. Serhan, A. Loste, C. Bleriot, J.B.J. Kamphuis, M. Grujic, L. Kjellen, G. Pejler, C. Paul, X. Dong, S.J. Galli, L.L. Reber, F. Ginhoux, M. Bajenoff, R. Gentek, and N. Gaudenzio. 2023. Landscape of mast cell populations across organs in mice and humans. *J Exp Med* 220:

Timms, B.G. 2008. Prostate development: a historical perspective. *Differentiation* 76:565-577.

Tuong, Z.K., K.W. Loudon, B. Berry, N. Richoz, J. Jones, X. Tan, Q. Nguyen, A. George, S. Hori, S. Field, A.G. Lynch, K. Kania, P. Coupland, A. Babbage, R. Grenfell, T. Barrett, A.Y. Warren, V. Gnanapragasam, C. Massie, and M.R. Clatworthy. 2021. Resolving the immune landscape of human prostate at a single-cell level in health and cancer. *Cell Rep* 37:110132.

Veglia, F., A. Hashimoto, H. Dweep, E. Sanseviero, A. De Leo, E. Tcyganov, A. Kossenkov, C. Mulligan, B. Nam, G. Masters, J. Patel, V. Bhargava, P. Wilkinson, D. Smirnov, M.A. Sepulveda, S. Singhal, E.B. Eruslanov, R. Cristescu, A. Loboda, Y. Nefedova, and D.I. Gabrilovich. 2021. Analysis of classical neutrophils and polymorphonuclear myeloid-derived suppressor cells in cancer patients and tumor-bearing mice. *J Exp Med* 218:

Wu, Y., J. Ma, X. Yang, F. Nan, T. Zhang, S. Ji, D. Rao, H. Feng, K. Gao, X. Gu, S. Jiang, G. Song, J. Pan, M. Zhang, Y. Xu, S. Zhang, Y. Fan, X. Wang, J. Zhou, L. Yang, J. Fan, X. Zhang, and Q. Gao. 2024. Neutrophil profiling illuminates anti-tumor antigen-presenting potency. *Cell* 187:1422-1439 e1424.

Xie, X., Q. Shi, P. Wu, X. Zhang, H. Kambara, J. Su, H. Yu, S.Y. Park, R. Guo, Q. Ren, S. Zhang, Y. Xu, L.E. Silberstein, T. Cheng, F. Ma, C. Li, and H.R. Luo. 2020. Single-cell transcriptome profiling reveals neutrophil heterogeneity in homeostasis and infection. *Nat Immunol* 21:1119-1133.

Yalcin, F., H. Haneke, I.E. Efe, L.D. Kuhrt, E. Motta, B. Nickl, C. Fluh, M. Synowitz, O. Dzaye, M. Bader, and H. Kettenmann. 2024. Tumor associated microglia/macrophages utilize GPNMB to promote tumor growth and alter immune cell infiltration in glioma. *Acta Neuropathol Commun* 12:50.

Yan, L., M. Wu, T. Wang, H. Yuan, X. Zhang, H. Zhang, T. Li, V. Pandey, X. Han, P.E. Lobie, and T. Zhu. 2024. Breast Cancer Stem Cells Secrete MIF to Mediate Tumor Metabolic Reprogramming That Drives Immune Evasion. *Cancer Res* 84:1270-1285.

Zhao, J., I. Andreev, and H.M. Silva. 2024. Resident tissue macrophages: Key coordinators of tissue homeostasis beyond immunity. *Sci Immunol* 9:eadd1967.

Zhu, G., Y. Tang, N. Geng, M. Zheng, J. Jiang, L. Li, K. Li, Z. Lei, W. Chen, Y. Fan, X. Ma, L. Li, X. Wang, and X. Liang. 2014. HIF-alpha/MIF and NF-kappaB/IL-6 axes contribute to the recruitment of CD11b+Gr-1+ myeloid cells in hypoxic microenvironment of HNSCC. *Neoplasia* 16:168-179.

Zilionis, R., C. Engblom, C. Pfirschke, V. Savova, D. Zemmour, H.D. Saatcioglu, I. Krishnan, G. Maroni, C.V. Meyerovitz, C.M. Kerwin, S. Choi, W.G. Richards, A. De Rienzo, D.G. Tenen, R. Bueno, E. Levantini, M.J. Pittet, and A.M. Klein. 2019. Single-Cell Transcriptomics of Human and Mouse Lung Cancers Reveals Conserved Myeloid Populations across Individuals and Species. *Immunity* 50:1317-1334 e1310.

Discussion & Perspectives

Prostate cancer (PCa) is the most commonly diagnosed cancer and the second leading cause of cancer-related deaths in men in Western societies. Despite significant progress over the last decade, PCa remains incurable. Immune checkpoint inhibitors (ICIs), which have revolutionized the field of immunotherapy, produced disappointing results in PCa trials, contrasting with their efficacy on other types of cancer. This limited efficacy of ICI-based immunotherapies is attributed to the sparse tumor-infiltrating T cells and the immunosuppressive traits of the prostate tumor microenvironment (TME) (Liu and Sun, 2021; Maleki Vareki, 2018). Therefore, understanding the composition, phenotypic states, and functions of intratumoral immune cells is crucial for developing effective immunotherapeutic strategies against PCa.

Hence, my PhD project aimes to address this knowledge gap using an innovative pre-clinical model that closely recapitulates human PCa features. The advantage of the inducible PTEN$^{(i)pe-/-}$ mouse model relies on the temporal control of the tumor induction, via tamoxifen administration at adulthood, and the slow tumor progression. More specifically, adult PTEN$^{(i)pe-/-}$ mice develop PIN lesions and adenocarcinoma after a latency phase of 3- and 9-months post tamoxifen administration respectively, and this slow tumor progression is mimicking human PCa staging. This PSA-PTEN$^{(i)pe-/-}$ model exhibits full tumor penetrance and allows to study the immune cells in the tumor microenvironment and to test therapeutic strategies during PCa progression using homogeneous groups of age-matched treated/non-treated male mice. Previous studies by our collaborators (Abu El Maaty et al., 2022; Parisotto et al., 2018b; Ratnacaram et al., 2008) have demonstrated that the tumor microenvironment of the PTEN$^{(i)pe-/-}$ prostates is senescent and highly hypoxic, characterized by increased GR1^{+} infiltration starting from 2 months onwards after *Pten* ablation, that account for ~3% of the total prostate cells, while in age-matched control animals they account for less than 0.07% of total prostate cells. Following-up on these studies, I performed an in-depth characterization of myeloid and lymphoid infiltrates in the PTEN$^{(i)pe-/-}$ model along tumor progression, using state-of-the art technologies.

Using single cell RNA sequencing on the CD45^{+} immune cells of PTEN$^{(i)pe-/-}$and age-matched littermate control prostates, I aimed to decipher the immune cell heterogeneity and functions at early and late tumor stages. Our thorough longitudinal analysis of immune infiltrates at the single cell level from early and advanced stages at prostatic intraepithelial neoplasia (PIN) (3- and 5-months post-Tamoxifen) and adenocarcinoma and advanced adenocarcinoma stages (9- and 12-months post-Tamoxifen), revealed a myeloid dominant landscape, with diversity and plasticity within the immune compartment. This analysis led to the creation of a high-resolution immune cell atlas of murine prostate cancer and paved the way for new immunotherapeutic targets against prostate cancer. In the parallel, I conducted a comprehensive characterization of macrophage heterogeneity and ontogeny in normal mouse prostate, representing the first detailed exploration of this organ.

In the following section, I will discuss the findings obtained from immunophenotyping techniques, including scRNA sequencing, flow-cytometry and confocal microscopy, on both healthy and tumorous PTEN$^{(i)pe-/-}$ prostates.

These analyses revealed that, similar to many other tissues, prostate contains a large heterogeneity of immune cell types, including neutrophils, dendritic cell subsets, macrophage

subsets of embryonic or monocytic origin, conventional and unconventional T cells, NK cells, B cells, and non-immune endothelial, epithelial, and fibroblast cells. Interestingly, we observed that the 50:50 balanced lymphoid : myeloid composition in healthy control prostates is shifting to a myeloid-dominated profile in PTEN$^{(i)pe-/-}$ prostates. This is highlighted by massive Ly6G^{+}CD11b^{+} neutrophils recruitment, from the neoplastic stage onwards, and significant increase of F4/80^{+} macrophages. In contrast, the lymphoid cells remain relatively stable at low levels upon tumor formation. Confocal microscopy confirmed the flow cytometric findings, demonstrating Ly6G^{+} neutrophils infiltration in the cancerous epithelium and the lumen, and stromal localization of newly recruited Iba1^{+} macrophages along with low levels of CD3^{+} T lymphocytes.

Notably, our annotated immunophenotyping matched greatly with the recent report on primary prostate tumor samples and normal controls by (Hirz et al., 2023). This study revealed that patients with localized prostate cancer have an immune suppressive tumor microenvironment associated with suppressive myeloid populations, exhausted T-cells, and high stromal angiogenic activity. Indeed, among a plethora of lymphoid cells, including CD4^{+} T, CD8^{+} T, NK and ILCs found in prostate tissue, the main difference between healthy and cancerous prostates was the increase of exhausted CD8^{+} T cells (cluster 3) already from the precancerous stage. This cluster exhibited increased expression of *Pdcd1*, *Lag3* and *Havcr2* genes in PTEN$^{(i)pe-/-}$ prostates compared to WT controls. These genes corresponding to the PD-1, Lag3 and Tim3 proteins respectively are associated with CD8^{+} T cell exhaustion (Chen and Mellman, 2017). Flow cytometric analysis confirmed the appearance of PD-1^{hi}Tim3^{hi} exhausted CD8^{+} T cells in PTEN$^{(i)pe-/-}$ prostates. Overall, while the total number of CD8^{+} T cells in the tumorous prostates increases slightly, they remain at overall low levels but exhibit a phenotype switch to exhausted (PD-1^{high}Tim3^{+}) state, from the very early PCa stage, 2 months post tamoxifen administration.

These findings support the notion that the murine PTEN$^{(i)pe-/-}$ prostate tumor effectively models the “cold” TME of human prostate cancer, characterized by low CD8^{+} T cell infiltration and exhaustion (Bronte et al., 2005; Japp et al., 2015; Sfanos et al., 2009). Importantly, this immunosuppressive tumor microenvironment is already established at the neoplastic stage.

Since myeloid cells were the dominant population within the prostatic tumor microenvironment we focused our attention on the myeloid subsets. scRNAseq and flow cytometry enabled us to map the myeloid cells residing in healthy prostate tissue and upon prostate cancer development.

Equipped with our team's valuable expertise in disentangling the mononuclear phagocytic system in skin and melanoma cancer (Malissen et al., 2014; Tamoutounour et al., 2013) and using different macrophage- and dendritic cell-reporter mouse models, I was able to decipher the myeloid heterogeneity in prostate tissue. Based on the heterogeneity indicated by scRNA sequencing, I designed a multiparametric myeloid-specific flow cytometry panel, allowing me to distinguish 2 Dendritic Cell subsets (cDC1: **Xcr1^{+}Zbtb46^{+}**CD11b^{-} CD11c^{+}MHCII^{+}, and cDC2: **DC-Sign^{+}Zbtb46^{+}**CD11b^{+}CD11c^{+}MHCII^{+}), 2 monocyte subsets (P1 classical monocytes: **Ly6C^{high}**MHCII^{-}CD11b^{+}CD64^{-} & P2 non-classical monocytes: **Ly6C^{int}**MHCII^{+}CD11b^{+} CD64^{-}) and 3 distinct macrophage subsets

(**CD11b$^+$Tim4$^+$**FolR2$^+$Lyve1$^+$CD206$^+$CD64$^+$ CD88$^+$F4/80$^+$Slco2b1$^+$, **CD11b$^+$Tim4$^-$**FolR2^{+or-} CX3CR1$^+$CD64$^+$CD88$^+$F4/80$^+$Slco2b1$^+$, and **CD11b$^-$Tim4$^-$**CX3CR1$^+$CD64$^+$CD88$^+$ F4/80$^+$Slco2b1$^+$) as well as a Lyz$^+$ population (Lyz$^+$CD11b$^+$CD11c$^+$MHCII$^+$CD64$^-$CD88$^-$). Additional macrophage populations, cDC1 subclusters, pDCs, CCR7$^+$ DCs and mast cells revealed by scRNAseq could not be identified by facs due to their scarcity or the lack of specific marker. For instance, Mac1,2,3,4 detected by scRNAseq must be included in the **CD11b$^+$Tim4$^-$FolR2$^-$** population. Remarkably, the gene signature of our annotated clusters shows great matching with gene signatures of the corresponding subsets recently described in other organs by (Chakarov et al., 2019; Dick et al., 2022; Dwyer et al., 2016; Liu et al., 2023).

Elucidating the origins, developmental trajectories, and homeostatic mechanisms of tissue-resident macrophages is fundamental for developing strategies to modulate macrophage functions at specific tissue sites. Thus, to better characterize the macrophage subsets in steady-state adult prostate tissue, I further investigated their origin and renewal using bone-marrow chimeras and, transgenic mouse model for depletion strategy. The general consensus indicates that macrophages are classified into two distinct groups based on their origin: a) the tissue-resident macrophages (RTMs), which originate from the yolk sac and fetal liver, and b) the infiltrating macrophages, which originate from bone marrow-derived monocytes (Park et al., 2022). Although all tissues are populated with fetal macrophages at birth, these cells can gradually be replaced by HSC-derived progenitors over time, varying by location or pathological condition, as reviewed by (Ginhoux and Guilliams, 2016; Park et al., 2022). For instance, parabiosis experiments initially demonstrated the involvement of adult precursors in certain tissue-resident macrophages and their continuous turnover during adulthood. Our laboratory has previously showed that at adulthood, the replacement of tissue macrophages in the dermis was dependent on the recruitment of Ly6C^{hi} monocytes after they exited the BM using the chemokine receptor CCR2. This was evidenced by the significant reduction of macrophage populations in mice lacking CCR2 and their reconstitution almost exclusively from wild-type BM-derived cells in WT:Ccr2$^{-/-}$ competitive chimeras (Tamoutounour et al., 2013). Similar findings were observed for macrophages in the intestine and pancreas (Bain et al., 2014b; Calderon et al., 2015).

Given that the origin of macrophages in prostate tissue was not explored before, I performed experiments to address this question. Knowing that one prostatic macrophage population expresses Tim4, a marker associated with long-term residency, we hypothesized minimal replacement by monocyte-derived cells population, as shown for other tissues, like gut and liver (Scott et al., 2016; Shaw et al., 2018). Indeed, protected BM chimeric experiments revealed that CD11b$^+$Tim4$^+$ Mac and CD11b$^-$Tim4$^-$ Mac populations have a very low turnover, compared to the CD11b$^+$Tim4$^-$ Mac that were reconstituted by BM donor cells at 30%. This suggested that CD11b$^+$Tim4$^+$ Mac and CD11b$^-$Tim4$^-$ Mac are long-lived cells, while some of CD11b$^+$Tim4$^-$ Mac are reconstituted by BM-derived monocytes. Furthermore, following complete irradiation the majority of CD11b$^+$Tim4$^-$ Mac and CD11b$^+$Tim4$^+$ Mac were donor-derived, whereas CD11b$^-$Tim4$^-$ Mac were only 50% donor-derived.

Consistent with (Guilliams et al., 2020) report, the replenishment of resident macrophages with monocytes follows a consistent pattern across tissues in which the RTM death triggers transient inflammation, then monocyte engraftment occurs in a single wave

during this inflammation, leading to partial and inefficient repopulation. Subsequently both monocyte-derived and the remaining resident macrophages proliferate to complete the repopulation and compete for niches. Thus, the extent of resident macrophage replacement by monocyte-derived macrophages depends on the degree of depletion, the intensity of inflammation (varied by the type of macrophage death), and the accessibility of the niche to monocytes. Indeed, we observed this pattern when comparing the levels of reconstitution in complete irradiation to the protected one. In the latter, the RTM population is intact and antagonizes with the mo-derived donor cells. Thus, we might speculate that in the protected chimeras, the prostatic RTMs that are not eradicated have a certain advantage by primarily repopulating the niche through proliferation and maintaining tissue equilibrium.

Additionally, use of $CCR2^{-/-}$ mouse model, in which monocytes are unable to exit the bone marrow, we remarked that all three prostate macrophage population are intact, indicating minimal contribution of HSC-derived cells, and suggesting an embryonic origin. Fate-mapping models, such as $Cdh5^{CreERT2}$ $Rosa^{Tomato}$ mice as described by (Gentek et al., 2018), could be used to label fetal HSCs, responsible for definite hematopoiesis and then trace their progeny in adulthood.

To further elucidate prostate macrophage reconstitution, I used diphtheria toxin (DT) to ablate tissue-resident macrophages and monocyte-derived cells in adult $CD64^{DTR}$ mice, and subsequently assess the kinetics of macrophage reconstitution in prostates. I observed that all macrophage subsets present prior to DT treatment, were eventually reconstituted from HSCs in normal ratios and numbers, although with different kinetics. The $CD11b^{+}Tim4^{-}$ macrophages showed the fastest reconstitution, reappearing within 3 days post-depletion, while $CD11b^{-}Tim4^{-}$ Mac exhibited the slowest turnover, taking 1.5 month to return to normal levels. Additionally, $Tim4^{+}$ Mac reconstitution occurred with initial upregulation of FolR2 expression (7 days after depletion) by $CD11b^{+}Tim4^{-}$ macrophages. This finding suggests that $CD11b^{-}Tim4^{-}$ Mac cells may not be HSC-derived. Last, I performed competitive WT:$Ccr2^{-/-}$ bone marrow chimera on fully irradiated mice, indicating that once the niche is empty, all three macrophage subsets can be derived from monocytes exiting the BM using Ccr2.

Conclusively our findings suggest that while all 3 macrophage subsets residing in prostate are likely of embryonic origin, they can be completely reconstituted by monocyte derived BM macrophages upon depletions depending on the eradication degree of the cells. To further validate these origins, we could use fate-mapping models, such as the $Cx3cr1^{cre}$ or the $Cx3cr1^{creER}$ described by (Yona et al., 2013) or the granulocyte-monocyte $Ms4a3^{Cre}$-$Rosa^{TdT}$ described by (Liu et al., 2019).

Following these experiments and given that Colony-stimulating factor 1 (CSF-1) is crucial for the survival, proliferation, and differentiation of mononuclear phagocytic cells (Cecchini et al., 1994), we next evaluated the CSF-1 dependency of prostate macrophages. Using the inhibitory anti-CSF1R antibody *in vivo*, we observed that all three macrophage populations were CSF-1 dependent as they were depleted from steady state prostate tissue. We also assessed their dependency on the conserved enhancer of CSF-1, called FIRE. Flow cytometric analysis as well confocal microscopy revealed that the $CD11b^{+}Tim4^{+}$ Mac were independent of the FIRE enhancer, while the other two subsets were absent from the $Csf1r^{\Delta FIRE/\Delta FIRE}$ mice. These findings are in line with other tissue-resident macrophages that

express Tim4 and are found to be independent of the FIRE enhancer (eg. liver Kupffer cells, dermis, spleen and bone) (Hume et al., 2017; Rojo et al., 2019).

Last, we found that CD11b^{+}Tim4^{+} Mac exhibit the highest capacity to bind and phagocytose fluorescent beads *ex vivo* and to internalizing blood-circulating fluorescent dextran *in vivo*. This scavenging is most likely facilitated by the mannose receptor (CD206) expressed by CD11b^{+}Tim4^{+} Mac. Furthermore, confocal microscopy revealed that CD11b^{+}Tim4^{+} Mac are located in close proximity to the blood vessels in the stromal area outside of the glands, where they uptake the fluorescent dextran. Additionally, these cells express also the surface marker Lyve1, indicative of their perivascular localization, as described by (Chakarov et al., 2019) in many tissues. Altogether, these findings concatenated, are in line with the notion that the homeostatic functions of macrophages are linked to specific tissue "niches" that control their population size and imprint their tissue-specific identity (Guilliams et al., 2020).

In summary, this part of my thesis provides unprecedented insights into prostate macrophage heterogeneity, indicating 3 distinct resident subsets, their reconstitution dynamics upon depletions, their CSF-1 and FIRE enhancer dependency, as well as their functional response related to their localization in the prostate niche.

Following the detailed characterization of myeloid cells in healthy prostate tissue, we shifted our attention to myeloid cells infiltrating the induced murine PTEN$^{(i)pe-/-}$ prostate cancer. Tumors secrete various cytokines to recruit monocytes and macrophages, the latter are known as tumor-associated macrophages (TAMs). TAMs exhibit distinct phenotypic and functional properties compared to macrophages in healthy tissues, therefore deciphering their behavior and heterogeneity is pivotal for understanding disease pathogenesis. For a long time, TAMs have been classified into M1, classically activated macrophages that are pro-inflammatory and protective against infections and tumors, and M2, alternatively activated macrophages that are anti-inflammatory and promote tumor growth by supporting angiogenesis and immunosuppression, leading to lower patient survival. Clinical and preclinical studies showed that prostate tumors are dominated by pro-tumoral M2 macrophages expressing CD206, CD68, CD163, which correlate with pro-metastatic properties and worse overall survival (Copeland et al., 2019; Hu et al., 2015). Nonetheless, the M1/M2 nomenclature is overly simplistic to describe the complex heterogeneity of macrophages in cancer.

Equipped with the knowledge we provided on the myeloid heterogeneity in healthy prostate tissue, we proceeded on characterizing the myeloid subsets in the inducible PTEN$^{(i)pe-/-}$ prostate tumors monitoring the changes from early neoplastic stages to advanced adenocarcinoma. Longitudinal multiparametric flow cytometry on PTEN$^{(i)pe-/-}$ prostates compared to age matched littermates, revealed a significant increase of CD11b^{+}Tim4^{-} macrophage subset from the PIN stage, at 3months post tamoxifen, onwards to late adenocarcinoma stage. Additionally, the CD64^{-}CD11b^{+} population, containing monocytes, cDC2 and Lyz cells, was increased in PTEN$^{(i)pe-/-}$ prostate tumors. On the contrary, the CD11b^{+}Tim4^{+} and CD11b^{-}Tim4^{-} macrophage populations, and cDC1 were maintained in stable levels during tumor development.

Comparative gene expression profiling analysis of the scRNA-seq revealed the appearance of a novel cluster in PTEN$^{(i)pe-/-}$ prostate tumors from the PIN stage: the Trem2^{+} Tumor Associated Macrophages (cluster 4). Trem2^{+} TAMs express *Trem2, Gpnmb, Spp1, Vegfa, Cxcl10, Bglap, Apoe, Rsad* genes, indicative of immunosuppression, neoangiogenesis, lipid metabolism and suggesting an overall pro-tumoral identity. Additionally, the monocytes (cluster 6) and Tim4^{-}FolR2^{+} Mac (cluster 1), were increased in the tumor context. As we speculated, flow cytometry confirmed that Trem2^{+} TAM population was appearing in prostate tumor from PIN stage within the CD11b^{+}Tim4^{-}FolR2^{-} subset, validating the scRNA seq findings that Trem2^{+}Tim4^{-}FolR2^{-} Mac (corresponding to cluster 4), Tim4^{-}FolR2^{+} Mac (corresponding to cluster 1) and Trem2^{-}Tim4^{-}FolR2^{-} Mac (a pool of various macrophages clusters) expand during prostate cancer progression.

Functional enrichment of the myeloid cells based on their differential gene expression profile, indicated that most monocyte/macrophage/DC clusters upregulated pathways related to leukocyte and neutrophil migration/chemotaxis to attract more immune cells on the TME and increased their phagocytic capacity, except the Trem2^{+} TAM cluster. The latter, exhibit intense metabolic activity, generating precursor metabolites and ATP, performing cellular and aerobic respiration and oxidative phosphorylation, inducing necroptosis and ferroptosis cell death, without significant phagocytic activity or neutrophil chemotaxis. Confocal microscopy and flow cytometry revealed that while in steady state prostates it is mainly the perivascular Tim4^{+} cells, that express CD206 and internalize blood-circulating dextran, in the tumor context, where there is higher vascularization in the TME and greater diffusion of dextran from the blood vessels, the Tim4^{-}Trem2^{-} cells upregulate CD206 and uptake dextran too. Trem2^{+} TAM however did not scavenge dextran, suggesting a distal localization from the vasculature.

Literature review highlights that TREM2, initially studied for its role in Alzheimer diseases (Ulland and Colonna, 2018), has been recently recognized as a key marker of monocyte-derived macrophages (mo-macs) in tumors with a pro-tumoral function. The group of (Katzenelenbogen et al., 2020) described two Arg1^{+}TREM2^{+} macrophage subsets in fibrosarcoma-bearing mice: the TAMs expressing *C1qa, Spp1, Cx3Cr1, Apoe* genes, and the monocytic regulatory cells (Mreg) expressing *Gpnmb, Il7r, Hilpda, Vegfa, Hmox1, Clec4d* genes. The Trem2^{+} TAM in PTEN$^{(i)pe-/-}$ prostate tumors exhibit *Trem2, Gpnmb, Spp1, Vegfa, Cxcl10, Bglap, Apoe, Rsad* gene expression similar to the Mreg cluster described by (Katzenelenbogen et al., 2020) and colleagues. TREM2 deletion reduced Mreg populations and increased immune reactivity, enhancing NK and cytotoxic T cell activity (Katzenelenbogen et al., 2020). Similarly, the group of (Molgora et al., 2020) showed that TREM2 knockout mice exhibited reduced tumor growth, and anti-TREM2 monoclonal antibody treatment, especially with anti-PD-1, inhibited tumor growth. These studies in various cancer types, reveal TREM2's role in myeloid cell suppression in the tumor microenvironment and its potential as a target for reactivating anti-tumor immunity.

In the same line, the recent study of (Nalio Ramos et al., 2022) described two distinct APOE^{+} populations of TAMs in human and mouse breast cancer tumors: the TREM2^{+} macrophages expressing *Trem2* and *Spp1* genes, and the FOLR2^{+} macrophages expressing *FolR2, Lyve1, Mrc1* genes. TREM2^{+} TAMs were rare in healthy breast tissues but increased with tumor progression, while FOLR2^{+} macrophages were RTMs found in healthy mammary glands

prior to cancer development. The latter corresponds to the prostate RTMs Tim4^{+}FolR2^{+} Mac (cluster 3) that pre-exist in healthy prostates, as indicated by the high scoring with the gene signature of the breast RTMs FOLR2^{+} Mac (Nalio Ramos et al., 2022). Similarly, the gene signature from PCa-specific Trem2^{+} TAM (cluster 4) is matching greatly with the breast cancer-specific Trem2^{+} TAM. Moreover, the authors described that the FOLR2^{+} macrophages localize in perivascular areas of tumor stroma, interact with CD8^{+} T cells, and effectively prime effector CD8^{+} T cells *ex vivo*. Importantly, higher densities of FOLR2^{+} macrophages in breast tumors correlated with improved patient survival. This study underscored the specific roles of distinct TAM subsets and suggested potential subset-targeted therapies in macrophage-based cancer treatments.

Another study by (Sharma et al., 2020) identified two TAM populations in hepatocellular carcinoma (HCC) characterized by FOLR2 (TAM1) and SPP1 (TAM2) markers. However, using RNA velocity analysis, the authors showed that FOLR2^{+} TAM1 macrophages originate from monocytes (mo-mac), whereas SPP1^{+} TAM2 are tissue-resident macrophages (RTMs), contradicting to the results obtained of Nalio Ramos et al. (2022). Additionally, FOLR2^{+} TAM1 displayed more immunosuppressive interactions with regulatory T cells (Tregs) and higher levels of immunomodulatory chemokines (CXCL12, CXCL16) and CD86, suggesting that FOLR2^{+} TAM1 contribute to the immunosuppressive microenvironment in HCC. Taking all these observations into consideration, we could infer that the function and origin of phenotypically similar populations could differ among various cancer types. Notably, this is a great example indicating the perplexity of characterizing the immune cells by cancer type which can be impacted by each particular tumor microenvironment and could potentially explain why treatments effective for some cancer types are proven ineffective for others.

Interestingly very recently the study of (Gao et al., 2023) revealed a significant upregulation of TREM2 expression in prostate adenocarcinoma patients. Elevated TREM2 expression correlated strongly with adverse clinicopathological features, suggesting its role as an independent prognostic biomarker for progression-free interval (PFI) in PCa patients at the stage of adenocarcinoma. Furthermore, TREM2 knockdown substantially impaired the migratory capacity of prostate cancer cell lines via the AKT/PI3K signaling pathway in prostate adenocarcinoma cell lines. Thus, TREM2 may serve as a predictive biomarker and a target for antitumor strategies, particularly in the context of immunotherapy.

Functional assays to investigate the impact of PTEN$^{(i)pe-/-}$ macrophage subsets *ex vivo* on CD8^{+} T cells proliferation was limited by the low cell number of each subset after sorting, despite the pool of at least 10 prostates. Thus, it seems rather difficult to assess the function of the different subsets of macrophages in the PTEN$^{(i)pe-/-}$ model *ex vivo*. Bulk CD11b^{+} macrophages were sorted from PTEN$^{(i)pe-/-}$ (PIN) and cocultured with CD8^{+} T cells and showed no significant effect on CD8^{+} T cell proliferation. Although we cannot exclude that the immunosuppressive functions of individual macrophage population were obscured using bulk analysis.

To specifically assess the role of Trem2 macrophages in PCa, we could cross PTEN$^{(i)pe-/-}$ prostate cancer mice with Trem2$^{-/-}$ deficient mice, which consistently restrict the growth of various tumors, driving a complex remodeling of macrophage infiltrate and promoting enrichment and activation of T and NK cells. However, since the generation of this new mouse

line would require quite some time, an alternative approach would be to use the anti-TREM2 monoclonal antibody to deplete TREM2^{+} macrophages. Previous studies demonstrated that TREM2 targeting with the effector-enhanced anti-TREM2 antibody (eFc mAb) could restrict tumor growth in EMT6 breast cancer and ID8 ovarian cancer models (Binnewies et al., 2021). Moreover, in an anti-PD-1 resistant colon carcinoma model (CT26), combining eFc anti-TREM2 and anti-PD-1 induced tumor rejection in 20–60% of mice and increased activated CD8^{+} T cell infiltration. The residual TAMs displayed a more inflammatory phenotype with higher expression of co-stimulatory molecules. The translational potential of TREM2 targeting with a depleting antibody is under assessment in a clinical trial of the anti-TREM2 mAb PY314, alone or with Pembrolizumab (NCT04691375) tested in a large cohort of patients having various solid cancers. Of note, prostate cancer patients are not included in this study, which was recently completed, and results are pending.

Alternatively, Trem2 targeting could be used to reprogram TREM2^{+} TAM, as demonstrated by (Molgora et al., 2020) using the 178 mAb, which inhibits TREM2 ligand binding *in vitro* , although its *in vivo* mechanisms remain unclear. Notably, strategies aiming to reprogram macrophages to regain an anti-tumor effect might potentially be more beneficial than macrophage elimination *per se*. Given the pro-tumoral gene signature of Trem2^{+} TAMs in PTEN$^{(i)pe-/-}$ prostate tumors, reprogramming them using the 178 mAb could alter tumor progression and immune infiltration. Considering the presence of Trem2^{+} TAMs from the precancerous stage of neoplasia, we could consider that an early intervention may enhance therapeutic efficacy.

Additionally, our scRNAseq dataset revealed upregulated pathways related to leukocyte & neutrophil migration/chemotaxis in macrophages, monocytes, DCs subsets, CD4^{+} T, CD8^{+} T, NK, ILCs and B cells in the PTEN$^{(i)pe-/-}$ samples compared to control. This suggests that the immune cells, whether pre-existing or newly recruited, within the prostate tumor microenvironment are emitting mobilization signals to attract additional leukocytes, particularly neutrophils, to the tumorous area. Preliminary cell-chat communication analysis among the various immune cell clusters, indicated strong interaction on the MIF-CD74-CXCR2 axis.

MIF (Macrophage Migration Inhibitory Factor) is a pro-inflammatory cytokine exhibiting chemokine-like properties. In response to various harmful stimuli, such as hypoxia, cancer and stromal cells release MIF which fosters a tumor-promoting microenvironment. Acting as an autocrine/ paracrine factor, MIF boosts tumor cell proliferation, migration, and angiogenesis, promoting tumor survival and adaptation by facilitating epithelial to mesenchymal transition, inducing the expression of matrix metalloproteinases (MMPs) and recruiting macrophages and neutrophils in the TME (Noe and Mitchell, 2020). Its overexpression is noted in various cancers, including prostate cancer, and is linked to tumor aggressiveness (Mora Barthelmess et al., 2023). Elevated MIF levels in advanced PCa, correlate with disease progression, with MIF levels in patients with metastasis significantly elevated compared to those with localized PCa (Muramaki et al., 2006). Additionally, the study of (Meyer-Siegler et al., 2005) demonstrated that MIF and its receptor (CD74) were localized to prostatic epithelium and increased secreted MIF was also detected in culture medium from prostate cancer cell lines (LNCaP and PC-3). Our scRNAseq dataset showed high *Mif* gene

expression in Trem2$^+$ TAMs in the PTEN$^{(i)pe-/-}$ prostate tumors, which also co-express cathepsin genes (*Ctsd*, *Ctss*) and glycolysis related genes (*Gapdh, Pgk1, Eno1, Pkm, and Ldha*), suggesting their implication on the remodeling of the extracellular matrix and metabolic activity. Trem2$^+$ TAM also express *Cxcl10* gene suggesting a complex functional profile with potential pro-inflammatory function, as described in ovarian carcinoma by (Ardighieri et al., 2021). Nonetheless, this potent anti-tumoral function might be hindered by the governing pro-tumoral functions.

Interestingly, the literature highlights a synergistic relationship between HIF-1α and MIF under hypoxic conditions, where HIF-1α upregulates MIF expression, which in turn prevents HIF-1α degradation and amplifies its transcriptional response. Notably, the prostate tumor microenvironment in PTEN$^{(i)pe-/-}$ prostate tumors is highly hypoxic, as previously reported by our collaborators (Abu El Maaty et al., 2022). Considering our study's additional observation of MIF expression by Trem2$^+$ TAMs, we can hypothesize that Trem2$^+$ TAMs might enhance the hypoxic TME through a positive feedback loop between MIF and HIF-1α, reinforcing their suggested protumoral properties.

Reprogramming Trem2$^+$ TAM in the PTEN$^{(i)pe-/-}$ prostate tumors by targeting the MIF pathway, rather than usinganti-Trem2 antibodies could be an alternative therapeutic approach. Indeed, pre-clinical studies showed that neutralizing MIF with antibodies inhibits PCa growth by preventing MIF-induced activation of ERK1/2 and AKT, promoting apoptosis through activation of caspase-3 and leading to inhibition of PC3 xenografts in a dose-dependent manner (Hussain et al., 2013). This immunotherapeutic approach could disrupt the MIF-Hif-1a loop, creating a more immunogenic microenvironment and potentially enhancing anti-tumor immunity.

Finally, we deciphered the Ly-6G$^+$ neutrophils which were the prevalent immune cell population in the PTEN$^{(i)pe-/-}$ prostate tumors, present from the precancerous stage of PIN, and exponentially increasing upon tumor progression. This rise in neutrophil levels was prostate-specific, as neutrophil counts in the blood and spleen remained unchanged.

It has been suggested that while in physiological conditions, the vast majority of neutrophils complete their maturation in the bone marrow, in cancer, neutrophils may leave the bone marrow prematurely. The infiltrating and circulating neutrophils in some cancers are less mature (Ly6G$^+$CD101$^-$) compared to the fully differentiated mature neutrophils (Ly6G$^+$CD101$^+$) that typically infiltrate organs under steady-state conditions (Evrard et al., 2018; Mackey et al., 2019). For instance, (Sagiv et al., 2015) demonstrated the existence of ring like, banded and segmented nuclei of circulating neutrophils from mammary and lung tumor models. In contrast, we observed that neutrophils in PTEN$^{(i)pe-/-}$ prostate tumors have a mature morphology characterized by the distinct segmented nucleus and CD101 expression . Notably, prostate neutrophils, unlike blood neutrophils, downregulate the expression of CXCR2, a tissue homing signal, that enables the circulating neutrophils to enter the tissues (Evrard et al., 2018).

scRNA sequencing analysis indicated that the bulk neutrophil cluster in the tumorous samples exhibits differential expression of genes related to immunosuppression and tumor progression, such as *S100a8, S100a9, Arg2, Ptgs2, CD276, Mreg, Il1rn* and *Ilb* (Kaplanov et al., 2019; Veglia et al., 2021b). Moreover, we demonstrated that Ly6G$^+$ neutrophils sorted from

tumorous PTEN$^{(i)pe-/-}$ prostates at PIN stage suppressed CD8^{+} T cell proliferation *ex vivo*, indicating their putative immunosuppressive properties.

Reclustering the neutrophils revealed hidden heterogeneity, uncovering 8 distinct clusters that could not be detected by facs due to marker limitations, suggesting a more complex landscape of neutrophil subpopulations within the tumor microenvironment than initially recognized. This highlights the need for new protein markers to characterize neutrophil heterogeneity at the protein level, similar to how we characterized Trem2 in tumor-associated macrophages. This will also enable us to assess their distinct functions *in vivo* or *ex vivo*, which may be currently obscured when analyzed as a bulk population. Proposed markers identified on MDSCs, such as CD84 identified in human and murine breast cancer by (Alshetaiwi et al., 2020) or Trem2 identified in the murine prostate cancer PB-Cre4 PTEN$^{pc-/-}$ model by (Bancaro et al., 2023), were not expressed on neutrophils infiltrating tumorous PTEN$^{(i)pe-/-}$ prostates.

This highlights the differences in observations that may arise from using various models. In my view, this is the hidden beauty of science, reminding us to remain critical in our interpretations, avoid generalizations, and take the time to thoroughly evaluate generated results while considering the different variables involved. In the PTEN$^{(i)pe-/-}$ mouse model, used in our study, the use of CreER^{T2} recombinase and PSA promoter permits to control the *PTEN* gene ablation in adult prostatic luminal epithelial cells, leading to *Pten* ablation in a fully developed prostate and well-differentiated prostatic luminal epithelial cells, resulting in PIN observed after 3months post tamoxifen and adenocarcinoma after 9months. Conversely, in the PTEN$^{pc-/--}$ model used by (Bancaro et al., 2023), the *Pten* ablation is driven by Pb-4 promoter with a constitutively active Cre recombinase and occurs in the immature prostate bud of newborns, leading to faster progression, with PIN at 4 weeks and adenocarcinoma at 2 months. Indeed, previous studies have shown that PIN development is accelerated when *Pten* is ablated before puberty. Consequently, the PTEN$^{(i)pe-/-}$ model, with slower progression mirrors human PCa more closely, and may shape a different immune microenvironment with infiltrating cell exhibiting different properties and phenotypes.

Despite the lack of additional markers to elucidate neutrophil subset functions *ex vivo*, we explored their properties based on their gene expression provided by our scRNAseq dataset. Surprisingly, all neutrophil clusters were present in WT prostates but scarcely dispersed. N3, the dominant cluster in the WT prostates corresponds to typical mature neutrophils identified in steady state tissues and early tumor stages, as indicated by the gene signature of mature neutrophils curated by (Xie et al., 2020) and PMN1 or T1 clusters described by (Veglia et al., 2021a) and (Ng et al., 2024) respectively.

Interestingly, RNA velocity analysis predicted that N3 gives rise to N2 at PIN stage and N3 will also give rise to N5 at adenocarcinoma stage. Statistical analysis indicated that N0 & N2 prevail at PIN stage while N5 & N7dominated at n the adenocarcinoma stage. Cluster N0 bears a strong interferon-stimulated-gene signature (ISG), characterized by *Cxcl10, Ifit1, Ifit3b, Rsad2* gene expression, and resemble the Sell^{hi}Cxcl10^{hi} ISG-bearing neutrophils from (Gungabeesoon et al., 2023) and the Ifit1^{+}Isg15^{+} from (Wu et al., 2024). This suggests that N0 could exert anti-tumor properties via its strong pro-inflammatory profile. At the same time though, the N0 exhibits high levels of PD-L1 (*Cd274* gene), involved in immunosuppression.

This underlines the plasticity of the N0 cells, bearing a dual role depending on the environmental cues. Indeed, gene ontology analysis indicated that N0 cells upregulate pathways related to response to virus, cytokine mediating signaling and autophagy, as well as TNF and TLR signaling, necroptosis, ferroptosis, antigen presentation and Hif-1 signaling. Therefore, suggesting that on the one hand this cluster helps on the antitumoral immunity via antigen presentation and autophagy thanks to its ISG signature, but at the same time presents pro-tumoral properties by inducing necroptosis (possibly via TNfa/TLR signaling that are upregulated), ferroptosis and hypoxia (possibly via Hif-1 signaling). Indeed, the literature indicates that necroptosis likely accounts for tumor necrosis and is often associated with tumor aggressiveness and metastasis for solid cancers (Yan et al., 2022). Unlike apoptotic cell death, for which dead cells are efficiently removed without breakage of the plasma membrane, necroptotic cell death leads to "leakage" and subsequent release of intracellular components. We could therefore speculate that the N0 cells, as the dominant neutrophil group at the PIN stage, initially receive inflammatory signals from the tumors, leading to ISG signature, but later adopt a protumoral profile once present in the tumor. Thus, we could consider them as highly plastic as they can have dual and contradictory roles in cancer initiation, progression, and metastasis depending on the environmental cues, as previously stated by (Coffelt et al., 2016).

Interestingly, (Xie et al., 2020) showed that ISG-neutrophils are present in blood and spleen of human & mice and expand during bacterial infections. So, although our analysis showed no changes in the numbers of circulating neutrophils, they may exhibit phenotypic alterations such as ISG expression.

Cluster N2, the second most dominant cluster at the PIN stage, upregulates pathways related to transendothelial migration of leukocyte, VEGF & Hif-1 signaling, chemokine signaling, leukocyte cell-cell adhesion and chemotaxis, regulation of actin cytoskeleton. We could therefore speculate that N2 have a pro-metastatic role, promoting neoangiogenesis, ECM alterations and leukocyte migration to the TME. The prevalent N0 and N2 observed at PIN stage seem to have pro-tumoral functions, which could also explain our previously mentioned findings on suppressing the $CD8^+$ T cell proliferation *ex vivo* when sorted as a bulk.

Clusters N5 and N7 were prevalent at the adenocarcinoma stage. N5 gene signature matches greatly with the PMN3 cluster described by (Veglia et al., 2021a) with potent suppressive properties. Additionally, N5 expresses the gene *Tnfrsf23* encoding for the protein dcTRAIL-R1 expressed by the protumoral and long-lived T3 cluster described by (Ng et al., 2024). Gene enrichment analysis indicated that N5 & N7, upregulate pathways related to efferocytosis, necroptosis, Hif-1 signaling, neutrophil/leukocyte migration and cell-cell adhesion. This suggests that N5 & N7 recruit more immune cells in the TME and promote angiogenesis and invasion within the hypoxic TME of $PTEN^{(i)pe-/-}$ tumors, described by our collaborators (Abu El Maaty et al., 2022). Moreover, many neutrophil clusters express MIF receptors genes, *Cd74* and *Cd44*, suggesting possible interaction between MIF from $Trem2^+$ TAM, and CD74/CD44 on neutrophils.

In summary, our comprehensive analysis of neutrophils in $PTEN^{(i)pe-/-}$ prostate tumors revealed, for the first time, significant heterogeneity, identifying eight distinct clusters with varying composition from neoplastic stage to adenocarcinoma and overall

immunosuppressive and pro-tumoral functions evident from the PIN stage, validated by the impaired proliferation of $CD8^+$ T cells *ex vivo*. Our neutrophil map captured known neutrophil subpopulation features and revealed potentially uncharacterized subsets, enhancing our understanding of neutrophil roles in prostate cancer.

Therefore, our study raises new questions requiring further investigation: What are the mechanisms underlying $CD8^+$ T cells immunosuppression, and which specific neutrophil cluster(s) are responsible for this effect? Considering that neutrophil presence in the blood of prostate cancer patients correlates with poor prognosis and given that the observed gene signatures suggest many neutrophil clusters may drive neoangiogenesis, hypoxia and ECM remodeling, could neutrophils in PCa facilitate tumor cell extravasation and metastasis, as observed in other cancer types? If so, what are the underlying mechanisms?

I thus attempted to verify the pro-tumoral role of neutrophils. Studying neutrophil biology in *ex vivo* cultures is challenging due to their short lifespan, making *in vivo* studies preferable. An additional obstacle in testing the role of each described subset remains the lack of markers to discriminate these subsets at the protein level. Therefore, we decided to deplete them *in vivo* as a bulk and assess the impact on the tumor progression and the potential for generating a more immunogenic tumor microenvironment. Researchers commonly use anti-Gr1 and anti-Ly6G antibodies to deplete neutrophils, but these methods have limitations. Anti-Gr1 (clone RB6-8C5, rat IgG2b) efficiently depletes neutrophil, but is not neutrophil-specific, as it also depletes the inflammatory monocytes and other Ly6C-expressing cells, such as T cells. On the other hand, anti-Ly6G (clone 1A8, rat IgG2a), is neutrophil-specific, but not effective long-term, as neutrophils quickly return in tumor-bearing mice (Moses et al., 2016). This posed a significant challenge that I faced during my PhD. Given that the tumor in the inducible $PTEN^{(i)pe-/-}$ model progresses very slowly, taking months to be developed, I had to apply a long-term treatment of at least one month to observe an effect on the tumor growth. Moreover, based on my longitudinal analysis, showing that neutrophil infiltration is observed already from 2months post tamoxifen, I initiated the treatment at this timepoint, with a read out at 3mo post Tamoxifen.

Aware of the challenges reported in the literature for *in vivo* neutrophil depletion, I followed the combination treatment described in (Boivin et al., 2020). The authors proposed a more durable protocol via co-administration of rat anti-mouse Ly6G and anti-rat mAbs, which enhance the killing efficacy of anti-Ly6G to deplete neutrophils for at least 18 days in C57BL/6 models. Following this approach, I treated 2months bearing tumors $PTEN^{(i)pe-/-}$ mice with rat-anti mouse a-Ly6G (1A8) daily (25µg the first week, and 50µg the rest of the days), and every 2 days with anti-rat kappa light chain (MAR 18.5) for 20 days (**Sup Figure 8A**). While I observed a successful complete neutrophil depletion from blood and prostate during the 2-day treatment, this depletion was not maintained for 20 days treatment in our tumor bearing $PTEN^{(i)pe-/-}$ mice (**Sup Figure 8B,C**). Therefore, I hypothesized that excessive neutrophilia and reduced efficacy might result from increased clearance of injected rat Ab due to anti-rat response generated in mice during the treatment.

To overcome this interspecies reactivity, I decided to use the murinized anti-Ly6G (1A8) specifically designed to tackle this problematic, as described by (Olofsen et al., 2022). Following their scheme and dose (100µg/mouse), neutrophil depletion was once again not

maintained during the treatment period of 27 days. Similar to the previous approach, neutrophils were depleted for 7 days but returned afterwards (**Sup Figure 8D-F**). Consequently, we concluded that long-term neutrophil depletion in the induced PTEN$^{(i)pe-/-}$ prostate cancer mouse model, is challenging, preventing us from evaluate their immunosuppressive role *in vivo*. As an alternative approach, I applied a 2-step treatment by first depleting the neutrophils with a 7-days treatment with murinized anti-Ly6G 1A8 (100µg), followed by daily injection of CXCR2 inhibitor SB225002 (10mg/kg) for 2 weeks, preventing them to enter the tissue, as proposed by (Nywening et al., 2018) for pancreatic cancer and also currently tested in a clinical trial for mCRPC patients (NCT03177187). However, this approach also failed, and neutrophils were found in the prostates after treatment, (**Sup Figure 8G-I**). Testing different doses of the CXCR2i might eventually be effective, but time constraints and limited number of mice, prevented further pursuit. Thus, considering these *in vivo* depletion attempts, we recognize the critical role of neutrophils in the body's system that comes with a great difficulty to manipulate them *in vivo* for a long period.

Lastly, based on our observations of immunosuppressive myeloid cells and exhausted CD8^{+} T cells in PTEN$^{(i)pe-/-}$ tumors, and recognizing the short-term efficacy of neutrophil depletion alone, we opted for a combination immunotherapy approach. We depleted neutrophils using murinized anti-Ly6G and total macrophages using anti-CSF1R, simultaneously administering anti-PD1 immune checkpoint inhibitor to rewire the exhausted T cells. Given the slow tumor development in this mouse model, we did not expect immediate impact on tumor growth. Therefore, we assessed potential changes in IFNγ and TNFα production by CD8^{+} T cells but observed no alterations in treated animals (**Sup Figure 8J-L**).

At this point, it is crucial to emphasize the importance of validating neutrophil depletion using appropriate markers. It is imperative to avoid using the use of Ly-6G marker in flow cytometry, as antigen masking can result in false-negative staining in blood (**Sup Figure 8M**). Proper verification method involves using the Ly-6C marker, where neutrophils will appear as Ly6C^{int}, or utilizing the SSC parameter to distinguish neutrophils based on their high granularity size (SSC^{high}). Surprisingly, many studies still claim successful prolonged *in vivo* neutrophil depletion using anti-Ly6G for more than a week. However, in most cases, the authors either do not verify the depletion or assess it using the Ly-6G marker to stain circulating blood from treated animals, leading to false-negative results due to antibody masking. This highlights the need to remain critical on conclusions regarding the pro-tumoral or anti-tumoral functions of neutrophils in studies where neutrophil depletion was applied. It is possible that the observed tumor progression or remission is due to factors other than the intended neutrophil depletion, as reviewed also by (Boivin et al., 2020).

Given that long-term *in vivo* depletion methods have proven ineffective in PTEN$^{(i)pe-/-}$ model, alternative approaches to assess neutrophil function *in vivo* are needed. One option is to cross the PTEN$^{(i)pe-/-}$ prostate cancer model, with a neutrophil tracking model, such as the Catchup mice (Hasenberg et al., 2015). This model includes a fluorescent reporter, allowing for the monitoring of mature neutrophil function using *in vivo* imaging and a Cre recombinase allowing to deplete neutrophil-derived molecules specifically at later stages of neutrophil differentiation. This model could yield valuable insights into the roles of neutrophils and their molecular products in prostate tumor initiation, and growth. Nevertheless, this model is based

on Ly-6G-driven Cre recombinase and having 2 Cre driver genes with different reporters could generate additional complications.

Alternatively, we could consider crossing the PTEN$^{(i)pe-/-}$ model with the Genista mice, which completely lack mature neutrophils (Ordoñez-Rueda et al., 2012), due to a point mutation in the Gfi-1. These mice are not based on cre/loxp system, and they exhibit neutropenia without affecting mouse growth or causing mortality. This approach would allow us to assess whether the complete absence of mature neutrophils leads to slower tumor progression and a more immunogenic microenvironment. However, eliminating all neutrophils does not resolve the need to evaluate specific functions of each subset, leading to the concept that we may consider that it could be more advantageous to reprogram neutrophils, given their flexibility and ability to respond to tumor cues, and potentially altering their role from supporting tumor growth to suppressing it.

For instance, Pten ablation stimulates proliferation of prostatic epithelial cells within 1 month to form PINs, followed by a progressive growth arrest with characteristics of cell senescence (latency phase) governed by a hypoxic TME in the PTEN$^{(i)pe-/-}$ model (Abu El Maaty et al., 2022; Parisotto et al., 2018b). Oncogene-induced senescence (OIS) promotes the recruitment of neutrophils, which may either scavenge pre-malignant cells or sustain inflammation promoting tissue aging and cancer. This suggests that neutrophils may either suppress or promote cancer, by respectively antagonizing or promoting cellular senescence, confirming their controversial function in cancer. However, this still may be context-dependent and reflect the tissue specificity of neutrophil dynamics and heterogeneity (Quail et al., 2022). Other studies using the Pb4-CRE driven PTEN$^{-/-}$ mice showed that the progression of PTEN loss–induced PIN is antagonized by cell senescence, driven by infiltrated IL-1RA secreting GR1-positive myeloid cells, allowing proliferation of PTEN-deficient prostatic epithelial cells and, thereby, PIN formation (Di Mitri et al., 2014). However, (Parisotto et al., 2018b) demonstrated that the GR1-positive cells and IL-1RA mRNA are not present in the prostate at 1 month after gene ablation in PTEN$^{(i)pe-/-}$ mice and, thus, cannot contribute to the high proliferation rate and the absence of senescence markers at this stage. They concluded that the first temporal consequence of *Pten* ablation in mouse prostatic epithelial cells is their rate of proliferation, allowing PIN formation in most prostate ducts within 1 month. Signs of senescence are observed only later, after several weeks of active proliferation (at 2months post Tamoxifen administration). Notably, our longitudinal analysis of the immune infiltrates in the PTEN$^{(i)pe-/-}$ mice confirms that increases in neutrophils and macrophages are not observed at 1 month post tamoxifen but starts from 2 months onwards.

Additionally, the concept of neutrophil adaptability and reprogramming in cancer has been recently proposed by (Ng et al., 2024). They examined the neutrophil ontogeny in murine orthotopic pancreatic cancer and uncovered their flexibility in adapting to environmental cues. They showed that both immature and mature neutrophils migrate into tumors, where they undergo differentiation, forming transitional populations. These transitional populations are reprogrammed to eventually adopt a terminal neutrophil state. Reprogrammed neutrophils exhibit strong expression of VEGFα and localize to a specific hypoxic-glycolytic niche near the tumor core. This localization positions them strategically to promote angiogenesis in hypoxic and nutrient-poor regions of the tumor, thereby supporting tumor

growth. Similar to this study, we could consider that neutrophils in PTEN$^{(i)pe-/-}$ prostate model will be equally plastic and adapted to the TME cues.

A more relevant prostate cancer model progressing to metastasis would be require to address the pro-metastatic role of the neutrophils. The PTEN/p53$^{(i)pe-/-}$ mouse model, also developed by the team of D. Metzger (Parisotto et al., 2018b), presents depletion of both *PTEN* and *TP53* genes, allows faster tumor progression from PIN to adenocarcinoma stage, within 5months post Tamoxifen, and unlike PTEN$^{(i)pe-/-}$ mice, it develops metastasis located in bones and liver (D. Metzger, personal communication). Comparative analysis of the immune infiltration in both models, demonstrated that they are myeloid dominant with the neutrophils prevailing. These data, presented in appendix as a collaborative article is under review, and demonstrate that p53-loss induced prostatic epithelial cell plasticity and invasion is driven by a crosstalk with the tumor microenvironment. It would be thus, interesting to further evaluate the suggested neoangiogenic and invasive role of neutrophils in this model. While there was no difference in the numbers of the infiltrating neutrophils subsets between the 2 models, it is likely that comparing the gene signatures of the neutrophil clusters may reveal stronger pro-metastatic properties of the PTEN/p53$^{(i)pe-/-}$ neutrophils.

Under this perspective and considering the dual role of the cluster N0 bearing both a pro-inflammatory ISG signature and contributing to hypoxia and necroptosis, we could consider reprogramming the neutrophils to boost their anti-tumoral properties. Inspired by the study of (Gungabeesoon et al., 2023), where a-CD40 treatment in orthotopic lung adenocarcinoma reduced tumor growth with an increase of ISG-neutrophils, we could consider applying anti-CD40 treatment to boost the pro-inflammatory function of ISG-bearing neutrophils (N0) in the PTEN$^{(i)pe-/-}$ prostate tumors and prevent tumor growth. This treatment could also restore the IFN production that is undermined by the absence of PTEN signaling in the tumor cells, as reported in various tumors by (Cetintas and Batada, 2020; Vidotto et al., 2020). The antitumoral properties of ISG-neutrophils could be further enhanced if the treatment is applied in early stages, highlighting the importance of early PCa diagnosis and treatment from the PIN stage by appropriate immunotherapy.

My PhD study provides new insights and stimulates a re-evaluation of the role and diversity of neutrophils and macrophages residing in healthy murine prostate and infiltrating PTEN$^{(i)pe-/-}$ cancerous prostate. It reveals important information regarding their ontogeny, diversity, plasticity, and impact on the TME. The longitudinal and thorough description of the myeloid compartment in PCa in the inducible PTEN$^{(i)pe-/-}$ prostate model from neoplasia to adenocarcinoma, paves the way for new therapeutic options and raises new challenges, emphasizing the need for new markers to explore neutrophil functions *in* and *ex vivo*. Considering neutrophils as potential therapeutic targets in PCa is now essential as they are the prevailing immune cell population in the TME. Numerous studies have recognized the microenvironment as a prognostic factor in prostate cancer, underscoring its importance.

Moreover, given the strong link between increased age and prostate cancer formation, coupled with the growing elderly population, it appears unlikely that cancer will be eradicated in the foreseeable future. Thus, the focus of cancer prevention research extends beyond simply preventing cancer occurrences to also minimize or avert the adverse consequences associated with cancer. History has shown that earlier diagnosis and treatment improves

outcome and overall survival of cancer patients. Certainly, a greater number of cancer-related deaths could be prevented through early detection and intervention. Our study highlights that the immune compartment is mobilized very early in tumor formation from the precancerous stage of prostatic intraepithelial neoplasia. Notably, the TME appears immunosuppressive and rather pro-tumoral from this stage. Therefore, an early combinatory myeloid targeting treatment is likely to be more effective in rewiring the immune compartment to target tumor cells, potentially delaying or eradicating cancer.

Given the challenges in maintaining long-term neutrophil depletion in this model, similar issues might arise when attempting to deplete Trem2$^+$ TAM longtermly. Instead of aiming for complete depletion of cell populations, we should focus on leveraging the plasticity of immune cells to potentiate their anti-tumoral properties. This strategy would also reduce adverse effects by avoiding neutropenia due to complete neutrophils depletion with anti-Ly6G and the complete lack of macrophages caused by anti-CSFR1. Notably, reprogramming the myeloid cells appears more feasible and closer to implementation and application in human PCa patients. Given the heterogeneity of the prostate immune TME and the numerous suggested immunosuppressive mechanisms, immunotherapy targeting both myeloid and lymphoid compartments holds promise. We propose a combinatory approach of reprogramming both protumoral neutrophils (e.g., using anti-CD40) and Trem2$^+$ TAMs (via anti-Trem2 or modulation of the MIF axis using anti-MIF) and rewiring exhausted CD8$^+$ T cells (with anti-PD1) from the PIN stage could induce the necessary switch in the immune microenvironment. This strategy could convert “cold” prostate cancer tumors into “hot” tumors, characterized by infiltration of cytotoxic cells.

Combining the proposed myeloid-targeting immunotherapeutic approach with standard treatments, such as androgen deprivation therapy or chemotherapy, which are proven beneficial for stalling tumor growth, could enhance the overall efficacy of prostate cancer treatment.

General Conclusions

The results of this PhD study shed light on the immune composition of mouse prostate in physiological condition and elucidate the changes on the immune infiltrates upon cancer initiation and progression (***Figure 24***). It provides a high-resolution immune cell atlas indicating the myeloid and lymphoid diversity within the prostate gland. Given the gap in the knowledge on macrophage diversity of prostate tissue, we described for the first time three distinct resident macrophage subsets found in physiological prostate (Tim4^{+} Mf, Tim4^{-} Mf, CD11b^{-} Mf). We further elucidated their reconstitution dynamics upon depletions, their dependency on CSF-1, as well as their functional response related to their localization in the prostate niche. Our findings suggest that all three macrophage subsets are CSF-1 dependent and while they are likely of embryonic origin, they can be completely reconstituted by monocyte derived BM macrophages upon depletions depending on the eradication degree of the resident cells. Additionally, we observed that the Tim4^{+} Mf colocalize with CD31^{+} endothelial cells, corresponding to the perivascular macrophages that have been described in other tissues. These cells co-express FolR2 and Lyve-1 markers and exhibit high scavenging capacity of blood circulating ligands (dextran).

Comprehensive longitudinal analysis of the myeloid-dominant prostate tumors of the inducible PTEN$^{(i)pe-/-}$ prostate model that highly mimics human prostate cancer features, demonstrated that the immune compartment undergoes significant changes as early as the neoplastic stage, marked by a dominant immunosuppressive signature. Throughout the progression of prostate cancer, neutrophils massively infiltrate the prostate epithelium and remain the predominant immune cell population. We underscored a great neutrophil diversity, identifying eight distinct clusters. Our neutrophil map captured known neutrophil subpopulation features and revealed potentially uncharacterized subsets, enhancing our understanding of neutrophil roles in prostate cancer. We observed reprogramming and functional diversification of neutrophils as the tumor evolves, with ISG- and dcTRAIL-R1-states being predominant at the PIN and adenocarcinoma stages respectively. Besides the pro-inflammatory gene signature of the N0 cluster (ISG-tumor associated neutrophils), we remarked a dual role of these cells bearing also immunosuppressive traits. This was validated by the impaired proliferation of CD8^{+} T cells *ex vivo* in presence of bulk neutrophils from PIN tumors. Additionally, our study revealed that in PTEN$^{(i)pe-/-}$ prostates, the primary change in the mononuclear phagocyte compartment already from the neoplastic stage is the recruitment of Trem2^{+} TAMs. These cells bear an intense metabolic and immunosuppressive signature and express high levels of macrophage migration inhibitory factor (MIF), as indicated by scRNAseq analysis. Furthermore, our findings indicate that the murine PTEN$^{(i)pe-/-}$ prostate tumor effectively models the "cold" TME of human prostate cancer, characterized by low CD8^{+} T cell infiltration and exhaustion (PD1^{+}Tim3^{+}) already form the neoplastic stage.

Conclusively, our study encourages a re-evaluation of the role and diversity of neutrophils and macrophages by emphasizing the need for new markers that will enable the

investigation of neutrophil functions *in vivo* and *ex vivo*. Given that neutrophils and macrophages are the predominant immune cell population within the TME, it is now crucial to consider them as potential therapeutic targets in prostate cancer.

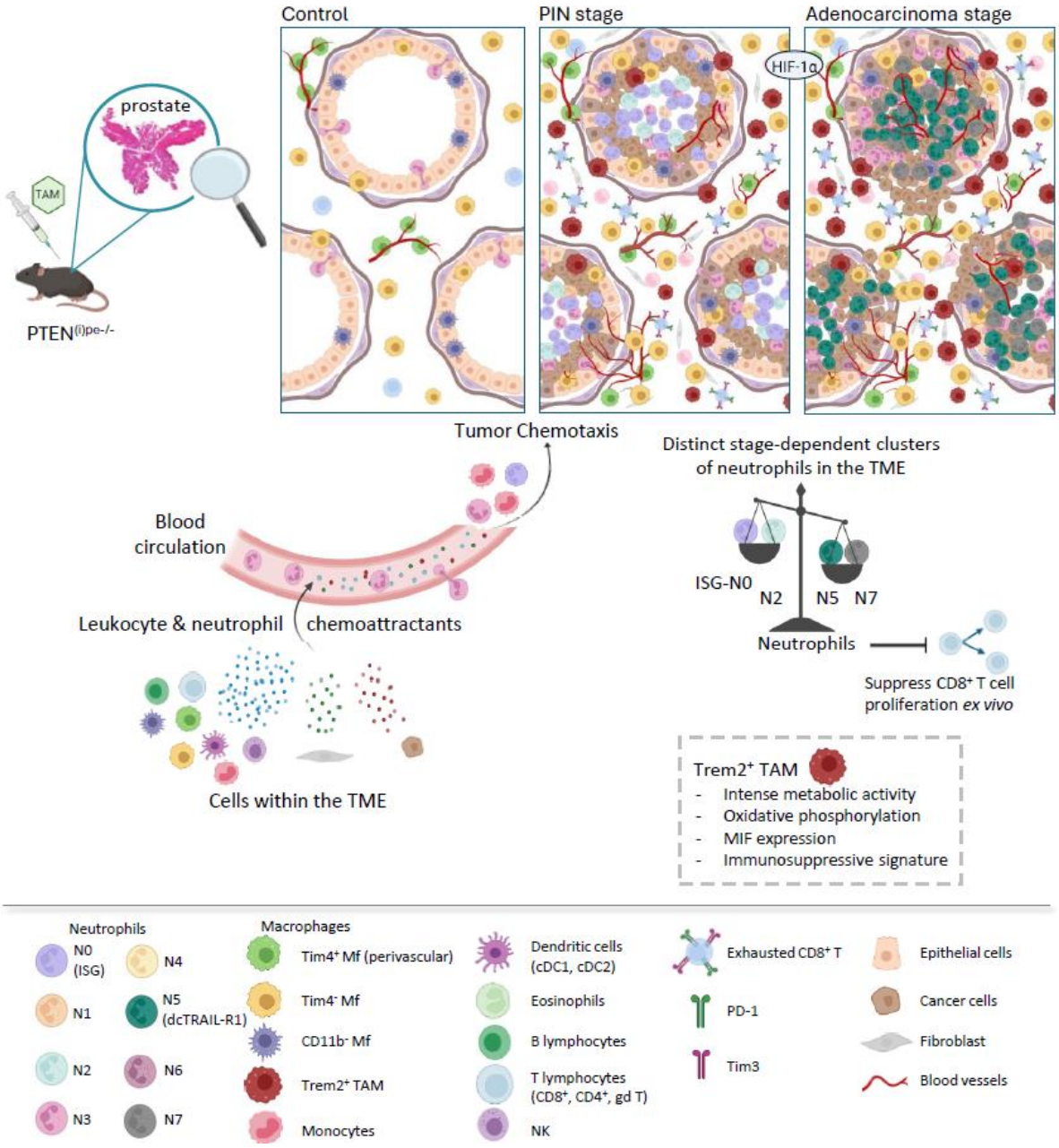

Figure 24. Graphical abstract recapitulating the findings of my PhD study.

Appendix: Contributing author in submitted article

In the following section I enclose the manuscript entitled “p53-loss induced prostatic epithelial cell plasticity and invasion is driven by a crosstalk with the tumor microenvironment”. As a contributing author in this article, I have participated in the methodology, investigation, visualization and formal analysis of the immunophenotyping experiments presented in *Figures S3 & S6*. This manuscript has been submitted in ***Cell Death and Disease*** journal (*CDDIS-24-2925-T*) on 17th of June 2024 and it is under peer reviewing.

p53-loss induced prostatic epithelial cell plasticity and invasion is driven by a crosstalk with the tumor microenvironment

Darya Yanushko[1,2,3,4†], Beatriz German Falcon[1,2,3,4,6†], Rana El Bizri[1,2,3,4,7†], **Despoina Pervizou**[5], Céline Keime[1,2,3,4], Tao Ye[1,2,3,4], Christelle Thibault-Carpentier[1,2,3,4], Sandrine Henri[5], Gilles Laverny[1,2,3,4*] and Daniel Metzger[1,2,3,4*]

[1] Institut de Génétique et de Biologie Moléculaire et Cellulaire, Illkirch, France.

[2] Centre National de la Recherche Scientifique (CNRS), UMR7104, Illkirch, France.

[3] Institut National de la Santé et de la Recherche Médicale (INSERM), U1258, Illkirch, France.

[4] Université de Strasbourg, Strasbourg, France.

[5] Centre d'Immunologie de Marseille-Luminy, Aix Marseille Université, INSERM, CNRS, 13288 Marseille, France

Current address:

[6] Center for Prostate Disease Research, Murtha Cancer Center Research Program, Departement of Surgery, Walter Reed Army Medical Center and Uniformed University of the Health Sciences, The Henry M. Jackson Foundation for the Advancement of Military Medicine, Bethesda, USA

[7] Bellvitge Institute for Biomedical Research (IDIBELL), 08908, Barcelona, Spain.

* Gilles Laverny laverny@igbmc.fr, Daniel Metzger metzger@igbmc.fr.

† Contributed equally to this study

Abstract

Prostate cancer is a heterogeneous disease with a slow progression and a highly variable clinical outcome. The tumor suppressor genes *PTEN* and *TP53* are frequently mutated in prostate cancer and predictive of an early metastatic dissemination and unfavorable patient outcome. The progression of solid tumors to metastasis is often associated with increased cell plasticity, but the complex events underlying *TP53*-loss induced disease aggressiveness remain incompletely understood. Using genetically engineered mice, we show that *Trp53* deficiency in *Pten*-null prostatic epithelial cells (PECs) does not impact the early cell proliferation and neoplasia formation, nor growth arrest and senescence entry at later time. However, *Trp53*-deficiency enhances invasive adenocarcinoma development and promotes metastatic cell dissemination. Importantly, our single-cell transcriptomic and chromatin accessibility analyses combined with histological examinations uncovered an epithelial cell population characterized by an induction of Jak/Stat3 signaling and displaying mesenchymal features. Moreover, our *in vivo* and organoid-based co-culture experiments provide evidence that PEC plasticity occurs through a bi-directional communication with cancer-associated fibroblasts (CAFs). Thus, our study demonstrates that p53 loss induces a protumorigenic crosstalk between PECs and CAFs and identifies new vulnerabilities that might be targeted to limit cancer progression.

Keywords: prostate cancer, p53, tumor microenvironment, EMT, CAF.

Introduction

Prostate cancer is the most commonly diagnosed non-cutaneous male malignancy and the second cause of cancer-related death in western countries (1). It is a heterogeneous disease with a slow progression and a highly variable clinical outcome. The tumor suppressors *PTEN* and *TP53* are among the most frequently altered genes in prostate cancer (2). *PTEN* mutations have been identified in 10–15% of all prostate tumors and in up to 60% of advanced prostate cancers (3,4). Moreover, *TP53* mutations are present in up to 75% of advanced tumors and are highly associated with metastatic disease (2,3). However, there is emerging evidence that *TP53* mutations are already present at a high frequency in primary prostatic tumors and are predictive of an early metastatic dissemination and an unfavorable patient outcome (5,6). Though, the molecular and cellular mechanisms underlying the progression of indolent PTEN- and p53-deficient tumors to aggressive and metastatic cancer remain elusive.

Over the recent years, single-cell analyses uncovered a large cellular heterogeneity of localized prostatic tumors (7–9). While tumorigenesis initiates in prostatic epithelial cells, various cell types, including cancer associated fibroblasts (CAF), immune and endothelial cells produce extra-cellular matrix and secrete signaling molecules that might exert protumorigenic effects, and thus contribute to tumor progression (10,11). However, the complex communication network during tumor progression remains poorly characterized.

We have previously shown that Pten$^{(i)pe-/-}$ mice, in which *Pten* is inactivated in prostatic luminal cells at adulthood, develop prostatic intraepithelial neoplasia (PINs) due to enhanced proliferation of prostatic epithelial cells (PECs), featuring stabilization of p53, followed by a progressive growth arrest with characteristics of cell senescence. Some PINs progress to adenocarcinoma, but no metastases were observed (12,13). Moreover, Chen et al. reported that Pb-Cre4-mediated inactivation of *Pten* and *Trp53* in prostatic epithelial cells induces more aggressive tumors with no signs of senescence (14).

To unravel the mechanisms underlying increased aggressiveness induced by *Trp53* loss, we performed detailed longitudinal studies of Pten/Trp53$^{(i)pe-/-}$ mice, in which *Pten* and *Trp53* are selectively inactivated in prostatic luminal cells at adulthood. Our results show that p53 deficiency does not impact the early proliferation of *Pten*-null epithelial cells and PIN formation, nor growth arrest and senescence entry at later time. However, it induces epithelial cell plasticity, enhances adenocarcinoma formation and promotes their metastatic potential. Importantly, we unravel that epithelial cell plasticity is induced in a non-cell-autonomous manner by a feedforward loop stimulating IL6 production by CAFs, that in turn enhances Jak/Stat3 signaling in epithelial cells. Importantly, aggressive and metastatic prostate tumors in patients were characterized by a high score of the transcriptomic signature identified in PECs of Pten/Trp53$^{(i)pe-/-}$ mice. Thus, p53 loss promotes prostate cancer progression by inducing a pro-tumorigenic crosstalk between *PTEN*-deficient prostatic epithelial cells and cancer-associated fibroblasts.

Results

Prostatic epithelial cells of Pten/Trp53$^{(i)pe-/-}$ mice become senescent after a proliferation phase

To determine the impact of p53 deficiency in Pten-null prostatic epithelial cells (PECs), we compared prostate tumorigenesis of Pten$^{(i)pe-/-}$ and Pten/Trp53$^{(i)pe-/-}$ mice (13). As expected, most PECs were phosphorylated AKT (S473) positive in PINs 3 months after gene inactivation (AGI). Moreover, PECs of both mouse lines expressed TROP2, a marker of Luminal-C cells, that were previously shown to be the main epithelial cell population of *Pten*-deficient prostatic tumors (15) (Supp. Fig. 1a). In contrast, p53 protein was detected in the nuclei of PECs of Pten$^{(i)pe-/-}$ mice, but not in those of Pten/Trp53$^{(i)pe-/-}$ mice (Supp. Fig. 1b), demonstrating efficient inactivation of *Pten* and *Trp53* in prostatic luminal cells of Pten/Trp53$^{(i)pe-/-}$ mice.

The average prostate weight of control mice, as well as of Pten$^{(i)pe-/-}$ and Pten/Trp53$^{(i)pe-/-}$ mice 1 month AGI, was around 100 mg, and increased to 180 mg in both mutant mice 3 months AGI, but not in controls (Fig. 1a). Hematoxylin and eosin (HE) staining of prostatic sections showed the presence of PINs and a stromal reaction in dorso-lateral prostates (DLPs) of both mutant mice 3 months AGI (Fig. 1b). The proliferation rate was 2.5-fold higher in PINs of the DLP of mutant mice 1 month AGI than in PEC of aged-matched control mice, and further increased 3 months AGI. However, it was below 1% in control and mutant mice 5 months AGI (Fig. 1c & 1d), and PINs of both Pten$^{(i)pe-/-}$ and Pten/Trp53$^{(i)pe-/-}$ mice were positive for senescence-associated β-galactosidase (SA-βGal), a faithful marker of cell senescence (16) (Fig. 1e, Supp. Fig. 1c). Moreover, while most PECs of Pten$^{(i)pe-/-}$ mice expressed the cyclin-dependent kinase inhibitor p21, no p21-positive cells were detected in PINs of Pten/Trp53$^{(i)pe-/-}$ mice 5 months AGI (Fig. 1f). In contrast, the proportion of p16-positive cells was 5-fold higher in DLP of Pten/Trp53$^{(i)pe-/-}$ mice than of Pten$^{(i)pe-/-}$ mice (Fig. 1f & g, Supp. Fig. 1c). In addition, SA-ßgal staining and abundant p16-positive cells were still present in glands of DLP of Pten/Trp53$^{(i)pe-/-}$ mice 7 months AGI (Fig. 1h & 1i). Together, these results show that p53 loss does not affect early PIN formation induced by *Pten* inactivation at adulthood, and that both *Pten*- and *Pten/Trp53*-deficient PINs in DLP become senescent.

As PECs in the anterior prostate (AP) of control, Pten$^{(i)pe-/-}$ and Pten/Trp53$^{(i)pe-/-}$ mice were SA-ßGal-positive 5 moths AGI (Supp. Fig. 1d), possibly due to the expression of the ß-galactosidase isoform *Glb1l3* (17), this assay could not be used to assess cell senescence in this lobe. However, some p16-positive cells were detected in TROP2-positive luminal cells in the AP (Supp. Fig. 1e), indicative of senescent cells. Moreover, as PIN formation, severity and tumor progression were highly variable in the AP amongst mice and glands of a given mouse (Supp. Fig. 1e and f), these results show that p53 loss does not prevent PECs senescence, and underline lobe-specific prostate tumor progression.

Trp53 deficiency promotes PECs dissemination

Between 5- and 7-months AGI, all Pten$^{(i)pe-/-}$ and Pten/Trp53$^{(i)pe-/-}$ mice harbored PINs and intraductal carcinomas within the DLPs, but invasive tumors were twice more frequent in Pten/Trp53$^{(i)pe-/-}$ mice (Fig. 2a & b). Whereas the proliferation rate in tumors of Pten$^{(i)pe-/-}$ mice was below 4%, it went up to 11 % in Pten/Trp53$^{(i)pe-/-}$ mice, with an average of 4% (Fig. 2c & d). Of note, 20% of Pten/Trp53$^{(i)pe-/-}$ mice had a prostate mass above 300 mg and developed

large tumoral masses with sarcomatoid histology in the AP (Supp. Fig. 2a & b). Importantly, Pten/Trp53$^{(i)pe-/-}$ mice with a prostate weight below 300 mg never harbored sarcomatoid tumors, and their prostate weight was similar to that of Pten$^{(i)pe-/-}$ mice (Supp. Fig. 2c), but 50% of them presented cell infiltrates in the liver (Supp. Fig. 2d). These infiltrates contained pan-cytokeratin positive cells surrounded by many CD45positive cells (Fig. 2e). In contrast, mice with sarcomatoid tumors never presented such infiltrates. As such infiltrates were not observed in Pten$^{(i)pe-/-}$ mice, in agreement with our previous analyses (12), p53 loss promotes the dissemination of *Pten*-deficient PECs.

Altogether, these data demonstrate that tumors in DLP of Pten/Trp53$^{(i)pe-/-}$ mice are more aggressive than those of Pten$^{(i)pe-/-}$ mice.

As senescent cells secrete a cocktail of cytokines, chemokines, growth factors and matrix remodeling factors, termed senescence-associated secretory phenotype (SASP), that might remodel their immune microenvironment and impact tumor progression (18), we immunophenotyped the prostates of control, Pten$^{(i)pe-/-}$ and Pten/Trp53$^{(i)pe-/-}$ mice 5 months AGI by flow cytometry. The abundance of immune cells (CD45^{+}) was similar in Pten$^{(i)pe-/-}$ and Pten/Trp53$^{(i)pe-/-}$ mice, though higher than in control mice (Supp. Fig. 3a). The number of the myeloid cells [Ly6G+ neutrophils (Supp. Fig. 3b) and CD11b^{+} macrophages (Supp. Fig. 3c)], and of the lymphoid populations [CD4^{+} and CD8^{+} T-cells] (Supp. Fig. 3d-f) was similarly increased in both mutant mice. Note that 60% of CD8+ T-cells expressed the exhaustion marker PD-1 in both mouse models (Supp. Fig. 3g). As Ly6G+ neutrophils are the major immune subpopulation of the DLP and the majority of CD8 T lymphocytes express PD-1, the tumor microenvironment of both mutant mice has immunosuppressive characteristics.

p53 deficiency promotes plasticity of *Pten*-null PECs via JAK/STAT3 signaling.

To investigate the molecular mechanisms underlying PIN progression, we performed single-cell RNA sequencing (scRNAseq) and recovered 5449 cells isolated from 3 dissociated sarcomatoid-free prostates of Pten/Trp53$^{(i)pe-/-}$ mice 5 months AGI. Annotation of the 23 identified cell clusters based on lineage markers revealed Immune (*Ptprc*, clusters 2, 3, 5, 6, 7, 8, 12, 13, 14, 17, 20, 21, 22), CAFs (*Vim, Col1a1,* clusters 0, 9, 10, 11), Endothelial (*Pecam1,* cluster 18), contaminant seminal vesicle (SV) (*Pate4*, cluster 23) and Epithelial (*Cdh1, Epcam*, clusters 4, 16 & 19) populations (Fig. 3a & 3b, Supp. table 1), the latter encompassing basal, luminal-B (LumB) (17) and luminal-C (LumC) cells (Supp. Fig. 4a & b) , as previously observed in Pten$^{(i)pe-/-}$ mice (15). However, one cluster (cluster 15) could not be annotated using lineage markers used in our previous analysis of Pten$^{(i)pe-/-}$ mice. The signature of these cells, defined as globally distinguishing genes of this cluster that are upregulated in transcriptomes of tumors of the TCGA PRAD cohort (Fig. 3c, see Methods), was not detected in epithelial cells of Pten$^{(i)pe-/-}$ mice 3-, 6- or 9-months AIG (15) (Supp. Fig. 4c). Interestingly, gene set enrichment analysis (GSEA) of cluster 15 signature revealed hallmarks of inflammatory and TGFβ signaling, as well as of Epithelial-to-Mesenchymal Transition (EMT) (19) (Supp. Fig. 4d, Supp. table 2). Cells of this cluster also expressed high levels of *Cdkn2a* (p16/p19) and of *Hoxb13* encoding a lineage marker conserved throughout prostate cancer progression (20) (Supp. Fig. 4e), indicating their luminal epithelial origin. This cluster was thus annotated as EMT cells (EMTc).

Recently, 3 transcriptional subtypes of human prostate cancer were reported: (i) androgen receptor pathway-positive prostate cancer (ARPC), (ii) mesenchymal and stem-like prostate

cancer (MSPC) and (iii) neuroendocrine prostate cancer (NEPC) (6). Interestingly, EMTc cells had a much higher signature score of MSPC than of ARPC and NEPC (Fig. 3d). In addition, the EMTc signature score (Fig. 3c) was higher in tumors of prostate cancer patients with mutated TP53 than of those with wild-type TP53, and in those with high-risk disease (Gleason score 8-10) in the TCGA cohort (Fig. 3e & 3f). Finally, the score of this signature was higher in patients with localized disease than in benign prostates, and it was even higher in patients with metastases in the dataset reported by Grasso et al. (21) (Fig. 3g and Supp. Fig. 5). Together, our data uncover a subset of luminal cells in murine *Pten*- and *Trp53*-deficient tumors that shares transcriptomic features with human prostate tumors exhibiting increased mesenchymal and stem-like characteristics and metastasis.

To further characterize the cell populations present in the DLP of sarcomatoid-free Pten/Trp53$^{(i)pe-/-}$ mice 5 months AGI, we performed single-nuclei Assay for Transposase Accessible Chromatin sequencing (snATACseq). Cluster annotation identified similar cell populations than those obtained by scRNAseq, namely Immune (clusters 2, 17, 5, 19, 20, 16), Endothelial (cluster 9), CAF populations (clusters 0, 14, 18), Epithelial subpopulations [LumC (clusters 3, 8, 1, 4, 10), LumB (cluster 7), Basal (cluster 13)], SV (cluster 11)] and, importantly, EMTc (cluster 15) (Fig. 4a, Supp. Table 3). To identify candidate factors driving cell-specific gene expression, we performed single-cell multiomic inference of enhancers and gene regulatory networks (SCENIC+) analyses (22) by integrating chromatin accessibility and gene expression profiles obtained from snATACseq (Fig. 4a) and scRNAseq (Fig. 3a) datasets, respectively. This analysis revealed eRegulons of Runx3, Rel and Izkf1 selectively in the immune populations, of Sox7, Sox17 and Sox18 selectively in the endothelial cluster, and of Twist1 and Tcf21 selectively in the CAF populations (Fig. 4b & Supp. Table 4). In addition, within epithelial subpopulations, the eRegulon of Trp63 was selective to the basal cluster, whereas Foxa1 and Androgen receptor (Ar) eRegulons were enriched in the LumC cluster. In contrast, Foxa1 and Ar eRegulons were low in the EMTc. Moreover, Stat3 expression and its target site accessibility were higher in EMTc than in LumC cells. Interestingly, GSEA of differentially expressed genes (DEGs) between EMTc and LumC cells revealed an enrichment of epithelial-mesenchymal transition (e.g. *Vim* and *Sparc*), as well as IL6/Jak/Stat3 signaling related genes (e.g. *Csf1 and Il6ra)* (Fig. 4c & 4d, and Supp. Tables 5 & 6). Importantly, immunofluorescent analyses showed that pStat3 (T705)-positive PECs were much more abundant in PINs of Pten/Trp53$^{(i)pe-/-}$ mice than of Pten$^{(i)pe-/-}$ mice 5 months AGI, and were mainly located near the basal lamina, in proximity to the stroma (Fig. 4e & f). Thus, Stat3 signaling induced in *Pten*- and *Trp53*-deficient PECs might require signals from the stroma to induce their plasticity.

IL6 produced by cancer-associated fibroblasts induces plasticity of PTEN- and p53deficient PECs.

To identify cell types and molecular factors that might promote Stat3 signaling in PECs of Pten/Trp53$^{(i)pe-/-}$ mice, we interrogated the scRNAseq data using CellPhoneDB (23). These analyses predicted that epithelial populations interact mostly with CAFs (Fig. 4g, Supp. table 7). To determine whether CAFs from prostates of mutant mice secrete factors that promote PEC plasticity, Pten$^{-/-}$ and Pten/Trp53$^{-/-}$ organoids were treated for 48 h with the supernatants of CAFs isolated from prostates of Pten$^{(i)pe-/-}$ or Pten/Trp53$^{(i)pe-/-}$ mice 5 months AGI (Fig. 4h). Whereas all cells in organoids from both lines were E-cadherin positive, some also expressed

Vimentin (Vim) in Pten/Trp53$^{-/-}$ organoids treated with supernatants of CAFs isolated from prostates of Pten/Trp53$^{(i)pe-/-}$ mice, but not of Pten$^{(i)pe/-}$ones (Fig. 4i). Importantly, co-treatment of Pten/Trp53$^{pe-/-}$ organoids with Pten/Trp53$^{(i)pe-/-}$ CAF supernatants and the Jak kinase inhibitor Ruxolitinib reduced the proportion of Vim^{+} cells (Fig. 4j & 4k), demonstrating the driver role of Jak/Stat signaling in plasticity induction. In contrast, no Vim^{+} cells were detected in Pten$^{-/-}$ organoids treated with supernatants of CAFs isolated from prostates of Pten/Trp53$^{-/-}$ mice, indicating a crosstalk between PECs and CAFs selectively in Pten/Trp53$^{(i)pe-/-}$ tumors.

Molecules secreted by CAFs might induce extracellular matrix remodeling, immunomodulation, metabolic regulation, and contribute to tumor progression, invasion and immune escape (24). CAF sub clustering revealed 3 populations that were annotated based on the expression of previously reported selective marker genes (25–27): ductal fibroblasts (*Wnt2, Rorb*), myofibroblastic CAFs ("myCAFs" [*Acta2, Tagln, Mmp11, Myl9, Postn, Tpm1, Tpm2]*), and inflammatory CAFs ("iCAFs" [*Il6, Cxcl12, Dpt, Has1, Cxcl1, Ccl2*]) (Fig. 5a). As expected, GSEA of their transcriptomic signatures revealed an enrichment of pathways related to extracellular matrix organization in myCAF and ductal fibroblasts, and immune system activation in iCAFs (Supp. Fig. 4f). Given the IL6/JAK/STAT3 signaling enrichment in EMTc compared to LumC cells (Fig. 4c), we interrogated the predicted interactions through secreted molecules between iCAFs and LumC cells or EMTc. The most significant and specific interaction was between *Il6* expressed by iCAFs and IL6 receptor (*Il6ra*) of EMTc (Fig. 5b & Supp. table 8). Moreover, whereas culture supernatants of Pten$^{-/-}$ and Pten/Trp53$^{-/-}$ organoids contained low IL6 levels, those of CAFs from Pten$^{(i)pe-/-}$ mice and Pten/Trp53$^{(i)pe-/-}$ ones contained 10-fold and 20-fold higher IL6 levels, respectively (Fig. 5c). Importantly, IL6 induced Vimentin expression in dose-dependent manner in Pten/Trp53$^{-/-}$ organoids, but not in Pten$^{-/-}$ ones (Fig. 5d). Together, these results show that *Trp53* deficiency in PECs enhances IL6 production in CAFs, that in turn promotes Jak/Stat-induced epithelial cell plasticity (Fig. 5e).

Discussion

PTEN and *TP53* genomic alterations are frequent in advanced prostate tumors and are associated with prostate cancer aggressivity. However, as some occur in preneoplastic lesions, and as the impact of combined *PTEN* and *TP53* loss in PECs on their progression is poorly characterized, we compared prostate tumorigenesis in Pten/Trp53$^{(i)pe-/-}$ and Pten$^{(i)pe-/-}$ mice, in which *Trp53* and/or *Pten* are inactivated in prostatic luminal cells at adulthood. Moreover, we addressed the clinical relevance of our findings by interrogating human prostate cancer datasets.

We show that *Trp53* and/or *Pten* are efficiently inactivated in luminal cells of the DLP of adult Pten/Trp53$^{(i)pe-/-}$ and Pten$^{(i)pe-/-}$ mice, respectively, and that these PECs actively proliferate between 1- and 3-months AGI, leading to PINs at high incidence in these prostatic lobes of both mutant mice, in agreement with our previous study (13). Moreover, we demonstrate that both *Pten*- and *Pten/Trp53*-null PECs are growth arrested at later time and are SA-ß-gal-positive. However, whereas PECs of Pten$^{(i)pe-/-}$ mice express the cell cycle inhibitors p21 and p16, those of Pten/Trp53$^{(i)pe-/-}$ mice only express p16. Thus, both *Pten*- and *Pten/Trp53*-deficient PECs become senescent in DLP after the proliferation phase, but their senescence state might be different. Chen and colleagues reported the development of large prostatic tumors in the anterior prostate (AP) of Pten$^{pc/-}$/Trp53$^{pc-/-}$ mice, in which the tumor suppressor genes are inactivated in PECs before puberty by the Cre recombinase expressed under the control of the Probasin promoter (14). As no SA-ß-gal activity was observed in these PECs in contrast to those of aged-matched Pten$^{pc-/-}$ mice, it was concluded that senescence of *Pten*-deficient tumors is p53mediated. Even though PSA-CreER^{T2}-mediated gene inactivation is less efficient in the AP than in the DLP (12), and tumor formation is heterogeneous in this lobe, we detected p16-positive cells in PINs, and observed large sarcomatoid tumors in the AP in about 20% of Pten/Trp53$^{(i)pe-/-}$ mice between 5 and 7 months AGI. Taken together, these data show that *Pten*– deficient PECs enter senescence in the absence of p53 in the DLP, and highlight lobe-specific tumor progression.

Importantly, our multiomic single-cell analyses revealed that combined loss of PTEN and p53 leads to an emergence of a subset of luminal cells during the senescent phase, termed EMTc, characterized by an epithelial-to-mesenchymal transition signature. Further investigation of tumor progression in the DLP, shown to resemble human prostate peripheral zone where most adenocarcinoma develop (28), revealed that Pten/Trp53$^{(i)pe-/-}$ mice present more invasive adenocarcinoma than Pten$^{(i)pe-/-}$ mice, as well as cell infiltrates in the liver at a 50% penetrance. Importantly, such infiltrates were never observed in Pten/Trp53$^{(i)pe-/-}$ mice with sarcomatoid tumors, nor in Pten$^{(i)pe-/-}$ mice at similar age, indicating that metastatic spreading selectively originates from *Pten/Trp53*-null adenocarcinoma. These results are in line with previous observations in breast tumors, showing that those with a partial EMT state display a higher metastatic capacity than fully dedifferentiated ones (29), and in prostate cancer mouse models showing that KRas overexpression in Pten-null PECs promotes intermediate epithelial-mesenchymal states with high tumoroid-forming capacity and metastasis to soft tissues (30,31).

Our single cell analyses revealed that EMTc are characterized by an induction of Jak/Stat3 signaling and a strong *Cdkn2a* (p16/p19) signature. Importantly, we demonstrate that tumors

of patients with high-risk prostate cancer and with metastatic disease have a high EMTc signature. In addition, EMTc share a transcriptomic signature with the recently identified human mesenchymal and stem-like prostate cancer (MSPC) subtype, that is present in treatment-naïve patients, enriched in metastatic prostate cancer, and frequently mutated for *PTEN* and *TP53* (6). Moreover, as patients with MSPC are poor responders to androgen receptor signaling inhibitors, impairing the emergence of this cell population represents an attractive strategy to prevent tumor progression.

Previous studies reported that IL6/Jak/Stat3 pathways is operating at multiple levels during prostate tumor progression. Pencik et al. showed an increased aggressivity of prostate tumors in $Pten^{pc-/-}/Stat3^{pc-/-}$ mice, with a concomitant deregulation of the senescent state by disrupting the ARF–MDM2–p53 tumor suppressor axis (32). In contrast, Toso et al. showed decreased prostate cancer progression in $Pten^{pc-/-}/Stat3^{pc-/-}$ mice, promoted by clearance of senescent cells by the immune microenvironment (33). Furthermore, Nowak et al. reported IL6 production in PECs of $Pten^{pc-/-}/Trp53^{pc-/-}$ mice leading to an autocrine/paracrine STAT3 activation in PECs and CAFs, leading to MYC activation and metastasis (34). In addition, CAF-produced IL6 was shown to attenuate p53-mediated response to chemotherapy in LNCaP cells (11). Moreover, Trp53/Rb1-codeletion in prostatic epithelial cells induced Jak/Stat signaling and cell plasticity in a cell-autonomous manner leading to the progression of prostate tumors towards neuroendocrine prostate cancer and resistance to androgen receptor signaling (35,36). However, the potential impact of the TME on the induction of PTEN- and p53-deficient PECs plasticity was unknown.

We demonstrate that IL6 induces the expression of the mesenchymal marker Vimentin in PECs of $Pten/Trp53^{(i)pe-/-}$ mice, but not of $Pten^{(i)pe-/-}$ ones. Intriguingly, the number of pStat3-positive cells was much higher in DLP of $Pten/Trp53^{(i)pe-/-}$ mice than of $Pten^{(i)pe-/-}$ ones, and these cells were preferentially located in the vicinity of stromal cells, indicating that EMTc might be instructed by paracrine signals of the microenvironment. Importantly, we show that CAFs produce at least 10 times more IL6 than organoids from PECs of both mouse models, and that CAFs from prostates of $Pten/Trp53^{(i)pe-/-}$ mice produce twice as much IL6 than those of $Pten^{(i)pe-/-}$ ones, indicating that signals from Trp53-deficient tumors stimulate IL6 secretion by CAFs. Moreover, as culture supernatants of CAFs from $Pten/Trp53^{(i)pe-/-}$ mice but not from $Pten^{(i)pe-/-}$ ones induced Vimentin expression only in $Pten/Trp53^{-/-}$ PECs, and as this effect was dampened by Jak/Stat signaling inhibition, we conclude that epithelial cell plasticity is driven by a feedforward loop, involving CAF-produced IL6 promoting Jak/Stat3 pathway in PECs located in proximity of the TME, in addition to an autocrine/paracrine epithelial signaling proposed by previous studies (34). Whether PECs act directly on CAFs to enhance IL6 or through interactions with other cells (e.g. immune and endothelial cells) present in the TME requires further investigations.

Taken together, our study uncovers an epithelial population with partial EMT characteristics emerging selectively in PTEN- and p53-deficient senescent PINs. We provide evidence that this cell population is induced by signals from CAFs within the immune microenvironment containing immunosuppressive myeloid cells and exhausted lymphocytes. Importantly, as the presence of the EMTc cells correlates with metastatic dissemination, the identified crosstalk represents an attractive therapeutic target.

Competing Interest Statement

The authors declare no potential conflicts of interest.

Acknowledgments

We thank T. Mak and A. Suzuki for floxed PTEN mice, A. Berns for floxed p53 mice, JeanMarc Bornert, Anna Isavella Rerra, Camille Emprou, Kateryna Len, Régis Lutzing, Marie Cerciat, David Rodrigez, the IGBMC mouse, histopathology, cell culture and imaging facilities, the flow cytometry facility members C. Ebel and M. Phillips, and GenomEast, a member of the "France Génomique" consortium (ANR-10-INBS-0009), for excellent assistance. This study was supported by funds from the Centre National de la Recherche Scientifique (CNRS) (D.M.), Institut National de la Santé et de la Recherche Médicale (INSERM) (D.M.), Université de Strasbourg (D.M.), Interdisciplinary Thematic Institute IMCBio, as part of the ITI 2021-2028 program of the University of Strasbourg, CNRS and Inserm, supported by IdEx Unistra (ANR-10-IDEX-0002), and by SFRI-STRAT'US project (ANR 20-SFRI-0012) and EUR IMCBio (ANR-17-EURE-0023) under the framework of the French Investments for the Future Program (D.M.), Fondation pour la Recherche Médicale grant EQU201903007800 (D.M), ITMO Cancer within funds of the Cancer Plan 2014– 2019 (administrated by INSERM) and with a collaborative support from the French National Cancer Institute (D.M. and S.H.), INCa_16077 (D.M.), Ministère de l'enseignement supérieur et de la recherche (DY), Al Bizri Foundation (R.E.B.).

Author Contributions:

Conceptualization: DM, GL, SH, DY and BGF

Methodology: DY, BGF, REB, DP, CK, TY, CT-C, SH, GL

Investigation: DY, BGF, REB, DP, CK, TY, SH, GL

Visualization: DY, BGF, REB, DP, CK, TY, SH, GL

Supervision: SH, GL, DM

Writing – original draft: DY, BGF, SH, GL, DM

Formal analysis: DY, DP, SH, GL, DM

Funding acquisition: SH, DM

Materials and Methods

Sex as a biological variable

Only male mice were analyzed, as prostate cancer modeling is relevant only in animals of this sex.

Mice

Pten$^{(i)pe-/-}$ and Pten/Trp53$^{(i)pe-/-}$ male mice, as well as sex-matched Pten$^{L2/L2}$ and Pten/Trp53$^{L2/L2}$ control littermates (all on a C57BL/6 genetic background) were generated by intraperitoneal injection of Tamoxifen (1 mg/mouse/day) for 5 days to 8 to 10 week old PSA-CreERT2(Tg/0)/PtenL2/L2, PSA-CreERT2(Tg/0)/PtenL2/L2/Trp53L2/L2, PSACreERT2(0/0)/PtenL2/L2 and PSA-CreERT2(0/0)/PtenL2/L2/Trp53L2/L2 mice, respectively, as described (12,13). Mice breeding and maintenance were done in the accredited IGBMC/ICS animal house (D-67-218-37), in compliance with French and EU regulations on the use of laboratory animals for research. Animal experiments were approved by the Ethical committee Com'Eth (Comité d'Ethique pour l'Expérimentation Animale, Strasbourg, France), the Ethical committee CE14 (Marseille, France) and the French ministry of Higher Education and Research (APAFIS#36739-2022041912335718 v7, APAFIS #25240-2020042716503331 v5).

Histological examination

Five µm histological sections were prepared from paraffin embedded tissues and dried overnight at 37°C. Hematoxylin and eosin (HE) staining was performed according to standard protocols. Slides were scanned in brightfield mode with a NanoZoomer digital slide scanner (Hamamatsu) and analyzed with the NDP.view2 Viewing software (Hamamatsu). Representative images are provided.

Immunostaining

Five µm paraffin tissue sections were deparaffinized according to standard protocols and incubated for 20 min in SignalStain Citrate Unmasking Solution (10X) (CST 14746) in a pressure cooker for heat-induced antigen retrieval. The following primary antibodies were used: p53 (CM5) (Leica, P53-CM5P-L; 1:200), p21 (BD Pharmingen, 556430, 1:50), pAkt (S473) (D9E) XP (CST, 5315S; 1:200), Trop2 (R&D Systems, AF1122; 1:50), Ki-67 (Thermo Fisher Scientific, MA5-14520; 1:200), E-cad (CST, 14472S; 1:200), Vim (CST, 5741S; 1:200), pStat3 (Tyr705) (D3A7) XP (CST, 9145S; 1:200), CD45 (Abcam, ab10558; 1:200), p16 [EPR20418] (Abcam, ab211542; 1:600) and pan-keratin (Proteintech, 264111-AP; 1:1500).

For immunohistochemistry, one drop of SignalStain® Boost IHC Detection Reagent (CST 8114) was added to each section, and SignalStain® DAB Substrate Kit (CST 8059) used to develop the signal, according to the manufacturer's instructions. The sections were counterstained with hematoxylin and mounted. Images were acquired using a NanoZoomer digital slide scanner (Hamamatsu) and analyzed with the NDP.view2 Viewing software (Hamamatsu).

For immunofluorescence, secondary antibodies coupled to Alexa Fluor 555 (Invitrogen, A31570; 1:400), Alexa Fluor 647 (Invitrogen, A32849; 1:400) or Alexa Fluor 488 (Invitrogen, A21206; 1:400) were used. The sections were mounted with Fluoromount-G™ (Invitrogen,

00-4959-52). Images were acquired with a Leica DM 4000 B microscope equipped with a Photometrics CoolSNAP HQ2 camera.

The number of Ki-67-positive, p16-positive and pStat3-positive cells was determined with the QuPath software (37).

SA-ß-gal staining

SA-ß-gal staining was performed on 10 µm frozen prostate sections using the senescence ß-Galactosidase Staining Kit (CST 9860), following the manufacturer's instructions.

Sections were counterstained with hematoxylin.

Flow cytometry

To distinguish circulating cells from tissue resident cells, mice were injected intravenously with 3 µg of anti CD45.2-FITC 3 minutes before euthanasia. Prostates were collected, the DLP isolated, weighted, cut into small pieces and incubated for 20 min at room temperature with type II collagenase (Worthington Biochemical) and DNase I (Sigma) in 2% FCS RPMI under frequent pipetting. The enzymatic reaction was stopped by addition of 2% v/v of 0.5 M EDTA. The cellular suspension was passed through a 5 ml syringe with 18G needle for complete tissue dissociation. The single-cell solution was filtered through a 70 µm cell strainer and centrifuged. The pellet was resuspended in PBS, 5 mM EDTA, 2% FCS and was re-filtered through a 30 µm cell strainer (Miltenyi).

Cells were preincubated with anti-Fc receptor antibody (clone 2.4G2) and stained with appropriate antibodies in PBS-5 mM EDTA, 2% FCS at 4°C for 30 min at dark. Viability was assessed with Zombie UV™ Fixable Viability dye (Biolegend). Flow cytometry was performed on FACS Symphony or Fortessa X20 systems (BD Biosciences) and data analyzed with Flowjo software (Flowjo LLC). Doublets and dead cells were excluded from the analysis. For the analysis of myeloid cells (neutrophils and macrophages), B, T and NK cells were gated out using a Lin^- gate ($CD5^-$, $CD19^-$, $CD161c^-$). Antibodies used are listed in Supp. Table 9. The gating strategies for lymphoid and myeloid cells are presented on Fig. S6. Absolute numbers were estimated using CountBright™ absolute count microbeads for flow cytometry (Invitrogen) and normalized by the prostate weight.

scRNA-seq analysis

Mouse prostates were dissociated into single cells as described (15). Cells from 3 prostates were pooled, stained with DAPI and living cells (DAPI-negative) were FACSsorted using a BD FACSAriaTM Fusion flow cytometer. Trypan blue exclusion assay was used to determine cell number and viability of FACS-sorted cells using a Neubauer Chamber. Samples with a cell viability of >95% were processed with a Chromium Controller (10X Genomics, Leiden, The Netherlands). Sixteen thousand cells were loaded per well in nanoliter-scale Gel Beads-in-Emulsion (GEMs). Single-cell 3' mRNA-seq libraries were generated according to "User guide Chromium Next GEM Single Cell 3 prime Reagent Kits v3.1 (Dual index) (10X Genomics, PN CG000315 - Rev.D). Briefly, cells were partitioned into droplets with barcoded gel beads and reverse transcription master mix using Chromium Chip G. After complementary DNA (cDNA) synthesis and barcoding from poly-adenylated RNA, GEMs were disrupted and pooled before amplification of cDNA by 11 polymerase chain reaction (PCR) cycles. Following enzymatic

fragmentation and size selection of cDNA amplicons, sequencing libraries were constructed by adding Illumina P5 and P7 adapters (San Diego, USA) and i5 and i7 sample indexes by end repair, A-tailing, adaptor ligation, and 10 cycles of PCR amplification. Quality control and quantification of libraries was performed with a Bioanalyzer 2100 (Agilent Technologies, Santa Clara, CA). The generated library was sequenced on Illumina HiSeq 4000 as 100 bases paired-end reads and Illumina NextSeq 550 as 28+100 bases paired-end reads. RTA 2.7.7, bcl2fastq 2.20.0.422 and Cell Ranger 3.0.2 mkfastq were used for image analysis, base calling and demultiplexing. Cell Ranger 7.0.0 count was used for alignment, barcode and UMI (Unique Molecular Identifier) filtering and counting, with a reference created with Cell Ranger 7.0.0 mkref using GRCm39 assembly of Mus musculus genome, Ensembl release 107 annotations and $CreER^{T2}$ sequence. The Read10X function of the Seurat version (v) 4.3 (R v 4.2.2) was used to read the output of the Cell Ranger pipeline and obtain a matrix of the number of UMI of each gene detected in each cell.

snATAC-seq analysis

Mouse DLPs were dissociated into single cells as described (15). Nuclei were isolated from 800 000 cells by applying Nuclei isolation buffer (10 mM Tris-HCl pH 7.4, 10 mM NaCl, 3 mM MgCl2, 0.1% Tween-20, 0.1% IGEPAL CA-630, 0.01% Digitonin, 1% BSA) for 5 min and washed according to the 10X Demonstrated Protocol (CG000169). For each sample, 16 000 nuclei were loaded on a 10X Chromium Controller (10X Genomics, Leiden, The Netherlands) to recover 10 000 nuclei.

Chromium Next GEM Single Cell ATAC Reagent Kits v1.1 (10X Genomics ref. CG000209 Rev C) were used to generate single-nuclei libraries. Nuclei were fragmented and adapter sequences were added through a Transposition Mix. Gel beads with barcodes and a Master Mix were combined with the transposed nuclei on a Chromium Chip H to generate GEMs, which were then broken and pooled to produce barcoded single-stranded DNA. The leftover biochemical reagents and unused barcodes were removed from the reaction mixture using magnetic and SPRI beads. Library construction was performed via PCR with the addition of P7 and a sample index. Quality control and quantification of libraries were performed using a Bioanalyzer 2100 (Agilent Technologies, Santa Clara, CA). Generated libraries were sequenced on Illumina HiSeq 4000 and NextSeq 2000 sequencers as 100 bases paired-end reads. Cell Ranger ATAC 2.0.0 and the mouse reference cellranger-arc-mm10-2020-A-2.0.0 were used for demultiplexing, alignment, barcode filtering and counting. The Read10X function of the Seurat v 4.3.0 (R v 4.2.2) was used to read the output of the Cell Ranger pipeline and to obtain a matrix of the number of reads of each peak detected in each cell.

Reads from barcodes of the same cell type were pooled using Signac 1.9.0. Cell type specific peak calling was performed using macs2 2.2.7.1. Peaks were annotated to the nearest gene using Homer software mm10 genome ucsc v6.4. eRegulons were determined using the Scenic+ package (version 0.1.dev456+g9662363).

Culture and analysis of PEC-derived organoids and cancer associated fibroblasts

Mouse DLPs were dissociated into single cells, as described (15). For fibroblasts culture, single cell suspensions obtained from DLPs of $Pten^{(i)pe-/-}$ and $Pten/Trp53^{(i)pe-/-}$ mice 5 months AGI were seeded in DMEM [4.5 g/L glucose, 20% FCS, 1% penicillin/streptomycin] at

37°C and 5% CO_2. After 1 passage, only fibroblasts were maintained in culture. At 70% confluence, the media was replaced, collected 48h later, and centrifuged for 5 min at 400 g.

$Pten^{-/-}$ and $Pten/Trp53^{-/-}$ organoid cultures were established from DLPs of $Pten^{(i)pe-/-}$ and $Pten/Trp53^{(i)pe-/-}$ mice 3 months AGI, respectively, as described (15,38). 5 000 cells were seeded per Cultrex dome (R&D systems, 3533-010-02) and after 1 week, the culture media was replaced by conditioned medium from CAFs of $Pten^{(i)pe-/-}$ or $Pten/Trp53^{(i)pe-/-}$ mice, with or without Ruxolitinib (10 µM) (MedChemExpress, HY-50856), or with "organoid medium" supplemented with IL6 (at a final concentration of 2 or 4 ng/mL) (PeproTech, 216-16) for 48 hrs.

To perform histological analyses of organoids, matrigel domes were digested for 1 h at 37°C in dispase (2 mg/mL) (StemCell Technologies, 07913). Organoids were fixed in 10% formalin for 24 h, included in HistoGel™ (Epredia, HG-4000-012), embedded in paraffin and processed for HE staining or immunofluorescent detections following standard protocols. Brightfield images of organoids were acquired with EVOS™ M5000 imaging system (Invitrogen).

IL6 levels determination

The culture media of organoids and fibroblasts were replaced 1 week after seeding with cognate culture media, collected 48 h later, centrifuged at 400 g for 5 min and supernatants were collected. IL6 levels were determined with the Mouse IL-6 Uncoated ELISA Kit (Invitrogen, 88-7064-88) in 96-well plates (Corning, 9018), according to manufacturer's protocol.

EMTc signature and human datasets analyses

The EMTc signature was generated by selecting the top 25 globally distinguishing genes of the EMTc cluster with the lowest adjusted p-value and a log2 fold change>1 in the mouse scRNAseq data. This list of genes was then refined by selecting the genes upregulated in transcriptomes of tumor tissues versus healthy tissues from the TCGA PRAD cohort.

The correlation of EMTc signature with the *TP53* status and the Gleason score was analyzed in the TCGA PRAD cohort (n = 496 patients with prostate cancer) and in the cohort of Grasso et al. (n=76 patients with prostate cancer)(21). The score corresponds to the mean of the quartiles for each individual gene.

Data analysis

Statistical analysis was performed using the GraphPad Software Prism 9.

Code availability

Sequencing data are deposited at the Gene Expression Omnibus (GEO) database (GSE236042). Code for scRNAseq and snATACseq analysis is available at Github repository on demand.

Article References

1. Sung H, Ferlay J, Siegel RL, Laversanne M, Soerjomataram I, Jemal A, et al. Global Cancer Statistics 2020: GLOBOCAN Estimates of Incidence and Mortality Worldwide for 36 Cancers in 185 Countries. CA A Cancer J Clin. 2021 May;71(3):209–49.
2. Hamid AA, Gray KP, Shaw G, MacConaill LE, Evan C, Bernard B, et al. Compound Genomic Alterations of TP53, PTEN, and RB1 Tumor Suppressors in Localized and Metastatic Prostate Cancer. European Urology. 2019 Jul;76(1):89–97.
3. Abeshouse A, Ahn J, Akbani R, Ally A, Amin S, Andry CD, et al. The Molecular Taxonomy of Primary Prostate Cancer. Cell. 2015 Nov;163(4):1011–25.
4. Jamaspishvili T, Berman DM, Ross AE, Scher HI, De Marzo AM, Squire JA, et al. Clinical implications of PTEN loss in prostate cancer. Nat Rev Urol. 2018 Apr;15(4):222–34.
5. Teroerde M, Nientiedt C, Duensing A, Hohenfellner M, Stenzinger A, Duensing S. Revisiting the Role of p53 in Prostate Cancer. In: Urology Department, Frimley Park Hospital, Portsmouth Rd, Frimley, Camberley GU16 7UJ, UK, Bott SR, Lim Ng K, editors. Prostate Cancer [Internet]. Exon Publications; 2021 [cited 2023 Jun 16]. p. 113–24. Available from: https://exonpublications.com/index.php/exon/article/view/318
6. Han H, Wang Y, Curto J, Gurrapu S, Laudato S, Rumandla A, et al. Mesenchymal and stem-like prostate cancer linked to therapy-induced lineage plasticity and metastasis. Cell Reports. 2022 Apr;39(1):110595.
7. Abu El Maaty MA, Grelet E, Keime C, Rerra AI, Gantzer J, Emprou C, et al. Singlecell analyses unravel cell type–specific responses to a vitamin D analog in prostatic precancerous lesions. Sci Adv. 2021 Jul 30;7(31):eabg5982.
8. Wang G, Zhao D, Spring DJ, DePinho RA. Genetics and biology of prostate cancer. Genes Dev. 2018 Sep 1;32(17–18):1105–40.
9. Baures M, Dariane C, Tika E, Puig Lombardi E, Barry Delongchamps N, Blanpain C, et al. Prostate luminal progenitor cells: from mouse to human, from health to disease. Nat Rev Urol. 2022 Apr;19(4):201–18.
10. Owen JS, Clayton A, Pearson HB. Cancer-Associated Fibroblast Heterogeneity, Activation and Function: Implications for Prostate Cancer. Biomolecules. 2022 Dec;13(1):67.
11. Cheteh EH, Sarne V, Ceder S, Bianchi J, Augsten M, Rundqvist H, et al. Interleukin6 derived from cancer-associated fibroblasts attenuates the p53 response to doxorubicin in prostate cancer cells. Cell Death Discov. 2020 Jun 2;6(1):42.
12. Ratnacaram CK, Teletin M, Jiang M, Meng X, Chambon P, Metzger D. Temporally controlled ablation of PTEN in adult mouse prostate epithelium generates a model of invasive prostatic adenocarcinoma. Proc Natl Acad Sci USA. 2008 Feb 19;105(7):2521–6.

13. Parisotto M, Grelet E, El Bizri R, Dai Y, Terzic J, Eckert D, et al. PTEN deletion in luminal cells of mature prostate induces replication stress and senescence in vivo. Journal of Experimental Medicine. 2018 Jun 4;215(6):1749–63.

14. Chen Z, Trotman LC, Shaffer D, Lin HK, Dotan ZA, Niki M, et al. Crucial role of p53dependent cellular senescence in suppression of Pten-deficient tumorigenesis. Nature. 2005 Aug;436(7051):725–30.

15. Abu el Maaty MA, Terzic J, Keime C, Rovito D, Lutzing R, Yanushko D, et al. Hypoxia-mediated stabilization of HIF1A in prostatic intraepithelial neoplasia promotes cell plasticity and malignant progression. Sci Adv. 2022 Jul 22;8(29):eabo2295.

16. Dimri GP, Lee X, Basile G, Acosta M, Scott G, Roskelley C, et al. A biomarker that identifies senescent human cells in culture and in aging skin in vivo. Proceedings of the National Academy of Sciences. 1995 Sep;92(20):9363–7.

17. Graham MK, Chikarmane R, Wang R, Vaghasia A, Gupta A, Zheng Q, et al. Singlecell atlas of epithelial and stromal cell heterogeneity by lobe and strain in the mouse prostate. The Prostate. 2023 Feb;83(3):286–303.

18. Coppé JP, Desprez PY, Krtolica A, Campisi J. The Senescence-Associated Secretory Phenotype: The Dark Side of Tumor Suppression. Annu Rev Pathol Mech Dis. 2010 Jan 1;5(1):99–118.

19. Subramanian A, Tamayo P, Mootha VK, Mukherjee S, Ebert BL, Gillette MA, et al. Gene set enrichment analysis: A knowledge-based approach for interpreting genome-wide expression profiles. Proc Natl Acad Sci USA. 2005 Oct 25;102(43):15545–50.

20. Patel RA, Sayar E, Coleman I, Roudier MP, Hanratty B, Low J, et al. Characterization of HOXB13 expression patterns in localized and metastatic castration-resistant prostate cancer. The Journal of Pathology. 2024 Jan;262(1):105–20.

21. Grasso CS, Wu YM, Robinson DR, Cao X, Dhanasekaran SM, Khan AP, et al. The mutational landscape of lethal castration-resistant prostate cancer. Nature. 2012 Jul;487(7406):239–43.

22. Bravo González-Blas C, De Winter S, Hulselmans G, Hecker N, Matetovici I, Christiaens V, et al. SCENIC+: single-cell multiomic inference of enhancers and gene regulatory networks. Nat Methods [Internet]. 2023 Jul 13 [cited 2023 Aug 1]; Available from: https://www.nature.com/articles/s41592-023-01938-4

23. Efremova M, Vento-Tormo M, Teichmann SA, Vento-Tormo R. CellPhoneDB: inferring cell–cell communication from combined expression of multi-subunit ligand– receptor complexes. Nature Protocols 2020 15:4. 2020 Feb;15(4):1484–506.

24. Sahai E, Astsaturov I, Cukierman E, DeNardo DG, Egeblad M, Evans RM, et al. A framework for advancing our understanding of cancer-associated fibroblasts. Nat Rev Cancer. 2020 Mar;20(3):174–86.

25. Elyada E, Bolisetty M, Laise P, Flynn WF, Courtois ET, Burkhart RA, et al. CrossSpecies Single-Cell Analysis of Pancreatic Ductal Adenocarcinoma Reveals Antigen-Presenting Cancer-Associated Fibroblasts. Cancer Discovery. 2019 Aug 1;9(8):1102–23.

26. Öhlund D, Handly-Santana A, Biffi G, Elyada E, Almeida AS, Ponz-Sarvise M, et al. Distinct populations of inflammatory fibroblasts and myofibroblasts in pancreatic cancer. The Journal of experimental medicine. 2017 Mar;214(3):579–96.

27. Joseph DB, Henry GH, Malewska A, Reese JC, Mauck RJ, Gahan JC, et al. Singlecell analysis of mouse and human prostate reveals novel fibroblasts with specialized distribution and microenvironment interactions. Journal of Pathology. 2021 Oct;255(2):141–54.

28. Berquin IM, Min Y, Wu R, Wu H, Chen YQ. Expression Signature of the Mouse Prostate. Journal of Biological Chemistry. 2005 Oct;280(43):36442–51.

29. Pastushenko I, Brisebarre A, Sifrim A, Fioramonti M, Revenco T, Boumahdi S, et al. Identification of the tumour transition states occurring during EMT. Nature. 2018 Apr;556(7702):463–8.

30. Mulholland DJ, Kobayashi N, Ruscetti M, Zhi A, Tran LM, Huang J, et al. *Pten* Loss and RAS/MAPK Activation Cooperate to Promote EMT and Metastasis Initiated from Prostate Cancer Stem/Progenitor Cells. Cancer Research. 2012 Apr 1;72(7):1878– 89.

31. Aytes A, Mitrofanova A, Kinkade CW, Lefebvre C, Lei M, Phelan V, et al. *ETV4* promotes metastasis in response to activation of PI3-kinase and Ras signaling in a mouse model of advanced prostate cancer. Proc Natl Acad Sci USA [Internet]. 2013 Sep 10 [cited 2024 May 27];110(37). Available from: https://pnas.org/doi/full/10.1073/pnas.1303558110

32. Pencik J, Schlederer M, Gruber W, Unger C, Walker SM, Chalaris A, et al. STAT3 regulated ARF expression suppresses prostate cancer metastasis. Nat Commun. 2015 Jul 22;6(1):7736.

33. Toso A, Revandkar A, Di Mitri D, Guccini I, Proietti M, Sarti M, et al. Enhancing Chemotherapy Efficacy in Pten -Deficient Prostate Tumors by Activating the Senescence-Associated Antitumor Immunity. Cell Reports. 2014 Oct;9(1):75–89.

34. Nowak DG, Cho H, Herzka T, Watrud K, DeMarco DV, Wang VMY, et al. MYC Drives *Pten/Trp53* -Deficient Proliferation and Metastasis due to IL6 Secretion and AKT Suppression via PHLPP2. Cancer Discovery. 2015 Jun 1;5(6):636–51.

35. Deng S, Wang C, Wang Y, Xu Y, Li X, Johnson NA, et al. Ectopic JAK–STAT activation enables the transition to a stem-like and multilineage state conferring ARtargeted therapy resistance. Nat Cancer. 2022 Sep 5;3(9):1071–87.

36. Chan JM, Zaidi S, Love JR, Zhao JL, Setty M, Wadosky KM, et al. Lineage plasticity in prostate cancer depends on JAK/STAT inflammatory signaling. Science. 2022 Sep 9;377(6611):1180–91.

37. Bankhead P, Loughrey MB, Fernández JA, Dombrowski Y, McArt DG, Dunne PD, et al. QuPath: Open source software for digital pathology image analysis. Sci Rep. 2017 Dec 4;7(1):16878.

38. Drost J, Karthaus WR, Gao D, Driehuis E, Sawyers CL, Chen Y, et al. Organoid culture systems for prostate epithelial and cancer tissue. Nature Protocols. 2016 Feb;11(2):347–58.

Figure 1

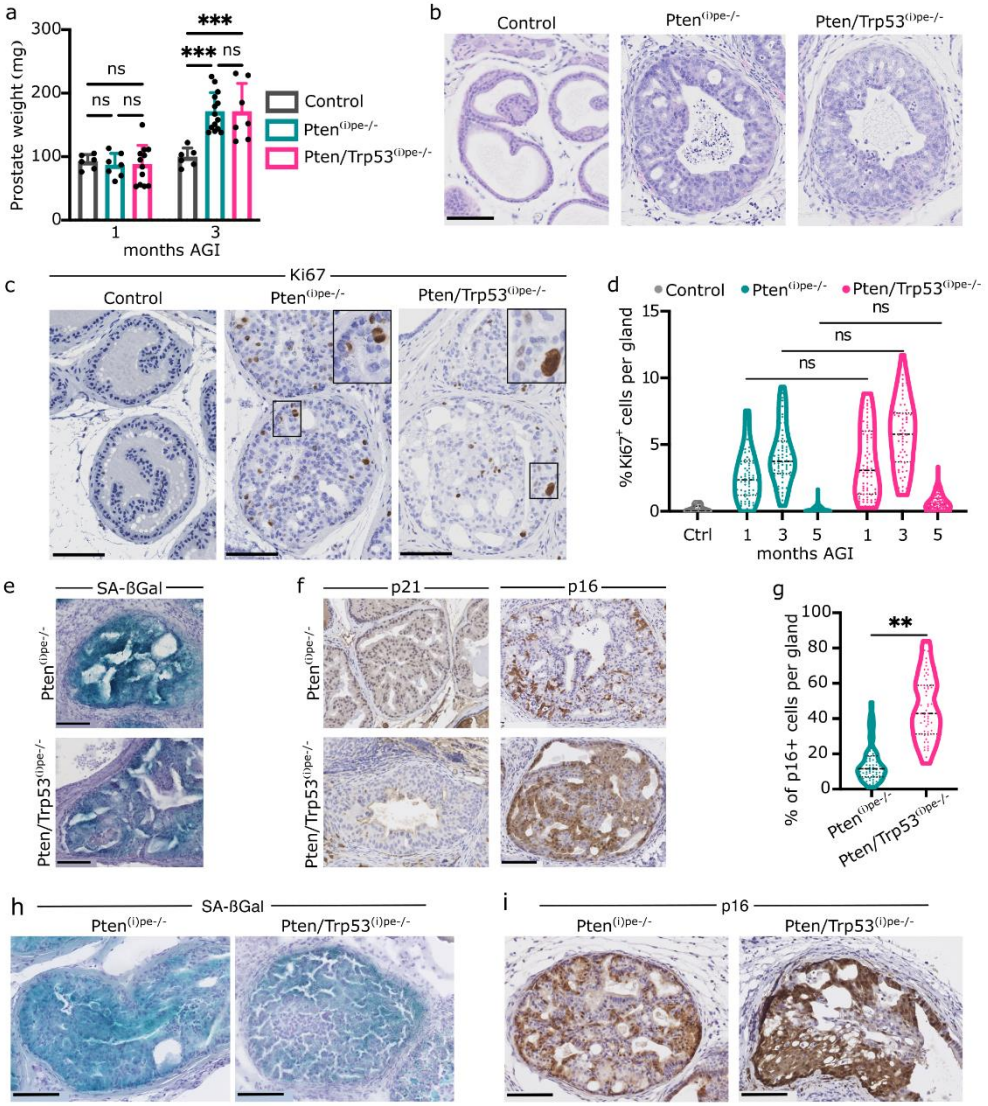
a
Prostate weight (mg)
300
200
100
0
ns
ns ns
*** ns
*** ns
1
3
months AGI
Control
Pten(i)pe-/-
Pten/Trp53(i)pe-/-
b
Control
Pten(i)pe-/-
Pten/Trp53(i)pe-/-
c
Ki67
Control
Pten(i)pe-/-
Pten/Trp53(i)pe-/-
d
Control
Pten(i)pe-/-
Pten/Trp53(i)pe-/-
% Ki67+ cells per gland
15
10
5
0
ns
ns
ns
Ctrl 1 3 5 1 3 5
months AGI
e
SA-ßGal
Pten(i)pe-/-
Pten/Trp53(i)pe-/-
f
p21
p16
Pten(i)pe-/-
Pten/Trp53(i)pe-/-
g
% of p16+ cells per gland
100
80
60
40
20
0
**
Pten(i)pe-/-
Pten/Trp53(i)pe-/-
h
SA-ßGal
Pten(i)pe-/-
Pten/Trp53(i)pe-/-
i
p16
Pten(i)pe-/-
Pten/Trp53(i)pe-/-

Figure 1. Characterization of early-stage prostate tumors in Pten/Trp53$^{(i)pe-/-}$ mice.

a. Prostate weight of control (Pten$^{L2/L2}$ or Pten/Trp53$^{L2/L2}$ mice), Pten$^{(i)pe-/-}$ and Pten/Trp53$^{(i)pe-/-}$ mice 1- and 3-months AGI. n≥6 per group. ns, non-significant, p≥0.05; *** p<0.001. Two-way ANOVA followed by Tukey's post-hoc test.

b. Representative hematoxylin-eosin (HE) staining of DLP sections from control, Pten$^{(i)pe/-}$ and Pten/Trp53$^{(i)pe-/-}$ mice, 3 months AGI. Scale bar: 100 µm. n ≥6 per group.

c-d. Representative Ki-67 staining (brown) of DLP sections from control, Pten$^{(i)pe-/-}$ and Pten/Trp53$^{(i)pe-/-}$ mice 3 months AGI **(c)** and quantification of Ki-67 positive PECs per gland at 1-, 3- and 5-months AGI (**d)**. n ≥3 mice per group. ns, non-significant, p≥0.05. Two-way ANOVA followed by Tukey's post-hoc test. Scale bar: 100 µm.

e. Representative Senescence-associated ß-galactosidase (SA-ßGal) staining (blue) of DLP sections from Pten$^{(i)pe-/-}$ and Pten/Trp53$^{(i)pe-/-}$ mice 5 months AGI. Scale bar: 100 µm. n = 3 mice per group.

f-g. Representative immunohistochemical staining of p21 and p16 (brown) **(f)** and quantification of p16 positive (+) PEC per gland **(g)** in DLP of Pten$^{(i)pe-/-}$ and Pten/Trp53$^{(i)pe/-}$ mice 5 months AGI. Scale bar: 100 µm. n≥3 per group. **, p<0.01; Student's t-test.

h. Representative SA-ßGal staining (blue) of DLP sections from Pten$^{(i)pe-/-}$ and Pten/Trp53$^{(i)pe-/-}$ mice 7 months AGI. Scale bar: 100 µm. n = 3 mice per group.

i. Representative immunohistochemical staining of p16 (brown) in DLP of Pten$^{(i)pe-/-}$ and Pten/Trp53$^{(i)pe-/-}$ mice 7 months AGI. Scale bar: 100 µm. n≥3 per group.

Figure 2

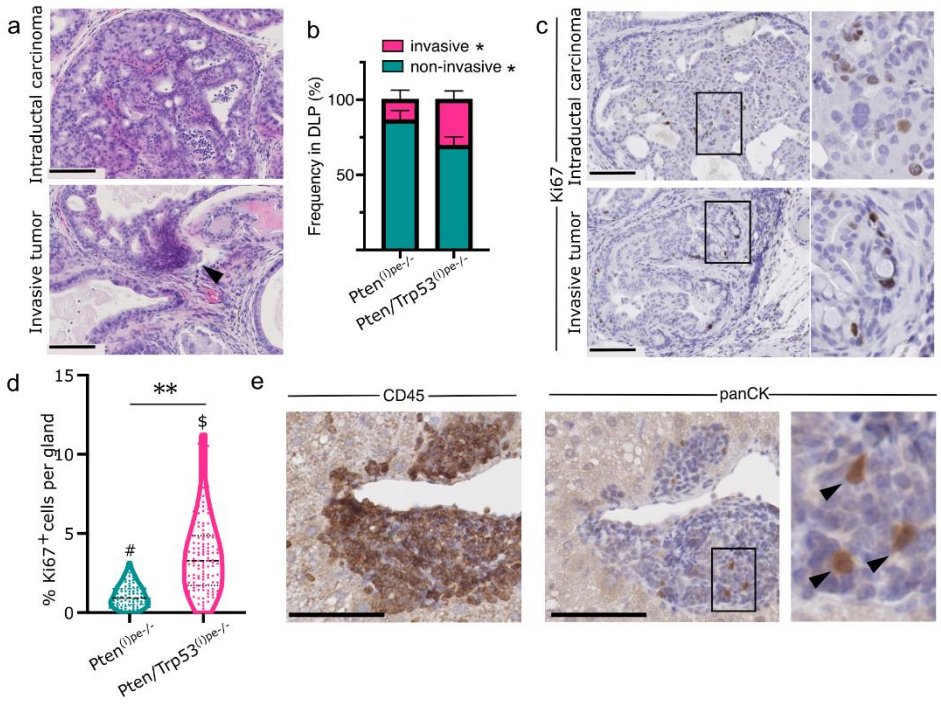

Figure 2. Characterization of tumor progression in Pten/Trp53$^{(i)pe-/-}$ mice

a. Representative HE staining of DLP of Pten/Trp53$^{(i)pe-/-}$ mice 7 months AGI. Top panel, intraductal adenocarcinoma (IDC); bottom panel, invasive adenocarcinoma (pointed by an arrow). Scale bar: 100 µm. n = 4 mice per group.

b. Frequency of invasive and non-invasive tumors in DLPs of Pten$^{(i)pe-/-}$ and Pten/Trp53$^{(i)pe/-}$ mice 5-7 months AGI. n=4 mice per group, n=100 glands per group. Paired t-tests. * $p<0.05$.

c. Representative Ki-67 staining of IDC and invasive adenocarcinoma in DLP sections of Pten/Trp53$^{(i)pe-/-}$ mice 7 months AGI. n=4 mice per group. Scale bar: 100 µm.

d. Quantification of Ki-67-positive PECs per gland in DLP of Pten$^{(i)pe-/-}$ and Pten/Trp53$^{(i)pe/-}$ mice 7 months AGI. n ≥ 4 mice per group. 2-way ANOVA followed by Tukey's post-hoc test. ** $p<0.01$; # $p\geq0.05$ compared to Pten$^{(i)pe-/-}$ 5 months AGI (Fig 1d); $ $p<0.05$ compared to Pten/Trp53$^{(i)pe-/-}$ 5 months AGI (Fig 1d).

e. Representative immunohistochemical detection of CD45 and pan-cytokeratin (panCK) in liver of Pten/Trp53$^{(i)pe-/-}$ mice 6 months AGI. Scale: 100 µm. n = 15 mice. Arrows point to panCK^{+} cells.

Figure 3

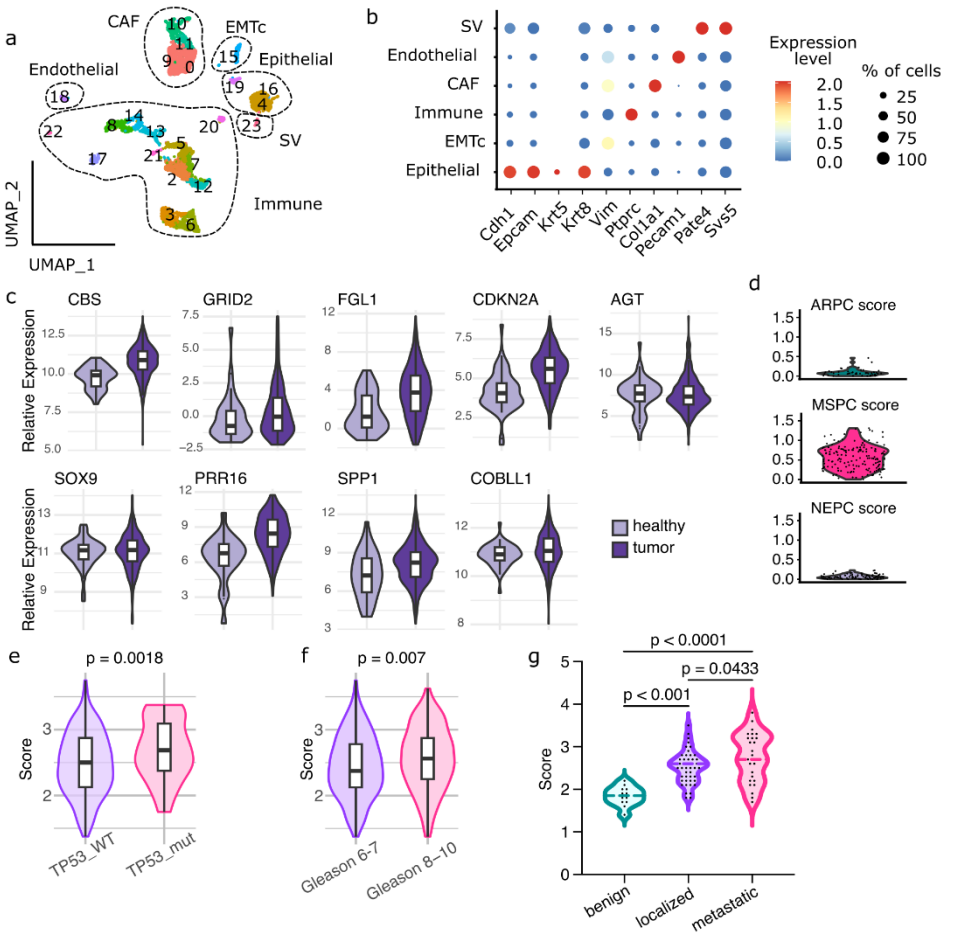

Figure 3. Single-cell transcriptomic analysis of Pten/Trp53$^{(i)pe-/-}$ prostates.

a. Uniform Manifold Approximation and Projection (UMAP) of single cell transcriptomic analysis of 5449 cells from dissociated prostates of Pten/Trp53$^{(i)pe-/-}$ mice 5 months AGI.

b. Dotplot of the average expression level of the marker genes used to annotate the cell populations, and the proportion of cell expressing them.

c. Violin plots of the 9 genes of the refined cluster 15 signature in prostate tumors and healthy tissue of the TCGA PRAD cohort.

d. Violin plots of the ARPC, MSPC and NEPC signature score described in Han et al. (2022) in EMTc cells.

e-f. Violin plots of the score of the EMTc signature in patients with wild-type (WT) or mutated TP53 (**e**) and in patients with intermediate risk (Gleason score 6-7) or high risk (Gleason score 8-10) prostate cancer (**f**) in the TCGA PRAD cohort. Unpaired Student T-test.

g. Violin plots of the score of the EMTc signature in benign tissue, localized or metastatic primary prostate tumors of patients (21). Multiple unpaired Student T-tests.

Figure 4

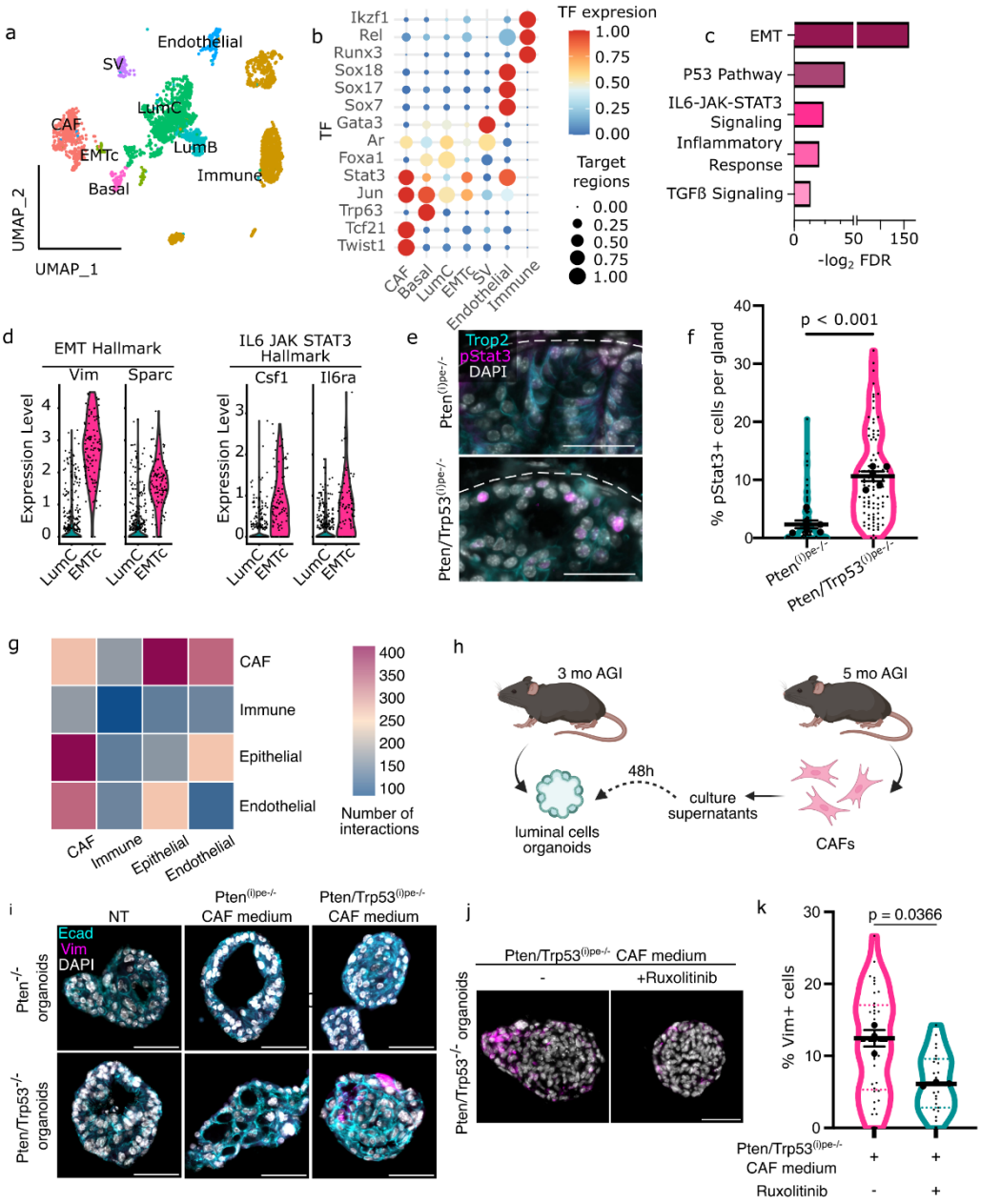
a
Endothelial
SV
LumC
CAF
LumB
EMTc
Immune
Basal
UMAP_2
UMAP_1
b
Ikzf1
Rel
Runx3
Sox18
Sox17
Sox7
Gata3
Ar
Foxa1
Stat3
Jun
Trp63
Tcf21
Twist1
TF
CAF
Basal
LumC
EMTc
SV
Endothelial
Immune
TF expresion
1.00
0.75
0.50
0.25
0.00
Target regions
0.00
0.25
0.50
0.75
1.00
c
EMT
P53 Pathway
IL6-JAK-STAT3 Signaling
Inflammatory Response
TGFß Signaling
0
50
150
-log2 FDR
d
EMT Hallmark
Vim
Sparc
Expression Level
IL6 JAK STAT3 Hallmark
Csf1
Il6ra
LumC
EMTc
e
Trop2
pStat3
DAPI
Pten(i)pe-/-
Pten/Trp53(i)pe-/-
f
p < 0.001
% pStat3+ cells per gland
g
CAF
Immune
Epithelial
Endothelial
Number of interactions
h
3 mo AGI
5 mo AGI
48h
culture supernatants
luminal cells organoids
CAFs
i
NT
Pten(i)pe-/- CAF medium
Pten/Trp53(i)pe-/- CAF medium
Ecad
Vim
DAPI
Pten-/- organoids
Pten/Trp53-/- organoids
j
Pten/Trp53(i)pe-/- CAF medium
-
+Ruxolitinib
Pten/Trp53-/- organoids
k
p = 0.0366
% Vim+ cells
Pten/Trp53(i)pe-/- CAF medium
Ruxolitinib

Figure 4. Characterisation of the signalling driving epithelial cell plasticity in prostatic tumors of Pten/Trp53$^{(i)pe-/-}$ mice

a. UMAP of Single-nuclei Assay for Transposase-Accessible Chromatin (ATAC) sequencing of 3973 cells from dissociated DLP of Pten/Trp53$^{(i)pe-/-}$ mice 5 months AGI.

b. Heatmap representing the eRegulons specific to the cell populations identified by SCENIC+. Color scale represents the transcript levels of the activator transcription factors (TF) and the dot size the enrichment of their motifs in open chromatin regions.

c. Gene Set Enrichment Analysis (GSEA) of transcripts upregulated in EMTc compared to LumC cells.

d. Violin plots of the transcript levels of the indicated genes selected from EMT and IL6JakStat3 hallmarks identified in **c**, in LumC cells and EMTc.

e. Representative immunofluorescent staining of pStat3 (magenta) and Trop2 (cyan) in DLP sections from Pten$^{(i)pe-/-}$ and Pten/Trp53$^{(i)pe-/-}$ mice 5 months AGI. Nuclei are stained with DAPI (white). Scale bar: 50 µm. n = 4 mice per genotype. Dashed line shows the limit of the gland.

f. Quantification of pStat3-positive cells located with less than 30 µm from basal lamina of glands in DLP of Pten$^{(i)pe-/-}$ and Pten/Trp53$^{(i)pe-/-}$ mice 5 months AGI. n ≥ 5 mice per group. Unpaired Student t-test.

g. Heatmap representing the number of interaction between the indicated cell populations in prostates of Pten/Trp53$^{(i)pe-/-}$ prostates 5 months AGI, determined by CellPhoneDB[21] analysis.

h. Schematic representation of the experimental procedure to evaluate the effect of culture media of CAFs isolated from mice 5 months AGI on organoids derived from DLPs of mutant mice 3 months AGI.

i. Representative immunofluorescent staining of E-cadherin (Ecad, cyan) and Vimentin (Vim, magenta) in Pten$^{-/-}$ and Pten/Trp53$^{-/-}$ organoids, treated or not (NT) with supernatants from cultured CAFs isolated from prostates of Pten$^{(i)pe-/-}$ or Pten/Trp53$^{(i)pe-/-}$ mice 5 months AGI. Nuclei are stained with DAPI (white). N = 3. Scale bar: 50 µm.

j-k. Representative immunofluorescent staining of Vimentin (Vim, magenta) (**j**) and quantification of Vim positive cells (**k**) in Pten/Trp53$^{-/-}$ organoids, treated with supernatants from cultured CAFs isolated from prostates of Pten/Trp53$^{(i)pe-/-}$ mice 5 months AGI, supplemented or not with Ruxolitinib (10 µM). Nuclei are stained with DAPI (white). N = 3. Scale bar: 50 µm. Unpaired Student t-test.

Figure 5

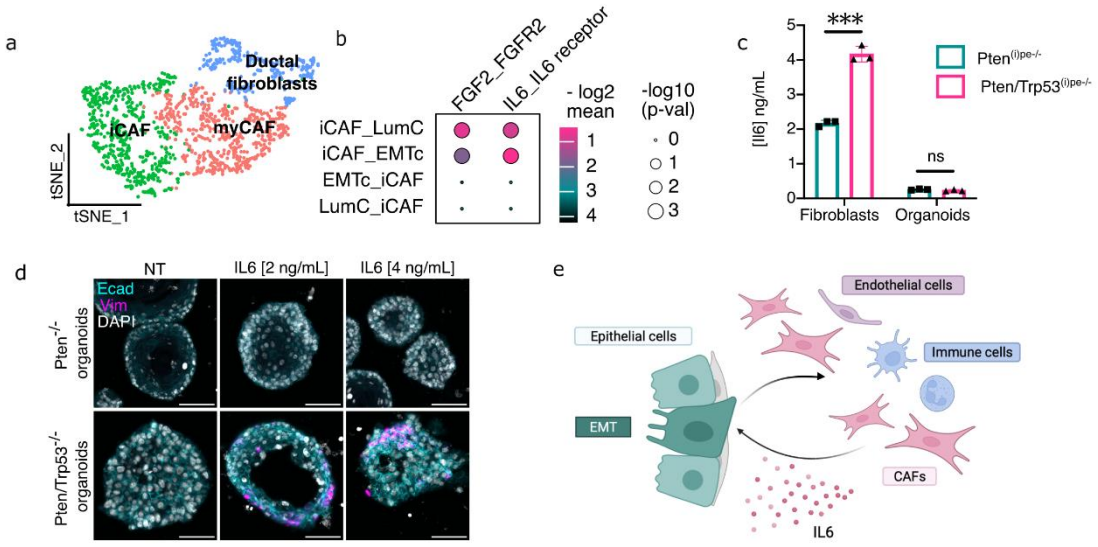

Figure 5. Characterization of the crosstalk between epithelial and stromal cells in prostatic tumors of Pten/Trp53$^{(i)pe-/-}$ mice.

a. t-SNE of fibroblast subpopulations in prostates of Pten/Trp53$^{(i)pe-/-}$ mice 5 months AGI.

b. Most significant unilateral interactions of the indicated secreted signaling between iCAFs and EMTc, or iCAFs and LumC cells. The first cell population in the interacting couple (interactant1_interactant2) expresses the ligand, and the second the receptor (ligand_receptor).

c. IL6 levels in culture supernatants of Pten$^{-/-}$ and Pten/Trp53$^{-/-}$organoids and fibroblasts isolated from prostates of Pten$^{(i)pe-/-}$ and Pten/Trp53$^{(i)pe-/-}$ mice, 5 months AGI. n = 3 mice per group. ns, non-significant, p≥0.05; *** p<0.001. Two-way ANOVA followed by Tukey's post-hoc.

d. Representative immunofluorescent staining of E-cadherin (Ecad, cyan) and Vimentin (Vim, magenta) in Pten$^{-/-}$ and Pten/Trp53$^{-/-}$ organoids, treated or not (NT) with IL6 at 2 and 4 ng/mL. Nuclei are stained with DAPI (white). Scale bar: 50 µm. n=3.

e. Schematic representation of the crosstalk between PECs and stromal cells stimulating CAFs to produce IL6 which in turn activates JAK/STAT3 signaling in PECs that promotes EMT.

Supplementary Figure 1

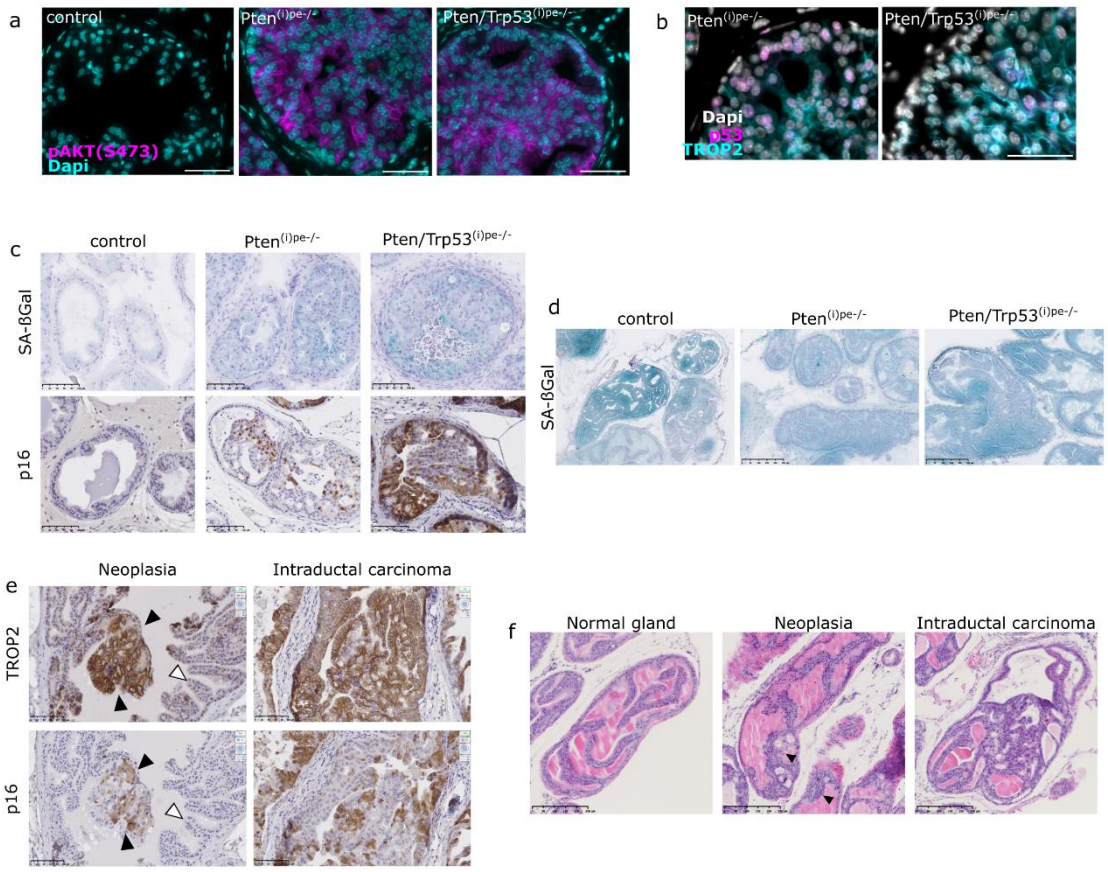

Figure S1. Validation of *Trp53* and/or *Pten* inactivation in PEC of mutant mice

a. Representative immunofluorescent staining of pAKT (S473) (magenta) in dorsolateral prostate (DLP) of control, Pten$^{(i)pe-/-}$ and Pten/Trp53$^{(i)pe-/-}$ mice 3 months AGI. Nuclei are stained with DAPI (cyan). Scale bar = 50 µm. n = 3 mice per group.

b. Representative immunofluorescent staining of p53 protein (magenta) and TROP2 (cyan) in DLP of Pten$^{(i)pe-/-}$ and Pten/Trp53$^{(i)pe-/-}$ mice 3 months AGI. Nuclei are stained with DAPI (white). Scale = 50 µm. n = 3 mice per group.

c. Representative staining of SA-ßGal and p16 immunodetection in DLP of control, Pten$^{(i)pe-/-}$ and Pten/Trp53$^{(i)pe-/-}$ mice 3 months AGI. Scale = 100 µm. n = 3 mice per group.

d. Representative staining of SA-ßGal in AP of control, Pten$^{(i)pe-/-}$ and Pten/Trp53$^{(i)pe-/-}$ mice 5 months AGI. Scale = 250 µm. n = 3 mice per group.

e. Representative TROP2 (upper panels) and p16 (lower panels) staining (brown) of AP sections from a Pten/Trp53$^{(i)pe-/-}$ mouse 5 months AGI**.** Low-grade neoplasia (left panels) and intraductal carcinoma (right panels). Black and white arrows point to neoplasia and normal epithelium, respectively. n ≥ 3 mice per group. Scale bar: 100 µm.

f. Representative HE staining of glands in AP of a Pten/Trp53$^{(i)pe-/-}$ mouse 5 months AGI. Left panel, normal gland; middle panel, PIN [arrow indicates neoplasia]; right panel, intraductal adenocarcinoma. Scale bar: 250 µm. n ≥ 3 mice per group.

Supplementary Figure 2

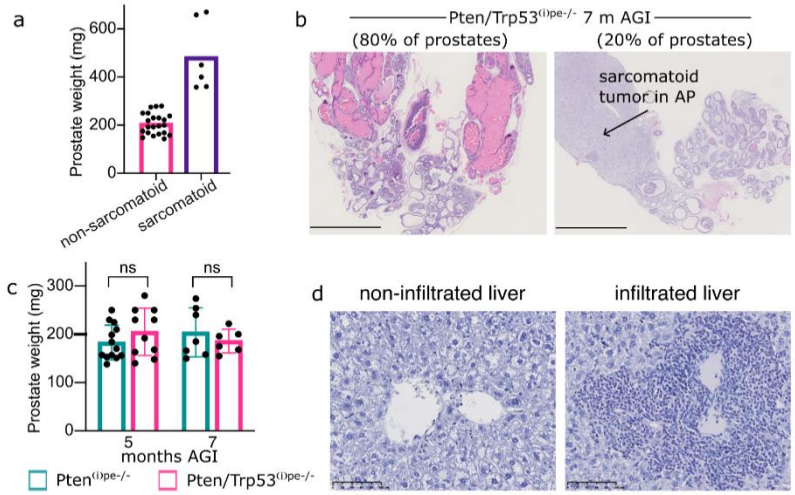

Figure S2. Characterization of prostate tumor progression in Pten/Trp53$^{(i)pe-/-}$ mice.

a. Weight of non-sarcomatoid and sarcomatoid prostates of Pten/Trp53$^{(i)pe-/-}$ mice 5-7 months AGI.

b. Representative HE staining of prostates of Pten/Trp53$^{(i)pe-/-}$ mice 7 months (m) AGI with (right) or without (left) a sarcomatoid tumor in the AP. Scale bar : 2.5 mm. n ≥ 5 mice per group.

c. Weight of non-sarcomatoid prostates of Pten$^{(i)pe-/-}$ and Pten/Trp53$^{(i)pe-/-}$ mice 5 and 7 months AGI.

d. Representative HE staining of non-infiltrated and infiltrated livers of Pten/Trp53$^{(i)pe-/-}$ mice 6 months AGI. Scale bar: 100 µm. n=15.

Supplementary Figure 3

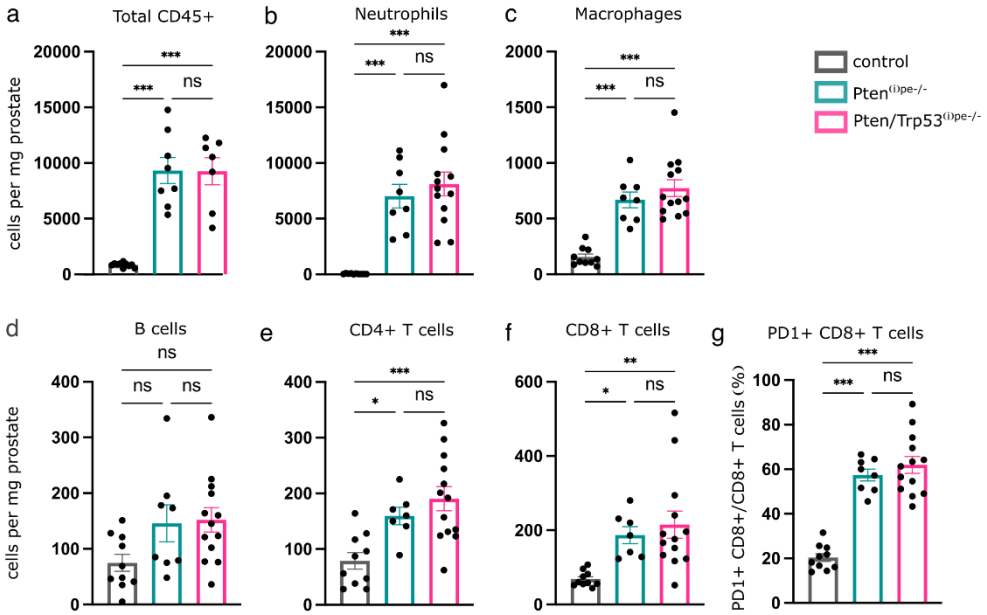

<u>Figure S3. Characterization of the immune microenvironment of Pten/Trp53$^{(i)pe-/-}$ mice 3 months AGI.</u>

a-f. Abundance of CD45^{+} cells **(a)**, Neutrophils **(b)**, Macrophages **(c)**, B-cells **(d)**, CD4+ T-cells **(e)** and CD8+ T-cells **(f)** in DLP of control, Pten$^{(i)pe-/-}$ and Pten/Trp53$^{(i)pe-/-}$ 5 months AGI. n ≥ 5 per group. 2-way ANOVA followed by Tukey's post-hoc test. ns, non-significant, p≥0,05; * p<0.05; ** p<0.01; *** p<0.001.

g. Proportion of PD1 positive cells among CD8^{+} T cells in DLPs of control, Pten$^{(i)pe-/-}$ and Pten/Trp53$^{(i)pe-/-}$ mice 3 months AGI. n ≥ 7 per group. 2-way ANOVA followed by Tukey's posthoc test. ns, non-significant, p≥0,05; *** p<0.001.

Supplementary Figure 4

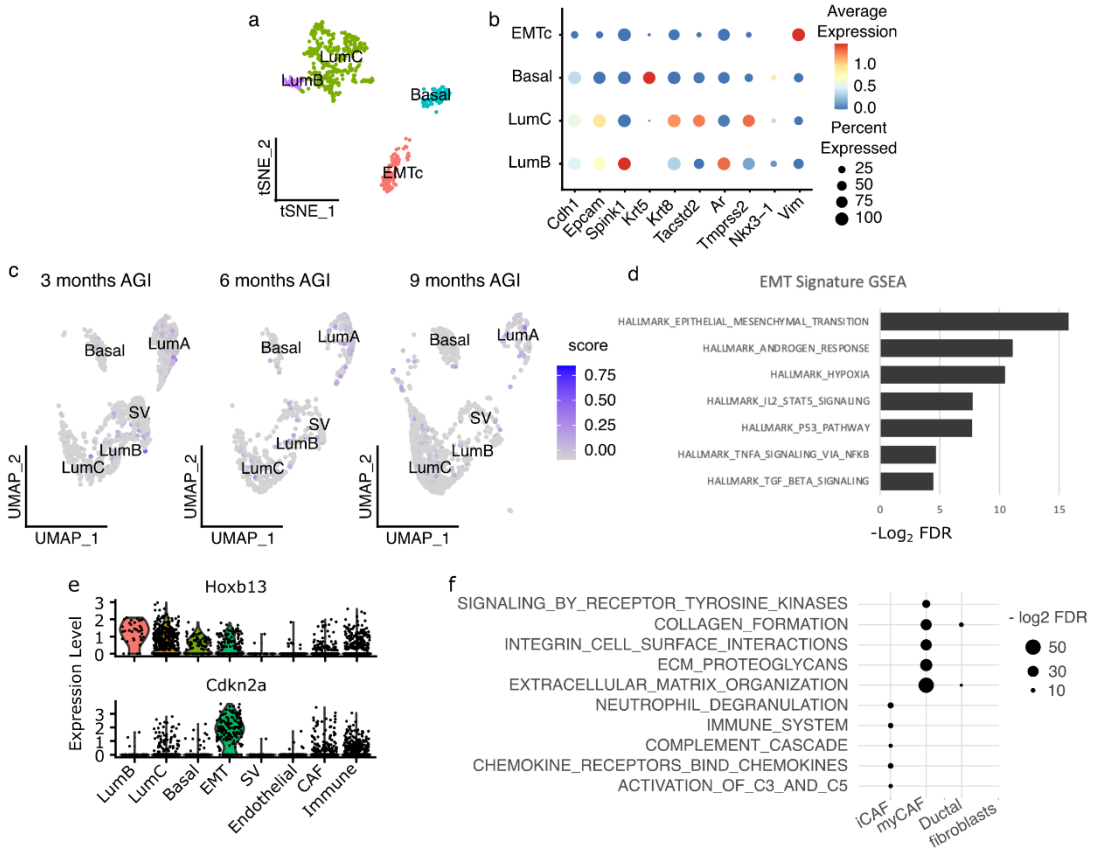

Figure S4. Single cell analyses of prostate tumors of Pten/Trp53$^{(i)pe-/-}$ mice.

a. t-SNE of epithelial subpopulations of Pten/Trp53$^{(i)pe-/-}$ prostates 5 months AGI identified by scRNAseq.

b. Dotplot of the average expression level of the marker genes used to annotate the cell populations shown in **a**, and the proportion of cell expressing them.

c. Cluster 15 signature score in PECs of Pten$^{(i)pe-/-}$ mice 3, 6 and 9 months AGI.

d. Gene Set Enrichment Analysis (GSEA) of the EMTc cluster signature.

e. Violin plots of *Hoxb13* and *Cdkn2a* in the indicated cell populations of a Pten/Trp53$^{(i)pe-/-}$ prostate 5 months AGI.

f. Gene Set Enrichment Analysis (GSEA) of signatures of CAF populations shown in **5a**.

Supplementary Figure 5

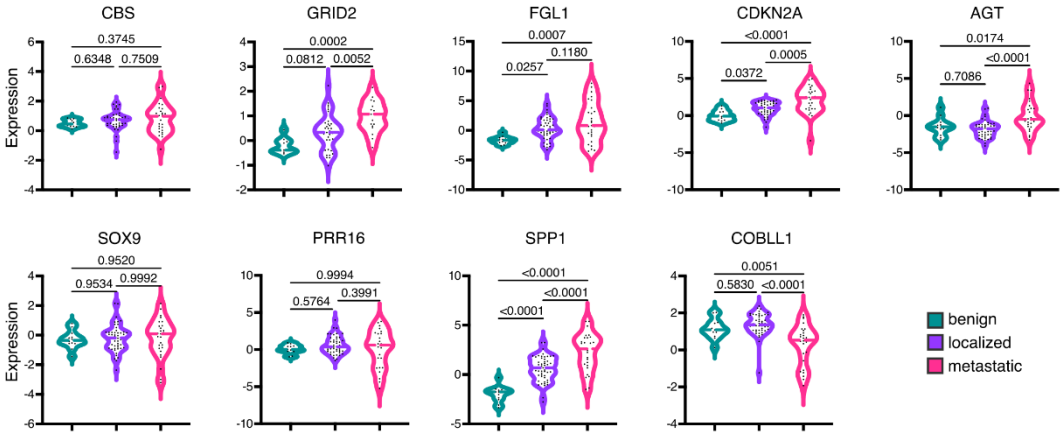

Figure S5. Expression level of genes of the EMTc signature in human prostate samples.
Violin plots of the 9 genes of the refined EMTc signature in the localized and metastatic human prostate tumors and benign tissues (Grasso et al., 2012).

Supplementary Figure 6

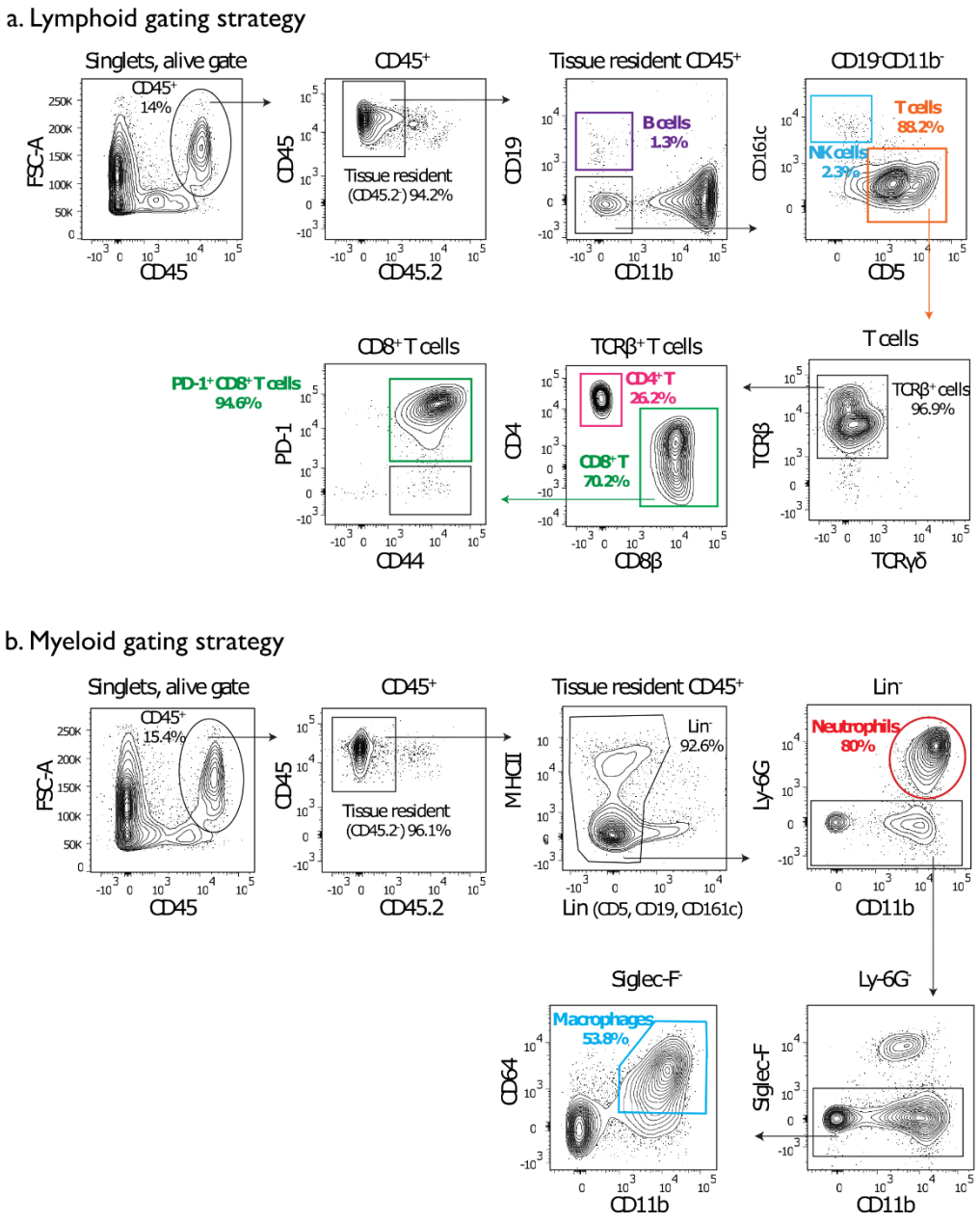

Figure S6. Strategy to quantify prostatic lymphoid and myeloid cells by flow cytometry.
Lymphoid cell (**a**) and myeloid cell (**b**) populations gating strategies. Dissociated cells of a DLP from a Pten/Trp53$^{(i)pe-/-}$ mouse 5 months AGI are shown.

Literature

Abate-Shen, C., Banach-Petrosky, W.A., Sun, X., Economides, K.D., Desai, N., Gregg, J.P., Borowsky, A.D., Cardiff, R.D., Shen, M.M., 2003. Nkx3.1; Pten mutant mice develop invasive prostate adenocarcinoma and lymph node metastases. Cancer Res. 63, 3886–3890.

Abate-Shen, C., Shen, M.M., Gelmann, E., 2008. Integrating differentiation and cancer: The Nkx3.1 homeobox gene in prostate organogenesis and carcinogenesis. Differentiation 76, 717–727. https://doi.org/10.1111/j.1432-0436.2008.00292.x

Abdulkadir, S.A., Magee, J.A., Peters, T.J., Kaleem, Z., Naughton, C.K., Humphrey, P.A., Milbrandt, J., 2002. Conditional Loss of *Nkx3.1* in Adult Mice Induces Prostatic Intraepithelial Neoplasia. Mol. Cell. Biol. 22, 1495–1503. https://doi.org/10.1128/MCB.22.5.1495-1503.2002

Abeshouse, A., Ahn, J., Akbani, R., Ally, A., Amin, S., Andry, C.D., Annala, M., Aprikian, A., Armenia, J., Arora, A., Auman, J.T., Balasundaram, M., Balu, S., Barbieri, C.E., Bauer, T., Benz, C.C., Bergeron, A., Beroukhim, R., Berrios, M., Bivol, A., Bodenheimer, T., Boice, L., Bootwalla, M.S., Borges dos Reis, R., Boutros, P.C., Bowen, J., Bowlby, R., Boyd, J., Bradley, R.K., Breggia, A., Brimo, F., Bristow, C.A., Brooks, D., Broom, B.M., Bryce, A.H., Bubley, G., Burks, E., Butterfield, Y.S.N., Button, M., Canes, D., Carlotti, C.G., Carlsen, R., Carmel, M., Carroll, P.R., Carter, S.L., Cartun, R., Carver, B.S., Chan, J.M., Chang, M.T., Chen, Y., Cherniack, A.D., Chevalier, S., Chin, L., Cho, J., Chu, A., Chuah, E., Chudamani, S., Cibulskis, K., Ciriello, G., Clarke, A., Cooperberg, M.R., Corcoran, N.M., Costello, A.J., Cowan, J., Crain, D., Curley, E., David, K., Demchok, J.A., Demichelis, F., Dhalla, N., Dhir, R., Doueik, A., Drake, B., Dvinge, H., Dyakova, N., Felau, I., Ferguson, M.L., Frazer, S., Freedland, S., Fu, Y., Gabriel, S.B., Gao, J., Gardner, J., Gastier-Foster, J.M., Gehlenborg, N., Gerken, M., Gerstein, M.B., Getz, G., Godwin, A.K., Gopalan, A., Graefen, M., Graim, K., Gribbin, T., Guin, R., Gupta, M., Hadjipanayis, A., Haider, S., Hamel, L., Hayes, D.N., Heiman, D.I., Hess, J., Hoadley, K.A., Holbrook, A.H., Holt, R.A., Holway, A., Hovens, C.M., Hoyle, A.P., Huang, M., Hutter, C.M., Ittmann, M., Iype, L., Jefferys, S.R., Jones, C.D., Jones, S.J.M., Juhl, H., Kahles, A., Kane, C.J., Kasaian, K., Kerger, M., Khurana, E., Kim, J., Klein, R.J., Kucherlapati, R., Lacombe, L., Ladanyi, M., Lai, P.H., Laird, P.W., Lander, E.S., Latour, M., Lawrence, M.S., Lau, K., LeBien, T., Lee, D., Lee, S., Lehmann, K.-V., Leraas, K.M., Leshchiner, I., Leung, R., Libertino, J.A., Lichtenberg, T.M., Lin, P., Linehan, W.M., Ling, S., Lippman, S.M., Liu, J., Liu, W., Lochovsky, L., Loda, M., Logothetis, C., Lolla, L., Longacre, T., Lu, Y., Luo, J., Ma, Y., Mahadeshwar, H.S., Mallery, D., Mariamidze, A., Marra, M.A., Mayo, M., McCall, S., McKercher, G., Meng, S., Mes-Masson, A.-M., Merino, M.J., Meyerson, M., Mieczkowski, P.A., Mills, G.B., Shaw, K.R.M., Minner, S., Moinzadeh, A., Moore, R.A., Morris, S., Morrison, C., Mose, L.E., Mungall, A.J., Murray, B.A., Myers, J.B., Naresh, R., Nelson, J., Nelson, M.A., Nelson, P.S., Newton, Y., Noble, M.S., Noushmehr, H., Nykter, M., Pantazi, A., Parfenov, M., Park, P.J., Parker, J.S., Paulauskis, J., Penny, R., Perou, C.M., Piché, A., Pihl, T., Pinto, P.A., Prandi, D., Protopopov, A., Ramirez, N.C., Rao, A., Rathmell, W.K., Rätsch, G., Ren, X., Reuter, V.E., Reynolds, S.M., Rhie, S.K., Rieger-Christ, K., Roach, J., Robertson, A.G., Robinson, B., Rubin, M.A., Saad, F., Sadeghi, S.,

Saksena, G., Saller, C., Salner, A., Sanchez-Vega, F., Sander, C., Sandusky, G., Sauter, G., Sboner, A., Scardino, P.T., Scarlata, E., Schein, J.E., Schlomm, T., Schmidt, L.S., Schultz, N., Schumacher, S.E., Seidman, J., Neder, L., Seth, S., Sharp, A., Shelton, C., Shelton, T., Shen, H., Shen, R., Sherman, M., Sheth, M., Shi, Y., Shih, J., Shmulevich, I., Simko, J., Simon, R., Simons, J.V., Sipahimalani, P., Skelly, T., Sofia, H.J., Soloway, M.G., Song, X., Sorcini, A., Sougnez, C., Stepa, S., Stewart, C., Stewart, J., Stuart, J.M., Sullivan, T.B., Sun, C., Sun, H., Tam, A., Tan, D., Tang, J., Tarnuzzer, R., Tarvin, K., Taylor, B.S., Teebagy, P., Tenggara, I., Têtu, B., Tewari, A., Thiessen, N., Thompson, T., Thorne, L.B., Tirapelli, D.P., Tomlins, S.A., Trevisan, F.A., Troncoso, P., True, L.D., Tsourlakis, M.C., Tyekucheva, S., Van Allen, E., Van Den Berg, D.J., Veluvolu, U., Verhaak, R., Vocke, C.D., Voet, D., Wan, Y., Wang, Q., Wang, W., Wang, Z., Weinhold, N., Weinstein, J.N., Weisenberger, D.J., Wilkerson, M.D., Wise, L., Witte, J., Wu, C.-C., Wu, J., Wu, Y., Xu, A.W., Yadav, S.S., Yang, Liming, Yang, Lixing, Yau, C., Ye, H., Yena, P., Zeng, T., Zenklusen, J.C., Zhang, H., Zhang, Jianhua, Zhang, Jiashan, Zhang, W., Zhong, Y., Zhu, K., Zmuda, E., 2015. The Molecular Taxonomy of Primary Prostate Cancer. Cell 163, 1011–1025. https://doi.org/10.1016/j.cell.2015.10.025

Abida, W., Cyrta, J., Heller, G., Prandi, D., Armenia, J., Coleman, I., Cieslik, M., Benelli, M., Robinson, D., Van Allen, E.M., Sboner, A., Fedrizzi, T., Mosquera, J.M., Robinson, B.D., De Sarkar, N., Kunju, L.P., Tomlins, S., Wu, Y.M., Nava Rodrigues, D., Loda, M., Gopalan, A., Reuter, V.E., Pritchard, C.C., Mateo, J., Bianchini, D., Miranda, S., Carreira, S., Rescigno, P., Filipenko, J., Vinson, J., Montgomery, R.B., Beltran, H., Heath, E.I., Scher, H.I., Kantoff, P.W., Taplin, M.-E., Schultz, N., deBono, J.S., Demichelis, F., Nelson, P.S., Rubin, M.A., Chinnaiyan, A.M., Sawyers, C.L., 2019. Genomic correlates of clinical outcome in advanced prostate cancer. Proc. Natl. Acad. Sci. 116, 11428–11436. https://doi.org/10.1073/pnas.1902651116

Abu El Maaty, M.A., Terzic, J., Keime, C., Rovito, D., Lutzing, R., Yanushko, D., Parisotto, M., Grelet, E., Namer, I.J., Lindner, V., Laverny, G., Metzger, D., 2022. Hypoxia-mediated stabilization of HIF1A in prostatic intraepithelial neoplasia promotes cell plasticity and malignant progression. Sci. Adv. 8, eabo2295. https://doi.org/10.1126/sciadv.abo2295

Ahn, J., Albanes, D., Peters, U., Schatzkin, A., Lim, U., Freedman, M., Chatterjee, N., Andriole, G.L., Leitzmann, M.F., Hayes, R.B., Prostate, Lung, Colorectal, and Ovarian Trial Project Team, 2007. Dairy products, calcium intake, and risk of prostate cancer in the prostate, lung, colorectal, and ovarian cancer screening trial. Cancer Epidemiol. Biomark. Prev. Publ. Am. Assoc. Cancer Res. Cosponsored Am. Soc. Prev. Oncol. 16, 2623–2630. https://doi.org/10.1158/1055-9965.EPI-07-0601

Ajmera, A., McKay, R.R., Stratton, K.L., 2023. Management of Metastatic Prostate Cancer. J. Natl. Compr. Canc. Netw. 21, 548–551. https://doi.org/10.6004/jnccn.2023.5004

Akinrinmade, O.A., Chetty, S., Daramola, A.K., Islam, M., Thepen, T., Barth, S., 2017. CD64: An Attractive Immunotherapeutic Target for M1-type Macrophage Mediated Chronic Inflammatory Diseases. Biomedicines 5, 56. https://doi.org/10.3390/biomedicines5030056

Almand, B., Clark, J.I., Nikitina, E., Van Beynen, J., English, N.R., Knight, S.C., Carbone, D.P., Gabrilovich, D.I., 2001. Increased Production of Immature Myeloid Cells in Cancer Patients: A Mechanism of Immunosuppression in Cancer. J. Immunol. 166, 678–689. https://doi.org/10.4049/jimmunol.166.1.678

Alshetaiwi, H., Pervolarakis, N., McIntyre, L.L., Ma, D., Nguyen, Q., Rath, J.A., Nee, K., Hernandez, G., Evans, K., Torosian, L., Silva, A., Walsh, C., Kessenbrock, K., 2020.

Defining the emergence of myeloid-derived suppressor cells in breast cancer using single-cell transcriptomics. Sci. Immunol. 5, eaay6017. https://doi.org/10.1126/sciimmunol.aay6017

Antonarakis, E.S., Piulats, J.M., Gross-Goupil, M., Goh, J., Ojamaa, K., Hoimes, C.J., Vaishampayan, U., Berger, R., Sezer, A., Alanko, T., De Wit, R., Li, C., Omlin, A., Procopio, G., Fukasawa, S., Tabata, K., Park, S.H., Feyerabend, S., Drake, C.G., Wu, H., Qiu, P., Kim, J., Poehlein, C., De Bono, J.S., 2020. Pembrolizumab for Treatment-Refractory Metastatic Castration-Resistant Prostate Cancer: Multicohort, Open-Label Phase II KEYNOTE-199 Study. J. Clin. Oncol. 38, 395–405. https://doi.org/10.1200/JCO.19.01638

Ardighieri, L., Missale, F., Bugatti, M., Gatta, L.B., Pezzali, I., Monti, M., Gottardi, S., Zanotti, L., Bignotti, E., Ravaggi, A., Tognon, G., Odicino, F., Calza, S., Missolo-Koussou, Y., Ries, C.H., Helft, J., Vermi, W., 2021. Infiltration by CXCL10 Secreting Macrophages Is Associated With Antitumor Immunity and Response to Therapy in Ovarian Cancer Subtypes. Front. Immunol. 12, 690201. https://doi.org/10.3389/fimmu.2021.690201

Arlen, P.M., Mohebtash, M., Madan, R.A., Gulley, J.L., 2009. Promising novel immunotherapies and combinations for prostate cancer. Future Oncol. 5, 187–196. https://doi.org/10.2217/14796694.5.2.187

Austyn, J.M., Gordon, S., 1981. F4/80, a monoclonal antibody directed specifically against the mouse macrophage. Eur. J. Immunol. 11, 805–815. https://doi.org/10.1002/eji.1830111013

Autio, K.A., Klebanoff, C.A., Schaer, D., Kauh, J.S.W., Slovin, S.F., Adamow, M., Blinder, V.S., Brahmachary, M., Carlsen, M., Comen, E., Danila, D.C., Doman, T.N., Durack, J.C., Fox, J.J., Gluskin, J.S., Hoffman, D.M., Kang, S., Kang, P., Landa, J., McAndrew, P.F., Modi, S., Morris, M.J., Novosiadly, R., Rathkopf, D.E., Sanford, R., Chapman, S.C., Tate, C.M., Yu, D., Wong, P., McArthur, H.L., 2020. Immunomodulatory Activity of a Colony-stimulating Factor-1 Receptor Inhibitor in Patients with Advanced Refractory Breast or Prostate Cancer: A Phase I Study. Clin. Cancer Res. 26, 5609–5620. https://doi.org/10.1158/1078-0432.CCR-20-0855

Baas, W., Gershburg, S., Dynda, D., Delfino, K., Robinson, K., Nie, D., Yearley, J.H., Alanee, S., 2017. Immune Characterization of the Programmed Death Receptor Pathway in High Risk Prostate Cancer. Clin. Genitourin. Cancer 15, 577–581. https://doi.org/10.1016/j.clgc.2017.04.002

Baeuerle, P.A., Reinhardt, C., 2009. Bispecific T-Cell Engaging Antibodies for Cancer Therapy. Cancer Res. 69, 4941–4944. https://doi.org/10.1158/0008-5472.CAN-09-0547

Bain, C.C., Bravo-Blas, A., Scott, C.L., Gomez Perdiguero, E., Geissmann, F., Henri, S., Malissen, B., Osborne, L.C., Artis, D., Mowat, A.M., 2014a. Constant replenishment from circulating monocytes maintains the macrophage pool in the intestine of adult mice. Nat. Immunol. 15, 929–937. https://doi.org/10.1038/ni.2967

Bain, C.C., Bravo-Blas, A., Scott, C.L., Gomez Perdiguero, E., Geissmann, F., Henri, S., Malissen, B., Osborne, L.C., Artis, D., Mowat, A.M., 2014b. Constant replenishment from circulating monocytes maintains the macrophage pool in the intestine of adult mice. Nat. Immunol. 15, 929–937. https://doi.org/10.1038/ni.2967

Bancaro, N., Calì, B., Troiani, M., Elia, A.R., Arzola, R.A., Attanasio, G., Lai, P., Crespo, M., Gurel, B., Pereira, R., Guo, C., Mosole, S., Brina, D., D'Ambrosio, M., Pasquini, E., Spataro, C., Zagato, E., Rinaldi, A., Pedotti, M., Di Lascio, S., Meani, F., Montopoli, M., Ferrari, M., Gallina, A., Varani, L., Pereira Mestre, R., Bolis, M., Gillessen Sommer, S., De Bono, J.,

Calcinotto, A., Alimonti, A., 2023. Apolipoprotein E induces pathogenic senescent-like myeloid cells in prostate cancer. Cancer Cell 41, 602-619.e11. https://doi.org/10.1016/j.ccell.2023.02.004

Baranska, A., Shawket, A., Jouve, M., Baratin, M., Malosse, C., Voluzan, O., Vu Manh, T.-P., Fiore, F., Bajénoff, M., Benaroch, P., Dalod, M., Malissen, M., Henri, S., Malissen, B., 2018. Unveiling skin macrophage dynamics explains both tattoo persistence and strenuous removal. J. Exp. Med. 215, 1115–1133. https://doi.org/10.1084/jem.20171608

Barbieri, C.E., Bangma, C.H., Bjartell, A., Catto, J.W.F., Culig, Z., Grönberg, H., Luo, J., Visakorpi, T., Rubin, M.A., 2013. The Mutational Landscape of Prostate Cancer. Eur. Urol. 64, 567–576. https://doi.org/10.1016/j.eururo.2013.05.029

Barclay, A.N., Brown, M.H., 2006. The SIRP family of receptors and immune regulation. Nat. Rev. Immunol. 6, 457–464. https://doi.org/10.1038/nri1859

Barclay, A.N., Van Den Berg, T.K., 2014. The Interaction Between Signal Regulatory Protein Alpha (SIRPα) and CD47: Structure, Function, and Therapeutic Target. Annu. Rev. Immunol. 32, 25–50. https://doi.org/10.1146/annurev-immunol-032713-120142

Bednarczyk, M., Stege, H., Grabbe, S., Bros, M., 2020. β2 Integrins—Multi-Functional Leukocyte Receptors in Health and Disease. Int. J. Mol. Sci. 21, 1402. https://doi.org/10.3390/ijms21041402

Beer, T.M., Kwon, E.D., Drake, C.G., Fizazi, K., Logothetis, C., Gravis, G., Ganju, V., Polikoff, J., Saad, F., Humanski, P., Piulats, J.M., Gonzalez Mella, P., Ng, S.S., Jaeger, D., Parnis, F.X., Franke, F.A., Puente, J., Carvajal, R., Sengeløv, L., McHenry, M.B., Varma, A., Van Den Eertwegh, A.J., Gerritsen, W., 2017. Randomized, Double-Blind, Phase III Trial of Ipilimumab Versus Placebo in Asymptomatic or Minimally Symptomatic Patients With Metastatic Chemotherapy-Naive Castration-Resistant Prostate Cancer. J. Clin. Oncol. 35, 40–47. https://doi.org/10.1200/JCO.2016.69.1584

Bellmunt, J., De Wit, R., Vaughn, D.J., Fradet, Y., Lee, J.-L., Fong, L., Vogelzang, N.J., Climent, M.A., Petrylak, D.P., Choueiri, T.K., Necchi, A., Gerritsen, W., Gurney, H., Quinn, D.I., Culine, S., Sternberg, C.N., Mai, Y., Poehlein, C.H., Perini, R.F., Bajorin, D.F., 2017. Pembrolizumab as Second-Line Therapy for Advanced Urothelial Carcinoma. N. Engl. J. Med. 376, 1015–1026. https://doi.org/10.1056/NEJMoa1613683

Bergers, G., Brekken, R., McMahon, G., Vu, T.H., Itoh, T., Tamaki, K., Tanzawa, K., Thorpe, P., Itohara, S., Werb, Z., Hanahan, D., 2000. Matrix metalloproteinase-9 triggers the angiogenic switch during carcinogenesis. Nat. Cell Biol. 2, 737–744. https://doi.org/10.1038/35036374

Berry, S.J., Coffey, D.S., Walsh, P.C., Ewing, L.L., 1984. The development of human benign prostatic hyperplasia with age. J. Urol. 132, 474–479. https://doi.org/10.1016/s0022-5347(17)49698-4

Bhatia-Gaur, R., Donjacour, A.A., Sciavolino, P.J., Kim, M., Desai, N., Young, P., Norton, C.R., Gridley, T., Cardiff, R.D., Cunha, G.R., Abate-Shen, C., Shen, M.M., 1999. Roles for Nkx3.1 in prostate development and cancer. Genes Dev. 13, 966–977. https://doi.org/10.1101/gad.13.8.966

Binnewies, M., Pollack, J.L., Rudolph, J., Dash, S., Abushawish, M., Lee, T., Jahchan, N.S., Canaday, P., Lu, E., Norng, M., Mankikar, S., Liu, V.M., Du, X., Chen, A., Mehta, R., Palmer, R., Juric, V., Liang, L., Baker, K.P., Reyno, L., Krummel, M.F., Streuli, M., Sriram, V., 2021. Targeting TREM2 on tumor-associated macrophages enhances immunotherapy. Cell Rep. 37, 109844. https://doi.org/10.1016/j.celrep.2021.109844

Bishop, J.L., Sio, A., Angeles, A., Roberts, M.E., Azad, A.A., Chi, K.N., Zoubeidi, A., 2015. PD-L1 is highly expressed in Enzalutamide resistant prostate cancer. Oncotarget 6, 234–242. https://doi.org/10.18632/oncotarget.2703

Blériot, C., Ginhoux, F., 2019. Understanding the Heterogeneity of Resident Liver Macrophages. Front. Immunol. 10, 2694. https://doi.org/10.3389/fimmu.2019.02694

Boivin, G., Faget, J., Ancey, P.-B., Gkasti, A., Mussard, J., Engblom, C., Pfirschke, C., Contat, C., Pascual, J., Vazquez, J., Bendriss-Vermare, N., Caux, C., Vozenin, M.-C., Pittet, M.J., Gunzer, M., Meylan, E., 2020. Durable and controlled depletion of neutrophils in mice. Nat. Commun. 11, 2762. https://doi.org/10.1038/s41467-020-16596-9

Borregaard, N., 2010. Neutrophils, from Marrow to Microbes. Immunity 33, 657–670. https://doi.org/10.1016/j.immuni.2010.11.011

Brinkmann, V., Reichard, U., Goosmann, C., Fauler, B., Uhlemann, Y., Weiss, D.S., Weinrauch, Y., Zychlinsky, A., 2004. Neutrophil Extracellular Traps Kill Bacteria. Science 303, 1532–1535. https://doi.org/10.1126/science.1092385

Brizzolara, A., Benelli, R., Venè, R., Barboro, P., Poggi, A., Tosetti, F., Ferrari, N., 2017. The ErbB family and androgen receptor signaling are targets of Celecoxib in prostate cancer. Cancer Lett. 400, 9–17. https://doi.org/10.1016/j.canlet.2017.04.025

Bronte, V., Kasic, T., Gri, G., Gallana, K., Borsellino, G., Marigo, I., Battistini, L., Iafrate, M., Prayer-Galetti, T., Pagano, F., Viola, A., 2005. Boosting antitumor responses of T lymphocytes infiltrating human prostate cancers. J. Exp. Med. 201, 1257–1268. https://doi.org/10.1084/jem.20042028

Brooks, C.L., Gu, W., 2006. p53 Ubiquitination: Mdm2 and Beyond. Mol. Cell 21, 307–315. https://doi.org/10.1016/j.molcel.2006.01.020

Brusa, D., Simone, M., Gontero, P., Spadi, R., Racca, P., Micari, J., Degiuli, M., Carletto, S., Tizzani, A., Matera, L., 2013. Circulating immunosuppressive cells of prostate cancer patients before and after radical prostatectomy: Profile comparison. Int. J. Urol. 20, 971–978. https://doi.org/10.1111/iju.12086

Burgess, M., Wicks, K., Gardasevic, M., Mace, K.A., 2019. Cx3CR1 Expression Identifies Distinct Macrophage Populations That Contribute Differentially to Inflammation and Repair. ImmunoHorizons 3, 262–273. https://doi.org/10.4049/immunohorizons.1900038

Burnet, F.M., 1970. The Concept of Immunological Surveillance, in: Schwartz, R.S. (Ed.), Progress in Tumor Research. S. Karger AG, pp. 1–27. https://doi.org/10.1159/000386035

Cai, C., Chen, Sen, Ng, P., Bubley, G.J., Nelson, P.S., Mostaghel, E.A., Marck, B., Matsumoto, A.M., Simon, N.I., Wang, H., Chen, Shaoyong, Balk, S.P., 2011. Intratumoral *De Novo* Steroid Synthesis Activates Androgen Receptor in Castration-Resistant Prostate Cancer and Is Upregulated by Treatment with CYP17A1 Inhibitors. Cancer Res. 71, 6503–6513. https://doi.org/10.1158/0008-5472.CAN-11-0532

Cai, T., Santi, R., Tamanini, I., Galli, I.C., Perletti, G., Bjerklund Johansen, T.E., Nesi, G., 2019. Current Knowledge of the Potential Links between Inflammation and Prostate Cancer. Int. J. Mol. Sci. 20, 3833. https://doi.org/10.3390/ijms20153833

Calcinotto, A., Kohli, J., Zagato, E., Pellegrini, L., Demaria, M., Alimonti, A., 2019. Cellular Senescence: Aging, Cancer, and Injury. Physiol. Rev. 99, 1047–1078. https://doi.org/10.1152/physrev.00020.2018

Calderon, B., Carrero, J.A., Ferris, S.T., Sojka, D.K., Moore, L., Epelman, S., Murphy, K.M., Yokoyama, W.M., Randolph, G.J., Unanue, E.R., 2015. The pancreas anatomy

conditions the origin and properties of resident macrophages. J. Exp. Med. 212, 1497–1512. https://doi.org/10.1084/jem.20150496

Cannarile, M.A., Weisser, M., Jacob, W., Jegg, A.-M., Ries, C.H., Rüttinger, D., 2017. Colony-stimulating factor 1 receptor (CSF1R) inhibitors in cancer therapy. J. Immunother. Cancer 5, 53. https://doi.org/10.1186/s40425-017-0257-y

Casanova-Acebes, M., Dalla, E., Leader, A.M., LeBerichel, J., Nikolic, J., Morales, B.M., Brown, M., Chang, C., Troncoso, L., Chen, S.T., Sastre-Perona, A., Park, M.D., Tabachnikova, A., Dhainaut, M., Hamon, P., Maier, B., Sawai, C.M., Agulló-Pascual, E., Schober, M., Brown, B.D., Reizis, B., Marron, T., Kenigsberg, E., Moussion, C., Benaroch, P., Aguirre-Ghiso, J.A., Merad, M., 2021. Tissue-resident macrophages provide a pro-tumorigenic niche to early NSCLC cells. Nature 595, 578–584. https://doi.org/10.1038/s41586-021-03651-8

Cecchini, M.G., Dominguez, M.G., Mocci, S., Wetterwald, A., Felix, R., Fleisch, H., Chisholm, O., Hofstetter, W., Pollard, J.W., Stanley, E.R., 1994. Role of colony stimulating factor-1 in the establishment and regulation of tissue macrophages during postnatal development of the mouse. Development 120, 1357–1372. https://doi.org/10.1242/dev.120.6.1357

Cetintas, V.B., Batada, N.N., 2020. Is there a causal link between PTEN deficient tumors and immunosuppressive tumor microenvironment? J. Transl. Med. 18, 45. https://doi.org/10.1186/s12967-020-02219-w

Cha, H.-R., Lee, J.H., Ponnazhagan, S., 2020. Revisiting Immunotherapy: A Focus on Prostate Cancer. Cancer Res. 80, 1615–1623. https://doi.org/10.1158/0008-5472.CAN-19-2948

Chakarov, S., Lim, H.Y., Tan, L., Lim, S.Y., See, P., Lum, J., Zhang, X.-M., Foo, S., Nakamizo, S., Duan, K., Kong, W.T., Gentek, R., Balachander, A., Carbajo, D., Bleriot, C., Malleret, B., Tam, J.K.C., Baig, S., Shabeer, M., Toh, S.-A.E.S., Schlitzer, A., Larbi, A., Marichal, T., Malissen, B., Chen, J., Poidinger, M., Kabashima, K., Bajenoff, M., Ng, L.G., Angeli, V., Ginhoux, F., 2019. Two distinct interstitial macrophage populations coexist across tissues in specific subtissular niches. Science 363, eaau0964. https://doi.org/10.1126/science.aau0964

Champion, B.R., Fisher, K., Seymour, L., 2016. A PTENtial cause for the selectivity of oncolytic viruses? Nat. Immunol. 17, 225–226. https://doi.org/10.1038/ni.3394

Chang, R.B., Beatty, G.L., 2020. The interplay between innate and adaptive immunity in cancer shapes the productivity of cancer immunosurveillance. J. Leukoc. Biol. JLB.3MIR0320-475R. https://doi.org/10.1002/JLB.3MIR0320-475R

Chaplin, D.D., 2010. Overview of the immune response. J. Allergy Clin. Immunol. 125, S3–S23. https://doi.org/10.1016/j.jaci.2009.12.980

Chen, D.S., Mellman, I., 2017. Elements of cancer immunity and the cancer–immune set point. Nature 541, 321–330. https://doi.org/10.1038/nature21349

Chen, Z., Trotman, L.C., Shaffer, D., Lin, H.-K., Dotan, Z.A., Niki, M., Koutcher, J.A., Scher, H.I., Ludwig, T., Gerald, W., Cordon-Cardo, C., Paolo Pandolfi, P., 2005. Crucial role of p53-dependent cellular senescence in suppression of Pten-deficient tumorigenesis. Nature 436, 725–730. https://doi.org/10.1038/nature03918

Cheng, S., Li, Z., Gao, R., Xing, B., Gao, Y., Yang, Yu, Qin, S., Zhang, L., Ouyang, H., Du, P., Jiang, L., Zhang, B., Yang, Yue, Wang, X., Ren, X., Bei, J.-X., Hu, X., Bu, Z., Ji, J., Zhang, Z., 2021. A pan-cancer single-cell transcriptional atlas of tumor infiltrating myeloid cells. Cell 184, 792-809.e23. https://doi.org/10.1016/j.cell.2021.01.010

Cheng, X., Wang, X., Nie, K., Cheng, L., Zhang, Z., Hu, Y., Peng, W., 2021. Systematic Pan-Cancer Analysis Identifies TREM2 as an Immunological and Prognostic Biomarker. Front. Immunol. 12, 646523. https://doi.org/10.3389/fimmu.2021.646523

Cheng, Y., Mo, F., Li, Q., Han, X., Shi, H., Chen, S., Wei, Y., Wei, X., 2021. Targeting CXCR2 inhibits the progression of lung cancer and promotes therapeutic effect of cisplatin. Mol. Cancer 20, 62. https://doi.org/10.1186/s12943-021-01355-1

Chi, N., Tan, Z., Ma, K., Bao, L., Yun, Z., 2014. Increased circulating myeloid-derived suppressor cells correlate with cancer stages, interleukin-8 and -6 in prostate cancer. Int. J. Clin. Exp. Med. 7, 3181–3192.

Chughtai, B., Forde, J.C., Thomas, D.D.M., Laor, L., Hossack, T., Woo, H.H., Te, A.E., Kaplan, S.A., 2016. Benign prostatic hyperplasia. Nat. Rev. Dis. Primer 2, 16031. https://doi.org/10.1038/nrdp.2016.31

Cleutjens, K.B.J.. M., Van Der Korput, H.A.G.M., Ehren-van Eekelen, C.C., Sikes, R.A., Fasciana, C., Chung, L.W., Trapman, J., 1997. A 6-kb Promoter Fragment Mimics in Transgenic Mice the Prostate-Specific and Androgen-Regulated Expression of the Endogenous Prostate-Specific Antigen Gene in Humans. Mol. Endocrinol. 11, 1256–1265. https://doi.org/10.1210/mend.11.9.9974

Coffelt, S.B., Wellenstein, M.D., De Visser, K.E., 2016. Neutrophils in cancer: neutral no more. Nat. Rev. Cancer 16, 431–446. https://doi.org/10.1038/nrc.2016.52

Colombo, M.P., Ferrari, G., Stoppacciaro, A., Parenza, M., Rodolfo, M., Mavilio, F., Parmiani, G., 1991. Granulocyte colony-stimulating factor gene transfer suppresses tumorigenicity of a murine adenocarcinoma in vivo. J. Exp. Med. 173, 889–897. https://doi.org/10.1084/jem.173.4.889

Conley-LaComb, M.K., Saliganan, A., Kandagatla, P., Chen, Y.Q., Cher, M.L., Chinni, S.R., 2013. PTEN loss mediated Akt activation promotes prostate tumor growth and metastasis via CXCL12/CXCR4 signaling. Mol. Cancer 12, 85. https://doi.org/10.1186/1476-4598-12-85

Cools-Lartigue, J., Spicer, J., McDonald, B., Gowing, S., Chow, S., Giannias, B., Bourdeau, F., Kubes, P., Ferri, L., 2013. Neutrophil extracellular traps sequester circulating tumor cells and promote metastasis. J. Clin. Invest. 123, 3446–3458. https://doi.org/10.1172/JCI67484

Copeland, B.T., Shallal, H., Shen, C., Pienta, K.J., Foss, C.A., Pomper, M.G., 2019. Imaging and Characterization of Macrophage Distribution in Mouse Models of Human Prostate Cancer. Mol. Imaging Biol. 21, 1054–1063. https://doi.org/10.1007/s11307-019-01318-5

Courtois-Cox, S., Jones, S.L., Cichowski, K., 2008. Many roads lead to oncogene-induced senescence. Oncogene 27, 2801–2809. https://doi.org/10.1038/sj.onc.1210950

Cowland, J.B., Borregaard, N., 2016. Granulopoiesis and granules of human neutrophils. Immunol. Rev. 273, 11–28. https://doi.org/10.1111/imr.12440

Cristofano, A.D., Pesce, B., Cordon-Cardo, C., Pandolfi, P.P., 1998. Pten is essential for embryonic development and tumour suppression. Nat. Genet. 19, 348–355. https://doi.org/10.1038/1235

Cunha, G.R., Donjacour, A.A., Cooke, P.S., Mee, H., Bigsby, R.M., Higgins, S.J., Sugimura, Y., 1987. The Endocrinology and Developmental Biology of the Prostate*. Endocr. Rev. 8, 338–362. https://doi.org/10.1210/edrv-8-3-338

Dagenais, A., Villalba-Guerrero, C., Olivier, M., 2023. Trained immunity: A “new” weapon in the fight against infectious diseases. Front. Immunol. 14, 1147476. https://doi.org/10.3389/fimmu.2023.1147476

Dai, X.-M., Ryan, G.R., Hapel, A.J., Dominguez, M.G., Russell, R.G., Kapp, S., Sylvestre, V., Stanley, E.R., 2002. Targeted disruption of the mouse colony-stimulating factor 1 receptor gene results in osteopetrosis, mononuclear phagocyte deficiency, increased primitive progenitor cell frequencies, and reproductive defects. Blood 99, 111–120. https://doi.org/10.1182/blood.V99.1.111

D’Amico, A.V., Whittington, R., Malkowicz, S.B., Schultz, D., Blank, K., Broderick, G.A., Tomaszewski, J.E., Renshaw, A.A., Kaplan, I., Beard, C.J., Wein, A., 1998. Biochemical outcome after radical prostatectomy, external beam radiation therapy, or interstitial radiation therapy for clinically localized prostate cancer. JAMA 280, 969–974. https://doi.org/10.1001/jama.280.11.969

De Groot, A.E., Myers, K.V., Krueger, T.E.G., Kiemen, A.L., Nagy, N.H., Brame, A., Torres, V.E., Zhang, Z., Trabzonlu, L., Brennen, W.N., Wirtz, D., De Marzo, A.M., Amend, S.R., Pienta, K.J., 2021. Characterization of tumor-associated macrophages in prostate cancer transgenic mouse models. The Prostate 81, 629–647. https://doi.org/10.1002/pros.24139

De Groot, C.J.A., Huppes, W., Sminia, T., Kraal, G., Dijkstra, C.D., 1992. Determination of the origin and nature of brain macrophages and microglial cells in mouse central nervous system, using non-radioactive in situ hybridization and immunoperoxidase techniques. Glia 6, 301–309. https://doi.org/10.1002/glia.440060408

Debacker, J.M., Gondry, O., Lahoutte, T., Keyaerts, M., Huvenne, W., 2021. The Prognostic Value of CD206 in Solid Malignancies: A Systematic Review and Meta-Analysis. Cancers 13, 3422. https://doi.org/10.3390/cancers13143422

Decker, K.F., Zheng, D., He, Y., Bowman, T., Edwards, J.R., Jia, L., 2012. Persistent androgen receptor-mediated transcription in castration-resistant prostate cancer under androgen-deprived conditions. Nucleic Acids Res. 40, 10765–10779. https://doi.org/10.1093/nar/gks888

Deegen, P., Thomas, O., Nolan-Stevaux, O., Li, S., Wahl, J., Bogner, P., Aeffner, F., Friedrich, M., Liao, M.Z., Matthes, K., Rau, D., Rattel, B., Raum, T., Kufer, P., Coxon, A., Bailis, J.M., 2021. The PSMA-targeting Half-life Extended BiTE Therapy AMG 160 has Potent Antitumor Activity in Preclinical Models of Metastatic Castration-resistant Prostate Cancer. Clin. Cancer Res. 27, 2928–2937. https://doi.org/10.1158/1078-0432.CCR-20-3725

Di Mitri, D., Mirenda, M., Vasilevska, J., Calcinotto, A., Delaleu, N., Revandkar, A., Gil, V., Boysen, G., Losa, M., Mosole, S., Pasquini, E., D’Antuono, R., Masetti, M., Zagato, E., Chiorino, G., Ostano, P., Rinaldi, A., Gnetti, L., Graupera, M., Martins Figueiredo Fonseca, A.R., Pereira Mestre, R., Waugh, D., Barry, S., De Bono, J., Alimonti, A., 2019. Re-education of Tumor-Associated Macrophages by CXCR2 Blockade Drives Senescence and Tumor Inhibition in Advanced Prostate Cancer. Cell Rep. 28, 2156-2168.e5. https://doi.org/10.1016/j.celrep.2019.07.068

Di Mitri, D., Toso, A., Chen, J.J., Sarti, M., Pinton, S., Jost, T.R., D’Antuono, R., Montani, E., Garcia-Escudero, R., Guccini, I., Da Silva-Alvarez, S., Collado, M., Eisenberger, M., Zhang, Z., Catapano, C., Grassi, F., Alimonti, A., 2014. Tumour-infiltrating Gr-1+ myeloid cells antagonize senescence in cancer. Nature 515, 134–137. https://doi.org/10.1038/nature13638

Dick, S.A., Wong, A., Hamidzada, H., Nejat, S., Nechanitzky, R., Vohra, S., Mueller, B., Zaman, R., Kantores, C., Aronoff, L., Momen, A., Nechanitzky, D., Li, W.Y., Ramachandran, P., Crome, S.Q., Becher, B., Cybulsky, M.I., Billia, F., Keshavjee, S., Mital, S., Robbins, C.S., Mak, T.W., Epelman, S., 2022. Three tissue resident macrophage subsets coexist across organs with conserved origins and life cycles. Sci. Immunol. 7, eabf7777. https://doi.org/10.1126/sciimmunol.abf7777

Ding, Z., Wu, C.-J., Jaskelioff, M., Ivanova, E., Kost-Alimova, M., Protopopov, A., Chu, G.C., Wang, G., Lu, X., Labrot, E.S., Hu, J., Wang, W., Xiao, Y., Zhang, H., Zhang, Jianhua, Zhang, Jingfang, Gan, B., Perry, S.R., Jiang, S., Li, L., Horner, J.W., Wang, Y.A., Chin, L., DePinho, R.A., 2012. Telomerase Reactivation following Telomere Dysfunction Yields Murine Prostate Tumors with Bone Metastases. Cell 148, 896–907. https://doi.org/10.1016/j.cell.2012.01.039

Dizman, N., Buchbinder, E.I., 2021. Cancer Therapy Targeting CD47/SIRPα. Cancers 13, 6229. https://doi.org/10.3390/cancers13246229

Dorff, T., Hirasawa, Y., Acoba, J., Pagano, I., Tamura, D., Pal, S., Zhang, M., Waitz, R., Dhal, A., Haynes, W., Shon, J., Scholz, M., Furuya, H., Chan, O.T.M., Huang, J., Rosser, C., 2021. Phase Ib study of patients with metastatic castrate-resistant prostate cancer treated with different sequencing regimens of atezolizumab and sipuleucel-T. J. Immunother. Cancer 9, e002931. https://doi.org/10.1136/jitc-2021-002931

Drachenberg, D.E., Elgamal, A.-A.A., Rowbotham, R., Peterson, M., Murphy, G.P., 1999. Circulating levels of interleukin-6 in patients with hormone refractory prostate cancer. The Prostate 41, 127–133. https://doi.org/10.1002/(SICI)1097-0045(19991001)41:2<127::AID-PROS7>3.0.CO;2-H

Drake, C.G., 2010. Prostate cancer as a model for tumour immunotherapy. Nat. Rev. Immunol. 10, 580–593. https://doi.org/10.1038/nri2817

Dunn, G.P., Old, L.J., Schreiber, R.D., 2004. The Immunobiology of Cancer Immunosurveillance and Immunoediting. Immunity 21, 137–148. https://doi.org/10.1016/j.immuni.2004.07.017

Dwyer, D.F., Barrett, N.A., Austen, K.F., 2016. Expression profiling of constitutive mast cells reveals a unique identity within the immune system. Nat. Immunol. 17, 878–887. https://doi.org/10.1038/ni.3445

Eash, K.J., Greenbaum, A.M., Gopalan, P.K., Link, D.C., 2010. CXCR2 and CXCR4 antagonistically regulate neutrophil trafficking from murine bone marrow. J. Clin. Invest. 120, 2423–2431. https://doi.org/10.1172/JCI41649

Eastham, J.A., Stapleton, A.M., Gousse, A.E., Timme, T.L., Yang, G., Slawin, K.M., Wheeler, T.M., Scardino, P.T., Thompson, T.C., 1995. Association of p53 mutations with metastatic prostate cancer. Clin. Cancer Res. Off. J. Am. Assoc. Cancer Res. 1, 1111–1118.

Eisermann, K., Wang, D., Jing, Y., Pascal, L.E., Wang, Z., 2013. Androgen receptor gene mutation, rearrangement, polymorphism. Transl. Androl. Urol. 2, 137–147. https://doi.org/10.3978/j.issn.2223-4683.2013.09.15

Ellis, P.M., Vella, E.T., Ung, Y.C., 2017. Immune Checkpoint Inhibitors for Patients With Advanced Non–Small-Cell Lung Cancer: A Systematic Review. Clin. Lung Cancer 18, 444-459.e1. https://doi.org/10.1016/j.cllc.2017.02.001

Ellwood-Yen, K., Graeber, T.G., Wongvipat, J., Iruela-Arispe, M.L., Zhang, J., Matusik, R., Thomas, G.V., Sawyers, C.L., 2003. Myc-driven murine prostate cancer shares

molecular features with human prostate tumors. Cancer Cell 4, 223–238. https://doi.org/10.1016/S1535-6108(03)00197-1

Epstein, J.I., Egevad, L., Amin, M.B., Delahunt, B., Srigley, J.R., Humphrey, P.A., Grading Committee, 2016. The 2014 International Society of Urological Pathology (ISUP) Consensus Conference on Gleason Grading of Prostatic Carcinoma: Definition of Grading Patterns and Proposal for a New Grading System. Am. J. Surg. Pathol. 40, 244–252. https://doi.org/10.1097/PAS.0000000000000530

Escamilla, J., Schokrpur, S., Liu, C., Priceman, S.J., Moughon, D., Jiang, Z., Pouliot, F., Magyar, C., Sung, J.L., Xu, J., Deng, G., West, B.L., Bollag, G., Fradet, Y., Lacombe, L., Jung, M.E., Huang, J., Wu, L., 2015. CSF1 Receptor Targeting in Prostate Cancer Reverses Macrophage-Mediated Resistance to Androgen Blockade Therapy. Cancer Res. 75, 950–962. https://doi.org/10.1158/0008-5472.CAN-14-0992

Esparza-Baquer, A., Labiano, I., Sharif, O., Agirre-Lizaso, A., Oakley, F., Rodrigues, P.M., Zhuravleva, E., O'Rourke, C.J., Hijona, E., Jimenez-Agüero, R., Riaño, I., Landa, A., La Casta, A., Zaki, M.Y.W., Munoz-Garrido, P., Azkargorta, M., Elortza, F., Vogel, A., Schabbauer, G., Aspichueta, P., Andersen, J.B., Knapp, S., Mann, D.A., Bujanda, L., Banales, J.M., Perugorria, M.J., 2021. TREM-2 defends the liver against hepatocellular carcinoma through multifactorial protective mechanisms. Gut 70, 1345–1361. https://doi.org/10.1136/gutjnl-2019-319227

Evrard, M., Kwok, I.W.H., Chong, S.Z., Teng, K.W.W., Becht, E., Chen, J., Sieow, J.L., Penny, H.L., Ching, G.C., Devi, S., Adrover, J.M., Li, J.L.Y., Liong, K.H., Tan, L., Poon, Z., Foo, S., Chua, J.W., Su, I.-H., Balabanian, K., Bachelerie, F., Biswas, S.K., Larbi, A., Hwang, W.Y.K., Madan, V., Koeffler, H.P., Wong, S.C., Newell, E.W., Hidalgo, A., Ginhoux, F., Ng, L.G., 2018. Developmental Analysis of Bone Marrow Neutrophils Reveals Populations Specialized in Expansion, Trafficking, and Effector Functions. Immunity 48, 364-379.e8. https://doi.org/10.1016/j.immuni.2018.02.002

Fizazi, K., Drake, C.G., Beer, T.M., Kwon, E.D., Scher, H.I., Gerritsen, W.R., Bossi, A., Den Eertwegh, A.J.M.V., Krainer, M., Houede, N., Santos, R., Mahammedi, H., Ng, S., Danielli, R., Franke, F.A., Sundar, S., Agarwal, N., Bergman, A.M., Ciuleanu, T.E., Korbenfeld, E., Sengeløv, L., Hansen, S., McHenry, M.B., Chen, A., Logothetis, C., 2020. Final Analysis of the Ipilimumab Versus Placebo Following Radiotherapy Phase III Trial in Postdocetaxel Metastatic Castration-resistant Prostate Cancer Identifies an Excess of Long-term Survivors. Eur. Urol. 78, 822–830. https://doi.org/10.1016/j.eururo.2020.07.032

Fong, L., Kwek, S.S., O'Brien, S., Kavanagh, B., McNeel, D.G., Weinberg, V., Lin, A.M., Rosenberg, J., Ryan, C.J., Rini, B.I., Small, E.J., 2009. Potentiating Endogenous Antitumor Immunity to Prostate Cancer through Combination Immunotherapy with CTLA4 Blockade and GM-CSF. Cancer Res. 69, 609–615. https://doi.org/10.1158/0008-5472.CAN-08-3529

Francini, E., Gray, K.P., Shaw, G.K., Evan, C.P., Hamid, A.A., Perry, C.E., Kantoff, P.W., Taplin, M.-E., Sweeney, C.J., 2019. Impact of new systemic therapies on overall survival of patients with metastatic castration-resistant prostate cancer in a hospital-based registry. Prostate Cancer Prostatic Dis. 22, 420–427. https://doi.org/10.1038/s41391-018-0121-2

Francisco, L.M., Sage, P.T., Sharpe, A.H., 2010. The PD-1 pathway in tolerance and autoimmunity. Immunol. Rev. 236, 219–242. https://doi.org/10.1111/j.1600-065X.2010.00923.x

Freeman, K.W., Welm, B.E., Gangula, R.D., Rosen, J.M., Ittmann, M., Greenberg, N.M., Spencer, D.M., 2003. Inducible prostate intraepithelial neoplasia with reversible hyperplasia in conditional FGFR1-expressing mice. Cancer Res. 63, 8256–8263.

Fridlender, Z.G., Sun, J., Kim, S., Kapoor, V., Cheng, G., Ling, L., Worthen, G.S., Albelda, S.M., 2009. Polarization of Tumor-Associated Neutrophil Phenotype by TGF-β: "N1" versus "N2" TAN. Cancer Cell 16, 183–194. https://doi.org/10.1016/j.ccr.2009.06.017

Gabrilovich, D.I., Bronte, V., Chen, S.-H., Colombo, M.P., Ochoa, A., Ostrand-Rosenberg, S., Schreiber, H., 2007. The Terminology Issue for Myeloid-Derived Suppressor Cells. Cancer Res. 67, 425–425. https://doi.org/10.1158/0008-5472.CAN-06-3037

Gann, P.H., 2002. Risk factors for prostate cancer. Rev. Urol. 4 Suppl 5, S3–S10.

Gannon, P.O., Godin-Ethier, J., Hassler, M., Delvoye, N., Aversa, M., Poisson, A.O., Péant, B., Alam Fahmy, M., Saad, F., Lapointe, R., Mes-Masson, A.-M., 2010. Androgen-Regulated Expression of Arginase 1, Arginase 2 and Interleukin-8 in Human Prostate Cancer. PLoS ONE 5, e12107. https://doi.org/10.1371/journal.pone.0012107

Gao, H., Yang, Z., Sun, H., Zhang, Y., Wang, Z., Liu, W., Wen, H., Qu, C., Wang, X., 2023. TREM2 as an independent predictor of poor prognosis promotes the migration via the PI3K/AKT axis in prostate cancer. Am J Transl Res 15, 779–798.

Gathirua-Mwangi, W.G., Zhang, J., 2014. Dietary factors and risk for advanced prostate cancer. Eur. J. Cancer Prev. Off. J. Eur. Cancer Prev. Organ. ECP 23, 96–109. https://doi.org/10.1097/CEJ.0b013e3283647394

Gentek, R., Ghigo, C., Hoeffel, G., Bulle, M.J., Msallam, R., Gautier, G., Launay, P., Chen, J., Ginhoux, F., Bajénoff, M., 2018. Hemogenic Endothelial Fate Mapping Reveals Dual Developmental Origin of Mast Cells. Immunity 48, 1160-1171.e5. https://doi.org/10.1016/j.immuni.2018.04.025

Gillette, C.M., Yette, G.A., Cramer, S.D., Graham, L.S., 2023. Management of Advanced Prostate Cancer in the Precision Oncology Era. Cancers 15, 2552. https://doi.org/10.3390/cancers15092552

Ginhoux, F., Guilliams, M., 2016. Tissue-Resident Macrophage Ontogeny and Homeostasis. Immunity 44, 439–449. https://doi.org/10.1016/j.immuni.2016.02.024

Gleason, D.F., 1966. Classification of prostatic carcinomas. Cancer Chemother. Rep. 50, 125–128.

Gordon, S., Plüddemann, A., Martinez Estrada, F., 2014. Macrophage heterogeneity in tissues: phenotypic diversity and functions. Immunol. Rev. 262, 36–55. https://doi.org/10.1111/imr.12223

Grabowska, M.M., DeGraff, D.J., Yu, X., Jin, R.J., Chen, Z., Borowsky, A.D., Matusik, R.J., 2014. Mouse models of prostate cancer: picking the best model for the question. Cancer Metastasis Rev. 33, 377–397. https://doi.org/10.1007/s10555-013-9487-8

Graff, J.N., Liang, L.W., Kim, J., Stenzl, A., 2021. KEYNOTE-641: a Phase III study of pembrolizumab plus enzalutamide for metastatic castration-resistant prostate cancer. Future Oncol. 17, 3017–3026. https://doi.org/10.2217/fon-2020-1008

Greenberg, N.M., DeMayo, F., Finegold, M.J., Medina, D., Tilley, W.D., Aspinall, J.O., Cunha, G.R., Donjacour, A.A., Matusik, R.J., Rosen, J.M., 1995. Prostate cancer in a transgenic mouse. Proc. Natl. Acad. Sci. 92, 3439–3443. https://doi.org/10.1073/pnas.92.8.3439

Grozescu, T., Popa, F., 2017. Prostate cancer between prognosis and adequate/proper therapy. J. Med. Life 10, 5–12.

Grzywa, T.M., Sosnowska, A., Matryba, P., Rydzynska, Z., Jasinski, M., Nowis, D., Golab, J., 2020. Myeloid Cell-Derived Arginase in Cancer Immune Response. Front. Immunol. 11, 938. https://doi.org/10.3389/fimmu.2020.00938

Guilliams, M., Thierry, G.R., Bonnardel, J., Bajenoff, M., 2020. Establishment and Maintenance of the Macrophage Niche. Immunity 52, 434–451. https://doi.org/10.1016/j.immuni.2020.02.015

Gulley, J.L., Borre, M., Vogelzang, N.J., Ng, S., Agarwal, N., Parker, C.C., Pook, D.W., Rathenborg, P., Flaig, T.W., Carles, J., Saad, F., Shore, N.D., Chen, L., Heery, C.R., Gerritsen, W.R., Priou, F., Langkilde, N.C., Novikov, A., Kantoff, P.W., 2019. Phase III Trial of PROSTVAC in Asymptomatic or Minimally Symptomatic Metastatic Castration-Resistant Prostate Cancer. J. Clin. Oncol. 37, 1051–1061. https://doi.org/10.1200/JCO.18.02031

Gungabeesoon, J., Gort-Freitas, N.A., Kiss, M., Bolli, E., Messemaker, M., Siwicki, M., Hicham, M., Bill, R., Koch, P., Cianciaruso, C., Duval, F., Pfirschke, C., Mazzola, M., Peters, S., Homicsko, K., Garris, C., Weissleder, R., Klein, A.M., Pittet, M.J., 2023. A neutrophil response linked to tumor control in immunotherapy. Cell 186, 1448-1464.e20. https://doi.org/10.1016/j.cell.2023.02.032

Hafron, J.M., Wilfehrt, H.M., Ferro, C., Harmon, M., Flanders, S.C., McKay, R.R., 2022. Real-World Effectiveness of Sipuleucel-T on Overall Survival in Men with Advanced Prostate Cancer Treated with Androgen Receptor-Targeting Agents. Adv. Ther. 39, 2515–2532. https://doi.org/10.1007/s12325-022-02085-6

Han, X., Shi, H., Sun, Y., Shang, C., Luan, T., Wang, D., Ba, X., Zeng, X., 2019. CXCR2 expression on granulocyte and macrophage progenitors under tumor conditions contributes to mo-MDSC generation via SAP18/ERK/STAT3. Cell Death Dis. 10, 598. https://doi.org/10.1038/s41419-019-1837-1

Hanahan, D., Weinberg, R.A., 2011. Hallmarks of Cancer: The Next Generation. Cell 144, 646–674. https://doi.org/10.1016/j.cell.2011.02.013

Hansen, A.R., Massard, C., Ott, P.A., Haas, N.B., Lopez, J.S., Ejadi, S., Wallmark, J.M., Keam, B., Delord, J.-P., Aggarwal, R., Gould, M., Yang, P., Keefe, S.M., Piha-Paul, S.A., 2018. Pembrolizumab for advanced prostate adenocarcinoma: findings of the KEYNOTE-028 study. Ann. Oncol. 29, 1807–1813. https://doi.org/10.1093/annonc/mdy232

Harshman, L.C., Wang, V.X., Hamid, A.A., Santone, G., Drake, C.G., Carducci, M.A., DiPaola, R.S., Fichorova, R.N., Sweeney, C.J., 2020. Impact of baseline serum IL-8 on metastatic hormone-sensitive prostate cancer outcomes in the Phase 3 CHAARTED trial (E3805). The Prostate 80, 1429–1437. https://doi.org/10.1002/pros.24074

Hasenberg, A., Hasenberg, M., Männ, L., Neumann, F., Borkenstein, L., Stecher, M., Kraus, A., Engel, D.R., Klingberg, A., Seddigh, P., Abdullah, Z., Klebow, S., Engelmann, S., Reinhold, A., Brandau, S., Seeling, M., Waisman, A., Schraven, B., Göthert, J.R., Nimmerjahn, F., Gunzer, M., 2015. Catchup: a mouse model for imaging-based tracking and modulation of neutrophil granulocytes. Nat. Methods 12, 445–452. https://doi.org/10.1038/nmeth.3322

Hashemi Goradel, N., Najafi, M., Salehi, E., Farhood, B., Mortezaee, K., 2019. Cyclooxygenase-2 in cancer: A review. J. Cell. Physiol. 234, 5683–5699. https://doi.org/10.1002/jcp.27411

Hashimoto, D., Chow, A., Noizat, C., Teo, P., Beasley, M.B., Leboeuf, M., Becker, C.D., See, P., Price, J., Lucas, D., Greter, M., Mortha, A., Boyer, S.W., Forsberg, E.C., Tanaka, M., van Rooijen, N., García-Sastre, A., Stanley, E.R., Ginhoux, F., Frenette, P.S., Merad, M.,

2013. Tissue-resident macrophages self-maintain locally throughout adult life with minimal contribution from circulating monocytes. Immunity 38, 792–804. https://doi.org/10.1016/j.immuni.2013.04.004

Hatano, K., Nonomura, N., 2022. Genomic Profiling of Prostate Cancer: An Updated Review. World J. Mens Health 40, 368. https://doi.org/10.5534/wjmh.210072

Hayashi, N., Sugimura, Y., Kawamura, J., Donjacour, A.A., Cunha, G.R., 1991. Morphological and Functional Heterogeneity in the Rat Prostatic Gland1. Biol. Reprod. 45, 308–321. https://doi.org/10.1095/biolreprod45.2.308

Heinlein, C.A., Chang, C., 2004. Androgen Receptor in Prostate Cancer. Endocr. Rev. 25, 276–308. https://doi.org/10.1210/er.2002-0032

Hidalgo, A., Chilvers, E.R., Summers, C., Koenderman, L., 2019. The Neutrophil Life Cycle. Trends Immunol. 40, 584–597. https://doi.org/10.1016/j.it.2019.04.013

Hirz, T., Mei, S., Sarkar, H., Kfoury, Y., Wu, S., Verhoeven, B.M., Subtelny, A.O., Zlatev, D.V., Wszolek, M.W., Salari, K., Murray, E., Chen, F., Macosko, E.Z., Wu, C.-L., Scadden, D.T., Dahl, D.M., Baryawno, N., Saylor, P.J., Kharchenko, P.V., Sykes, D.B., 2023. Dissecting the immune suppressive human prostate tumor microenvironment via integrated single-cell and spatial transcriptomic analyses. Nat. Commun. 14, 663. https://doi.org/10.1038/s41467-023-36325-2

Hodi, F.S., O'Day, S.J., McDermott, D.F., Weber, R.W., Sosman, J.A., Haanen, J.B., Gonzalez, R., Robert, C., Schadendorf, D., Hassel, J.C., Akerley, W., Van Den Eertwegh, A.J.M., Lutzky, J., Lorigan, P., Vaubel, J.M., Linette, G.P., Hogg, D., Ottensmeier, C.H., Lebbé, C., Peschel, C., Quirt, I., Clark, J.I., Wolchok, J.D., Weber, J.S., Tian, J., Yellin, M.J., Nichol, G.M., Hoos, A., Urba, W.J., 2010. Improved Survival with Ipilimumab in Patients with Metastatic Melanoma. N. Engl. J. Med. 363, 711–723. https://doi.org/10.1056/NEJMoa1003466

Hu, W., Qian, Y., Yu, F., Liu, W., Wu, Y., Fang, X., Hao, W., 2015. Alternatively activated macrophages are associated with metastasis and poor prognosis in prostate adenocarcinoma. Oncol. Lett. 10, 1390–1396. https://doi.org/10.3892/ol.2015.3400

Hubbard, G.K., Mutton, L.N., Khalili, M., McMullin, R.P., Hicks, J.L., Bianchi-Frias, D., Horn, L.A., Kulac, I., Moubarek, M.S., Nelson, P.S., Yegnasubramanian, S., De Marzo, A.M., Bieberich, C.J., 2016. Combined *MYC* Activation and *Pten* Loss Are Sufficient to Create Genomic Instability and Lethal Metastatic Prostate Cancer. Cancer Res. 76, 283–292. https://doi.org/10.1158/0008-5472.CAN-14-3280

Hui, G.K., Gao, X., Gor, J., Lu, J., Sun, P.D., Perkins, S.J., 2023. The solution structure of the unbound IgG Fc receptor CD64 resembles its crystal structure: Implications for function. PLOS ONE 18, e0288351. https://doi.org/10.1371/journal.pone.0288351

Huijbers, E.J.M., Khan, K.A., Kerbel, R.S., Griffioen, A.W., 2022. Tumors resurrect an embryonic vascular program to escape immunity. Sci. Immunol. 7, eabm6388. https://doi.org/10.1126/sciimmunol.abm6388

Hume, D.A., Perry, V.H., Gordon, S., 1984. The mononuclear phagocyte system of the mouse defined by immunohistochemical localisation of antigen F4/80: Macrophages associated with epithelia. Anat. Rec. 210, 503–512. https://doi.org/10.1002/ar.1092100311

Hume, D.A., Ross, I.L., Himes, S.R., Sasmono, R.T., Wells, C.A., Ravasi, T., 2002. The mononuclear phagocyte system revisited. J. Leukoc. Biol. 72, 621–627. https://doi.org/10.1189/jlb.72.4.621

Hume, D.A., Wollscheid-Lengeling, E., Rojo, R., Pridans, C., 2017. The evolution of the macrophage-specific enhancer (Fms intronic regulatory element) within the CSF1R locus of vertebrates. Sci. Rep. 7, 17115. https://doi.org/10.1038/s41598-017-15999-x

Hummel, H.-D., Kufer, P., Grüllich, C., Deschler-Baier, B., Chatterjee, M., Goebeler, M.-E., Miller, K., De Santis, M., Loidl, W.C., Buck, A., Wittemer-Rump, S., Koca, G., Boix, O., Doecke, W.-D., Stienen, S., Sayehli, C., Bargou, R.C., 2019. Phase 1 study of pasotuxizumab (BAY 2010112), a PSMA-targeting Bispecific T cell Engager (BiTE) immunotherapy for metastatic castration-resistant prostate cancer (mCRPC). J. Clin. Oncol. 37, 5034–5034. https://doi.org/10.1200/JCO.2019.37.15_suppl.5034

Hussain, F., Freissmuth, M., Völkel, D., Thiele, M., Douillard, P., Antoine, G., Thurner, P., Ehrlich, H., Schwarz, H.-P., Scheiflinger, F., Kerschbaumer, R.J., 2013. Human Anti-Macrophage Migration Inhibitory Factor Antibodies Inhibit Growth of Human Prostate Cancer Cells *In Vitro* and *In Vivo*. Mol. Cancer Ther. 12, 1223–1234. https://doi.org/10.1158/1535-7163.MCT-12-0988

Irshad, S., Abate-Shen, C., 2013. Modeling prostate cancer in mice: something old, something new, something premalignant, something metastatic. Cancer Metastasis Rev. 32, 109–122. https://doi.org/10.1007/s10555-012-9409-1

Janeway, C.A., Medzhitov, R., 2002. Innate Immune Recognition. Annu. Rev. Immunol. 20, 197–216. https://doi.org/10.1146/annurev.immunol.20.083001.084359

Japp, A.S., Kursunel, M.A., Meier, S., Mälzer, J.N., Li, X., Rahman, N.A., Jekabsons, W., Krause, H., Magheli, A., Klopf, C., Thiel, A., Frentsch, M., 2015. Dysfunction of PSA-specific CD8+ T cells in prostate cancer patients correlates with CD38 and Tim-3 expression. Cancer Immunol. Immunother. 64, 1487–1494. https://doi.org/10.1007/s00262-015-1752-y

Jhunjhunwala, S., Hammer, C., Delamarre, L., 2021. Antigen presentation in cancer: insights into tumour immunogenicity and immune evasion. Nat. Rev. Cancer 21, 298–312. https://doi.org/10.1038/s41568-021-00339-z

Jiang, Y., Li, Y., Zhu, B., 2015. T-cell exhaustion in the tumor microenvironment. Cell Death Dis. 6, e1792–e1792. https://doi.org/10.1038/cddis.2015.162

Jin, C., McKeehan, K., Wang, F., 2003. Transgenic mouse with high cre recombinase activity in all prostate lobes, seminal vesicle, and ductus deferens. The Prostate 57, 160–164. https://doi.org/10.1002/pros.10283

Jin, H.-T., Anderson, A.C., Tan, W.G., West, E.E., Ha, S.-J., Araki, K., Freeman, G.J., Kuchroo, V.K., Ahmed, R., 2010. Cooperation of Tim-3 and PD-1 in CD8 T-cell exhaustion during chronic viral infection. Proc. Natl. Acad. Sci. 107, 14733–14738. https://doi.org/10.1073/pnas.1009731107

Kaltenmeier, C., Yazdani, H.O., Morder, K., Geller, D.A., Simmons, R.L., Tohme, S., 2021. Neutrophil Extracellular Traps Promote T Cell Exhaustion in the Tumor Microenvironment. Front. Immunol. 12, 785222. https://doi.org/10.3389/fimmu.2021.785222

Kane, N., Romero, T., Diaz-Perez, S., Rettig, M.B., Steinberg, M.L., Kishan, A.U., Schaue, D., Reiter, R.E., Knudsen, B.S., Nickols, N.G., 2023. Significant changes in macrophage and CD8 T cell densities in primary prostate tumors 2 weeks after SBRT. Prostate Cancer Prostatic Dis. 26, 207–209. https://doi.org/10.1038/s41391-022-00498-6

Kaplanov, I., Carmi, Y., Kornetsky, R., Shemesh, A., Shurin, G.V., Shurin, M.R., Dinarello, C.A., Voronov, E., Apte, R.N., 2019. Blocking IL-1β reverses the immunosuppression in mouse breast cancer and synergizes with anti–PD-1 for tumor abrogation. Proc. Natl. Acad. Sci. 116, 1361–1369. https://doi.org/10.1073/pnas.1812266115

Kasper, S., Sheppard, P.C., Yan, Y., Pettigrew, N., Borowsky, A.D., Prins, G.S., Dodd, J.G., Duckworth, M.L., Matusik, R.J., 1998. Development, progression, and androgen-dependence of prostate tumors in probasin-large T antigen transgenic mice: a model for prostate cancer. Lab. Investig. J. Tech. Methods Pathol. 78, 319–333.

Katzenelenbogen, Y., Sheban, F., Yalin, A., Yofe, I., Svetlichnyy, D., Jaitin, D.A., Bornstein, C., Moshe, A., Keren-Shaul, H., Cohen, M., Wang, S.-Y., Li, B., David, E., Salame, T.-M., Weiner, A., Amit, I., 2020. Coupled scRNA-Seq and Intracellular Protein Activity Reveal an Immunosuppressive Role of TREM2 in Cancer. Cell 182, 872-885.e19. https://doi.org/10.1016/j.cell.2020.06.032

Kazandjian, D., Suzman, D.L., Blumenthal, G., Mushti, S., He, K., Libeg, M., Keegan, P., Pazdur, R., 2016. FDA Approval Summary: Nivolumab for the Treatment of Metastatic Non-Small Cell Lung Cancer With Progression On or After Platinum-Based Chemotherapy. The Oncologist 21, 634–642. https://doi.org/10.1634/theoncologist.2015-0507

Khaled, Y.S., Ammori, B.J., Elkord, E., 2014. Increased Levels of Granulocytic Myeloid-Derived Suppressor Cells in Peripheral Blood and Tumour Tissue of Pancreatic Cancer Patients. J. Immunol. Res. 2014, 1–9. https://doi.org/10.1155/2014/879897

Kieu, T.Q., Tazawa, K., Kawashima, N., Noda, S., Fujii, M., Nara, K., Hashimoto, K., Han, P., Okiji, T., 2022. Kinetics of LYVE-1-positive M2-like macrophages in developing and repairing dental pulp in vivo and their pro-angiogenic activity in vitro. Sci. Rep. 12, 5176. https://doi.org/10.1038/s41598-022-08987-3

Kim, C.H., Axup, J.Y., Lawson, B.R., Yun, H., Tardif, V., Choi, S.H., Zhou, Q., Dubrovska, A., Biroc, S.L., Marsden, R., Pinstaff, J., Smider, V.V., Schultz, P.G., 2013. Bispecific small molecule–antibody conjugate targeting prostate cancer. Proc. Natl. Acad. Sci. 110, 17796–17801. https://doi.org/10.1073/pnas.1316026110

Kim, M.J., Bhatia-Gaur, R., Banach-Petrosky, W.A., Desai, N., Wang, Y., Hayward, S.W., Cunha, G.R., Cardiff, R.D., Shen, M.M., Abate-Shen, C., 2002. Nkx3.1 mutant mice recapitulate early stages of prostate carcinogenesis. Cancer Res. 62, 2999–3004.

Kissick, H.T., Sanda, M.G., Dunn, L.K., Pellegrini, K.L., On, S.T., Noel, J.K., Arredouani, M.S., 2014. Androgens alter T-cell immunity by inhibiting T-helper 1 differentiation. Proc. Natl. Acad. Sci. 111, 9887–9892. https://doi.org/10.1073/pnas.1402468111

Korfage, I.J., Essink-Bot, M.-L., Borsboom, G.J.J.M., Madalinska, J.B., Kirkels, W.J., Habbema, J.D.F., Schröder, F.H., de Koning, H.J., 2005. Five-year follow-up of health-related quality of life after primary treatment of localized prostate cancer. Int. J. Cancer 116, 291–296. https://doi.org/10.1002/ijc.21043

Kurihara, T., Warr, G., Loy, J., Bravo, R., 1997. Defects in Macrophage Recruitment and Host Defense in Mice Lacking the CCR2 Chemokine Receptor. J. Exp. Med. 186, 1757–1762. https://doi.org/10.1084/jem.186.10.1757

Kwon, E.D., Drake, C.G., Scher, H.I., Fizazi, K., Bossi, A., Van Den Eertwegh, A.J.M., Krainer, M., Houede, N., Santos, R., Mahammedi, H., Ng, S., Maio, M., Franke, F.A., Sundar, S., Agarwal, N., Bergman, A.M., Ciuleanu, T.E., Korbenfeld, E., Sengeløv, L., Hansen, S., Logothetis, C., Beer, T.M., McHenry, M.B., Gagnier, P., Liu, D., Gerritsen, W.R., 2014. Ipilimumab versus placebo after radiotherapy in patients with metastatic castration-resistant prostate cancer that had progressed after docetaxel chemotherapy (CA184-043): a multicentre, randomised, double-blind, phase 3 trial. Lancet Oncol. 15, 700–712. https://doi.org/10.1016/S1470-2045(14)70189-5

Lasek, W., 2022. Cancer immunoediting hypothesis: history, clinical implications and controversies. Cent. Eur. J. Immunol. 47, 168–174. https://doi.org/10.5114/ceji.2022.117376

Le Magnen, C., Dutta, A., Abate-Shen, C., 2016. Optimizing mouse models for precision cancer prevention. Nat. Rev. Cancer 16, 187–196. https://doi.org/10.1038/nrc.2016.1

Leach, S.M., Gibbings, S.L., Tewari, A.D., Atif, S.M., Vestal, B., Danhorn, T., Janssen, W.J., Wager, T.D., Jakubzick, C.V., 2020. Human and Mouse Transcriptome Profiling Identifies Cross-Species Homology in Pulmonary and Lymph Node Mononuclear Phagocytes. Cell Rep. 33, 108337. https://doi.org/10.1016/j.celrep.2020.108337

Leibowitz-Amit, R., Templeton, A.J., Omlin, A., Pezaro, C., Atenafu, E.G., Keizman, D., Vera-Badillo, F., Seah, J.-A., Attard, G., Knox, J.J., Sridhar, S.S., Tannock, I.F., De Bono, J.S., Joshua, A.M., 2014. Clinical variables associated with PSA response to abiraterone acetate in patients with metastatic castration-resistant prostate cancer. Ann. Oncol. 25, 657–662. https://doi.org/10.1093/annonc/mdt581

LeRoy, B.E., Northrup, N., 2009. Prostate cancer in dogs: Comparative and clinical aspects. Vet. J. 180, 149–162. https://doi.org/10.1016/j.tvjl.2008.07.012

Li, S., Zhu, M., Pan, R., Fang, T., Cao, Y.-Y., Chen, S., Zhao, X., Lei, C.-Q., Guo, L., Chen, Y., Li, C.-M., Jokitalo, E., Yin, Y., Shu, H.-B., Guo, D., 2016. The tumor suppressor PTEN has a critical role in antiviral innate immunity. Nat. Immunol. 17, 241–249. https://doi.org/10.1038/ni.3311

Li, X., Liu, R., Su, X., Pan, Y., Han, X., Shao, C., Shi, Y., 2019. Harnessing tumor-associated macrophages as aids for cancer immunotherapy. Mol. Cancer 18, 177. https://doi.org/10.1186/s12943-019-1102-3

Lin, C., Jan, Y., Kuo, L., Wang, B., Huo, C., Jiang, S.S., Chen, S., Kuo, Y., Chang, C., Chuu, C., 2018. Elevation of androgen receptor promotes prostate cancer metastasis by induction of epithelial-mesenchymal transition and reduction of KAT 5. Cancer Sci. 109, 3564–3574. https://doi.org/10.1111/cas.13776

Lipson, E.J., Drake, C.G., 2011. Ipilimumab: An Anti-CTLA-4 Antibody for Metastatic Melanoma. Clin. Cancer Res. 17, 6958–6962. https://doi.org/10.1158/1078-0432.CCR-11-1595

Litman, G.W., Cooper, M.D., 2007. Why study the evolution of immunity? Nat. Immunol. 8, 547–548. https://doi.org/10.1038/ni0607-547

Liu, P., Liang, Y., Jiang, L., Wang, H., Wang, S., Dong, J., 2018. CX3CL1/fractalkine enhances prostate cancer spinal metastasis by activating the Src/FAK pathway. Int. J. Oncol. https://doi.org/10.3892/ijo.2018.4487

Liu, X., Hoft, D.F., Peng, G., 2022. Tumor microenvironment metabolites directing T cell differentiation and function. Trends Immunol. 43, 132–147. https://doi.org/10.1016/j.it.2021.12.004

Liu, Y., Xu, R., Gu, H., Zhang, E., Qu, J., Cao, W., Huang, X., Yan, H., He, J., Cai, Z., 2021. Metabolic reprogramming in macrophage responses. Biomark. Res. 9, 1. https://doi.org/10.1186/s40364-020-00251-y

Liu, Y.-T., Sun, Z.-J., 2021. Turning cold tumors into hot tumors by improving T-cell infiltration. Theranostics 11, 5365–5386. https://doi.org/10.7150/thno.58390

Liu, Z., Wang, Haiting, Li, Z., Dress, R.J., Zhu, Y., Zhang, S., De Feo, D., Kong, W.T., Cai, P., Shin, A., Piot, C., Yu, J., Gu, Y., Zhang, M., Gao, C., Chen, L., Wang, Honglin, Vétillard, M., Guermonprez, P., Kwok, I., Ng, L.G., Chakarov, S., Schlitzer, A., Becher, B., Dutertre, C.-A., Su, B., Ginhoux, F., 2023. Dendritic cell type 3 arises from Ly6C+ monocyte-dendritic

cell progenitors. Immunity 56, 1761-1777.e6. https://doi.org/10.1016/j.immuni.2023.07.001

Liu, Zhaoyuan, Gu, Y., Chakarov, S., Bleriot, C., Kwok, I., Chen, X., Shin, A., Huang, W., Dress, R.J., Dutertre, C.-A., Schlitzer, A., Chen, J., Ng, L.G., Wang, H., Liu, Zhiduo, Su, B., Ginhoux, F., 2019. Fate Mapping via Ms4a3-Expression History Traces Monocyte-Derived Cells. Cell 178, 1509-1525.e19. https://doi.org/10.1016/j.cell.2019.08.009

Lorente, D., Mateo, J., Templeton, A.J., Zafeiriou, Z., Bianchini, D., Ferraldeschi, R., Bahl, A., Shen, L., Su, Z., Sartor, O., De Bono, J.S., 2015. Baseline neutrophil–lymphocyte ratio (NLR) is associated with survival and response to treatment with second-line chemotherapy for advanced prostate cancer independent of baseline steroid use. Ann. Oncol. 26, 750–755. https://doi.org/10.1093/annonc/mdu587

Luchman, H.A., Friedman, H.C., Villemaire, M.L., Peterson, A.C., Jirik, F.R., 2008. Temporally controlled prostate epithelium-specific gene alterations. genesis 46, 229–234. https://doi.org/10.1002/dvg.20386

Luongo, F., Colonna, F., Calapà, F., Vitale, S., Fiori, M.E., De Maria, R., 2019. PTEN Tumor-Suppressor: The Dam of Stemness in Cancer. Cancers 11, 1076. https://doi.org/10.3390/cancers11081076

Lyons, L.S., Rao, S., Balkan, W., Faysal, J., Maiorino, C.A., Burnstein, K.L., 2008. Ligand-Independent Activation of Androgen Receptors by Rho GTPase Signaling in Prostate Cancer. Mol. Endocrinol. 22, 597–608. https://doi.org/10.1210/me.2007-0158

Ma, X., Ziel-van Der Made, A.C., Autar, B., Van Der Korput, H.A., Vermeij, M., Van Duijn, P., Cleutjens, K.B., De Krijger, R., Krimpenfort, P., Berns, A., Van Der Kwast, T.H., Trapman, J., 2005. Targeted Biallelic Inactivation of *Pten* in the Mouse Prostate Leads to Prostate Cancer Accompanied by Increased Epithelial Cell Proliferation but not by Reduced Apoptosis. Cancer Res. 65, 5730–5739. https://doi.org/10.1158/0008-5472.CAN-04-4519

Ma, Z., Zhang, W., Dong, B., Xin, Z., Ji, Y., Su, R., Shen, K., Pan, J., Wang, Q., Xue, W., 2022. Docetaxel remodels prostate cancer immune microenvironment and enhances checkpoint inhibitor-based immunotherapy. Theranostics 12, 4965–4979. https://doi.org/10.7150/thno.73152

MacDonald, K.P.A., Palmer, J.S., Cronau, S., Seppanen, E., Olver, S., Raffelt, N.C., Kuns, R., Pettit, A.R., Clouston, A., Wainwright, B., Branstetter, D., Smith, J., Paxton, R.J., Cerretti, D.P., Bonham, L., Hill, G.R., Hume, D.A., 2010. An antibody against the colony-stimulating factor 1 receptor depletes the resident subset of monocytes and tissue- and tumor-associated macrophages but does not inhibit inflammation. Blood 116, 3955–3963. https://doi.org/10.1182/blood-2010-02-266296

Mackey, J.B.G., Coffelt, S.B., Carlin, L.M., 2019. Neutrophil Maturity in Cancer. Front. Immunol. 10, 1912. https://doi.org/10.3389/fimmu.2019.01912

Maddison, L.A., Nahm, H., DeMayo, F., Greenberg, N.M., 2000. Prostate specific expression of Cre recombinase in transgenic mice. genesis 26, 154–156. https://doi.org/10.1002/(SICI)1526-968X(200002)26:2<154::AID-GENE18>3.0.CO;2-2

Maleki Vareki, S., 2018. High and low mutational burden tumors versus immunologically hot and cold tumors and response to immune checkpoint inhibitors. J. Immunother. Cancer 6, 157, s40425-018-0479–7. https://doi.org/10.1186/s40425-018-0479-7

Malissen, B., Tamoutounour, S., Henri, S., 2014. The origins and functions of dendritic cells and macrophages in the skin. Nat. Rev. Immunol. 14, 417–428. https://doi.org/10.1038/nri3683

Mantovani, A., Cassatella, M.A., Costantini, C., Jaillon, S., 2011. Neutrophils in the activation and regulation of innate and adaptive immunity. Nat. Rev. Immunol. 11, 519–531. https://doi.org/10.1038/nri3024

Mantovani, A., Schioppa, T., Porta, C., Allavena, P., Sica, A., 2006. Role of tumor-associated macrophages in tumor progression and invasion. Cancer Metastasis Rev. 25, 315–322. https://doi.org/10.1007/s10555-006-9001-7

Marcel, V., Nguyen Van Long, F., Diaz, J.-J., 2018. 40 Years of Research Put p53 in Translation. Cancers 10, 152. https://doi.org/10.3390/cancers10050152

Marcus, L., Lemery, S.J., Keegan, P., Pazdur, R., 2019. FDA Approval Summary: Pembrolizumab for the Treatment of Microsatellite Instability-High Solid Tumors. Clin. Cancer Res. 25, 3753–3758. https://doi.org/10.1158/1078-0432.CCR-18-4070

Marhold, M., Kramer, G., Krainer, M., Le Magnen, C., 2022. The prostate cancer landscape in Europe: Current challenges, future opportunities. Cancer Lett. 526, 304–310. https://doi.org/10.1016/j.canlet.2021.11.033

Markiewski, M.M., DeAngelis, R.A., Benencia, F., Ricklin-Lichtsteiner, S.K., Koutoulaki, A., Gerard, C., Coukos, G., Lambris, J.D., 2008. Modulation of the antitumor immune response by complement. Nat. Immunol. 9, 1225–1235. https://doi.org/10.1038/ni.1655

Marshall, C.H., Fu, W., Wang, H., Park, J.C., DeWeese, T.L., Tran, P.T., Song, D.Y., King, S., Afful, M., Hurrelbrink, J., Manogue, C., Cotogno, P., Moldawer, N.P., Barata, P.C., Drake, C.G., Posadas, E.M., Armstrong, A.J., Sartor, O., Antonarakis, E.S., 2021. Randomized Phase II Trial of Sipuleucel-T with or without Radium-223 in Men with Bone-metastatic Castration-resistant Prostate Cancer. Clin. Cancer Res. 27, 1623–1630. https://doi.org/10.1158/1078-0432.CCR-20-4476

Martin, A.M., Nirschl, T.R., Nirschl, C.J., Francica, B.J., Kochel, C.M., Van Bokhoven, A., Meeker, A.K., Lucia, M.S., Anders, R.A., DeMarzo, A.M., Drake, C.G., 2015. Paucity of PD-L1 expression in prostate cancer: innate and adaptive immune resistance. Prostate Cancer Prostatic Dis. 18, 325–332. https://doi.org/10.1038/pcan.2015.39

Martin, C., Burdon, P.C.E., Bridger, G., Gutierrez-Ramos, J.-C., Williams, T.J., Rankin, S.M., 2003. Chemokines Acting via CXCR2 and CXCR4 Control the Release of Neutrophils from the Bone Marrow and Their Return following Senescence. Immunity 19, 583–593. https://doi.org/10.1016/S1074-7613(03)00263-2

Marvel, D., Gabrilovich, D.I., 2015. Myeloid-derived suppressor cells in the tumor microenvironment: expect the unexpected. J. Clin. Invest. 125, 3356–3364. https://doi.org/10.1172/JCI80005

Massari, F., Ciccarese, C., Caliò, A., Munari, E., Cima, L., Porcaro, A.B., Novella, G., Artibani, W., Sava, T., Eccher, A., Ghimenton, C., Bertoldo, F., Scarpa, A., Sperandio, N., Porta, C., Bronte, V., Chilosi, M., Bogina, G., Zamboni, G., Tortora, G., Samaratunga, H., Martignoni, G., Brunelli, M., 2016. Magnitude of PD-1, PD-L1 and T Lymphocyte Expression on Tissue from Castration-Resistant Prostate Adenocarcinoma: An Exploratory Analysis. Target. Oncol. 11, 345–351. https://doi.org/10.1007/s11523-015-0396-3

Masumori, N., Thomas, T.Z., Chaurand, P., Case, T., Paul, M., Kasper, S., Caprioli, R.M., Tsukamoto, T., Shappell, S.B., Matusik, R.J., 2001. A probasin-large T antigen transgenic mouse line develops prostate adenocarcinoma and neuroendocrine carcinoma with metastatic potential. Cancer Res. 61, 2239–2249.

Matos, A., Carvalho, M., Bicho, M., Ribeiro, R., 2021. Arginine and Arginases Modulate Metabolism, Tumor Microenvironment and Prostate Cancer Progression. Nutrients 13, 4503. https://doi.org/10.3390/nu13124503

Maxwell, P.J., Neisen, J., Messenger, J., Waugh, D.J.J., 2014. Tumor-derived CXCL8 signaling augments stroma-derived CCL2-promoted proliferation and CXCL12-mediated invasion of PTEN-deficient prostate cancer cells. Oncotarget 5, 4895–4908. https://doi.org/10.18632/oncotarget.2052

McNeal, J.E., 1981. The zonal anatomy of the prostate. The Prostate 2, 35–49. https://doi.org/10.1002/pros.2990020105

McNeal, J.E., Bostwick, D.G., 1986. Intraductal dysplasia: A premalignant lesion of the prostate. Hum. Pathol. 17, 64–71. https://doi.org/10.1016/S0046-8177(86)80156-3

Mehrabadi, A.Z., Ranjbar, R., Farzanehpour, M., Shahriary, A., Dorostkar, R., Hamidinejad, M.A., Ghaleh, H.E.G., 2022. Therapeutic potential of CAR T cell in malignancies: A scoping review. Biomed. Pharmacother. 146, 112512. https://doi.org/10.1016/j.biopha.2021.112512

Merrimen, J.L., Jones, G., Walker, D., Leung, C.S., Kapusta, L.R., Srigley, J.R., 2009. Multifocal high grade prostatic intraepithelial neoplasia is a significant risk factor for prostatic adenocarcinoma. J. Urol. 182, 485–490; discussion 490. https://doi.org/10.1016/j.juro.2009.04.016

Metzger, D., 1999. Engineering the mouse genome by site-specific recombination. Curr. Opin. Biotechnol. 10, 470–476. https://doi.org/10.1016/S0958-1669(99)00012-9

Metzger, D., Chambon, P., 2001. Site- and Time-Specific Gene Targeting in the Mouse. Methods 24, 71–80. https://doi.org/10.1006/meth.2001.1159

Meyer-Siegler, K.L., Iczkowski, K.A., Vera, P.L., 2005. Further evidence for increased macrophage migration inhibitory factor expression in prostate cancer. BMC Cancer 5, 73. https://doi.org/10.1186/1471-2407-5-73

Mills, C.D., Kincaid, K., Alt, J.M., Heilman, M.J., Hill, A.M., 2017. Pillars Article: M-1/M-2 Macrophages and the Th1/Th2 Paradigm. *J. Immunol* . 2000. 164: 6166–6173. J. Immunol. 199, 2194–2201. https://doi.org/10.4049/jimmunol.1701141

Mitsumori, K., Elwell, M.R., 1988. Proliferative lesions in the male reproductive system of F344 rats and B6C3F1 mice: incidence and classification. Environ. Health Perspect. 77, 11–21. https://doi.org/10.1289/ehp.887711

Mittmann, L.A., Haring, F., Schaubächer, J.B., Hennel, R., Smiljanov, B., Zuchtriegel, G., Canis, M., Gires, O., Krombach, F., Holdt, L., Brandau, S., Vogl, T., Lauber, K., Uhl, B., Reichel, C.A., 2021. Uncoupled biological and chronological aging of neutrophils in cancer promotes tumor progression. J. Immunother. Cancer 9, e003495. https://doi.org/10.1136/jitc-2021-003495

Molgora, M., Esaulova, E., Vermi, W., Hou, J., Chen, Y., Luo, J., Brioschi, S., Bugatti, M., Omodei, A.S., Ricci, B., Fronick, C., Panda, S.K., Takeuchi, Y., Gubin, M.M., Faccio, R., Cella, M., Gilfillan, S., Unanue, E.R., Artyomov, M.N., Schreiber, R.D., Colonna, M., 2020. TREM2 Modulation Remodels the Tumor Myeloid Landscape Enhancing Anti-PD-1 Immunotherapy. Cell 182, 886-900.e17. https://doi.org/10.1016/j.cell.2020.07.013

Mora Barthelmess, R., Stijlemans, B., Van Ginderachter, J.A., 2023. Hallmarks of Cancer Affected by the MIF Cytokine Family. Cancers 15, 395. https://doi.org/10.3390/cancers15020395

Morris, L., Graham, C.F., Gordon, S., 1991. Macrophages in haemopoietic and other tissues of the developing mouse detected by the monoclonal antibody F4/80. Development 112, 517–526. https://doi.org/10.1242/dev.112.2.517

Morrissey, C., Vessella, R.L., 2007. The role of tumor microenvironment in prostate cancer bone metastasis. J. Cell. Biochem. 101, 873–886. https://doi.org/10.1002/jcb.21214

Moseman, A.P., Moseman, E.A., Schworer, S., Smirnova, I., Volkova, T., Von Andrian, U., Poltorak, A., 2013. Mannose Receptor 1 Mediates Cellular Uptake and Endosomal Delivery of CpG-Motif Containing Oligodeoxynucleotides. J. Immunol. 191, 5615–5624. https://doi.org/10.4049/jimmunol.1301438

Moses, K., Klein, J.C., Männ, L., Klingberg, A., Gunzer, M., Brandau, S., 2016. Survival of residual neutrophils and accelerated myelopoiesis limit the efficacy of antibody-mediated depletion of Ly-6G+ cells in tumor-bearing mice. J. Leukoc. Biol. 99, 811–823. https://doi.org/10.1189/jlb.1HI0715-289R

Mossadegh-Keller, N., Sarrazin, S., Kandalla, P.K., Espinosa, L., Stanley, E.R., Nutt, S.L., Moore, J., Sieweke, M.H., 2013. M-CSF instructs myeloid lineage fate in single haematopoietic stem cells. Nature 497, 239–243. https://doi.org/10.1038/nature12026

Motzer, R.J., Escudier, B., McDermott, D.F., George, S., Hammers, H.J., Srinivas, S., Tykodi, S.S., Sosman, J.A., Procopio, G., Plimack, E.R., Castellano, D., Choueiri, T.K., Gurney, H., Donskov, F., Bono, P., Wagstaff, J., Gauler, T.C., Ueda, T., Tomita, Y., Schutz, F.A., Kollmannsberger, C., Larkin, J., Ravaud, A., Simon, J.S., Xu, L.-A., Waxman, I.M., Sharma, P., 2015. Nivolumab versus Everolimus in Advanced Renal-Cell Carcinoma. N. Engl. J. Med. 373, 1803–1813. https://doi.org/10.1056/NEJMoa1510665

Movahedi, K., Laoui, D., Gysemans, C., Baeten, M., Stangé, G., Van Den Bossche, J., Mack, M., Pipeleers, D., In't Veld, P., De Baetselier, P., Van Ginderachter, J.A., 2010. Different Tumor Microenvironments Contain Functionally Distinct Subsets of Macrophages Derived from Ly6C(high) Monocytes. Cancer Res. 70, 5728–5739. https://doi.org/10.1158/0008-5472.CAN-09-4672

Muenst, S., Läubli, H., Soysal, S.D., Zippelius, A., Tzankov, A., Hoeller, S., 2016. The immune system and cancer evasion strategies: therapeutic concepts. J. Intern. Med. 279, 541–562. https://doi.org/10.1111/joim.12470

Mulholland, D.J., Tran, L.M., Li, Y., Cai, H., Morim, A., Wang, S., Plaisier, S., Garraway, I.P., Huang, J., Graeber, T.G., Wu, H., 2011. Cell Autonomous Role of PTEN in Regulating Castration-Resistant Prostate Cancer Growth. Cancer Cell 19, 792–804. https://doi.org/10.1016/j.ccr.2011.05.006

Mumenthaler, S.M., Yu, H., Tze, S., Cederbaum, S.D., Pegg, A.E., Seligson, D.B., Grody, W.W., 2008. Expression of arginase II in prostate cancer. Int. J. Oncol. 32, 357–365.

Muramaki, M., Miyake, H., Yamada, Y., Hara, I., 2006. Clinical utility of serum macrophage migration inhibitory factor in men with prostate cancer as a novel biomarker of detection and disease progression. Oncol. Rep. 15, 253–257.

Murray, P.J., Allen, J.E., Biswas, S.K., Fisher, E.A., Gilroy, D.W., Goerdt, S., Gordon, S., Hamilton, J.A., Ivashkiv, L.B., Lawrence, T., Locati, M., Mantovani, A., Martinez, F.O., Mege, J.-L., Mosser, D.M., Natoli, G., Saeij, J.P., Schultze, J.L., Shirey, K.A., Sica, A., Suttles, J., Udalova, I., van Ginderachter, J.A., Vogel, S.N., Wynn, T.A., 2014. Macrophage Activation and Polarization: Nomenclature and Experimental Guidelines. Immunity 41, 14–20. https://doi.org/10.1016/j.immuni.2014.06.008

Nalio Ramos, R., Missolo-Koussou, Y., Gerber-Ferder, Y., Bromley, C.P., Bugatti, M., Núñez, N.G., Tosello Boari, J., Richer, W., Menger, L., Denizeau, J., Sedlik, C., Caudana, P.,

Kotsias, F., Niborski, L.L., Viel, S., Bohec, M., Lameiras, S., Baulande, S., Lesage, L., Nicolas, A., Meseure, D., Vincent-Salomon, A., Reyal, F., Dutertre, C.-A., Ginhoux, F., Vimeux, L., Donnadieu, E., Buttard, B., Galon, J., Zelenay, S., Vermi, W., Guermonprez, P., Piaggio, E., Helft, J., 2022. Tissue-resident FOLR2+ macrophages associate with CD8+ T cell infiltration in human breast cancer. Cell 185, 1189-1207.e25. https://doi.org/10.1016/j.cell.2022.02.021

Narayan, V., Barber-Rotenberg, J., Fraietta, J., Hwang, W.-T., Lacey, S.F., Plesa, G., Carpenter, E.L., Maude, S.L., Lal, P., Vapiwala, N., Melenhorst, J.J., Sebro, R., Farwell, M., Moniak, M., Gilmore, J., Lledo, L., Dengel, K., June, C.H., Haas, N.B., 2021. A phase I clinical trial of PSMA-directed/TGFβ-insensitive CAR-T cells in metastatic castration-resistant prostate cancer. J. Clin. Oncol. 39, 125–125. https://doi.org/10.1200/JCO.2021.39.6_suppl.125

Netea, M.G., Domínguez-Andrés, J., Barreiro, L.B., Chavakis, T., Divangahi, M., Fuchs, E., Joosten, L.A.B., Van Der Meer, J.W.M., Mhlanga, M.M., Mulder, W.J.M., Riksen, N.P., Schlitzer, A., Schultze, J.L., Stabell Benn, C., Sun, J.C., Xavier, R.J., Latz, E., 2020. Defining trained immunity and its role in health and disease. Nat. Rev. Immunol. 20, 375–388. https://doi.org/10.1038/s41577-020-0285-6

Nevedomskaya, E., Baumgart, S., Haendler, B., 2018. Recent Advances in Prostate Cancer Treatment and Drug Discovery. Int. J. Mol. Sci. 19, 1359. https://doi.org/10.3390/ijms19051359

Ng, M.S.F., Kwok, I., Tan, L., Shi, C., Cerezo-Wallis, D., Tan, Y., Leong, K., Calvo, G.F., Yang, K., Zhang, Y., Jin, J., Liong, K.H., Wu, D., He, R., Liu, D., Teh, Y.C., Bleriot, C., Caronni, N., Liu, Z., Duan, K., Narang, V., Ballesteros, I., Moalli, F., Li, M., Chen, J., Liu, Yao, Liu, L., Qi, J., Liu, Yingbin, Jiang, L., Shen, B., Cheng, H., Cheng, T., Angeli, V., Sharma, A., Loh, Y., Tey, H.L., Chong, S.Z., Iannacone, M., Ostuni, R., Hidalgo, A., Ginhoux, F., Ng, L.G., 2024. Deterministic reprogramming of neutrophils within tumors. Science 383, eadf6493. https://doi.org/10.1126/science.adf6493

Noe, J.T., Mitchell, R.A., 2020. MIF-Dependent Control of Tumor Immunity. Front. Immunol. 11, 609948. https://doi.org/10.3389/fimmu.2020.609948

Nonomura, N., Takayama, H., Nakayama, M., Nakai, Y., Kawashima, A., Mukai, M., Nagahara, A., Aozasa, K., Tsujimura, A., 2011. Infiltration of tumour-associated macrophages in prostate biopsy specimens is predictive of disease progression after hormonal therapy for prostate cancer. BJU Int. 107, 1918–1922. https://doi.org/10.1111/j.1464-410X.2010.09804.x

Nywening, T.M., Belt, B.A., Cullinan, D.R., Panni, R.Z., Han, B.J., Sanford, D.E., Jacobs, R.C., Ye, J., Patel, A.A., Gillanders, W.E., Fields, R.C., DeNardo, D.G., Hawkins, W.G., Goedegebuure, P., Linehan, D.C., 2018. Targeting both tumour-associated CXCR2 $^{+}$ neutrophils and CCR2 $^{+}$ macrophages disrupts myeloid recruitment and improves chemotherapeutic responses in pancreatic ductal adenocarcinoma. Gut 67, 1112–1123. https://doi.org/10.1136/gutjnl-2017-313738

Olingy, C.E., Dinh, H.Q., Hedrick, C.C., 2019. Monocyte heterogeneity and functions in cancer. J. Leukoc. Biol. 106, 309–322. https://doi.org/10.1002/JLB.4RI0818-311R

Oliveira, D.S.M., Dzinic, S., Bonfil, A.I., Saliganan, A.D., Sheng, S., Bonfil, R.D., 2016. The mouse prostate: a basic anatomical and histological guideline. Bosn. J. Basic Med. Sci. https://doi.org/10.17305/bjbms.2016.917

Olofsen, P.A., Stip, M.C., Jansen, J.H.M., Chan, C., Nederend, M., Tieland, R.G., Tsioumpekou, M., Leusen, J.H.W., 2022. Effective, Long-Term, Neutrophil Depletion Using a

Murinized Anti-Ly-6G 1A8 Antibody. Cells 11, 3406. https://doi.org/10.3390/cells11213406

Ordoñez-Rueda, D., Jönsson, F., Mancardi, D.A., Zhao, W., Malzac, A., Liang, Y., Bertosio, E., Grenot, P., Blanquet, V., Sabrautzki, S., De Angelis, M.H., Méresse, S., Duprez, E., Bruhns, P., Malissen, B., Malissen, M., 2012. A hypomorphic mutation in the Gfi1 transcriptional repressor results in a novel form of neutropenia. Eur. J. Immunol. 42, 2395–2408. https://doi.org/10.1002/eji.201242589

Orkin, S.H., 2000. Diversification of haematopoietic stem cells to specific lineages. Nat. Rev. Genet. 1, 57–64. https://doi.org/10.1038/35049577

Orkin, S.H., Zon, L.I., 2008. Hematopoiesis: An Evolving Paradigm for Stem Cell Biology. Cell 132, 631–644. https://doi.org/10.1016/j.cell.2008.01.025

Page, S.T., Plymate, S.R., Bremner, W.J., Matsumoto, A.M., Hess, D.L., Lin, D.W., Amory, J.K., Nelson, P.S., Wu, J.D., 2006. Effect of medical castration on CD4 $^{+}$ CD25 $^{+}$ T cells, CD8 $^{+}$ T cell IFN-γ expression, and NK cells: a physiological role for testosterone and/or its metabolites. Am. J. Physiol.-Endocrinol. Metab. 290, E856–E863. https://doi.org/10.1152/ajpendo.00484.2005

Palicelli, A., Croci, S., Bisagni, A., Zanetti, E., De Biase, D., Melli, B., Sanguedolce, F., Ragazzi, M., Zanelli, M., Chaux, A., Cañete-Portillo, S., Bonasoni, M.P., Soriano, A., Ascani, S., Zizzo, M., Castro Ruiz, C., De Leo, A., Giordano, G., Landriscina, M., Carrieri, G., Cormio, L., Berney, D.M., Gandhi, J., Santandrea, G., Bonacini, M., 2021. What Do We Have to Know about PD-L1 Expression in Prostate Cancer? A Systematic Literature Review. Part 4: Experimental Treatments in Pre-Clinical Studies (Cell Lines and Mouse Models). Int. J. Mol. Sci. 22, 12297. https://doi.org/10.3390/ijms222212297

Papayannopoulos, V., 2018. Neutrophil extracellular traps in immunity and disease. Nat. Rev. Immunol. 18, 134–147. https://doi.org/10.1038/nri.2017.105

Pardoll, D.M., 2012. The blockade of immune checkpoints in cancer immunotherapy. Nat. Rev. Cancer 12, 252–264. https://doi.org/10.1038/nrc3239

Parisotto, M., Grelet, E., El Bizri, R., Dai, Y., Terzic, J., Eckert, D., Gargowitsch, L., Bornert, J.-M., Metzger, D., 2018a. *PTEN* deletion in luminal cells of mature prostate induces replication stress and senescence in vivo. J. Exp. Med. 215, 1749–1763. https://doi.org/10.1084/jem.20171207

Parisotto, M., Grelet, E., El Bizri, R., Dai, Y., Terzic, J., Eckert, D., Gargowitsch, L., Bornert, J.-M., Metzger, D., 2018b. PTEN deletion in luminal cells of mature prostate induces replication stress and senescence in vivo. J. Exp. Med. 215, 1749–1763. https://doi.org/10.1084/jem.20171207

Parisotto, M., Metzger, D., 2013. Genetically engineered mouse models of prostate cancer. Mol. Oncol. 7, 190–205. https://doi.org/10.1016/j.molonc.2013.02.005

Park, M.D., Silvin, A., Ginhoux, F., Merad, M., 2022. Macrophages in health and disease. Cell 185, 4259–4279. https://doi.org/10.1016/j.cell.2022.10.007

Parker, C., Gillessen, S., Heidenreich, A., Horwich, A., 2015. Cancer of the prostate: ESMO Clinical Practice Guidelines for diagnosis, treatment and follow-up. Ann. Oncol. 26, v69–v77. https://doi.org/10.1093/annonc/mdv222

Patsoukis, N., Wang, Q., Strauss, L., Boussiotis, V.A., 2020. Revisiting the PD-1 pathway. Sci. Adv. 6, eabd2712. https://doi.org/10.1126/sciadv.abd2712

Peehl, D.M., 2005. Primary cell cultures as models of prostate cancer development. Endocr. Relat. Cancer 12, 19–47. https://doi.org/10.1677/erc.1.00795

Pelletier, M., Maggi, L., Micheletti, A., Lazzeri, E., Tamassia, N., Costantini, C., Cosmi, L., Lunardi, C., Annunziato, F., Romagnani, S., Cassatella, M.A., 2010. Evidence for a cross-talk between human neutrophils and Th17 cells. Blood 115, 335–343. https://doi.org/10.1182/blood-2009-04-216085

Peng, W., Chen, J.Q., Liu, C., Malu, S., Creasy, C., Tetzlaff, M.T., Xu, C., McKenzie, J.A., Zhang, C., Liang, X., Williams, L.J., Deng, W., Chen, G., Mbofung, R., Lazar, A.J., Torres-Cabala, C.A., Cooper, Z.A., Chen, P.-L., Tieu, T.N., Spranger, S., Yu, X., Bernatchez, C., Forget, M.-A., Haymaker, C., Amaria, R., McQuade, J.L., Glitza, I.C., Cascone, T., Li, H.S., Kwong, L.N., Heffernan, T.P., Hu, J., Bassett, R.L., Bosenberg, M.W., Woodman, S.E., Overwijk, W.W., Lizée, G., Roszik, J., Gajewski, T.F., Wargo, J.A., Gershenwald, J.E., Radvanyi, L., Davies, M.A., Hwu, P., 2016. Loss of PTEN Promotes Resistance to T Cell–Mediated Immunotherapy. Cancer Discov. 6, 202–216. https://doi.org/10.1158/2159-8290.CD-15-0283

Peprotech Inc, 2021, n.d. Cells of the Immune System.

Perdiguero, E.G., Geissmann, F., 2016. The development and maintenance of resident macrophages. Nat. Immunol. 17, 2–8. https://doi.org/10.1038/ni.3341

Perica, K., Varela, J.C., Oelke, M., Schneck, J., 2015. Adoptive T Cell Immunotherapy For Cancer. Rambam Maimonides Med. J. 6, e0004. https://doi.org/10.5041/RMMJ.10179

Pernar, C.H., Ebot, E.M., Wilson, K.M., Mucci, L.A., 2018. The Epidemiology of Prostate Cancer. Cold Spring Harb. Perspect. Med. 8, a030361. https://doi.org/10.1101/cshperspect.a030361

Petrylak, D.P., Loriot, Y., Shaffer, D.R., Braiteh, F., Powderly, J., Harshman, L.C., Conkling, P., Delord, J.-P., Gordon, M., Kim, J.W., Sarkar, I., Yuen, K., Kadel, E.E., Mariathasan, S., O'Hear, C., Narayanan, S., Fassò, M., Carroll, S., Powles, T., 2021. Safety and Clinical Activity of Atezolizumab in Patients with Metastatic Castration-Resistant Prostate Cancer: A Phase I Study. Clin. Cancer Res. 27, 3360–3369. https://doi.org/10.1158/1078-0432.CCR-20-1981

Pfeiffer, M.J., Smit, F.P., Sedelaar, J.P.M., Schalken, J.A., 2011. Steroidogenic Enzymes and Stem Cell Markers Are Upregulated during Androgen Deprivation in Prostate Cancer. Mol. Med. 17, 657–664. https://doi.org/10.2119/molmed.2010.00143

Philippe, I., Hubert, L., 2016. The reduced concentration of citrate in cancer cells: An indicator of cancer aggressiveness and a possible therapeutic target. Drug Resist. Updat. 29, 47–53. https://doi.org/10.1016/j.drup.2016.09.003

Philippou, Y., Sjoberg, H.T., Murphy, E., Alyacoubi, S., Jones, K.I., Gordon-Weeks, A.N., Phyu, S., Parkes, E.E., Gillies McKenna, W., Lamb, A.D., Gileadi, U., Cerundolo, V., Scheiblin, D.A., Lockett, S.J., Wink, D.A., Mills, I.G., Hamdy, F.C., Muschel, R.J., Bryant, R.J., 2020. Impacts of combining anti-PD-L1 immunotherapy and radiotherapy on the tumour immune microenvironment in a murine prostate cancer model. Br. J. Cancer 123, 1089–1100. https://doi.org/10.1038/s41416-020-0956-x

Phin, S., Moore, M.W., Cotter, P.D., 2013. Genomic Rearrangements of PTEN in Prostate Cancer. Front. Oncol. 3. https://doi.org/10.3389/fonc.2013.00240

Podsypanina, K., Ellenson, L.H., Nemes, A., Gu, J., Tamura, M., Yamada, K.M., Cordon-Cardo, C., Catoretti, G., Fisher, P.E., Parsons, R., 1999. Mutation of *Pten/Mmac1* in mice causes neoplasia in multiple organ systems. Proc. Natl. Acad. Sci. 96, 1563–1568. https://doi.org/10.1073/pnas.96.4.1563

Powles, T., Yuen, K.C., Gillessen, S., Kadel, E.E., Rathkopf, D., Matsubara, N., Drake, C.G., Fizazi, K., Piulats, J.M., Wysocki, P.J., Buchschacher, G.L., Alekseev, B., Mellado, B.,

Karaszewska, B., Doss, J.F., Rasuo, G., Datye, A., Mariathasan, S., Williams, P., Sweeney, C.J., 2022. Atezolizumab with enzalutamide versus enzalutamide alone in metastatic castration-resistant prostate cancer: a randomized phase 3 trial. Nat. Med. 28, 144–153. https://doi.org/10.1038/s41591-021-01600-6

Priceman, S.J., Sung, J.L., Shaposhnik, Z., Burton, J.B., Torres-Collado, A.X., Moughon, D.L., Johnson, M., Lusis, A.J., Cohen, D.A., Iruela-Arispe, M.L., Wu, L., 2010. Targeting distinct tumor-infiltrating myeloid cells by inhibiting CSF-1 receptor: combating tumor evasion of antiangiogenic therapy. Blood 115, 1461–1471. https://doi.org/10.1182/blood-2009-08-237412

Pyonteck, S.M., Akkari, L., Schuhmacher, A.J., Bowman, R.L., Sevenich, L., Quail, D.F., Olson, O.C., Quick, M.L., Huse, J.T., Teijeiro, V., Setty, M., Leslie, C.S., Oei, Y., Pedraza, A., Zhang, J., Brennan, C.W., Sutton, J.C., Holland, E.C., Daniel, D., Joyce, J.A., 2013. CSF-1R inhibition alters macrophage polarization and blocks glioma progression. Nat. Med. 19, 1264–1272. https://doi.org/10.1038/nm.3337

Qian, B.-Z., Li, J., Zhang, H., Kitamura, T., Zhang, J., Campion, L.R., Kaiser, E.A., Snyder, L.A., Pollard, J.W., 2011. CCL2 recruits inflammatory monocytes to facilitate breast-tumour metastasis. Nature 475, 222–225. https://doi.org/10.1038/nature10138

Quail, D.F., Amulic, B., Aziz, M., Barnes, B.J., Eruslanov, E., Fridlender, Z.G., Goodridge, H.S., Granot, Z., Hidalgo, A., Huttenlocher, A., Kaplan, M.J., Malanchi, I., Merghoub, T., Meylan, E., Mittal, V., Pittet, M.J., Rubio-Ponce, A., Udalova, I.A., Van Den Berg, T.K., Wagner, D.D., Wang, P., Zychlinsky, A., De Visser, K.E., Egeblad, M., Kubes, P., 2022. Neutrophil phenotypes and functions in cancer: A consensus statement. J. Exp. Med. 219, e20220011. https://doi.org/10.1084/jem.20220011

Ratnacaram, C.K., Teletin, M., Jiang, M., Meng, X., Chambon, P., Metzger, D., 2008. Temporally controlled ablation of PTEN in adult mouse prostate epithelium generates a model of invasive prostatic adenocarcinoma. Proc. Natl. Acad. Sci. 105, 2521–2526. https://doi.org/10.1073/pnas.0712021105

Rawla, P., 2019. Epidemiology of Prostate Cancer. World J. Oncol. 10, 63–89. https://doi.org/10.14740/wjon1191

Rebuzzi, S.E., Rescigno, P., Catalano, F., Mollica, V., Vogl, U.M., Marandino, L., Massari, F., Pereira Mestre, R., Zanardi, E., Signori, A., Buti, S., Bauckneht, M., Gillessen, S., Banna, G.L., Fornarini, G., 2022. Immune Checkpoint Inhibitors in Advanced Prostate Cancer: Current Data and Future Perspectives. Cancers 14, 1245. https://doi.org/10.3390/cancers14051245

Reith, W., LeibundGut-Landmann, S., Waldburger, J.-M., 2005. Regulation of MHC class II gene expression by the class II transactivator. Nat. Rev. Immunol. 5, 793–806. https://doi.org/10.1038/nri1708

Robinson, D., Van Allen, E.M., Wu, Y.-M., Schultz, N., Lonigro, R.J., Mosquera, J.-M., Montgomery, B., Taplin, M.-E., Pritchard, C.C., Attard, G., Beltran, H., Abida, W., Bradley, R.K., Vinson, J., Cao, X., Vats, P., Kunju, L.P., Hussain, M., Feng, F.Y., Tomlins, S.A., Cooney, K.A., Smith, D.C., Brennan, C., Siddiqui, J., Mehra, R., Chen, Y., Rathkopf, D.E., Morris, M.J., Solomon, S.B., Durack, J.C., Reuter, V.E., Gopalan, A., Gao, J., Loda, M., Lis, R.T., Bowden, M., Balk, S.P., Gaviola, G., Sougnez, C., Gupta, M., Yu, E.Y., Mostaghel, E.A., Cheng, H.H., Mulcahy, H., True, L.D., Plymate, S.R., Dvinge, H., Ferraldeschi, R., Flohr, P., Miranda, S., Zafeiriou, Z., Tunariu, N., Mateo, J., Perez-Lopez, R., Demichelis, F., Robinson, B.D., Schiffman, M., Nanus, D.M., Tagawa, S.T., Sigaras, A., Eng, K.W., Elemento, O., Sboner, A., Heath, E.I., Scher, H.I., Pienta, K.J., Kantoff, P.,

de Bono, J.S., Rubin, M.A., Nelson, P.S., Garraway, L.A., Sawyers, C.L., Chinnaiyan, A.M., 2015. Integrative Clinical Genomics of Advanced Prostate Cancer. Cell 161, 1215–1228. https://doi.org/10.1016/j.cell.2015.05.001

Roehrborn, C.G., 2008. Pathology of benign prostatic hyperplasia. Int. J. Impot. Res. 20 Suppl 3, S11-18. https://doi.org/10.1038/ijir.2008.55

Rojo, R., Raper, A., Ozdemir, D.D., Lefevre, L., Grabert, K., Wollscheid-Lengeling, E., Bradford, B., Caruso, M., Gazova, I., Sánchez, A., Lisowski, Z.M., Alves, J., Molina-Gonzalez, I., Davtyan, H., Lodge, R.J., Glover, J.D., Wallace, R., Munro, D.A.D., David, E., Amit, I., Miron, V.E., Priller, J., Jenkins, S.J., Hardingham, G.E., Blurton-Jones, M., Mabbott, N.A., Summers, K.M., Hohenstein, P., Hume, D.A., Pridans, C., 2019. Deletion of a Csf1r enhancer selectively impacts CSF1R expression and development of tissue macrophage populations. Nat. Commun. 10, 3215. https://doi.org/10.1038/s41467-019-11053-8

Roos, D., Van Bruggen, R., Meischl, C., 2003. Oxidative killing of microbes by neutrophils. Microbes Infect. 5, 1307–1315. https://doi.org/10.1016/j.micinf.2003.09.009

Rosenberg, J.E., Hoffman-Censits, J., Powles, T., Van Der Heijden, M.S., Balar, A.V., Necchi, A., Dawson, N., O'Donnell, P.H., Balmanoukian, A., Loriot, Y., Srinivas, S., Retz, M.M., Grivas, P., Joseph, R.W., Galsky, M.D., Fleming, M.T., Petrylak, D.P., Perez-Gracia, J.L., Burris, H.A., Castellano, D., Canil, C., Bellmunt, J., Bajorin, D., Nickles, D., Bourgon, R., Frampton, G.M., Cui, N., Mariathasan, S., Abidoye, O., Fine, G.D., Dreicer, R., 2016. Atezolizumab in patients with locally advanced and metastatic urothelial carcinoma who have progressed following treatment with platinum-based chemotherapy: a single-arm, multicentre, phase 2 trial. The Lancet 387, 1909–1920. https://doi.org/10.1016/S0140-6736(16)00561-4

Rybak, A.P., Bristow, R.G., Kapoor, A., 2015. Prostate cancer stem cells: deciphering the origins and pathways involved in prostate tumorigenesis and aggression. Oncotarget 6. https://doi.org/10.18632/oncotarget.2953

Sadhu, C., Ting, H.J., Lipsky, B., Hensley, K., Garcia-Martinez, L.F., Simon, S.I., Staunton, D.E., 2007. CD11c/CD18: novel ligands and a role in delayed-type hypersensitivity. J. Leukoc. Biol. 81, 1395–1403. https://doi.org/10.1189/jlb.1106680

Sagiv, J.Y., Michaeli, J., Assi, S., Mishalian, I., Kisos, H., Levy, L., Damti, P., Lumbroso, D., Polyansky, L., Sionov, R.V., Ariel, A., Hovav, A.-H., Henke, E., Fridlender, Z.G., Granot, Z., 2015. Phenotypic Diversity and Plasticity in Circulating Neutrophil Subpopulations in Cancer. Cell Rep. 10, 562–573. https://doi.org/10.1016/j.celrep.2014.12.039

Samaniego, R., Domínguez-Soto, Á., Ratnam, M., Matsuyama, T., Sánchez-Mateos, P., Corbí, Á.L., Puig-Kröger, A., 2020. Folate Receptor β (FRβ) Expression in Tissue-Resident and Tumor-Associated Macrophages Associates with and Depends on the Expression of PU.1. Cells 9, 1445. https://doi.org/10.3390/cells9061445

Sarker, D., Reid, A.H.M., Yap, T.A., De Bono, J.S., 2009. Targeting the PI3K/AKT Pathway for the Treatment of Prostate Cancer. Clin. Cancer Res. 15, 4799–4805. https://doi.org/10.1158/1078-0432.CCR-08-0125

Sasaki, Y., Ohsawa, K., Kanazawa, H., Kohsaka, S., Imai, Y., 2001. Iba1 Is an Actin-Cross-Linking Protein in Macrophages/Microglia. Biochem. Biophys. Res. Commun. 286, 292–297. https://doi.org/10.1006/bbrc.2001.5388

Schadendorf, D., Hodi, F.S., Robert, C., Weber, J.S., Margolin, K., Hamid, O., Patt, D., Chen, T.-T., Berman, D.M., Wolchok, J.D., 2015. Pooled Analysis of Long-Term Survival Data

From Phase II and Phase III Trials of Ipilimumab in Unresectable or Metastatic Melanoma. J. Clin. Oncol. 33, 1889–1894. https://doi.org/10.1200/JCO.2014.56.2736
Schatten, H., 2018. Brief Overview of Prostate Cancer Statistics, Grading, Diagnosis and Treatment Strategies, in: Schatten, H. (Ed.), Cell & Molecular Biology of Prostate Cancer. Springer International Publishing, Cham, pp. 1–14. https://doi.org/10.1007/978-3-319-95693-0_1
Schenk, J.M., Kristal, A.R., Arnold, K.B., Tangen, C.M., Neuhouser, M.L., Lin, D.W., White, E., Thompson, I.M., 2011. Association of symptomatic benign prostatic hyperplasia and prostate cancer: results from the prostate cancer prevention trial. Am. J. Epidemiol. 173, 1419–1428. https://doi.org/10.1093/aje/kwq493
Schmalstieg, F.C., Goldman, A.S., 2008. Ilya Ilich Metchnikoff (1845–1915) and Paul Ehrlich (1854–1915): the Centennial of the 1908 Nobel Prize in Physiology or Medicine. J. Med. Biogr. 16, 96–104. https://doi.org/10.1258/jmb.2008.008006
Schulz, C., Perdiguero, E.G., Chorro, L., Szabo-Rogers, H., Cagnard, N., Kierdorf, K., Prinz, M., Wu, B., Jacobsen, S.E.W., Pollard, J.W., Frampton, J., Liu, K.J., Geissmann, F., 2012. A Lineage of Myeloid Cells Independent of Myb and Hematopoietic Stem Cells. Science 336, 86–90. https://doi.org/10.1126/science.1219179
Scott, C.L., Zheng, F., De Baetselier, P., Martens, L., Saeys, Y., De Prijck, S., Lippens, S., Abels, C., Schoonooghe, S., Raes, G., Devoogdt, N., Lambrecht, B.N., Beschin, A., Guilliams, M., 2016. Bone marrow-derived monocytes give rise to self-renewing and fully differentiated Kupffer cells. Nat. Commun. 7, 10321. https://doi.org/10.1038/ncomms10321
Sehgal, P.D., Bauman, T.M., Nicholson, T.M., Vellky, J.E., Ricke, E.A., Tang, W., Xu, W., Huang, W., Ricke, W.A., 2019. Tissue-specific quantification and localization of androgen and estrogen receptors in prostate cancer. Hum. Pathol. 89, 99–108. https://doi.org/10.1016/j.humpath.2019.04.009
Sender, R., Weiss, Y., Navon, Y., Milo, I., Azulay, N., Keren, L., Fuchs, S., Ben-Zvi, D., Noor, E., Milo, R., 2023. The total mass, number, and distribution of immune cells in the human body. Proc. Natl. Acad. Sci. 120, e2308511120. https://doi.org/10.1073/pnas.2308511120
Sfanos, K.S., Bruno, T.C., Meeker, A.K., De Marzo, A.M., Isaacs, W.B., Drake, C.G., 2009. Human prostate-infiltrating CD8 $^{+}$ T lymphocytes are oligoclonal and PD-1 $^{+}$. The Prostate 69, 1694–1703. https://doi.org/10.1002/pros.21020
Sharma, A., Seow, J.J.W., Dutertre, C.-A., Pai, R., Blériot, C., Mishra, A., Wong, R.M.M., Singh, G.S.N., Sudhagar, S., Khalilnezhad, S., Erdal, S., Teo, H.M., Khalilnezhad, A., Chakarov, S., Lim, T.K.H., Fui, A.C.Y., Chieh, A.K.W., Chung, C.P., Bonney, G.K., Goh, B.K.-P., Chan, J.K.Y., Chow, P.K.H., Ginhoux, F., DasGupta, R., 2020. Onco-fetal Reprogramming of Endothelial Cells Drives Immunosuppressive Macrophages in Hepatocellular Carcinoma. Cell 183, 377-394.e21. https://doi.org/10.1016/j.cell.2020.08.040
Shaw, T.N., Houston, S.A., Wemyss, K., Bridgeman, H.M., Barbera, T.A., Zangerle-Murray, T., Strangward, P., Ridley, A.J.L., Wang, P., Tamoutounour, S., Allen, J.E., Konkel, J.E., Grainger, J.R., 2018. Tissue-resident macrophages in the intestine are long lived and defined by Tim-4 and CD4 expression. J. Exp. Med. 215, 1507–1518. https://doi.org/10.1084/jem.20180019
Sheikh, N.A., Petrylak, D., Kantoff, P.W., Dela Rosa, C., Stewart, F.P., Kuan, L.-Y., Whitmore, J.B., Trager, J.B., Poehlein, C.H., Frohlich, M.W., Urdal, D.L., 2013. Sipuleucel-T immune parameters correlate with survival: an analysis of the randomized phase 3 clinical trials

in men with castration-resistant prostate cancer. Cancer Immunol. Immunother. CII 62, 137–147. https://doi.org/10.1007/s00262-012-1317-2

Shen, H., Lentsch, A.B., 2004. Progressive dysregulation of transcription factors NF-κB and STAT1 in prostate cancer cells causes proangiogenic production of CXC chemokines. Am. J. Physiol.-Cell Physiol. 286, C840–C847. https://doi.org/10.1152/ajpcell.00335.2003

Shen, J., Hilgenbrink, A.R., Xia, W., Feng, Y., Dimitrov, D.S., Lockwood, M.B., Amato, R.J., Low, P.S., 2014. Folate receptor-β constitutes a marker for human proinflammatory monocytes. J. Leukoc. Biol. 96, 563–570. https://doi.org/10.1189/jlb.2AB0713-372R

Sherr, C.J., Rettenmier, C.W., Sacca, R., Roussel, M.F., Look, A.T., Stanley, E.R., 1985. The c-fms proto-oncogene product is related to the receptor for the mononuclear phagocyte growth factor, CSF 1. Cell 41, 665–676. https://doi.org/10.1016/S0092-8674(85)80047-7

Shin, H.C., Seo, I., Jeong, H., Byun, S.J., Kim, S., Bae, S.U., Kwon, S.Y., Lee, H.W., 2021. Prognostic Impact of Tumor-Associated Macrophages on Long-Term Oncologic Outcomes in Colorectal Cancer. Life 11, 1240. https://doi.org/10.3390/life11111240

Shroka, T.M., Kufareva, I., Salanga, C.L., Handel, T.M., 2023. The dual-function chemokine receptor CCR2 drives migration and chemokine scavenging through distinct mechanisms. Sci. Signal. 16, eabo4314. https://doi.org/10.1126/scisignal.abo4314

Siegel, R.L., Giaquinto, A.N., Jemal, A., 2024. Cancer statistics, 2024. CA. Cancer J. Clin. 74, 12–49. https://doi.org/10.3322/caac.21820

Sircar, K., Yoshimoto, M., Monzon, F.A., Koumakpayi, I.H., Katz, R.L., Khanna, A., Alvarez, K., Chen, G., Darnel, A.D., Aprikian, A.G., Saad, F., Bismar, T.A., Squire, J.A., 2009. *PTEN* genomic deletion is associated with p-Akt and AR signalling in poorer outcome, hormone refractory prostate cancer. J. Pathol. 218, 505–513. https://doi.org/10.1002/path.2559

Siret, C., Van Lessen, M., Bavais, J., Jeong, H.W., Reddy Samawar, S.K., Kapupara, K., Wang, S., Simic, M., De Fabritus, L., Tchoghandjian, A., Fallet, M., Huang, H., Sarrazin, S., Sieweke, M.H., Stumm, R., Sorokin, L., Adams, R.H., Schulte-Merker, S., Kiefer, F., Van De Pavert, S.A., 2022. Deciphering the heterogeneity of the Lyve1+ perivascular macrophages in the mouse brain. Nat. Commun. 13, 7366. https://doi.org/10.1038/s41467-022-35166-9

Stanley, E.R., Chitu, V., 2014. CSF-1 Receptor Signaling in Myeloid Cells. Cold Spring Harb. Perspect. Biol. 6, a021857–a021857. https://doi.org/10.1101/cshperspect.a021857

Steele, C.W., Karim, S.A., Leach, J.D.G., Bailey, P., Upstill-Goddard, R., Rishi, L., Foth, M., Bryson, S., McDaid, K., Wilson, Z., Eberlein, C., Candido, J.B., Clarke, M., Nixon, C., Connelly, J., Jamieson, N., Carter, C.R., Balkwill, F., Chang, D.K., Evans, T.R.J., Strathdee, D., Biankin, A.V., Nibbs, R.J.B., Barry, S.T., Sansom, O.J., Morton, J.P., 2016. CXCR2 Inhibition Profoundly Suppresses Metastases and Augments Immunotherapy in Pancreatic Ductal Adenocarcinoma. Cancer Cell 29, 832–845. https://doi.org/10.1016/j.ccell.2016.04.014

Stenzl, A., Feyerabend, S., Syndikus, I., Sarosiek, T., Kübler, H., Heidenreich, A., Cathomas, R., Grüllich, C., Loriot, Y., Perez Gracia, S.L., Gillessen, S., Klinkhardt, U., Schröder, A., Schönborn-Kellenberger, O., Reus, V., Koch, S.D., Hong, H.S., Seibel, T., Fizazi, K., Gnad-Vogt, U., 2017. Results of the randomized, placebo-controlled phase I/IIB trial of CV9104, an mRNA based cancer immunotherapy, in patients with metastatic

castration-resistant prostate cancer (mCRPC). Ann. Oncol. 28, v408–v409. https://doi.org/10.1093/annonc/mdx376.014

Sternberg, N., Hamilton, D., 1981. Bacteriophage P1 site-specific recombination. J. Mol. Biol. 150, 467–486. https://doi.org/10.1016/0022-2836(81)90375-2

Sugimura, Y., Cunha, G.R., Donjacour, A.A., 1986. Morphogenesis of Ductal Networks in the Mouse Prostate1. Biol. Reprod. 34, 961–971. https://doi.org/10.1095/biolreprod34.5.961

Sun, C., Mezzadra, R., Schumacher, T.N., 2018. Regulation and Function of the PD-L1 Checkpoint. Immunity 48, 434–452. https://doi.org/10.1016/j.immuni.2018.03.014

Tamoutounour, S., Guilliams, M., Montanana Sanchis, F., Liu, H., Terhorst, D., Malosse, C., Pollet, E., Ardouin, L., Luche, H., Sanchez, C., Dalod, M., Malissen, B., Henri, S., 2013. Origins and Functional Specialization of Macrophages and of Conventional and Monocyte-Derived Dendritic Cells in Mouse Skin. Immunity 39, 925–938. https://doi.org/10.1016/j.immuni.2013.10.004

Tamoutounour, S., Henri, S., Lelouard, H., De Bovis, B., De Haar, C., Van Der Woude, C.J., Woltman, A.M., Reyal, Y., Bonnet, D., Sichien, D., Bain, C.C., Mowat, A.McI., Reis E Sousa, C., Poulin, L.F., Malissen, B., Guilliams, M., 2012. CD 64 distinguishes macrophages from dendritic cells in the gut and reveals the T h1-inducing role of mesenteric lymph node macrophages during colitis. Eur. J. Immunol. 42, 3150–3166. https://doi.org/10.1002/eji.201242847

Tan, M.E., Li, J., Xu, H.E., Melcher, K., Yong, E., 2015. Androgen receptor: structure, role in prostate cancer and drug discovery. Acta Pharmacol. Sin. 36, 3–23. https://doi.org/10.1038/aps.2014.18

Tang, J., Xiao, L., Cui, R., Li, D., Zheng, X., Zhu, L., Sun, H., Pan, Y., Du, Y., Yu, X., 2016. CX3CL1 increases invasiveness and metastasis by promoting epithelial-to-mesenchymal transition through the TACE/TGF-α/EGFR pathway in hypoxic androgen-independent prostate cancer cells. Oncol. Rep. 35, 1153–1162. https://doi.org/10.3892/or.2015.4470

Tang, Z., Davidson, D., Li, R., Zhong, M.-C., Qian, J., Chen, J., Veillette, A., 2021. Inflammatory macrophages exploit unconventional pro-phagocytic integrins for phagocytosis and anti-tumor immunity. Cell Rep. 37, 110111. https://doi.org/10.1016/j.celrep.2021.110111

Tarling, J.D., Lin, H., Hsu, S., 1987. Self-Renewal of Pulmonary Alveolar Macrophages: Evidence From Radiation Chimera Studies. J. Leukoc. Biol. 42, 443–446. https://doi.org/10.1002/jlb.42.5.443

Tauber, A.I., 2003. Metchnikoff and the phagocytosis theory. Nat. Rev. Mol. Cell Biol. 4, 897–901. https://doi.org/10.1038/nrm1244

Taylor, B.S., Schultz, N., Hieronymus, H., Gopalan, A., Xiao, Y., Carver, B.S., Arora, V.K., Kaushik, P., Cerami, E., Reva, B., Antipin, Y., Mitsiades, N., Landers, T., Dolgalev, I., Major, J.E., Wilson, M., Socci, N.D., Lash, A.E., Heguy, A., Eastham, J.A., Scher, H.I., Reuter, V.E., Scardino, P.T., Sander, C., Sawyers, C.L., Gerald, W.L., 2010. Integrative Genomic Profiling of Human Prostate Cancer. Cancer Cell 18, 11–22. https://doi.org/10.1016/j.ccr.2010.05.026

Taylor, P., Gordon, S., Martinezpomares, L., 2005. The mannose receptor: linking homeostasis and immunity through sugar recognition. Trends Immunol. 26, 104–110. https://doi.org/10.1016/j.it.2004.12.001

Taylor, P.R., Martinez-Pomares, L., Stacey, M., Lin, H.-H., Brown, G.D., Gordon, S., 2005. MACROPHAGE RECEPTORS AND IMMUNE RECOGNITION. Annu. Rev. Immunol. 23, 901–944. https://doi.org/10.1146/annurev.immunol.23.021704.115816

Teijeira, Á., Garasa, S., Gato, M., Alfaro, C., Migueliz, I., Cirella, A., De Andrea, C., Ochoa, M.C., Otano, I., Etxeberria, I., Andueza, M.P., Nieto, C.P., Resano, L., Azpilikueta, A., Allegretti, M., De Pizzol, M., Ponz-Sarvisé, M., Rouzaut, A., Sanmamed, M.F., Schalper, K., Carleton, M., Mellado, M., Rodriguez-Ruiz, M.E., Berraondo, P., Perez-Gracia, J.L., Melero, I., 2020. CXCR1 and CXCR2 Chemokine Receptor Agonists Produced by Tumors Induce Neutrophil Extracellular Traps that Interfere with Immune Cytotoxicity. Immunity 52, 856-871.e8. https://doi.org/10.1016/j.immuni.2020.03.001

Templeton, A.J., McNamara, M.G., Šeruga, B., Vera-Badillo, F.E., Aneja, P., Ocaña, A., Leibowitz-Amit, R., Sonpavde, G., Knox, J.J., Tran, B., Tannock, I.F., Amir, E., 2014a. Prognostic Role of Neutrophil-to-Lymphocyte Ratio in Solid Tumors: A Systematic Review and Meta-Analysis. JNCI J. Natl. Cancer Inst. 106. https://doi.org/10.1093/jnci/dju124

Templeton, A.J., Pezaro, C., Omlin, A., McNamara, M.G., Leibowitz-Amit, R., Vera-Badillo, F.E., Attard, G., De Bono, J.S., Tannock, I.F., Amir, E., 2014b. Simple prognostic score for metastatic castration-resistant prostate cancer with incorporation of neutrophil-to-lymphocyte ratio. Cancer 120, 3346–3352. https://doi.org/10.1002/cncr.28890

Thomas, L., 1982. On immunosurveillance in human cancer. Yale J. Biol. Med. 55, 329–333.

Timms, B.G., 2008. Prostate development: a historical perspective. Differentiation 76, 565–577. https://doi.org/10.1111/j.1432-0436.2008.00278.x

Titov, A., Valiullina, A., Zmievskaya, E., Zaikova, E., Petukhov, A., Miftakhova, R., Bulatov, E., Rizvanov, A., 2020. Advancing CAR T-Cell Therapy for Solid Tumors: Lessons Learned from Lymphoma Treatment. Cancers 12, 125. https://doi.org/10.3390/cancers12010125

Tobin, R.P., Jordan, K.R., Kapoor, P., Spongberg, E., Davis, D., Vorwald, V.M., Couts, K.L., Gao, D., Smith, D.E., Borgers, J.S.W., Robinson, S., Amato, C., Gonzalez, R., Lewis, K.D., Robinson, W.A., Borges, V.F., McCarter, M.D., 2019. IL-6 and IL-8 Are Linked With Myeloid-Derived Suppressor Cell Accumulation and Correlate With Poor Clinical Outcomes in Melanoma Patients. Front. Oncol. 9, 1223. https://doi.org/10.3389/fonc.2019.01223

Toivanen, R., Shen, M.M., 2017. Prostate organogenesis: tissue induction, hormonal regulation and cell type specification. Development 144, 1382–1398. https://doi.org/10.1242/dev.148270

Topalian, S.L., Hodi, F.S., Brahmer, J.R., Gettinger, S.N., Smith, D.C., McDermott, D.F., Powderly, J.D., Carvajal, R.D., Sosman, J.A., Atkins, M.B., Leming, P.D., Spigel, D.R., Antonia, S.J., Horn, L., Drake, C.G., Pardoll, D.M., Chen, L., Sharfman, W.H., Anders, R.A., Taube, J.M., McMiller, T.L., Xu, H., Korman, A.J., Jure-Kunkel, M., Agrawal, S., McDonald, D., Kollia, G.D., Gupta, A., Wigginton, J.M., Sznol, M., 2012. Safety, Activity, and Immune Correlates of Anti–PD-1 Antibody in Cancer. N. Engl. J. Med. 366, 2443–2454. https://doi.org/10.1056/NEJMoa1200690

Turvey, S.E., Broide, D.H., 2010. Innate immunity. J. Allergy Clin. Immunol. 125, S24–S32. https://doi.org/10.1016/j.jaci.2009.07.016

Ulland, T.K., Colonna, M., 2018. TREM2 — a key player in microglial biology and Alzheimer disease. Nat. Rev. Neurol. 14, 667–675. https://doi.org/10.1038/s41582-018-0072-1

Valkenburg, K.C., Williams, B.O., 2011. Mouse Models of Prostate Cancer. Prostate Cancer 2011, 1–22. https://doi.org/10.1155/2011/895238

Van Bokhoven, A., Caires, A., Maria, M.D., Schulte, A.P., Lucia, M.S., Nordeen, S.K., Miller, G.J., Varella-Garcia, M., 2003. Spectral karyotype (SKY) analysis of human prostate carcinoma cell lines. The Prostate 57, 226–244. https://doi.org/10.1002/pros.10291

van Furth, R., Cohn, Z.A., Hirsch, J.G., Humphrey, J.H., Spector, W.G., Langevoort, H.L., 1972. The mononuclear phagocyte system: a new classification of macrophages, monocytes, and their precursor cells. Bull. World Health Organ. 46, 845–852.

Van Weerden, W.M., Bangma, C., De Wit, R., 2009. Human xenograft models as useful tools to assess the potential of novel therapeutics in prostate cancer. Br. J. Cancer 100, 13–18. https://doi.org/10.1038/sj.bjc.6604822

Veglia, F., Hashimoto, A., Dweep, H., Sanseviero, E., De Leo, A., Tcyganov, E., Kossenkov, A., Mulligan, C., Nam, B., Masters, G., Patel, J., Bhargava, V., Wilkinson, P., Smirnov, D., Sepulveda, M.A., Singhal, S., Eruslanov, E.B., Cristescu, R., Loboda, A., Nefedova, Y., Gabrilovich, D.I., 2021a. Analysis of classical neutrophils and polymorphonuclear myeloid-derived suppressor cells in cancer patients and tumor-bearing mice. J. Exp. Med. 218, e20201803. https://doi.org/10.1084/jem.20201803

Veglia, F., Sanseviero, E., Gabrilovich, D.I., 2021b. Myeloid-derived suppressor cells in the era of increasing myeloid cell diversity. Nat. Rev. Immunol. 21, 485–498. https://doi.org/10.1038/s41577-020-00490-y

Vidotto, T., Melo, C.M., Castelli, E., Koti, M., Dos Reis, R.B., Squire, J.A., 2020. Emerging role of PTEN loss in evasion of the immune response to tumours. Br. J. Cancer 122, 1732–1743. https://doi.org/10.1038/s41416-020-0834-6

Vidotto, T., Saggioro, F.P., Jamaspishvili, T., Chesca, D.L., Picanço De Albuquerque, C.G., Reis, R.B., Graham, C.H., Berman, D.M., Siemens, D.R., Squire, J.A., Koti, M., 2019. PTEN-deficient prostate cancer is associated with an immunosuppressive tumor microenvironment mediated by increased expression of IDO1 and infiltrating FoxP3+ T regulatory cells. The Prostate 79, 969–979. https://doi.org/10.1002/pros.23808

Visakorpi, T., Hyytinen, E., Koivisto, P., Tanner, M., Keinänen, R., Palmberg, C., Palotie, A., Tammela, T., Isola, J., Kallioniemi, O.-P., 1995. In vivo amplification of the androgen receptor gene and progression of human prostate cancer. Nat. Genet. 9, 401–406. https://doi.org/10.1038/ng0495-401

Vivier, E., Rebuffet, L., Narni-Mancinelli, E., Cornen, S., Igarashi, R.Y., Fantin, V.R., 2024. Natural killer cell therapies. Nature 626, 727–736. https://doi.org/10.1038/s41586-023-06945-1

Von Amsberg, G., Alsdorf, W., Karagiannis, P., Coym, A., Kaune, M., Werner, S., Graefen, M., Bokemeyer, C., Merkens, L., Dyshlovoy, S.A., 2022. Immunotherapy in Advanced Prostate Cancer—Light at the End of the Tunnel? Int. J. Mol. Sci. 23, 2569. https://doi.org/10.3390/ijms23052569

Wadosky, K.M., Koochekpour, S., 2016. Molecular mechanisms underlying resistance to androgen deprivation therapy in prostate cancer. Oncotarget 7, 64447–64470. https://doi.org/10.18632/oncotarget.10901

Wang, S., Gao, J., Lei, Q., Rozengurt, N., Pritchard, C., Jiao, J., Thomas, G.V., Li, G., Roy-Burman, P., Nelson, P.S., Liu, X., Wu, H., 2003. Prostate-specific deletion of the murine Pten tumor suppressor gene leads to metastatic prostate cancer. Cancer Cell 4, 209–221. https://doi.org/10.1016/S1535-6108(03)00215-0

Wang, X., Julio, M.K., Economides, K.D., Walker, D., Yu, H., Halili, M.V., Hu, Y.-P., Price, S.M., Abate-Shen, C., Shen, M.M., 2009. A luminal epithelial stem cell that is a cell of origin for prostate cancer. Nature 461, 495–500. https://doi.org/10.1038/nature08361

Wang, X., Yuwen, T., Zhong, Y., Li, Z.-G., Wang, X.-Y., 2023. A new method for predicting the prognosis of colorectal cancer patients through a combination of multiple tumor-associated macrophage markers at the invasive front. Heliyon 9, e13211. https://doi.org/10.1016/j.heliyon.2023.e13211

Wang, X.-Q., Tao, B.-B., Li, B., Wang, X.-H., Zhang, W.-C., Wan, L., Hua, X.-M., Li, S.-T., 2016. Overexpression of TREM2 enhances glioma cell proliferation and invasion: a therapeutic target in human glioma. Oncotarget 7, 2354–2366. https://doi.org/10.18632/oncotarget.6221

Wang, Z., Chen, C., Su, Y., Ke, N., 2022. Function and characteristics of TIM-4 in immune regulation and disease (Review). Int. J. Mol. Med. 51, 10. https://doi.org/10.3892/ijmm.2022.5213

Welch, D.R., Schissel, D.J., Howrey, R.P., Aeed, P.A., 1989. Tumor-elicited polymorphonuclear cells, in contrast to “normal” circulating polymorphonuclear cells, stimulate invasive and metastatic potentials of rat mammary adenocarcinoma cells. Proc. Natl. Acad. Sci. 86, 5859–5863. https://doi.org/10.1073/pnas.86.15.5859

Welch, H.G., Black, W.C., 2010. Overdiagnosis in Cancer. JNCI J. Natl. Cancer Inst. 102, 605–613. https://doi.org/10.1093/jnci/djq099

Wu, X., Wu, J., Huang, J., Powell, W.C., Zhang, J., Matusik, R.J., Sangiorgi, F.O., Maxson, R.E., Sucov, H.M., Roy-Burman, P., 2001. Generation of a prostate epithelial cell-specific Cre transgenic mouse model for tissue-specific gene ablation. Mech. Dev. 101, 61–69. https://doi.org/10.1016/S0925-4773(00)00551-7

Wu, Y., Ma, J., Yang, X., Nan, F., Zhang, T., Ji, S., Rao, D., Feng, H., Gao, K., Gu, X., Jiang, S., Song, G., Pan, J., Zhang, M., Xu, Y., Zhang, S., Fan, Y., Wang, X., Zhou, J., Yang, L., Fan, J., Zhang, X., Gao, Q., 2024. Neutrophil profiling illuminates anti-tumor antigen-presenting potency. Cell 187, 1422-1439.e24. https://doi.org/10.1016/j.cell.2024.02.005

Xiao, S., Qin, D., Hou, X., Tian, L., Yu, Y., Zhang, R., Lyu, H., Guo, D., Chen, X.-Z., Zhou, C., Tang, J., 2023. Cellular senescence: a double-edged sword in cancer therapy. Front. Oncol. 13, 1189015. https://doi.org/10.3389/fonc.2023.1189015

Xie, X., Shi, Q., Wu, P., Zhang, X., Kambara, H., Su, J., Yu, H., Park, S.-Y., Guo, R., Ren, Q., Zhang, S., Xu, Y., Silberstein, L.E., Cheng, T., Ma, F., Li, C., Luo, H.R., 2020. Single-cell transcriptome profiling reveals neutrophil heterogeneity in homeostasis and infection. Nat. Immunol. 21, 1119–1133. https://doi.org/10.1038/s41590-020-0736-z

Xiong, W., Gao, Y., Wei, W., Zhang, J., 2021. Extracellular and nuclear PD-L1 in modulating cancer immunotherapy. Trends Cancer 7, 837–846. https://doi.org/10.1016/j.trecan.2021.03.003

Xiong, X., Liao, X., Qiu, S., Xu, H., Zhang, S., Wang, S., Ai, J., Yang, L., 2022. CXCL8 in Tumor Biology and Its Implications for Clinical Translation. Front. Mol. Biosci. 9, 723846. https://doi.org/10.3389/fmolb.2022.723846

Yan, J., Wan, P., Choksi, S., Liu, Z.-G., 2022. Necroptosis and tumor progression. Trends Cancer 8, 21–27. https://doi.org/10.1016/j.trecan.2021.09.003

Yona, S., Kim, K.-W., Wolf, Y., Mildner, A., Varol, D., Breker, M., Strauss-Ayali, D., Viukov, S., Guilliams, M., Misharin, A., Hume, D.A., Perlman, H., Malissen, B., Zelzer, E., Jung, S., 2013. Fate Mapping Reveals Origins and Dynamics of Monocytes and Tissue

Macrophages under Homeostasis. Immunity 38, 79–91. https://doi.org/10.1016/j.immuni.2012.12.001

Yu, Y.-R., Ho, P.-C., 2019. Sculpting tumor microenvironment with immune system: from immunometabolism to immunoediting. Clin. Exp. Immunol. 197, 153–160. https://doi.org/10.1111/cei.13293

Yunger, S., Bar El, A., Zeltzer, L., Fridman, E., Raviv, G., Laufer, M., Schachter, J., Markel, G., Itzhaki, O., Besser, M.J., 2019. Tumor-infiltrating lymphocytes from human prostate tumors reveal anti-tumor reactivity and potential for adoptive cell therapy. OncoImmunology 8, e1672494. https://doi.org/10.1080/2162402X.2019.1672494

Zarif, J.C., Baena-Del Valle, J.A., Hicks, J.L., Heaphy, C.M., Vidal, I., Luo, J., Lotan, T.L., Hooper, J.E., Isaacs, W.B., Pienta, K.J., De Marzo, A.M., 2019. Mannose Receptor–positive Macrophage Infiltration Correlates with Prostate Cancer Onset and Metastatic Castration-resistant Disease. Eur. Urol. Oncol. 2, 429–436. https://doi.org/10.1016/j.euo.2018.09.014

Zhai, L., Bell, A., Ladomersky, E., Lauing, K.L., Bollu, L., Sosman, J.A., Zhang, B., Wu, J.D., Miller, S.D., Meeks, J.J., Lukas, R.V., Wyatt, E., Doglio, L., Schiltz, G.E., McCusker, R.H., Wainwright, D.A., 2020. Immunosuppressive IDO in Cancer: Mechanisms of Action, Animal Models, and Targeting Strategies. Front. Immunol. 11, 1185. https://doi.org/10.3389/fimmu.2020.01185

Zhang, X., Lee, C., Ng, P.-Y., Rubin, M., Shabsigh, A., Buttyan, R., 2000. Prostatic neoplasia in transgenic mice with prostate-directed overexpression of the c-myc oncoprotein. The Prostate 43, 278–285. https://doi.org/10.1002/1097-0045(20000601)43:4<278::AID-PROS7>3.0.CO;2-4

Zhang, X., Wang, L.-P., Ziober, A., Zhang, P.J., Bagg, A., 2021. Ionized Calcium Binding Adaptor Molecule 1 (IBA1). Am. J. Clin. Pathol. 156, 86–99. https://doi.org/10.1093/ajcp/aqaa209

Zhang, X., Wang, W., Li, P., Wang, X., Ni, K., 2018. High TREM2 expression correlates with poor prognosis in gastric cancer. Hum. Pathol. 72, 91–99. https://doi.org/10.1016/j.humpath.2017.10.026

Zhang, Y., Chandra, V., Riquelme Sanchez, E., Dutta, P., Quesada, P.R., Rakoski, A., Zoltan, M., Arora, N., Baydogan, S., Horne, W., Burks, J., Xu, H., Hussain, P., Wang, H., Gupta, S., Maitra, A., Bailey, J.M., Moghaddam, S.J., Banerjee, S., Sahin, I., Bhattacharya, P., McAllister, F., 2020. Interleukin-17–induced neutrophil extracellular traps mediate resistance to checkpoint blockade in pancreatic cancer. J. Exp. Med. 217, e20190354. https://doi.org/10.1084/jem.20190354

Zheng, Y., Sun, H., Yang, S., Liu, W., Jiang, G., 2024. Identification of Molecular Subtype and Prognostic Signature for Prostate Adenocarcinoma based on Neutrophil Extracellular Traps. J. Cancer 15, 2678–2690. https://doi.org/10.7150/jca.93275

Zhou, X., Franklin, R.A., Adler, M., Jacox, J.B., Bailis, W., Shyer, J.A., Flavell, R.A., Mayo, A., Alon, U., Medzhitov, R., 2018. Circuit Design Features of a Stable Two-Cell System. Cell 172, 744-757.e17. https://doi.org/10.1016/j.cell.2018.01.015

Zhu, Y., Knolhoff, B.L., Meyer, M.A., Nywening, T.M., West, B.L., Luo, J., Wang-Gillam, A., Goedegebuure, S.P., Linehan, D.C., DeNardo, D.G., 2014. CSF1/CSF1R Blockade Reprograms Tumor-Infiltrating Macrophages and Improves Response to T-cell Checkpoint Immunotherapy in Pancreatic Cancer Models. Cancer Res. 74, 5057–5069. https://doi.org/10.1158/0008-5472.CAN-13-3723